Hierarchical Association of Subcomplexes Drives pre-rRNA Folding during Ribosome Biogenesis in *Saccharomyces cerevisiae*

Jason Talkish

B.S. (Honors) Biology

B.S. (Honors) Forensic and Investigative Sciences

2006

West Virginia University, Morgantown, WV, USA

Submitted in partial fulfillment of the requirement for the degree of

Doctor of Philosophy

Department of Biological Sciences

Carnegie Mellon University

4400 Fifth Avenue

Pittsburgh, PA 15213

September 17, 2013

Thesis Advisor: Dr. John L. Woolford, Jr.

Acknowledgements

I would first and foremost like to thank my advisor and mentor John Woolford. His approach to science, teaching, lab management, and life is truly inspiring. He has always been someone I can turn to for advice, both about science and life in general, and for this I will always be grateful. I honestly believe that I could not have received better training, guidance, and support from anyone else or any other laboratory. I am forever thankful that John welcomed me into his laboratory and for his unending support and guidance.

I would like to thank the members of my thesis committee, Dr. Aaron P. Mitchell, Dr. C. Joel McManus, and Dr. Jeffrey Brodsky for challenging me to think deeply about my research. Their advice and guidance over the past few years has been invaluable to my work.

I would also like to thank all of the members of the Woolford Laboratory, both past and present, especially Michael Gamalinda, Madhumitha Ramesh, Salini Konikkat, Beril Kumcuoglu, Dr. Jingyu Zhang, and Dr. Aarti Sahasranaman. I am lucky to have worked with such brilliant and passionate scientists. But more importantly, I am grateful that I have made new friends and developed new relationships with so many caring, thoughtful, and supportive people. The close-knit nature of the Woolford Laboratory has made my time there truly enjoyable.

I want to give a special acknowledgement to my friend and (second) mentor, Jelena Jakovljevic for all of her support and guidance during my time in the Woolford Laboratory. I often looked forward to coming to lab just to chat and laugh with Jelena. She is someone I

admire very much and I am grateful that I had the opportunity to work with her and become friends with her.

I would like to thank the undergraduates that I had the opportunity to train, Lynley Doonan, Ian Campbell, and Anna Park. They were always a pleasure to work with and have helped me to become a better mentor.

I would also like to thank my friends from home who have always been there for me and supported me during my graduate studies. I am grateful to have had such a close group of people that I could turn to for a quick pick-me-up when my thesis work was not going smoothly.

I would also like to thank my family, especially those no longer with me, for their love and encouragement over the past few years. I could not have done this without their support.

Importantly, I want to express my sincerest gratitude to my girlfriend, Idil Ulengin. I am thankful that we both decided to do our graduate work at Carnegie Mellon University and that we had the opportunity to meet. Her unyielding love and support is what allowed me to make it trough the trials and tribulations of graduate school, and I can't imagine doing it without her.

Most importantly, I want to dedicate this work to my amazing parents, Robert and Barbara Talkish. They have always instilled in me good values and work ethic, encouraged me to always do my best, and supported me when things were at their worst. I consider myself lucky and truly blessed to have two people in my life who are so loving, caring, and thoughtful.

Hierarchical Assembly of Subcomplexes Drives pre-rRNA Folding During Ribosome Biogenesis in *Saccharomyces cerevisiae*

Jason Talkish

Carnegie Mellon University
Department of Biological Sciences
Pittsburgh, Pennsylvania

Abstract

Construction of eukaryotic ribosomes requires at least 180 assembly factors. These proteins are thought to drive forward the progressive folding and processing of pre-rRNAs, and binding of ribosomal proteins. Initial characterizations have revealed in which steps of pre-rRNA processing most of these factors function, but only recently have investigations begun to understand how each of these proteins contributes to folding of the nascent rRNA.

Work from our lab, part of which is presented in this thesis, has established an association hierarchy between 12 assembly factors and ribosomal proteins necessary for processing $27SA_3$ pre-rRNA. The most up-stream factors in this pathway are present in a subcomplex of four assembly factors and two ribosomal proteins. I focused on the understanding the roles of two of these proteins, Nop12 and Pwp1, in ribosome biogenesis. I investigated their timing of association with pre-ribosomes, their role in recruiting other proteins, and the effects on pre-rRNA folding in their absence. By doing so, I show that the effects observed on pre-rRNA processing in the absence of Nop12 and Pwp1 are not simply due to pre-ribosomes lacking a complete inventory of proteins, but rather due to a failure to properly fold the rRNA.

I also investigated the function of the DEAD-box protein Drs1 in ribosome biogenesis and show that it functions in two consecutive steps of ribosome assembly. Furthermore, physical and genetic interactions reveal that Drs1 is recruited to pre-ribosomes by a subcomplex of assembly factors that function in the same step of biogenesis.

Most importantly, in the course of investigating Drs1, I found that disruption of ribosome biogenesis results in a shift from pre-rRNAs being processed co-transcriptionally, to being processed post-transcriptionally. When this occurs, there is a breakdown of the global hierarchy of ribosome biogenesis. I show that normally late associating proteins associate with pre-ribosomes early in the biogenesis pathway, prior to any pre-rRNA processing steps occurring. Furthermore, I show this shift from co- to post-transcriptional processing is related to cell growth rates, and pre-rRNAs processed post-transcriptionally proceed down an alternative maturation pathway. These results have drastic implications for how we view the overall hierarchy of ribosome biogenesis.

Table of Contents

		Page
Chapter 1	**Introduction**	
1.1	Ribosome function and disease	2
1.2	Ribosome assembly and pre-rRNA processing are co-transcriptional	6
1.3	*Trans*-acting factors drive assembly of pre-ribosomes	16
1.3.1	Functions of assembly factors	25
1.3.2	RNA helicases/ATPases are the movers and shakers of ribosome biogenesis	25
1.4	Formation of pre-ribosomal particles	27
1.4.1	Subcomplexes of assembly factors reduce the complexity of assembly	32
1.5	Ribosome assembly is hierarchical, but heterogeneous	32
1.5.1	Ribosome assembly proceeds down multiple, parallel pathways	39
1.6	RNA folding	43
1.6.1	Secondary interactions are the driving force in RNA folding	44
1.6.2	Tertiary interactions generate the native, functional state during RNA folding	48
1.6.3	Compact intermediates in RNA folding	53
1.6.4	Parallel pathways of RNA folding – kinetic partitioning	54
1.6.5	Current approaches to probing RNA structure	57

1.6.6	Recent insights into *in vivo* pre-rRNA folding during ribosome biogenesis	64
1.6.6.1	The U3 snoRNA is required for proper folding of pre-18S rRNA	65
1.6.6.2	A conformational switch regulates pre-rRNA cleavage by Nob1	65
1.6.6.3	A subcomplex of assembly factors is required for proper folding of ITS2	66
Chapter 2	**Assembly factors Pwp1 and Nop12 function to fold 5.8S rRNA during ribosome biogenesis in *Saccharomyces cerevisiae***	
2.1	**Introduction**	68
2.2	**Results**	73
2.2.1	Pwp1 is nonessential and functions in 60S subunit biogenesis	73
2.2.2	Pwp1 is important for efficient processing of $27SA_2$ and $27SA_3$ pre-rRNAs	79
2.2.3	Pwp1 and Nop12 associate with 90S pre-ribosomes and are exported to the cytoplasm	86
2.2.4	Pwp1 is important for stable association with pre-ribosomes of assembly factors required for $27SA_3$ pre-rRNA processing	89
2.2.5	The composition of pre-ribosomes is largely unaffected	94

	in the absence of Nop12	
2.2.6	Pwp1 and Nop12 are not dependent of the A_3 factors for stable association with pre-ribosomes	95
2.2.7	Pwp1 and Nop12 are important for proper folding of 5.8S rRNA	99
2.3	**Discussion**	107
2.4	**Materials and Methods**	114
Chapter 3	**Disruption of ribosome biogenesis results in a shift from post- to co-transcriptional pre-rRNA processing and breakdown of the assembly hierarchy**	
3.1	**Introduction**	123
3.2	**Results**	126
3.2.1	Drs1 is required for processing of $27SA_2$ and $27SA_3$ pre-rRNAs	126
3.2.2	Association of Drs1 with pre-ribosomes requires the Nop7 subcomplex.	132
3.2.3	In the absence of Drs1, Nop7-contiaing pre-ribosomes are enriched for early associating 66S assembly factors and SSU components, but also late associating small subunit r-proteins	136
3.2.4	In the absence of Drs1, early 66S pre-ribosomes are enriched for late associating assembly factors	141
3.2.5	In the absence of Drs1, late associating 66S assembly	145

	factors and early associating 66S assembly factors are in the same pre-ribosomal particles	
3.2.6	Late 66S assembly factors co-immunoprecipitate early pre-rRNAs in the absence of Drs1	150
3.2.7	Nog2-containing pre-ribosomes are enriched with RNA polymerase I components upon depletion of Drs1	154
3.2.8	Clarifying discrepancies in my data	160
3.2.9	Pre-rRNA processing is dependent on cell growth rates	164
3.3	**Discussion**	172
3.4	**Materials and Methods**	179
Chapter 4	**Mod-seq: High-throughput sequencing for chemical probing of RNA structure**	
4.1	**Introduction**	185
4.2	**Results**	188
4.2.1	Overview of the Mod-seq strategy and pipeline	188
4.2.2	*In vivo* Mod-seq analysis of yeast rRNA	191
4.2.3	Detection of modified guanines by Mod-seq	212
4.2.4	Detection of RBP binding sites and RNP structural changes by Mod-seq	212
4.2.5	Mod-seq provides secondary structure information for pre-rRNAs	225
4.3	**Discussion**	228

4.4 **Materials and Methods** 232

Chapter 5 **Appendix**

5.1 Hierarchical recruitment into nascent ribosomes of assembly factors required for 27SB pre-rRNA processing in *Saccharomyces cerevisiae* 239

5.2 Ebp2 and Brx1 function cooperatively in 60S ribosomal subunit assembly 291

5.2.1 Depletion of Ebp2 and Brx1 block processing of $27SA_2$ and $27SA_3$ pre-rRNAs 291

5.2.2 A combination of *ebp2-14* and *brx1-102* or *brx1-172* mutations leads to synergistic defects in pre-rRNA processing 295

5.2.3 Ebp2 and Brx1 assemble into pre-ribosomes early, with pre-rRNPs containing 35S pre-rRNA 298

5.3 Timing of association of assembly factors 301

5.4 *In vivo* hydroxyl radical RNA structure probing in yeast 304

5.5 Cic1 and Nop15 are required for proper folding of ITS2 312

5.6 Screening for mutations in genes synthetically lethal with *drs1* missense mutants 318

5.7 Reducing the heterogeneity of pre-rRNAs for RNA 319

structure probing

5.8 Mutational analysis of Drs1 322

5.9 Association hierarchy of proteins that function in 27S pre-rRNA processing 326

References 327

List of Figures

Figure 1	Crystal structure of the *Saccharomyces cerevisiae* ribosome at 3.0Å	4
Figure 2	rDNA repeat in *Saccharomyces cerevisiae*	10
Figure 3	The majority of pre-rRNA processing in *Saccharomyces cerevisiae* occurs co-transcriptionally whereas a minority occurs post-transcriptionally	12
Figure 4	Pre-rRNA processing in *Saccharomyces cerevisiae*	14
Figure 5	Maturation of pre-ribosomal particles in *Saccharomyces cerevisiae*	30
Figure 6	*In vitro* assembly maps of *E. coli* small and large ribosomal subunits	37
Figure 7	Ribosome assembly proceeds down multiple, parallel Pathways	41
Figure 8	RNA secondary structure is composed of helices, loops, and junctions	46
Figure 9	COIN stacking is the dominant organizing force of RNA tertiary structure	51
Figure 10	Chemical probing of RNA structure	62
Figure 11	The Pwp1-subcomplex associates with pre-ribosomes near the ITS2-proximal stem	71
Figure 12	*PWP1* is nonessential and its deletion confers cold-	75

	Sensitivity	
Figure 13	Deletion of Pwp1 affects production of 60S ribosomal Subunits	77
Figure 14	Pwp1 functions in processing of $27SA_2$ and $27SA_3$ pre-rRNAs	82
Figure 15	Pre-ribosomes accumulate in the nucleolus in the absence of Pwp1	84
Figure 16	Pwp1 associates with pre-ribosomes in the nucleous and is exported to the cytoplasm	87
Figure 17	Changes in composition of pre-ribosomes in the absence of Pwp1 and Nop12	92
Figure 18	Pwp1 and Nop12 are not dependent on the interdependent A_3 factors for association with pre-ribosomes	97
Figure 19	Pwp1 and Nop12 are important for proper folding of 5.8S rRNA	103
Figure 20	Helix 5 of 5.8S rRNA is misfolded in the absence of Pwp1 and Nop12	105
Figure 21	*drs1* missense mutants block 27SB pre-rRNA Processing	128
Figure 22	Depletion of Drs1 blocks $27SA_2$ and $27SA_3$ pre-rRNA Processing	130
Figure 23	Drs1 functionally and physically interacts with the	133

	Nop7 subcomplex	
Figure 24	In the absence of Drs1, pre-ribosomes are enriched for early assembly factors and contain diminished amounts of late assembly factors	138
Figure 25	60S assembly factors Nop7 and Nog2 are associated with a different subset of pre-ribosomes upon depletion of Drs1	143
Figure 26	Late 60S pre-ribosomes are enriched for early assembly factors in the absence of Drs1	147
Figure 27	In the absence of Drs1, late associating assembly factors copurify early pre-rRNA intermediates	152
Figure 28	Nog2-containing pre-ribosomes are enriched with RNA polymerase I subunits upon depletion of Drs1	156
Figure 29	Depletion of Drs1 causes a shift from co-transcriptional pre-rRNA processing to post-transcriptional pre-rRNA processing	158
Figure 30	Model for clarifying discrepancies in our data	163
Figure 31	Growth of W303 from OD_{610} 0.1-6.0	167
Figure 32	Pre-rRNA processing in cells grown to high-density	169
Figure 33	Pre-rRNA processing in cells grown to high-density	171
Figure 34	Mapping DMS modification sites with high-throughput Sequencing	189
Figure 35	Sites of *in vivo* DMS modification of scR1 detected by	204

	Mod-seq	
Figure 36	Modified nucleotides in rRNA detected by Mod-seq	206
Figure 37	Sites of *in vivo* DMS modification of 5.8S rRNA identified by primer extension and PAGE analysis	210
Figure 38	Differentially modified nucleotides in the absence of r-protein L26 detected by Mod-seq	217
Figure 39	rRNA structural changes in the absence of r-protein L26 detected by Mod-seq	221
Figure 40	Differentially modified nucleotides in the absence of L26 localize near the SRP binding site	223
Figure 41	Mod-seq analysis of pre-rRNAs	226
Figure 42	Depletion of B-factors causes few changes in the SDS-PAGE profile of proteins contained in pre-ribosomes	245
Figure 43	All of the B-factors are necessary to recruit Nog2 to pre-ribosomes; only a subset of B-factors are required to recruit Nsa2 into pre-ribosomes	249
Figure 44	Stability of B-factors in the absence of others	251
Figure 45	Spb4 depends on Rpf2 to dock with pre-ribosomes	255
Figure 46	Nop2 and Nip7 co-sediment with pre-ribosomes, but also with each other when the function of Nip7 is compromised by TAP-tagging	259
Figure 47	Nop2 and Nip7 form a subcomplex, are	261

	interdependent for assembly into pre-ribosomes, and function in recruiting of other B-factors	
Figure 48	Nog1 and Rlp24 are important for association with pre-ribosomes of Tif6, as well as each other	265
Figure 49	Both Tif6 and Dbp10 are required for assembly of Rlp24 and Nog1 into pre-ribosomes	268
Figure 50	The TOR protein kinase pathway regulates assembly of 60S ribosomal subunits via targeting the B-factors Rpf2, Spb4, Nog1, and Nog2	271
Figure 51	The amounts of B-factors Rpf2, Spb4, Nog1, and Nog2 are decreased in whole cell extract upon inactivation of TOR signaling.	273
Figure 52	Physical and genetic interactions provide clues about the location of the B-factors in pre-ribosomes	285
Figure 53	Ebp2 and Brx1 are required for processing $27SA_2$ and $27SA_3$ pre-rRNAs	293
Figure 54	A combination of the *ebp2-14* and *brx1-102* or *brx1-172* mutations leads to synergistic defects in pre-rRNA processing	296
Figure 55	Ebp2 and Brx1 assemble into pre-ribosomes early, with pre-rRNPs containing 35S pre-rRNA	299
Figure 56	Timing of association of 66S assembly factors	302
Figure 57	*In vivo* hydroxyl radical RNA structure probing in	306

yeast

Figure 58 rRNA is cleaved in a dose-dependent manner by synchrotron-generated hydroxyl radicals 308

Figure 59 rRNA is cleaved in a solvent accessible manner by synchrotron-generated hydroxyl radicals 311

Figure 60 Cic1 and Nop15 are required for proper folding of ITS2 – ITS2 secondary structure 314

Figure 61 Cic1 and Nop15 are required for proper folding of ITS2 – autoradiograph 316

Figure 62 Catalytically inactive *drs1* mutants block 27SA pre-rRNA processing 324

Figure 63 Association hierarchy of proteins that function in 27S pre-rRNA processing 326

List of Tables

Table 1	Assembly factors that function in maturation of 60S ribosomal subunits in *S. cerevisiae*	19
Table 2	Numbers of high-throughput sequencing reads obtained by Mod-seq	192
Table 3	Mod-seq identified sites of DMS modification in yeast total RNA	193
Table 4	Ribosomal RNA positions with increased DMS-dependent modifications in the *rpl26Δ* strain	215
Table 5	Strain list	
Table 6	Oligonucleotide list	

CHAPTER 1: Introduction

My thesis work focused on understanding the roles of a number of proteins that function in two consecutive steps of 60S ribosomal subunit biogenesis in *Saccharomyces cerevisiae*. An underlying theme of my thesis is *in vivo* RNA folding during ribosome assembly. Studies of bacterial ribosome assembly *in vitro* have revealed many principles that govern folding of rRNA, but how rRNA folds in eukaryotic cells remains largely unaddressed. Much of the work regarding eukaryotic ribosome assembly has focused on understanding pre-rRNA processing, identifying the factors necessary to build a ribosome, and determining for which steps of ribosome biogenesis each of these factors is required. While this has been an important first step, the field of ribosome assembly is just beginning to understand the molecular mechanisms that govern ribosome biogenesis in eukaryotes. Thus, important and emerging aspects of eukaryotic ribosome assembly are how rRNA folds in nascent pre-ribosomes, how proteins that function in ribosome assembly contribute to this folding, and how rRNA folding regulates the assembly of other proteins and pre-rRNA processing. During my tenure in the Woolford Laboratory, one of my projects was to apply RNA structure probing techniques for determining rRNA structure *in vivo*. This culminated in a collaboration with the McManus group and the development of a new technique for assaying RNA structure by next-generation sequencing technology. In this introduction I will first provide a general background of ribosome biogenesis in eukaryotes, highlighting some of the principles that have been learned from *in vitro* studies of prokaryotic ribosomes. Then, I will focus on RNA folding, discussing the general principles that govern RNA folding, the challenges of folding large RNAs (such as rRNA),

current and emerging techniques to study RNA structure, and finally recent examples of *in vivo* studies of rRNA folding in eukaryotes.

1.1 Ribosome function and disease

Ribosomes are large ribonucleoprotein (RNP) machines responsible for translating the genetic code from mRNA to protein. All ribosomes consist of two subunits; a large 60S subunit (50S in prokaryotes) and a small 40S subunit (30S in prokaryotes). In yeast, the large subunit is composed of 3 rRNAs (25S, 5.8S, and 5S rRNA) and 47 ribosomal proteins (r-proteins) (Fig. 1A). The small subunit contains only one rRNA (18S) and 33 r-proteins (Fig. 1B). The large subunit contains the GTPase activation center, the polypeptide exit tunnel, and the petidyl transferase center (PTC). The PTC is comprised solely of RNA and functions in peptide bond formation. Thus, the ribosome functions as a ribozyme. The small subunit houses the decoding center, acting as a landing platform for mRNAs and tRNAs. Although highly conserved, particularly near the functional centers, eukaryotic ribosomes are larger and more complex than those in prokaryotes. Eukaryotic ribosomes have evolved additional sequences of rRNA called expansion segments (Gerbi, 1996). Furthermore, a number of r-proteins are specific to eukaryotes, and others have evolved eukaryotic-specific tails (Ben-Shem et al. 2011). Together, these expansion segments and eukaryotic specific r-proteins are thought to provide additional means of regulation to both ribosome assembly and ribosome function. Recent high-resolution crystal structures and cryo-EM reconstructions of *Tetraheymena,* yeast, fly, and human ribosomes highlight the extensive and intricate network of interactions between the rRNA and r-proteins (Fig. 1) (Armache et al. 2010a; Armache et al. 2010b; Ben-Shem et al. 2011; Anger et al. 2013).

Now armed with a blueprint of the final product, we are able to imagine, design, and implement more powerful experiments to better understand how these complex machines are assembled.

The production of ribosomes is a highly energetic process, consuming a significant fraction of cellular resources (Warner 1999). Approximately 60% of transcription in rapidly dividing yeast is devoted to the production of ribosomes (Woolford 1991; Woolford and Warner 1991). This equates to the cellular production of ~2000 ribosomes every minute. This high demand on cellular resources results in a tight linkage between cell growth rate, nutrient availability, and ribosome biogenesis. When cells are rapidly dividing and nutrients are available, the demand for the production of new ribosomes is high. In contrast, low nutrient availability, and consequently slower growth, leads to down regulation of ribosome production (Powers and Walter 1999).

Due to the essential nature of ribosomes, one would expect that significant defects in ribosome biogenesis or ribosome function would result in embryonic lethality. However, mutations in r-proteins or assembly factors that result in partial loss of function, as well as heterozygous null alleles, have been shown to result in a number of human diseases. (Freed et al. 2010; Narla and Ebert 2010) (Freed et al. 2010, Narla and Ebert, 2010). These diseases, termed ribosomopathies, often present as anemias, craniofacial abnormalities, short stature, limb and joint abnormalities, and mental retardation. A number of these diseases result in activation of P53, and therefore a predisposition to cancer (Freed et al. 2010). Thus, a detailed understanding of the molecular mechanisms that govern and drive ribosome biosynthesis is certain to advance our understanding, diagnosis, and treatment of ribosomopathies.

Figure 1

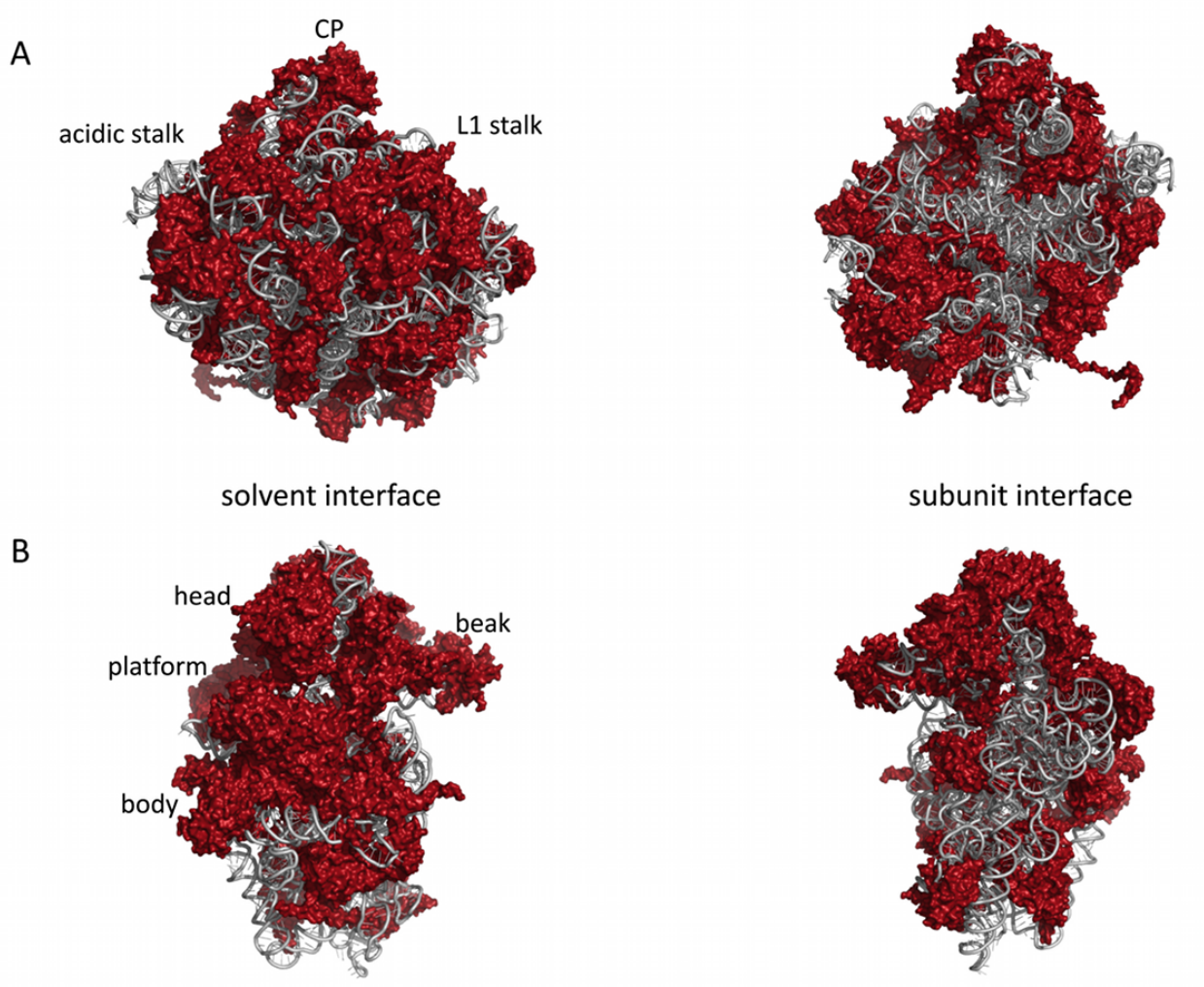

A
CP
acidic stalk
L1 stalk
solvent interface
subunit interface
B
head
beak
platform
body

Figure 1: Crystal structure of the *Saccharomyces cerevisiae* ribosome at 3.0Å

The 60S (A) and 40S (B) ribosomal subunits viewed from the solvent accessible side (left) and the subunit interface (right). Structural landmarks of the 60S subunit include the acidic stalk, the L1 stalk, and the central protuberance (CP). Landmarks of the 40S subunit include the head, body, platform, and beak.

1.2 Ribosome assembly and pre-rRNA processing are co-transcriptional

Ribosome assembly begins in the nucleolus, a subnuclear compartment organized around the rDNA genes. In *S. cerevisiae,* these genes are encoded on chromosome XII and are tandemly repeated approximately 150 times (Fig. 2). The sequences encoding 18S, 25S and 5.8S rRNAs are polycistronic and transcribed as a single unit by RNA Polymerase I (Pol I). The polycistronic nature of these precursors presumably ensures that rRNAs destined for the small (18S rRNA) and large (25S and 5.8S rRNA) subunits are transcribed in stoichiometric amounts. These pre-rRNAs are then processed though a series of endo- and exonucleolytic cleavages that eventually liberate the mature rRNAs (Fig 4, described in detail below). 5S rRNA is encoded by separate genes, transcribed by RNA Polymerase III, and processed independently of the other pre-rRNAs.

Pioneering work from Miller and Beatty (Miller and Beatty 1969) provided the first hints that ribosome assembly occurs co-transcriptionally. Electron micrographs of actively transcribed rDNA genes from amphibian oocytes revealed nascent rRNA transcripts decorated at their ends with electron dense knobs. More recently it was shown that disruption of ribosome biogenesis results in loss of these terminal knobs (Osheim et al. 2004). Furthermore, the mass of these knobs approximates that of initial pre-ribosomes. Together, these investigations provide ample evidence that ribosome assembly begins coincident with transcription of the rRNA.

Nevertheless, pre-rRNA processing in *S. cerevisiae* was thought to occur exclusively post-transcriptionally. Pioneering works from the Warner group and the Planta group independently showed that a 35S pre-rRNA could be synthesized and detected within a 90S RNP particle (Udem and Warner 1972; Trapman et al. 1975). When this occurs, Pol I

transcribes the entire length of the rDNA gene, producing a 35S pre-rRNA that is packaged into 90S pre-ribosomes (Fig 3A). This initial pre-rRNA is then cleaved endonucleolytically, resulting in two separate precursors that will mature into the rRNAs of the small and large ribosomal subunits. However, more recently it was shown that in rapidly dividing yeast, the majority of initial pre-rRNA processing steps occur co-transcriptionally. As Pol I moves down the rDNA unit, the pre-rRNA is cleaved co-transcriptionally to first release an RNP particle that will mature into the 40S subunit. Transcription termination then liberates a particle that is destined to mature into the 60S subunit (Fig 3B). It is now known that in rapidly dividing yeast, initial steps of pre-rRNA processing are in an equilibrium in which the majority occur co-transcriptionally, and a minority occur post-transcriptionally (Osheim et al. 2004). This equilibrium is related to cell growth and cell division rates, as cells that are in stationary phase process a greater fraction of pre-rRNAs post-transcriptionally. This will be discussed in greater detail in Chapter 3.

Pre-rRNA processing is once of the best studied and most well understood aspects of ribosome biogenesis (Venema and Tollervey 1999). When pre-rRNA processing occurs post-transcriptionally, the initial precursor is the 35S pre-rRNA (Fig 4A). In addition to the sequence encoding mature 18S, 25S, and 5.8S rRNAs, this initial transcript contains two external and two internal transcribed spacer sequences (ETS and ITS) that must be removed. Initial cleavages of the pre-rRNA at the A_0, A_1, and A_2 sites within the 5' ETS generate 20S and 27SA_2 pre-rRNAs that will mature into the rRNAs of the 40S and 60S subunits, respectively (Udem and Warner 1972; Hughes and Ares 1991; Beltrame et al. 1994). When pre-rRNA processing occurs co-transcriptionally, the nascent pre-rRNA is cleaved at the A_2 site within ITS1, soon after this processing site is transcribed by Pol I (Fig

4B) (Osheim et al. 2004; Kos and Tollervey 2010). This releases what is presumably 20S pre-rRNA, prior to the completion of transcription. It still remains unclear if processing at sites A_0 and A_1 can occur coincident with transcription. As Pol I reaches the end of the rDNA gene, transcription termination releases $27SA_2$ pre-rRNA (Kufel et al. 1999). Current knowledge indicates that 20S and $27SA_2$ pre-rRNAs are processed the same, regardless if they are generated co- or post-transcriptionally. However, recent work from our lab suggests that this might not be the case. Our data indicate that pre-rRNAs processed post-transcriptionally can follow a different processing pathway than those processed co-transcriptionally (discussed in Chapter 3).

Once generated, 20S pre-rRNA is rapidly exported to the cytoplasm where its 3' end is cleaved at the D site to produce mature 18S rRNA (Fatica et al. 2003a; Lamanna and Karbstein 2009; Lamanna and Karbstein 2010). This is the last known step of pre-rRNA processing during biogenesis of the 40S subunit. Processing of $27SA_2$ pre-rRNA, and subsequent generation of 5.8S and 25S rRNAs, follows a much more complex pathway. Alternative processing pathways of this intermediate results in the formation of two different populations of functional 5.8S rRNA, differing in length by six nucleotides at their 5' ends. The major pathway, occurring approximately 85% of the time, involves cleavage of $27SA_2$ pre-rRNA at the A_3 site in ITS1, creating the $27SA_3$ pre-rRNA (Shuai and Warner 1991; Lindahl et al. 1992; Schmitt and Clayton 1993; Chu et al. 1994; Lygerou et al. 1996). This is followed by 5' to 3' exonucleolytic digestion of the pre-rRNA to the B_s site, removing the remainder of ITS1 and producing the 5' end of $27SB_s$ pre-rRNA (Henry et al. 1994; Oeffinger et al. 2009). The minor pathway, occurring approximately 15% of the time, involves an endonucleolytic cleavage, by an unknown nuclease, at the B_L site to form $27SB_L$

pre-rRNA. Both 27SB pre-rRNAs are then cleaved at the C_2 site in ITS2, producing 25.5S pre-rRNA and $7S_S$ or $7S_L$ pre-rRNAs. The 3' ends of both 7S species are then removed by a series of exonucleolytic digestions, forming mature $5.8S_S$ and $5.8S_L$ rRNAs (Henry et al. 1994; Mitchell et al. 1996). Last, 25.5S pre-rRNA is trimmed at its 5' end by Rat1, generating mature 25S rRNA (Geerlings et al. 2000).

In addition to the various endo- and exonucleolytic cleavages involved in rRNA processing, there are a large number of covalent modifications of the rRNA that occur both co- and post-transcriptionally (Osheim et al. 2004; Kos and Tollervey 2010). The majority of these modifications are guided by small nucleolar ribonucleoprotein particles (snoRNPs) and involve the isomerization of uridines to pseudouridines and the methylation of 2'-hydroxyl groups of the riboses (reviewed in Woolford and Basserga, 2013). These modifications are thought to play a general role in rRNA conformation and stability.

Figure 2

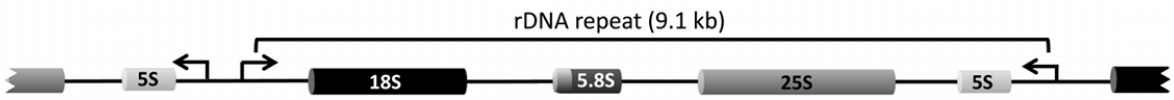


Figure 2: rDNA repeat in *Saccharomyces cerevisiae*

The 9.1 kb rDNA genes are located on chromosome XII and repeated ~150 times. 18S, 5.8S, and 25S rRNAs are transcribed as a single transcript by RNA polymerase I. 5S rRNA is encoded by separate genes and is transcribed in the opposite direction by RNA polymerase III.

Figure 3

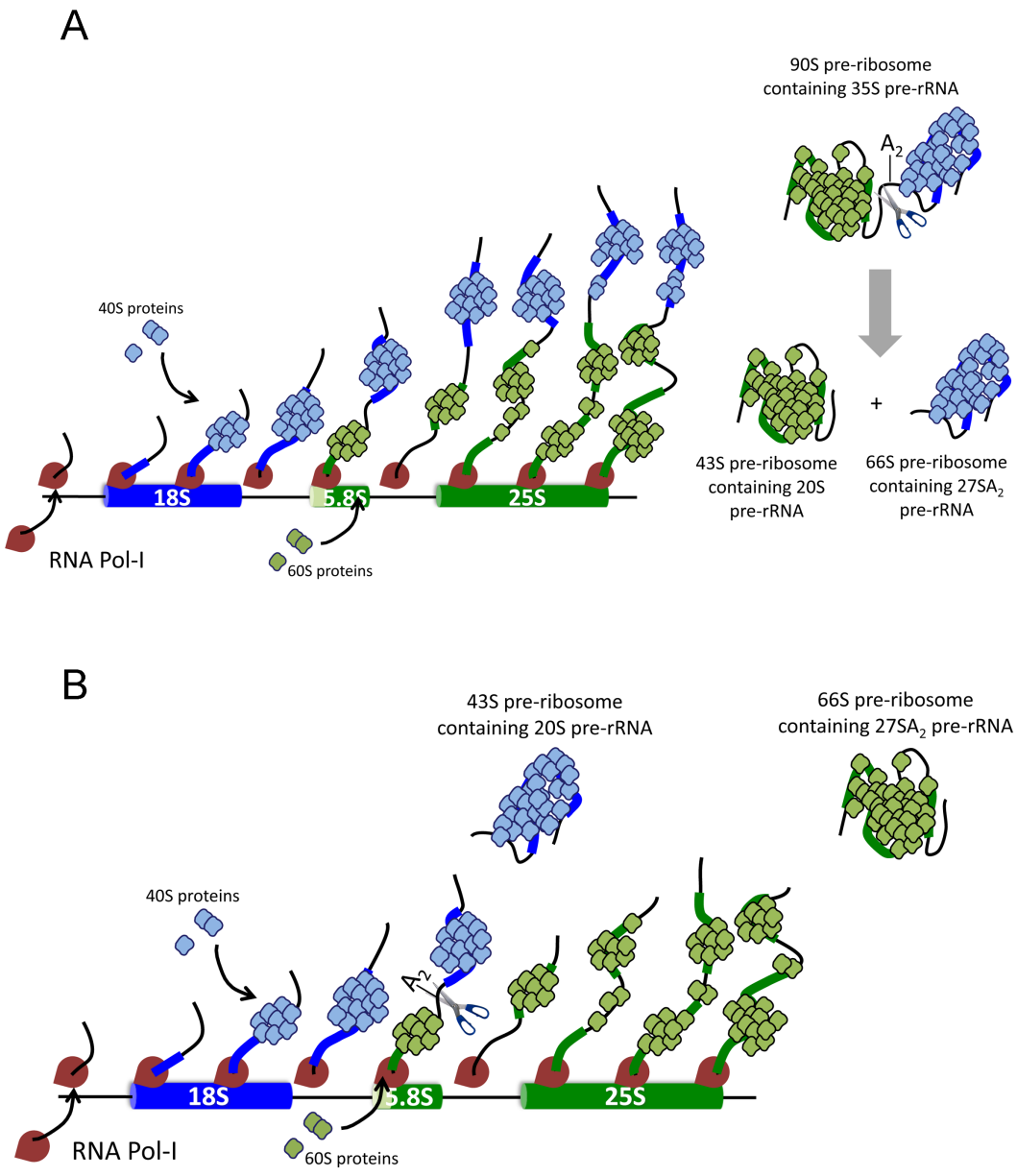

A
90S pre-ribosome
containing 35S pre-rRNA
A2
40S proteins
18S
5.8S
25S
RNA Pol-I
60S proteins
43S pre-ribosome
containing 20S
pre-rRNA
+
66S pre-ribosome
containing 27SA2
pre-rRNA
B
43S pre-ribosome
containing 20S pre-rRNA
66S pre-ribosome
containing 27SA2 pre-rRNA
40S proteins
A2
18S
5.8S
25S
RNA Pol-I
60S proteins

Figure 3: The majority of pre-rRNA processing in *Saccharomyces cerevisiae* occurs co-transcriptionally whereas a minority occurs post-transcriptionally.

(A) Traditionally, pre-rRNA processing was thought to occur post-transcriptionally. When this occurs, RNA polymerase I (red) transcribes the entire length of rRNA resulting in the formation of a 90S pre-ribosome containing 35S pre-rRNA and both 40S (blue) and 60S (green) proteins. Post-transcriptional cleavage at the A_2 site separates the maturation of 40S and 60S subunits. (B) New data suggests that in rapidly dividing yeast, early steps of pre-rRNA processing occur co-transcriptionally. Co-transcriptional cleavage at the A_2 site first releases a 43S pre-ribosome containing 20S pre-rRNA (blue) and transcription termination releases a 66S pre-ribosome containing $27SA_2$ pre-rRNA (green). In this scenario, 35S pre-rRNA is never produced.

Figure 4

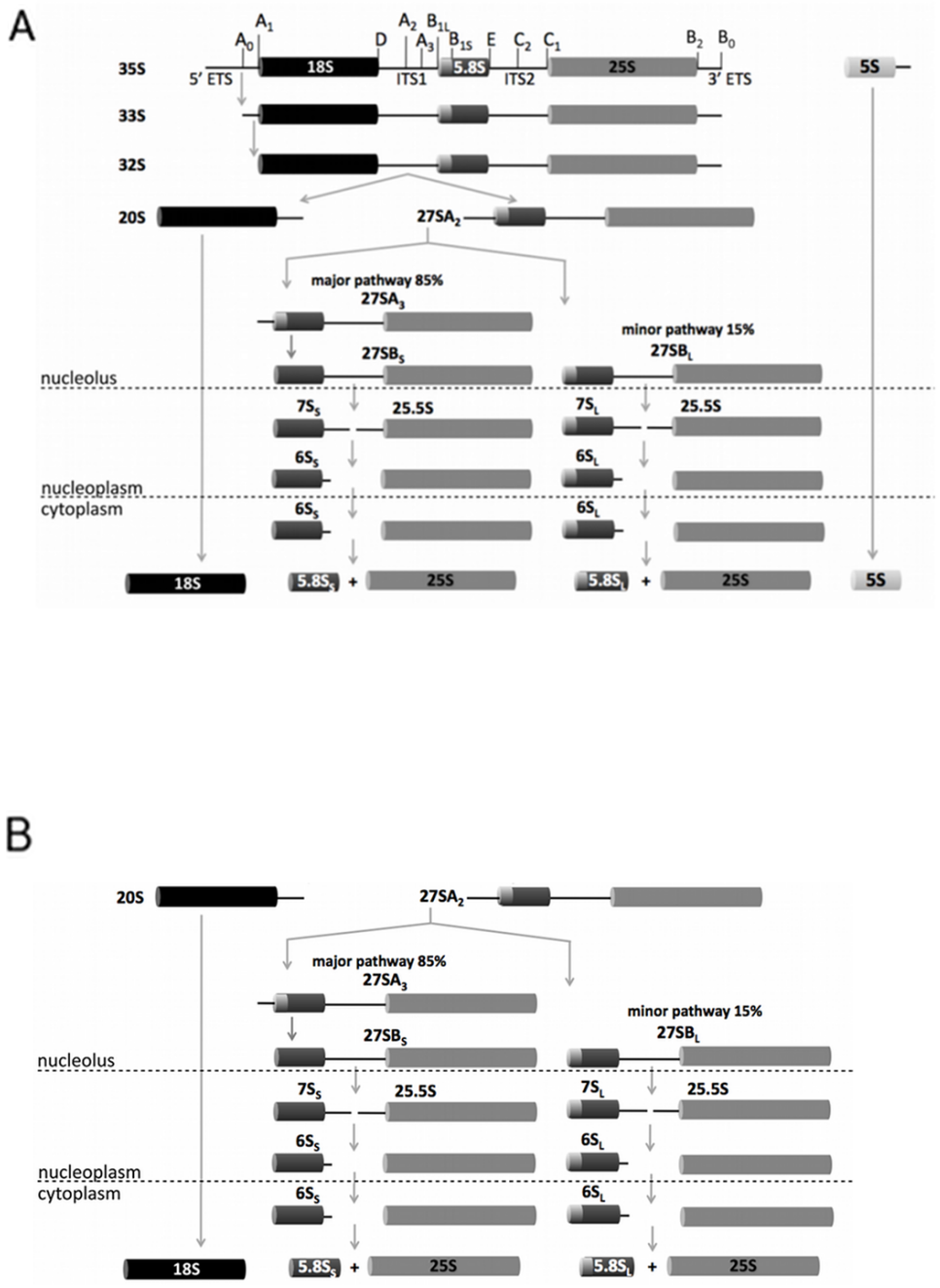

A
35S
33S
32S
20S
5' ETS
18S
ITS1
5.8S
ITS2
25S
3' ETS
5S
27SA2
major pathway 85%
27SA3
minor pathway 15%
27SBS
27SBL
nucleolus
7SS
25.5S
7SL
6SS
6SL
nucleoplasm
cytoplasm
18S
5.8SS
5.8SL
B

Figure 4. Pre-rRNA processing in *Saccharomyces cerevisiae*

(A) Post-transcriptional pre-rRNA processing initiates with 35S pre-rRNA, (B) whereas co-transcriptional pre-rRNA processing initiates with 20S and $27SA_2$ pre-rRNA. As described in 1.2, these initial intermediates undergo a series of endo and exonucleolytic processing steps to remove spacer sequences (5' ETS, ITS1, ITS2, and 3' ETS) and liberate mature 18S, 5.8S, and 25S rRNAs. Processing sites are indicated on the 35S pre-rRNA intermediate, and each of the consecutive pre-rRNA intermediates is labeled.

1.3 *Trans*-acting factors drive assembly of pre-ribosomes

In addition to r-proteins and rRNAs, ribosome biogenesis requires a large number of *trans*-acting factors, hereafter referred to as assembly factors. These factors were first discovered in 1972, but it took ~20 years to identify and understand the significance of these proteins. Sedimentation of ribosome precursor particles from HeLa cell nucleoli revealed "extra" proteins, distinguishable from r-proteins, associated with these RNPs (Kumar and Warner 1972). To date, at least 180 assembly factors have been shown to be required for ribosome assembly (Lafontaine and Tollervey 1995; Tollervey 1996; Kressler et al. 1999; Kressler et al. 2010). Many of these proteins are essential for life and are conserved from yeast to humans. These proteins, while important for ribosome assembly, do not function directly in protein synthesis and are not required for ribosome function. As biogenesis of the ribosome proceeds, these factors associate with the assembling particle, perform their function, and then are released and recycled for another round of ribosome synthesis. Assembly factors were first identified using classic genetic screens for mutants defective in ribosome assembly (Fabian and Hopper 1987; Sachs and Davis 1990; Tollervey et al. 1991; Ripmaster et al. 1992; Schmitt and Clayton 1993; Berges et al. 1994; Chu et al. 1994; Sun and Woolford 1994). These initial assembly mutants were then used in other screens (synthetic lethality, suppression, and two-hybrid) to identify additional assembly factors (Adams et al. 2002). Examination of pre-rRNA processing in assembly mutants identified three broad classes of assembly defects that still hold true: (1) Mutations that slow ribosome maturation but do not completely block it; (2) Mutations that block a step in assembly causing an accumulation of a specific assembly intermediate; (3) Mutations that block assembly and cause degradation of one or more of the intermediates.

Although genetics led to the identification and characterization of an initial subset of assembly factors, the ability to epitope-tag these proteins, affinity-purify ribosome assembly intermediates, and assay their constituents by mass spectrometry (MS) allowed the identification of a large number of additional factors associated with pre-ribosomes (Rigaut et al. 1999; Bassler et al. 2001; Harnpicharnchai et al. 2001; Dragon et al. 2002; Nissan et al. 2002). In yeast, approximately 90 proteins can be reproducibly found in precursors of the 60S subunit (Table 1). With the development of the tandem affinity purification (TAP) method, TAP-tagged assembly factors could be used as "molecular hooks" to purify all pre-ribosomes containing the tagged protein. Once purified, these particles could then be "dissected" using a variety of assays to examine both the RNA and protein constituents of each particle. Because most assembly factors are present in more than one consecutive pre-ribosomal intermediate, their timing of association with, and release from, pre-ribosome can be determined by examining the earliest and latest pre-rRNAs that co-purify with each factor. This has provided a "road map" of assembly. Initial characterizations of assembly have also determined for which steps in pre-rRNA processing most of these factors are required, but detailed mechanisms for how the majority of these proteins function are still lacking.

In vitro reconstitution of *E. coli* ribosomes suggested that the biogenesis of ribosomes is a "self assembly" process (Traub and Nomura 1968; Nierhaus and Dohme 1974; Nierhaus 1991). However, the reconstitution process is slow under physiological conditions, and non-physiological conditions (heating, high [Mg^{2+}], etc.) are required to drive the assembly process to completion. Assembly is slowed even further if precursor RNAs are used instead of mature rRNA, suggesting that proper processing of the rRNA is

necessary for efficient assembly (Mangiarotti et al. 1975). Ribosomal subunits assembled *in vitro* accumulate as intermediate particles at low temperature, containing an incomplete set of r-proteins. These intermediates only make the transition to mature, functional subunits upon heating to 40 °C (Held et al. 1973). This heating step is thought to provide the energy needed to rearrange the assembling particle and help facilitate stable joining of the remaining r-proteins. *In vivo*, this energy barrier is thought to be overcome by assembly factors.

TABLE 1

Table 1 Assembly factors that function in maturation of 60S ribosomal subunits in *S. cerevisiae*

Pre-rRNA processing step	Name/Alias	Human Ortholog; Accession Number	Comments	Ref.
A0, A1, A2, A3	Rrp5	PDCD11; NP_055791.1	S1-like RNA binding domains	Eppens *et al.* 1999; Vemema *et al*. 1996; Vos *et al*. 2004
	Nop4/Nop77	RBM28; NP_060547.2	4 RRMs	Sun *et al*. 1994
	Dbp6	DDX51; NP_778236.2	DEAD-box RNA helicase	Kressler *et al.* 1998
	Npa1/Urb1			Dez *et al*. 2004; Rosado *et al*. 2004
	Npa2/Urb2			Rosado *et al*. 2007
	Nop8		Coiled-coil and an RRM	Zanchin *et al*. 1999
	Rsa3			de la Cruz *et al*. 2004
	Noc1/Mak21	CEBPZ; NP_005751.2	CCAAT-binding factor	Milkereit *et al*. 2001
	Noc2 / Rix3	NOC2L; NP_056473.2	Coiled-coils	Milkereit *et al*. 2001
	Noc3	NOC3L; NP_071896.8	Coiled-coils	Milkereit *et al*. 2001
	Dbp2	DDX5; NP_004387.1	DEAD-box RNA helicase	Bond *et al*. 2001
	Dbp3	DDX42; NP_031398.2	DEAD-box RNA helicase	Weaver *et al*. 1997
	Dbp7	DDX31; NP_073616.6	DEAD-box RNA helicase	Daugeron and Linder 1998
	Dbp9	DDX56; NP_061955.1	DEAD-box RNA helicase	Daugeron *et al*. 2001
	Prp43/JA1	DHX15; NP_001349.2	DEAH-box RNA helicase; also involved in pre-mRNA splicing and SSU biogenesis	Combs *et al*. 2006; Leeds *et al*. 2006

	Loc1		Also involved in *ASH1* mRNA localization	Urbinati *et al*. 2006
	Mak5	DDX24; NP_065147.1	DEAD-box RNA helicase	Zagulski *et al*. 2003
	Cbf5		Pseudouridine synthase catalytic subunit of box H/ACA snoRNPs	Lafontaine *et al*. 1998
	Ssf1	PPAN; NP_064615.3	Brix domain	Fatica *et al*. 2002
	Ssf2	EIF6; NP_064615.3	Brx1 domain	
	Rrp14	SURF6; NP_006744.2	Coiled-coils	Oeffinger *et al*. 2007; Yamada *et al*. 2007
	Rrp15	?????		De Marchis *et al*. 2005
	Mak16	MAK16; NP_115898.2	HMG-like acidic region	Pellet *et al*. 2006
	Nop16	NOP16; NP_057475.2		Unpublished results J.W.
A_3 cleavage and A_3 processing	Rpf1	RPF1; NP_079341.2	s70-like RNA binding motif	Wehner and Baserga 2002
	Ebp2	EBNA1BP2; NP_001153408.1		Huber *et al*. 2000; Shimoji *et al*. 2012; Tsujii *et al*. 2000
	Brx1	BRIX1; NP_060791.3	s70-like RNA binding motif	Kaser *et al*. 2001; Shimoji *et al*. 2012
	Ytm1	WDR12; NP_060726.3	WD40 repeats	Miles *et al*. 2005; Sahasranaman *et al*. 2011
	Erb1	BOP1; NP_056016.1	WD40 repeats	Granneman *et al*. 2011; Pestov *et al*. 2001; Sahasranaman *et al*. 2011
	Nop7/Yph1	PES1; NP_055118.1	BRCT domain and coiled-coils	*Adams et al*. 2002; Granneman *et al*. 2011; Oeffinger *et al*. 2002; Sahasranaman *et al*. 2011
	Drs1	DDX27; NP_060365.7	DEAD-box RNA helicase	Merl *et al*. 2010; Unpublished results J.W.
	Nop15	MKI67IP; NP_115766.3	RRM	Granneman *et al*. 2011; Oeffinger *et al*. 2003; Sahasranaman *et al*. 2011

	Cic1/Nsa3		Ribosomal protein L1 domain	Fatica *et al*. 2003; Granneman *et al*. 2011; Sahasranaman *et al*. 2011
	Rlp7	RL7L; NP_940888	Similar to r-protein L7	Dunbar *et al*. 2000; Sahasranaman *et al*. 2011
	Rrp1	RRP1B; NP_055871.1		Horsey *et al*. 2004; Sahasranaman *et al*. 2011
	Nop12	RBM34; NP_055829.2	RRM	Granneman *et al*. 2011; Wu *et al*. 2001
	Has1	DDX18; NP_006764.3	DEAD-box RNA helicase; also required for SSU biogensis	Dembowski *et al*. in press
	Rai1	DOM3Z; NP_005501.2	Binds to and stabilizes the exoribonuclease Rat1	Xue *et al*. 2000
	Rat1/**Xrn2**	XRN2; NP_036387.2	Nuclear 5' to 3' single-stranded RNA exonuclease	Henry *et al*. 1994; Oeffinger *et al*. 2009
	Xrn1	SEP1; NP_061874.3	Cytoplasmic 5' to 3' RNA exonuclease; also involved in mRNA decay	Henry *et al*. 1994; Oeffinger *et al*. 2009
	Rrp17	NOL12; NP_077289	Nuclear 5' to 3' RNA exonuclease	Oeffinger *et al*. 2009
C_2 cleavage	Nip7	NIP7; NP_057185.1	PUA domain	Talkish *et al*. 2012; Zanchin *et al*. 1997
	Nop2/Yna1	NOP2; NP_006161.2	Putative RNA methyltransferase	Hong *et al*. 1997; Talkish *et al*. 2012
	Rpf2	RPF2; NP_115570.1	Brix domain	Morita *et al*. 2002; Wehner and Baserga 2002; Zhang *et al*. 2007
	Rrs1	RRS1; NP_055984.1		Tsuno *et al*. 2000; Zhang *et al*. 2007
	Spb4	DDX55; NP_065987.1	DEAD-box RNA helicase	de la Cruz *et al*. 1998; Garcia-Gomez *et al*. 2011
	Dbp10	DDX54; NP_001104792.1	DEAD-box RNA helicase	Burger *et al*. 2000
	Mak11	PAK1IP1; NP_060376.2	WD40 repeats	Saveanu *et al*. 2007
	Tif6 /Cdc95	EIF6; NP_852133.1	eIF6 domain	Basu *et al*. 2001; Senger *et al*. 2001

	Rlp24	RSL24D1; NP_057388.1	TRASH domain and a coiled-coil	Saveanu *et al*. 2003
	Nog1	GTPBP4; NP_036473.2	GTPase	Kallstrom *et al*. 2003; Saveanu *et al*. 2003
	Spb1	FTSJ3; NP_060117.3	Ado-Met dependent methyltransferase	Kressler *et al*. 1999
	Nsa2	NSA2; NP_055701.1	Member of the ribosomal protein S8e superfamily	Lebreton *et al*. 2006
	Nog2/Nug2	GNL2; NP_037417.1	GTPase	Bassler *et al*. 2001; Saveanu *et al*. 2001
	Nug1	GNL3L; NP_061940.1	GTPase	Bassler *et al*. 2001
	Cgr1	CCDC86; NP_077003.1	Coiled-coil	Moy *et al*. 2002
27SB stability	Rix7	NVL; NP_002524.2	AAA-ATPase	Gadal *et al*. 2001; Kressler *et al*. 2008
	Nsa1	WDR74; NP_060563.2	Released from pre-ribosomes by Rix7	Kressler *et al*. 2008
7S processing and nuclear release of assembly factors	Ipi3	WDR18; NP_077005.2	WD40 repeats	Galani *et al*. 2004; Krogan *et al.* 2004
	Ipi2/Rix1			Galani *et al*. 2004; Krogan *et al.* 2004
	Ipi1			Galani *et al*. 2004; Krogan *et al.* 2004
	Rea1/Mdn1	MDN1; NP_055426.1	Dynein related AAA-type ATPase; Releases Ytm1 and Rsa4 from pre-ribosomes	Bassler *et al*. 2010; Galani *et al*. 2004; Ulbrich *et al*. 2009
	Rsa4	NLE1; NP_060566.2	WD40 repeats	de la Cruz *et al*. 2005
	Mtr4/Dob1	SKIV2L2; NP_056175.3	DEAD-box RNA helicase	de la Cruz *et al*. 1998

Nuclear export	Nop53	GLTSCR2; NP_056525.2	Coiled-coil	Granato *et al*. 2005; Granato *et al*. 2008
	Sda1	SDAD1; NP_060585.2	Also required for actin cytoskeleton organization	Dez *et al*. 2006
	Rrp12	RRP12; NP_055994.2	HEAT-repeats	Oeffinger *et al*. 2004
	Arx1	PA2G4; NP_006182.2	Coiled-coil	Bradatsch *et al*. 2007; Bradatsch *et al*. 2012; Lebreton *et al*. 2006
	Alb1		Nuclear shuttling factor	Bradatsch *et al*. 2007; Bradatsch *et al*. 2012; Lebreton *et al*. 2006
	Nmd3/Src5	NMD3; NP_057022.2	Coiled-coil	Hedges *et al.* 2005; West *et al*. 2005
	Mex67	TAP; NP_006353.2	Also involved in nuclear RNA export	Yao *et al*. 2007; Yao *et al*. 2008
	Mtr2		Also involved in nuclear RNA export	Yao *et al*. 2007; Yao *et al*. 2008
	Bud20		Zinc finger domain	Bassler *et al*. 2012
6S processing	Ngl2		Ccr4-like Rnase	Faber *et al*. 2002; Thomson and Tollervey 2010
	Rex1/Rnh70	REX1; NP_065746.3	3' to 5' exoribonuclease	van Hoof *et al*. 2000
	Rex2		3' to 5' exoribonuclease	van Hoof *et al*. 2000
Cytoplasmic maturation	Drg1/Afg2	SPATA5; NP_660208.2	AAA-ATPase; Releases Nog1 and Rlp24	Pertschy *et al*. 2007
	Rei1	ZNF622; NP_219482.1	Zinc finger domains; Release of Arx1 and Alb1	Lebreton *et al*. 2006; Parnell and Bass 2009
	Reh1		Zinc finger domains	Lebreton *et al*. 2006; Parnell and Bass 2009
	Jjj1	DNAJC21; NP_919259.3	Contains a zinc finger domain and a DNA J domain; Release of Arx1 and Alb1	Demoinet *et al*. 2007; Greber *et al*. 2012; Meyer *et al*. 2007; Meyer *et al*. 2009

	Ssa1	HSP70; NP_005337.2	ATPase; Member of HSP70 family; Releases Arx1 and Alb1	Meyer *et al*. 2007
	Ssa2	HSC70; NP_006588.1	ATPase; Member of HSP70 family; Releases Arx1 and Alb1	Meyer *et al*. 2007
	Yvh1	DUSP12; NP_009171.1	Dual-specificity phosphatase	Kemmler *et al*. 2009; Lo *et al*. 2009
	Mrt4	MRT04; NP_057267.2	Similar to the r-protein P0	Kemmler *et al*. 2009; Rodriguez-Mateos *et al*. 2009
	Sdo1	SBDS; NP_057122.2	Responsible for Shwachman-Bodain-Diamond syndrome; Release of Tif6	Menne *et al*. 2007
	Efl1/Ria1	EFTUD1; NP_078856.4	Cytoplasmic GTPase; Releases Tif6	Senger *et al*. 2001
	Lsg1/Kre35	LSG1; NP_078856.4	Cytoplasmic GTPase; Releases Nmd3	Hedges *et al*. 2005; Kallstrom *et al*. 2003
	Sqt1	AAMP; NP_001078.2	WD40 repeats	West *et al*. 2005
	Puf6	KIAA0020; NP_055693.4	Pumilio family RNA binding domain	
Unknown	Fpr4		Peptidyl-prolyl cis-trans isomerase	
	Fpr3		Peptidyl-prolyl cis-trans isomerase	

Assembly factors isolated as a subcomplex are color-coded

1.3.1 Functions of assembly factors

Based on pre-rRNA processing defects, biochemical characterization, and sequence analysis, assembly factors can be broadly placed into functional groups: (1) Endo- and exonucleases required for the various cleavage events during pre-rRNA processing. While many of the nucleases that function in pre-rRNA processing have been identified, a few still remain to be determined; (2) Proteins associated with snoRNPs involved in base modification of the pre-rRNAs; (3) Enzymes that post-translationally modify r-proteins and/or assembly factors; (4) RNA binding proteins, RNA chaperones, and scaffolding proteins that stabilize and promote correct protein-protein, RNA-protein, and RNA-RNA interactions, preventing the formation of incorrect structures; (5) Factors that facilitate export of pre-ribosomes out of the nucleus; (6) RNA helicases/ATPases, AAA ATPases, and GTPases that utilize the energy of NTP hydrolysis to refold pre-rRNAs, reorganize pre-ribosome structure, release other proteins from the pre-ribosome, trigger pre-rRNA processing events, and act as potential "proof-readers" of assembly. The NTPases, due to their conserved nature and enzymatic function, are one of the most studied classes of assembly factors, yet precise molecular mechanisms of these proteins still remain elusive. A sub-section of Chapter 3 of my thesis focuses on the function of the DEAD-box protein Drs1. Thus, I will discuss the role of RNA helicases/ATPases in ribosome biogenesis, in more detail.

1.3.2 RNA helicases/ATPases are the movers and shakers of ribosome biogenesis

Large RNPs, such as the maturing ribosome, are dynamic complexes with continually changing RNA-RNA and RNA-protein interactions (Staley and Woolford 2009). Many of

these changing interactions require RNA structures, such as stem-loops and helices, to be unwound and refolded. These molecular rearrangements require "helper" proteins such as RNA helicases that can disrupt RNA-RNA interactions, dissociate proteins from RNA molecules, and assist in proper tertiary structure formation (Bleichert and Baserga 2007; Rodriguez-Galan et al. 2013). RNA helicases belong to a conserved superfamily of proteins, 39 of which are thought to function in RNA metabolism in *S. cerevisiae*. The largest subset of these helicases belong to the subfamily of the so-called DEAD-box proteins (DBPs). The yeast genome encodes 25 DBPs, the majority of which function in spliceosome and ribosome assembly. DBPs contain at least 11 amino acid motifs, nine of which are highly conserved and form the core of the two RecA-like domains. Motif II (Walker B motif) contains the amino acids D-E-A-D giving the family its name. The nine core motifs all cooperate to bind RNA, bind ATP, hydrolyze ATP, and couple ATP hydrolysis to cause structural rearrangements.

In *S. cerevisiae*, 20 putative RNA helicases, 15 of which are DBPs, are required for ribosome biogenesis (Kressler et al. 2010). It is thought that these proteins use the energy of NTP hydrolysis to remove or deliver assembly factors, act as reversible place holders, and cause conformational rearrangements in the nascent ribosome. A few helicases have been implicated in snoRNA removal (Kos and Tollervey 2005; Liang and Fournier 2006; Bohnsack et al. 2008). Others have been proposed to unwind helices or cause conformational rearrangements within pre-rRNAs to trigger exonucleolytic processing steps (de la Cruz et al. 1998; Pertschy et al. 2009; Dembowski et al. 2013).

Although not a DBP, the AAA-ATPase Rea1 is probably the best mechanistically understood assembly factor. Rea1, the largest protein in yeast (559 kD), was shown to

harness the energy of ATP hydrolysis to release itself, as well as a number of other assembly factors, from pre-ribosomes (Ulbrich et al. 2009; Bassler et al. 2010). Rea1 can be broadly defined as having a globular domain, containing the AAA motif, and a long flexible tail domain. Electron microscopy revealed that the flexible tail of Rea1 contacts specific assembly factors, and upon ATP hydrolysis removes these proteins (and itself) from pre-ribosomes. While this mechanism of action may be unique to Rea1, other assembly factors are certain to harness the energy of NTP hydrolysis to strip proteins off of the assembling ribosome.

1.4 Formation of pre-ribosomal particles

Ribosome biogenesis begins in the nucleolus with the formation of either a 90S pre-ribosome containing 35S pre-rRNA (post-trancriptionally generated), or separate 66S and 43S pre-ribosomes containing $27SA_2$ and 20S pre-rRNAs, respectively (co-transcriptionally generated)(Fig 5). As transcription proceeds, many assembly factors and r-proteins associate with the nascent RNA (Gallagher et al. 2004; Osheim et al. 2004; Granato et al. 2008; Wery et al. 2009; Kos and Tollervey 2010; Hierlmeier et al. 2012). 43S pre-ribosomes containing 20S pre-rRNA are rapidly exported to the cytoplasm where they undergo final steps of maturation to form functional 40S subunits. In contrast, maturation of the 60S subunit is more complicated and thus slower. Based on the pre-rRNA processing intermediates generated during assembly, at least four distinct 66S pre-ribosomes can be detected. Pre-ribosomes containing $27SA_2$, $27SA_3$, and 27SB pre-rRNA reside mainly in the nucleolus. It is thought that during processing of 27SB pre-rRNA, pre-ribosomes make the transition from being nucleolar to nucleoplasmic, although it still remains unclear how and

why pre-ribosomes are released from the nucleolus during this step. Late 66S pre-ribosomes are then exported from the nucleoplasm to the cytoplasm, where final steps of assembly occur, leading to the production of mature 60S ribosomal subunits.

During the biogenesis processes, assembly factors must associate with pre-ribosomes, perform their function, and then be released. While this occurs throughout the biogenesis pathway, two major "release points" during biogenesis of the 60S subunit have been identified. The first occurs prior to 66S pre-ribosome exiting the nucleus. In part, this is thought to reduce the size of the pre-ribosome enough to facilitate movement through the nuclear pore complex. At least two AAA ATPases function to release factors during this transition, one of which is the largest protein in yeast (Rea1; 559 kD) (Kressler et al. 2008; Ulbrich et al. 2009; Bassler et al. 2010; Kressler et al. 2011). The second major release of assembly factors occurs in the cytoplasm, and is one of the best understood aspects of ribosome assembly (Senger et al. 2001; Menne et al. 2007; Pertschy et al. 2007; Lo et al. 2010). Recent work has shown that a number of assembly factors remain associated with late pre-ribosomes to prevent pre-mature association of the subunits with each other, or with mRNAs and tRNAs (Gartmann et al. 2010; Sengupta et al. 2010; Strunk et al. 2011). Many of these assembly factors are bound to the subunit interfaces of these immature particles, or near what will become the functional sites of the mature ribosome. These late assembly factors are thought to ensure that immature subunits do not join prematurely.

Immediately prior to maturation, both immature subunits undergo a functional proofreading step, or "test drive". The immature 40S subunit performs a translation like cycle in which it associates with mature 60S subunits. During this time, the final steps of 18S maturation and release of the last remaining assembly factors test the functional

centers of these nearly mature particles (Lebaron et al. 2012; Strunk et al. 2012). A similar phenomenon has also been demonstrated for immature 60S subunits. It is thought that a flexible loop of r-protein L10 simultaneously probes the tRNA P-site, the catalytic center, and the GTPase activating site. This "functional proofreading" results in the release of factors bound the subunit interface of immature 60S subunits (Bussiere et al. 2012).

Figure 5

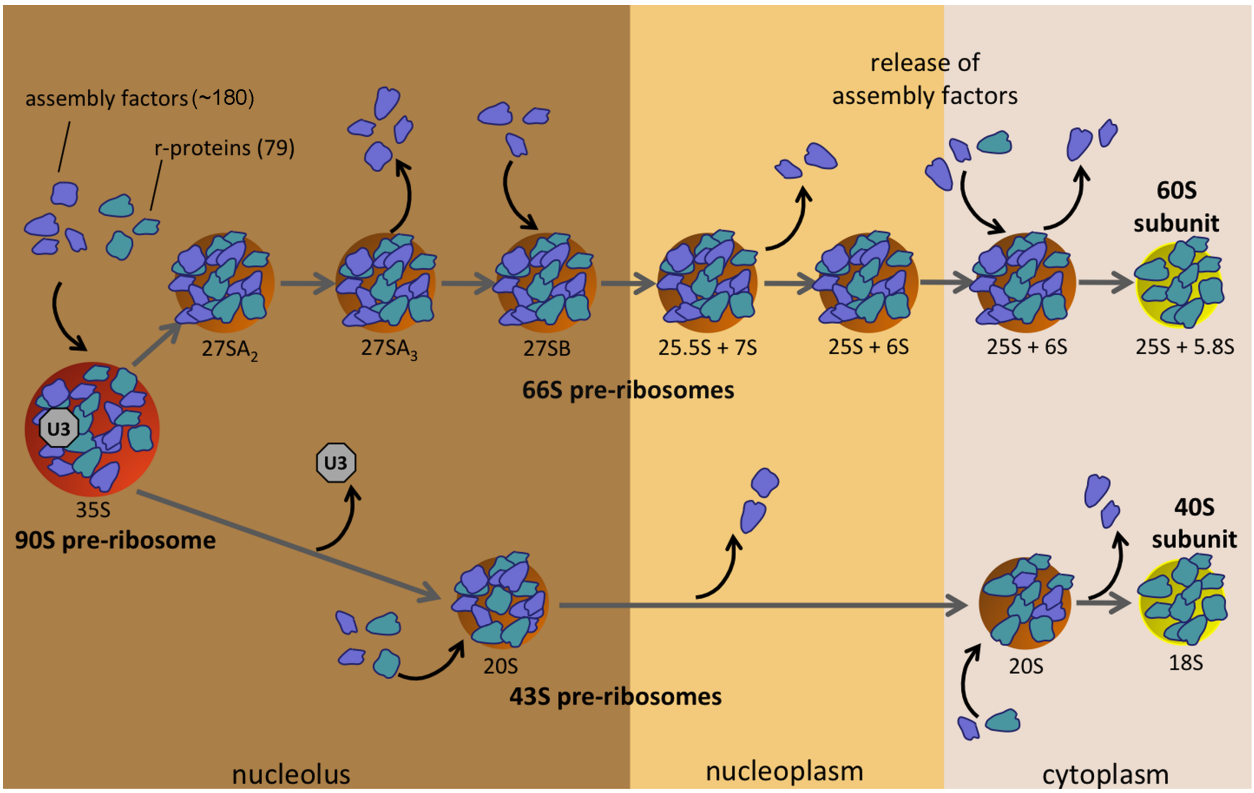

assembly factors (~180)
r-proteins (79)
release of
assembly factors
60S
subunit
27SA2
27SA3
27SB
25.5S + 7S
25S + 6S
25S + 6S
25S + 5.8S
66S pre-ribosomes
U3
35S
90S pre-ribosome
U3
40S
subunit
20S
18S
20S
43S pre-ribosomes
nucleolus
nucleoplasm
cytoplasm

Figure 5: Maturation of pre-ribosomal particles in *Saccharomyces cerevisiae*

Ribosome assembly begins in the nucleolus with either the formation of 90S pre-ribosomes (post-transcriptionally generated) or separate 43S and 66S pre-ribosomes (co-transcriptionally generated). As particles mature they are bound by assembly factors (purple) and r-proteins (teal), and transition from the nucleolus to the nucleoplasm. Final steps of maturation occur upon export of pre-ribosomes out of the nucleus and into the cytoplasm. Throughout this processes assembly factors perform their function and dissociate from pre-ribosomes before maturation is complete.

1.4.1 Subcomplexes of assembly factors reduce the complexity of assembly

Numerous studies have revealed that assembly factors and r-proteins do not always associate with ribosomes individually, but rather as part of a larger subcomplex (Xue et al. 2000; Harnpicharnchai et al. 2001; Milkereit et al. 2001; Granneman et al. 2003; Milkereit et al. 2003; Dosil and Bustelo 2004; Krogan et al. 2004; Nissan et al. 2004; Miles et al. 2005; Karbstein and Doudna 2006; Lebreton et al. 2006b; Rashid et al. 2006; Rosado et al. 2007; Zhang et al. 2007; Merl et al. 2010; Hierlmeier et al. 2012; Talkish et al. 2012) (Table 1, colored proteins). Subcomplexes of proteins are thought to reduce the complexity of ribosome synthesis, by targeting groups of proteins that function together during biogenesis to their respective assembly neighborhoods. These assembly modules contain 2-10 proteins and are thought to associate with pre-ribosomes *en bloc.* Subcomplexes were initially identified under conditions that disrupt interactions within pre-ribosomes, resulting in dissociation of the subcomplex from the assembling particle. Thus, subcomplexes are thought to represent the most stable interactions among assembly factors. Work from our lab has identified and characterized five subcomplexes that function in $27SA_3$ and 27SB pre-rRNA processing (Nop7-, Pwp1-, ITS2-, Nop2/Nip7-, and Rpf2-subcomplex), but at least six other subcomplexes have been shown to function in production of 60S ribosomal subunits. In most cases, proteins within a subcomplex function during the same steps of pre-rRNA processing, suggesting these proteins function cooperatively during ribosome biogenesis. The roles and implications of subcomplexes in 60S subunit assembly will be discussed in more detail in Chapter 2.

1.5 Ribosome assembly is hierarchical but heterogeneous

In vitro reconstitution of bacterial ribosomes revealed that ribosome biogenesis is a hierarchical process. The Nomura group showed that functional *E. coli* 30S subunits could be reconstituted using free rRNA and r-proteins, without additional components (Traub and Nomura 1968). Even more impressive, they later showed that this remarkable feat could be accomplished using individually purified proteins (or recombinant proteins) and rRNA transcribed *in vitro* (Mizushima and Nomura 1970). This was later demonstrated for the 50S subunit by Nierhaus and co-workers (Nierhaus and Dohme 1974; Rohl and Nierhaus 1982). By varying the order in which individual proteins were added, these studies revealed that r-protein binding was often interdependent and that there is an overall hierarchy that governs assembly (Fig. 6A and 6B). Assembly initiates with binding of a small subset of r-proteins to the rRNA (primary binding proteins). It is thought that these early binding events help organize and structure the rRNA to allow subsequent association other proteins (Stern et al. 1988). The remaining proteins, called secondary and tertiary binders, only associate with the assembling particle after previous association of primary binders. Although a general hierarchy exists, a collection of RNA structure probing experiments has demonstrated that each domain of 16S rRNA can assemble independently *in vitro* (Weitzmann et al. 1993; Samaha et al. 1994; Agalarov et al. 1999; Adilakshmi et al. 2008). Furthermore, assembly of these domains occurs primarily in a 5' to 3' direction (Powers et al. 1993; Holmes and Culver 2005; Adilakshmi et al. 2008).

The notion of hierarchical assembly also governs *in vivo* ribosome biogenesis in eukaryotes. Systematic investigation of the roles of small subunit r-proteins in yeast and mammalian cells revealed a correlation between the timing of association of r-proteins and the steps in pre-rRNA processing for which they are required (Ferreira-Cerca et al. 2005;

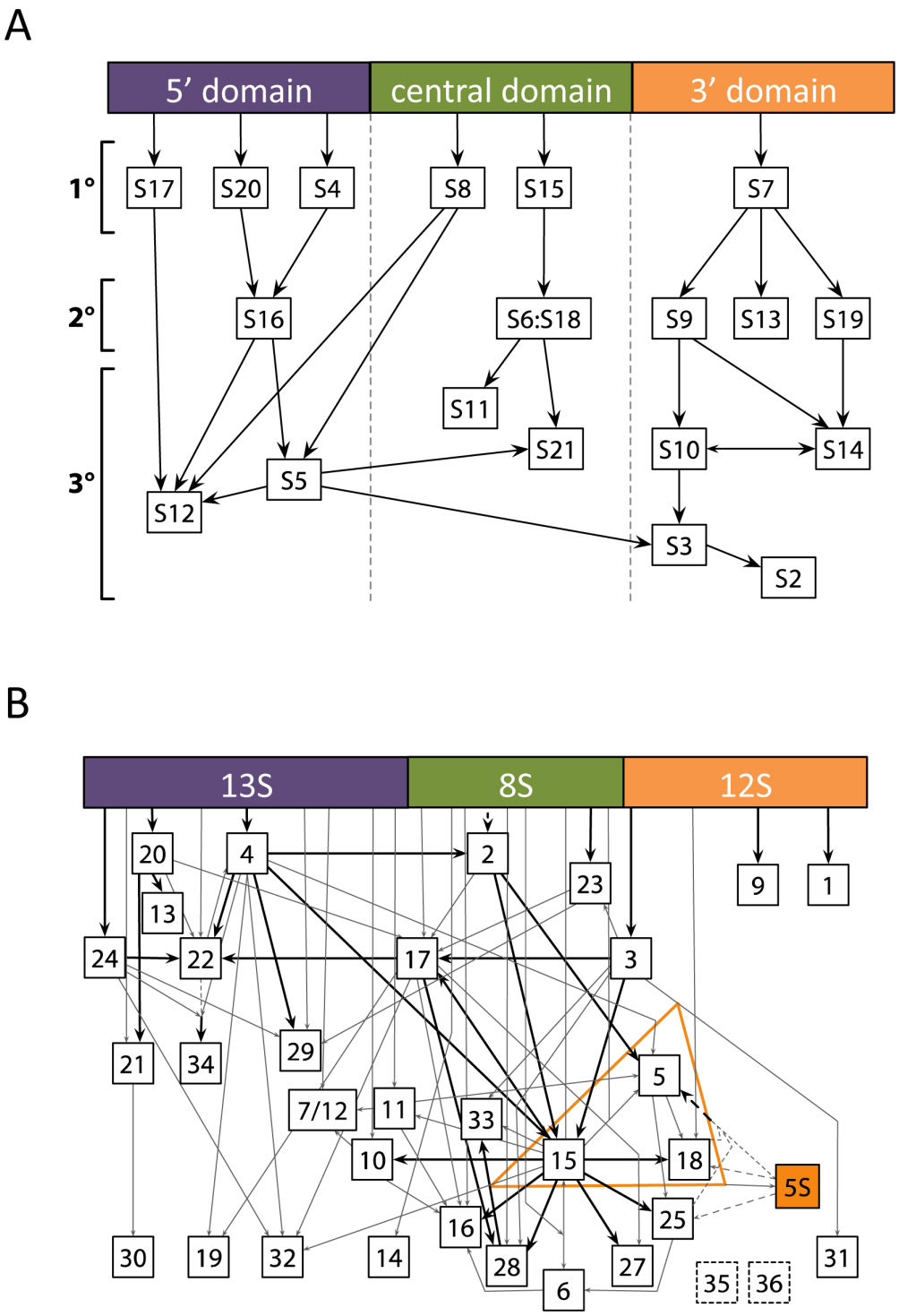
Ferreira-Cerca et al. 2007; O'Donohue et al. 2010). Eukaryotic homologues of *E. coli* primary binding proteins were found to often function in early steps of pre-rRNA processing, whereas homologues of secondary or tertiary binders were found to affect later steps. Furthermore, eukaryotic homologues of bacterial primary binding proteins localize mainly to the body of the small subunit (5' half of 18S rRNA) whereas homologues of secondary and tertiary binders were localized primarily to the head domain (3' half of 18S rRNA). While this did not hold true in every case, it suggests a general 5' to 3' directionality of r-protein association with 18S rRNA.

Recent work from our lab has demonstrated that many of these principles regulate assembly of the large ribosomal subunit as well (Gamalinda et al., submitted). Systematic depletion of yeast large subunit r-proteins and analysis of pre-rRNA processing and pre-ribosome composition revealed the following: (1) Based on pre-rRNA processing defects, r-proteins required for production of 60S subunits can be grouped as functioning during early, middle, or late steps of ribosome assembly. (2) Proteins within the same phenotypic class cluster together in the mature ribosome suggesting that they function together to organize particular neighborhoods within the assembling particle. (3) Early acting r-proteins generally bind the 5' half of 25S rRNA (domains I and II) whereas later acting proteins bind the 3' half of 25S rRNA (domain IV and V). Together, these systematic investigations reinforce the lessons learned in bacteria and show that in eukaryotes r-proteins hierarchically associate with rRNA in a 5' to 3' direction. The 5' to 3' directionality of assembly is in good agreement with the co-transcriptional nature of pre-rRNA processing.

A large collection of work has also demonstrated that assembly factors associate with nascent pre-ribosomes in a hierarchical manner. As stated above, the timing of association of assembly factors can be mapped by examining what pre-rRNAs co-purify with each factor (section 1.3). This has been determined for a number of proteins and has revealed that most assembly factors are present in more than one consecutive pre-ribosomal particle (Kressler et al. 2010). An orthogonal approach has been to use assembly factors present in pre-ribosomes at distinct intervals during the biogenesis pathway as molecular hooks to purify consecutive pre-ribosomal intermediates. Analysis of these consecutive intermediates by mass spectrometry has shown that a large number of assembly factors are present in early pre-ribosomal particles, and these particles become progressively less complex as maturation proceeds (Nissan et al. 2002). While these types of analyses have allowed us to group assembly factors as early, middle, or late binders, they often do not provide enough resolution to understand the precise timing of association of assembly factors relative to each other. It also provides little information about which proteins require previous binding of other proteins to associate with pre-ribosomes. To address these issues our lab has developed a strategy in which the constituents of pre-ribosomes are assayed upon depletion, deletion, or inactivation of a given protein. By systematically assaying the changes that occur in pre-ribosomes in the absence of individual assembly factors, we have developed a complex hierarchy of stable association for 24 assembly factors that function in two consecutive steps of ribosome biogenesis (Sahasranaman et al. 2011; Jakovljevic et al. 2012; Shimoji et al. 2012; Talkish et al. 2012; Dembowski et al. 2013). It should be noted that there is a difference between "timing of association" of an assembly factor and "stable incorporation" of that factor into pre-

ribosomes. Most assembly factors that function in early steps of 60S subunit biogenesis associate with pre-ribosomes early during assembly. In fact many of these proteins probably associate co-transcriptionally. However, work from our lab has revealed that they are "stably incorporated" into the structure in a hierarchical manner. Thus, a protein might be recruited to pre-ribosomes early in assembly, but only stably incorporated after prior stabilization of another protein. This likely reflects the idea of "encounter complexes" in which a protein initially binds an RNP weakly through a limited number of contacts. After the initial binding event, rearrangements within the RNP structure allow a greater number of more robust interactions to form, stably incorporating the protein into the RNP structure.

Figure 6



adapted from Shajani *et al.*, 2011

Figure 6: *In vitro* assembly maps of *E. coli* small and large ribosomal subunits

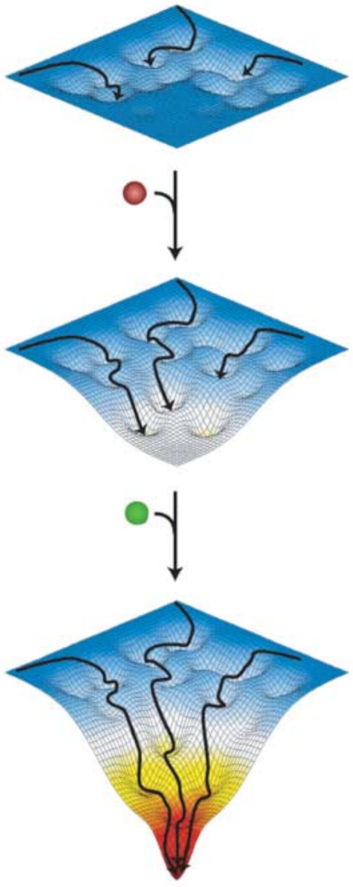
(A) The Nomura assembly map depicts order of protein binding during reconstitution of 30S ribosomal subunits *in vitro*. Primary binding proteins associate with rRNA first, followed by subsequent association of secondary and tertiary binders. (B) The Nierhaus assembly map depicts the order of ribosomal protein binding during construction of 50S ribosomal subunits.

1.5.1 Ribosome assembly proceeds down multiple, parallel pathways

More recent work from the Williamson group has expanded upon the initial principles of assembly laid out by *in vitro* reconstitution of bacterial ribosomes. While the Nomura and Nierhaus maps have been invaluable for establishing the fundamentals of assembly, they reflect the order of protein binding and thermodynamics during assembly at equilibrium. Using a combination of pulse-case monitored by quantitative mass spectrometry (PC/QMS), the Williamson group measured the binding kinetics of 20 r-proteins with 16S rRNA (Talkington et al. 2005). Many of their results correlated well with the initial Nomura and Nierhaus assembly maps. Generally, they observed faster binding kinetics for primary binding proteins than for secondary or tertiary binders. Previous *in vitro* assembly studies suggested that there was a single rate-limiting barrier during ribosome assembly. This was due to the accumulation of a single, homogeneous intermediate during assembly *in vitro*. By measuring the temperature dependence of the binding rates of each r-protein, the Williamson group showed that this is not the case. In fact assembly proceeds through multiple, often alternative, barriers, suggesting that ribosome assembly can proceed down multiple different pathways. This is not surprising since *in vitro*, r-proteins do not have an absolute dependence of association, but rather the order of binding can be slightly varied. The idea of multiple assembly pathways was solidified by examination of *in vitro* assembly intermediates using time-resolved electron microscopy (Mulder et al. 2010). Fourteen distinct assembly intermediates could be detected. Correlating these intermediates with the crystal structure of the 30S subunit, mass spectrometry data, and kinetic data revealed that these intermediates populate different, parallel assembly pathways (Fig. 7). Multiple assembly pathways may have

evolved to ensure that even under suboptimal conditions, ribosome biogenesis is not completely blocked. The parallel nature of ribosome assembly likely reflects the ability of RNA to fold into more than one structure at equilibrium. Some of these structures may be on-pathway intermediates, while others may be nonproductive (discussed in 1.6.3 and 1.6.4). Time-resolved hydroxyl radical footprinting of rRNA structure revealed that during *in vitro* reconstitution, assembly nucleates from multiple different points along 16S rRNA, indicating many early assembly intermediates (Adilakshmi et al. 2008). The rRNA may adopt slightly different conformations in these early intermediates and thus initiate slightly different r-protein association pathways.

Figure 7



Talkington *et al.*, 2005

Figure 7: Ribosome assembly proceeds down multiple, parallel pathways.

Shown is an "assembly landscape" for 30S ribosomal subunit assembly. The horizontal axes of the landscape represent the conformational space of 16S rRNA and the vertical axis is the free energy of these conformations. The native conformation of 16S is shown in the bottom corner (red). The arrows indicate parallel assembly pathways. Folding of the rRNA creates binding sites for proteins (red and green spheres), association of which alters the energy landscape and drives folding of 16S rRNA to the native state.

1.6 RNA Folding

Traditionally, RNA was thought to be simply a mediator of the genetic code. However, an enormous body of work from the last ~30 years has revealed that this is not the case. RNA is one of the most diverse and dynamic molecules in cells. RNAs regulate nearly every cellular process including transcription, splicing and mRNA editing, and mRNA stability and turnover, as well as protein synthesis, cell signaling, and mitosis. This wide array of functions stems from the ability of RNA to fold back upon itself and form an almost unlimited number of structures. These structures often form the binding sites for protein, ions, and small molecules that regulate the function of a particular RNA. However, RNA is not simply a structural molecule, but rather can function in an enzymatic fashion. For example, the ribosome and self-splicing introns are complex and dynamic ribozymes. Because RNA is intimately tied to almost every cellular process, disruption of RNA structure or function can lead to disease. Thus, to understand how this dynamic molecule functions, it is important to understand how it folds.

Three major themes are currently driving the field of RNA folding (Woodson 2010). The first is that RNA folding is hierarchical and cooperative. RNA folding begins with the formation of secondary interactions, followed by the formation of weaker, often long-range, tertiary interactions. However, this is not simply a linear process, but rather a cooperative one. Secondary structures often influence the formation of tertiary interactions, and likewise tertiary interactions can often lead to changes in secondary structure. The second major theme is that soon after the formation of secondary interactions, RNA molecules undergo a transition to a "collapsed state". This quasi-stable state is driven primarily by sampling of different tertiary interactions, and often requires proteins or ions to fine-tune

the RNA structure and drive folding to the native, functional state. The last major theme is that RNA folding pathways are heterogeneous and parallel. RNA molecules can often form more than one structure, many of which are not functional. This can be especially problematic for long RNAs, as the likelihood of misfolding increases with RNA length. The dynamic nature of RNA molecules often results in the formation of heterogeneous but parallel folding intermediates. Thus, it is important to understand the different folding pathways RNA can take, and the conditions and factors that influence these pathways.

**It is important to note that the principles of hierarchical, cooperative, and parallel folding are present throughout ribosome assembly, highlighting the integral role that RNA folding plays during the assembly process.

1.6.1 Secondary interactions are the driving force in RNA folding

Stable Watson-Crick base pairs, both intra- and intermolecular, are the dominant organizing force of RNA folding. RNA secondary structure can be broadly defined as double helices separated by various single-stranded loops (Fig. 8) (Holbrook 2008). Loops present at the end of a double helix are considered to be external loops (or hairpin loops), and include structural motifs such as the GNRA tetraloop-receptor and the kissing hairpin (Fig. 8A) (Chang and Tinoco 1994; Pley et al. 1994). External loops are thought to be generally local in nature, having little effect on the surrounding RNA secondary structure. However, interactions between external loops often contribute to tertiary structure. Internal loops, such as kink-turns and hook-turns, are formed by two single-stranded regions connecting two helices (Fig. 8B) (Klein et al. 2001; Szep et al. 2003). The single-stranded regions of

internal loops often significantly distort the orientation of the two connected helices by introducing sharp bends in the sugar-phosphate backbone. The combination of two or more internal loops can create complex junctions, further distorting the orientation of the surrounding helices (Fig. 8C). Thus, both internal and external loops directly influence RNA tertiary structure (discussed in section 1.6.2). Furthermore, proteins and small molecules that help fold or regulate the function of an RNA often recognize unique structures formed within loops.

The formation of RNA secondary structure occurs rapidly and is a spontaneous process. Temperature jump and NMR studies of short duplex forming RNAs showed that hairpins form in the range of 10 to 100 μs (Craig et al. 1971; Porschke and Eigen 1971). Kinetic analysis of duplex formation revealed that although nucleation of a helix is energetically unfavorable, the formation of each additional base pair results in free energy changes of -1 to -3.6 kcal/mol (Freier et al. 1986). Thus, these interactions are incredibly stable. However, this stability can result in misfolded RNAs that fall into kinetic traps (Brion and Westhof 1997). Because of the large negative net free energy changes during secondary structure formation, the chances of an RNA falling into a kinetic trap during early steps of folding are high.

FIGURE 8

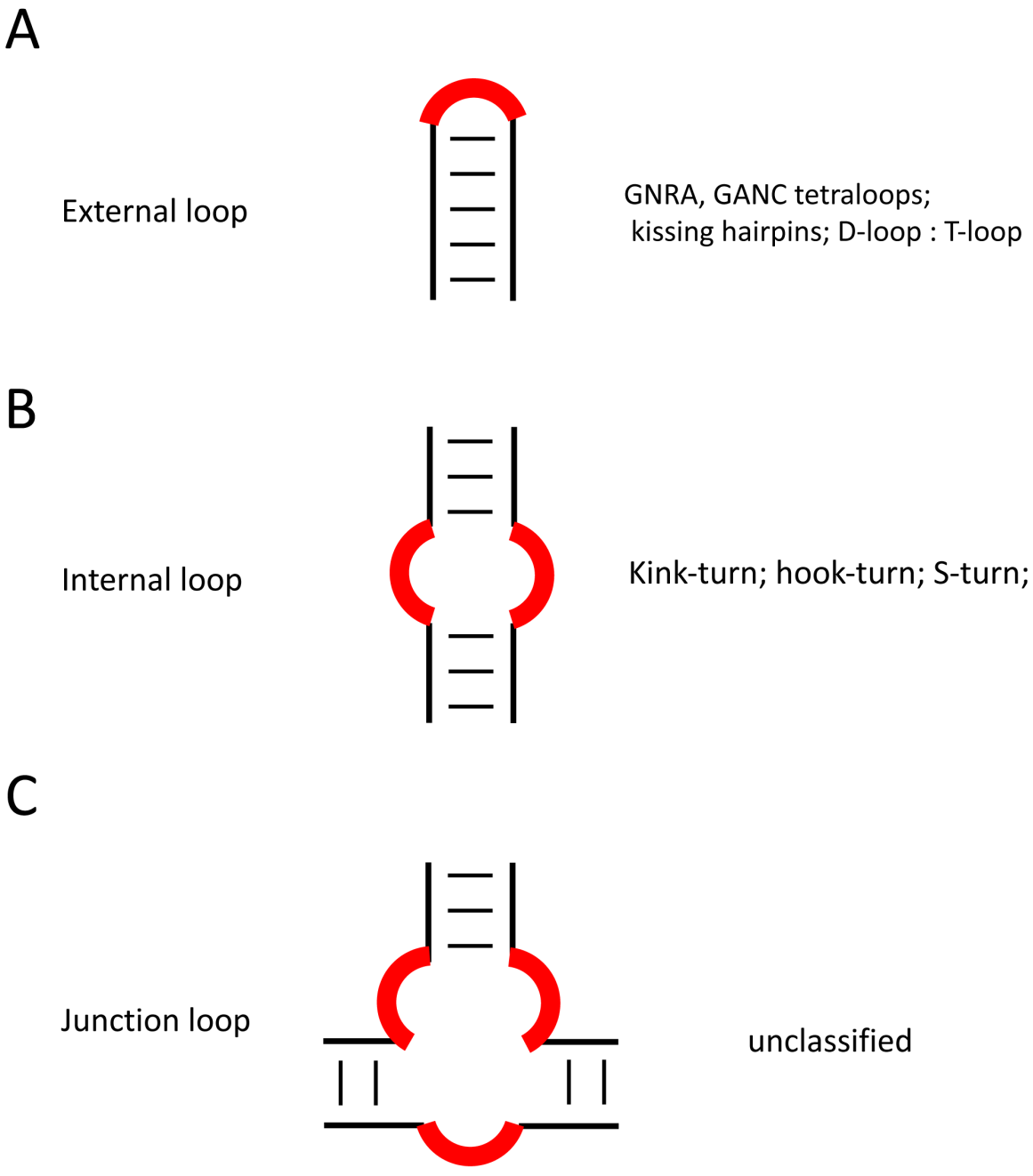

A
External loop
GNRA, GANC tetraloops;
kissing hairpins; D-loop : T-loop
B
Internal loop
Kink-turn; hook-turn; S-turn;
C
Junction loop
unclassified

Figure 8: RNA secondary structure is composed of helices, loops, and junctions

Types of RNA secondary structures. Helices are shown as black ladders and loops connecting the helices are shown as red semi-circles. Representative examples of secondary structural motifs are indicated.

1.6.2 Tertiary interactions generate the native, functional state during RNA folding

The determination of the three-dimensional crystal structure of tRNAs was a landmark event to understanding RNA folding (Kim et al. 1974; Suddath et al. 1974; Stout et al. 1976). For the first time, RNA was seen not as a simple two-dimensional molecule composed of hairpins and loops, but rather as a complex three-dimensional molecule structured by tertiary interactions consisting of non-canonical base pairs, base stacking, coaxial helix stacking, intercalated strands, and metal ions. Unlike secondary structure interactions, tertiary contacts are often weaker and can occur over long distances (Brion and Westhof 1997; Lescoute and Westhof 2006; Holbrook 2008; Woodson 2010). These interactions provide the glue to organize preformed secondary structures into a biologically functional architecture. In general, tertiary interactions are thought to increase the fidelity of RNA folding and direct helix assembly by biasing secondary interactions toward native-like structures (Chauhan and Woodson 2008). Many tertiary interactions can be grouped into recurrent motifs or structures. These include coaxial helices (Kim et al. 1974), tetraloop receptor interactions (Cate et al. 1996), A-minor motif interactions (Nissen et al. 2001), kissing loops (Chang and Tinoco 1994), tRNA-type D-loop-T-loop interactions (Kim et al. 1974), pseudoknots (Rietveld et al. 1982), and ribose zippers (Tamura and Holbrook 2002). The most dominant of these motifs is coaxial helical stacking, or COIN stacking.

RNA molecules attempt to maximize base-stacking, particularly at helix termini (Butcher and Pyle 2011). Stacking between the aromatic nucleic acid bases stabilizes the double-helical nature of RNA (Walter et al. 1994). If two helices are separated by a phosphodiester linkage, the terminal base pairs will stack and the two helices become colinear, or coaxially stacked. Thus, COIN stacking is thought to provide an overall

architecture to RNA molecules. One of best examples of this is the "L shaped" structure of tRNAs (Fig. 9). Analysis of the *T. thermophilis* small and the *H. marismortui* large rRNAs revealed that COIN stacking is a common feature of RNA molecules: ~85% of the helices in these rRNAs are present in COIN stacks (Ban et al. 2000; Wimberly et al. 2000). Similar to canonical helix formation, COIN stacking is energetically favorable, but sequence dependent. Helices surrounding complicated junctions in RNA secondary structure can often alternatively stack with each other, and in some cases act as conformational switches (Groeneveld et al. 1995; Poot et al. 1997; Lilley 1998; van Meerten et al. 2001). However, alternative stacking can also lead to the formation of kinetic traps.

While COIN stacking, particularly around RNA junctions, is thought to provide an overall organization to RNAs, other tertiary interactions help fine-tune and stabilize helix orientation. Kissing loops, formed by Watson-Crick base-pairing of external loop nucleotides between two helices, have been found in many RNAs and provide a mechanism to bring together secondary structures separated over long distances. Pseudoknots, formed by long-range base-pairing of single stranded RNA with an external loop, often function in the same fashion (Staple and Butcher 2005). The formation of a pseudoknot results in the generation of a second helix that can coaxially stack with the first. These structures are often important for the function of catalytic RNAs such as the hepatitis delta virus (HDV) ribozyme, self-splicing introns, and rRNA (Brink et al. 1993; Poot et al. 1996; Ferre-D'Amare et al. 1998; Adams et al. 2004). Tetraloop-receptor motifs are also extremely prevalent in RNA structures and assist in forming long-range interactions (Costa and Michel 1997). These motifs often involve a terminal hairpin loop contacting highly conserved internal loops or bulged bases. The terminal hairpin loop usually contains a

highly conserved consensus sequence such as GNRA or GANC. The receptors, although highly conserved, can often vary in structure and complexity. Last, a number of tertiary interactions occur within the major or minor grooves of RNA helices and include the formation of base-triples (A-minor motif), complex triple-stranded motifs, and interactions between 2'-hydroxyl groups of the RNA backbone (ribose zipper motif).

While individual tertiary interactions are energetically favorable, the net folding energies can be relatively small (Russell et al. 2002a; Chauhan et al. 2005). One reason is the enormous electrostatic forces generated by juxtaposition of phosphates in the RNA backbone. These phosphates are often much closer to each other in tertiary interactions than in canonical double helices. To circumvent these repulsive forces, RNA tertiary structures often fold around multivalent ions such as Mg^{2+} (Draper et al. 2005). A second reason is that RNA functional sites often lie within internal loops and helical junctions that distort the RNA backbone and create the binding sites for small molecules or proteins. Formation of these pockets often requires the disruption of previously formed Watson-Crick base pairs. Thus, the net free energy change during tertiary structure formation is often reduced by the energy needed to disrupt or reorganize secondary structures.

FIGURE 9

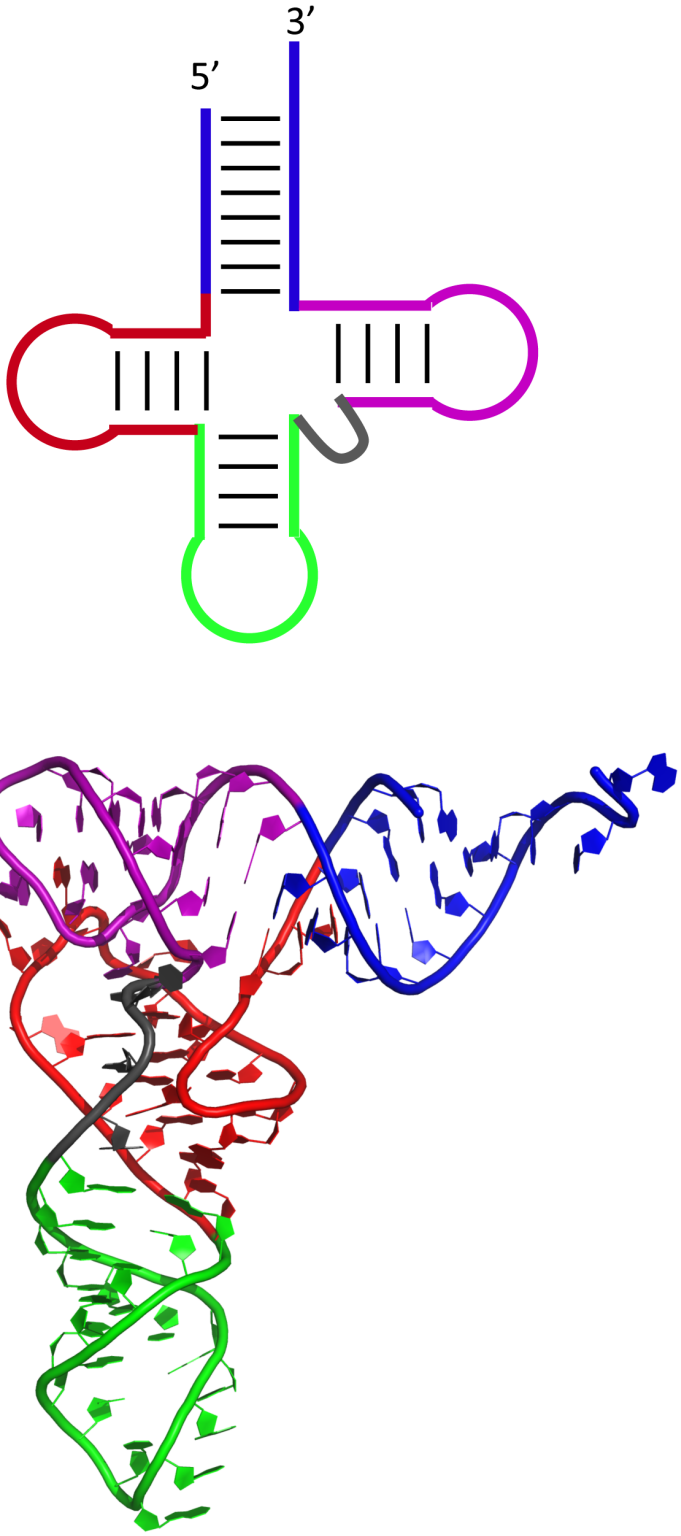


Figure 9: COIN stacking is the dominant organizing force of RNA tertiary structure

Shown is a schematic of tRNA secondary structure (top) and the crystal structure of phenylalanine tRNA (bottom; PDB: 6TNA). Coaxial stacking is observed between the blue and purple helices and the red and green helices.

1.6.3 Compact intermediates in RNA folding

A large collection of work has revealed that as RNAs fold to their native state, they undergo a collapse (or compaction), akin to the molten-globular state of protein folding (Woodson 2000; Woodson 2010). This was first observed using a combination of biochemical approaches and small angle x-ray scattering (SAXS) that showed large ribozymes collapse to a non-native intermediate ~5-15% larger than the native structure (Buchmueller et al. 2000; Russell et al. 2000). Time-resolved SAXS of the *Tetrahymena* group I ribozyme showed that this collapse occurs extremely rapidly, on the order of 10-20 ms (Russell et al. 2002a; Das et al. 2003). This results in an ensemble of intermediates, many of which only reach the native structure after 1-100 min *in vitro* (Zarrinkar and Williamson 1994; Pan et al. 1997; Russell et al. 2002b). It is during this collapsed state that the search for the final native structure occurs. RNA helices are largely formed and participate in transient tertiary interactions, but have not yet stably packed into a functional structure.

During the collapsed state, the formation of the final tertiary contacts and remodeling of secondary structures are highly cooperative. Using hydroxyl radical footprinting, the Woodson group showed that disruption of a single tertiary interaction in the *Azoarcus* ribozyme reduced cooperativity of helix assembly resulting in a larger fraction of misfolded RNA molecules (Chauhan and Woodson 2008). This led to destabilization of all other tertiary contacts as well as misfolding of secondary structures around the ribozyme core (Chauhan et al. 2009). Thus, the transition of RNAs to a collapsed state and the subsequent formation of native tertiary contacts is essential for accurate helix folding. It is likely that the tertiary interactions within the collapsed state

bias the ensemble of secondary structure conformations to native-like structures (Woodson 2010).

1.6.4 Parallel pathways of RNA folding – kinetic partitioning

To understand the thermodynamic parameters that govern RNA folding, it is important to briefly reflect on the principles that have emerged from the study of protein folding (Dill and Chan 1997). Pioneering work in the early 1960's showed that denatured bovine pancreatic ribonuclease could spontaneously refold to its native, functional state (Anfinsen et al. 1961; Anfinsen 1973). This suggested that protein folding is a self-assembly process and that the "information" required for a protein to fold into its native state was present in the primary amino acid sequence. Furthermore, this implied that the structure of some globular proteins is thermodynamically stable and represents global minima in their free energies. However, these experiments did not provide the mechanisms of protein folding. A breakthrough arose when Cyrus Levinthal raised a question in the late 1960s: With the nearly unlimited number of possible conformations, how does a protein search among all of them to reach its native state (Levinthal, 1969)? He postulated that a protein could not simply sample every one of the enormously large number of possible conformations (he estimated 10^{300}) and still fold in a biologically relevant time-scale. Instead, rapid formation of local interactions could stabilize and guide further folding events, continually reducing the number of possible confirmations. This thought experiment led to the idea that proteins fold to their native state along a number of different folding pathways, all occupying the same energy landscape. Because RNAs have the ability to form alternative structures, some

as energetically favorable as the native state, many of the questions raised and initial principles uncovered regarding protein folding are applicable to RNA folding.

The current view of RNA folding is that it is a stochastic search among probable conformations toward the most stable state (Woodson 2010). This occurs within an "energy landscape" defined by the free energies of the different conformations and the energy barriers between them (Thirumalai et al. 2001). Because of the relatively low complexity of the primary sequence and stability of RNA secondary structure, RNAs can fold into structures that are not always compatible with the native fold. The energy barriers needed to correct misfolded structures introduce minima into the landscape. Thus, energy landscapes are usually composed of a single global minima (representing the native state), surrounded by many local minima (representing folding intermediates and/or kinetic traps)(refer to Fig. 7). These local minima introduce alternative folding routes to the native state. Generally, more complex RNAs have a greater number of folding intermediates as well as a greater chance to misfold. This leads to "rough" energy landscapes that become "smoother" as the RNA continually folds to its native state.

In this model, known as the kinetic partitioning mechanism, a fraction of a population of unfolded RNAs rapidly folds to the native state by direct paths. The other fraction becomes trapped in stable, misfolded structures. *In vitro* analysis of the *Tetrahymena* self-splicing RNA revealed that only ~8% of the population folded directly to the native state, but briefly heating the misfolded population resulted in ~70% folding to the native state (Pan et al. 1997). Heating is thought to partially denature the trapped intermediates, allowing another opportunity to fold properly. Consistent with this, a greater fraction of RNAs folded to the native state in the presence of low concentrations of

denaturants such as urea (Pan et al. 1997; Pan and Sosnick 1997). Single molecule FRET experiments confirmed these results, showing that 6% of the RNAs transitioned rapidly from a low FRET state (unfolded) to a high-FRET state (folded), with a rate constant of 1 s^{-1}. The remaining fraction underwent much slower transitions and included an intermediate FRET state (Zhuang et al. 2000). Kinetic partitioning can be perturbed even further by mutations in the RNA that either destabilize interactions or introduce alternative, more stable structures. A single point mutation in the *Tetrahymena* self-splicing RNA resulted in only ~3% folding to the native state (Pan et al. 1997). Together these principles show that RNA folding can proceed down multiple pathways, some more productive than others. Generally, direct folding to the native state occurs fast, whereas molecules that fold through alternative pathways do so slowly (Zhuang et al. 2002). Due to the stability of secondary interactions, the folding pathway of an RNA is determined early in the folding processes. Furthermore, the fraction of RNA molecules that fold directly to the native state depends on the relative stability of alternative secondary structures, as well as the strength of tertiary interactions.

**Together, the principles of discussed in sections 1.6.1 – 1.6.4 reveal the following model of RNA folding: 1) Secondary structures are highly stable and form rapidly. However, this stability provides ample opportunity for misfolding. 2) Following secondary structure formation, RNAs transition to a collapsed state, in which tertiary contacts are loosely formed. During this time, sampling of different tertiary interactions can cause refolding of secondary structures further driving folding to the native state. 3) Tertiary interactions, while often weaker than secondary interactions, fold the RNA into a biologically functional

molecule. 4) RNA folding occurs within an energy landscape through parallel pathways. Some RNA molecules fold rapidly to the native state, whereas others become trapped in local minima and proceed down alternative folding routes.

1.6.5 Current approaches to probing RNA structure

Because the function of RNA is directly tied to its structure, it is important to understand how these molecules fold to their native state. While crystallographic and NMR approaches are powerful tools to understand the structure of RNA on the atomic level, they often only provide a snap-shot of the native state and fail to capture the dynamic nature of RNA as it folds. Tools such as SAXS have been applied to RNA structure determination, but often only provide structural changes on a global level. To better understand the dynamics and conformational changes during RNA folding, a barrage of techniques has been developed to probe the local environment of individual nucleotides (Peattie and Gilbert 1980; Ehresmann et al. 1987; Stern et al. 1988). These approaches often use small molecules, chemicals, or enzymes that modify or cleave RNA in a manner that reports secondary and tertiary structural information. Experiments are performed under conditions so that, on average, only one modification occurs per RNA molecule, reducing the risk of modification causing unintended structural changes. Many of these modifications sterically block processivity of reverse transcriptase, and thus can be detected as a reverse transcriptase stops using primer extension assays (Fig. 10A). While all of these techniques have been traditionally used *in vitro*, recent advances in technology and the development of new molecules that can penetrate the cell have allowed some of the approaches to be used *in vivo* (Wells et al. 2000; Spitale et al. 2012).

A number of reagents have been developed to probe the local environment of nucleobases (Fig. 10B) (Brunel and Romby 2000). The most common include dimethysulfate (DMS), kethoxal, diethyl polycarbonate (DEPC), CMCT, and bisulphate. These chemicals often modify the Watson-Crick face of nucleobases, and thus provide structural information about hydrogen bonding and base-pairing. Many of these reagents are base-specific and therefore multiple chemicals may have to be utilized to probe the environment of all nucleotides in an RNA. For example, DMS modifies N1 of adanines, N3 of cytosines, and N7 of guanines. However, uracils are not modified and traditional primer extension approaches do not detect modification of G(N7). Thus, to obtain information about guanines and uracils, other chemicals such as kethoxal (modifies G at N1 and N2) and CMCT (modifies G and N1 and U at N3) must also be employed. While most of these chemicals are limited to *in* vitro assays, DMS is applicable both *in vitro* and *in vivo* (discussed in Chapter 2 and Chapter 4). New developments of sequence-independent chemicals (SHAPE analysis) have addressed some of these issues by allowing interrogation of all nucleotides in an RNA both *in vitro* and *in vivo* (see below).

Many RNases have also been applied to structure probing experiments. Most RNases (T1, S1, etc.) cleave single-stranded RNA. However, RNase V1 from cobra venom exclusively cleaves double-stranded RNA. Therefore, secondary structure information can be obtained by comparing the cleavage patterns of RNA digested with single-stranded nucleases to RNA digested with double-stranded nucleases. Caution must be taken with this approach because cleavages within the RNA may induce conformational rearrangements that potentially provide new cleavage sites. Furthermore, because of the large size of many RNases, they are susceptible to steric hindrance and therefore may not

provide single nucleotide resolution. However, this approach has been successful in determining the overall secondary structure for a number of large RNAs, including rRNA (Kean and Draper 1985; Baudin et al. 1987; Mougel et al. 1987).

Hydroxyl radicals can also be used to probe RNA structure, providing high-resolution tertiary structure data (Tullius and Greenbaum 2005). These highly reactive and sequence-independent species cause strand scission by abstracting a hydrogen atom from the deoxyribose sugars. The small size of hydroxyl radicals means they are limited only by the solvent accessibility of RNA. Traditionally, hydroxyl radicals have been generated *in vitro* by reacting iron(II) EDTA with hydrogen peroxide. While this is still a widely used method, new approaches have begun utilizing high-energy, synchrotron-generated x-rays to produce hydroxyl radicals from radiolysis of water (Brenowitz et al. 2002). Syncrotron-generated hydroxyl radicals provide a number of advantages. First, there is no need for the addition of chemical reagents to the sample, reducing the risk of perturbing the RNA structure. Second, the generation of hydroxyl radicals by x-rays is extremely fast. Combining stopped-flow technology with synchrotron-generated hydroxyl radicals allows investigation of RNA folding at millisecond timescales, providing high-resolution snap-shots of RNA folding over time (Adilakshmi et al. 2006; Adilakshmi et al. 2008). Last, x-rays can be used to generate hydroxyl radicals *in vivo* by irradiation of frozen cell pellets. While this was originally developed using *E. coli*, I have shown that this technique is also feasible in yeast (Appendix 5.4).

The most recent addition to the arsenal of RNA structure probing techniques is selective 2'-hydroxyl acylation analyzed by primer extension (SHAPE) (Merino et al. 2005). SHAPE chemistry interrogates local nucleotide flexibility by reacting with the 2'-hydroxyl

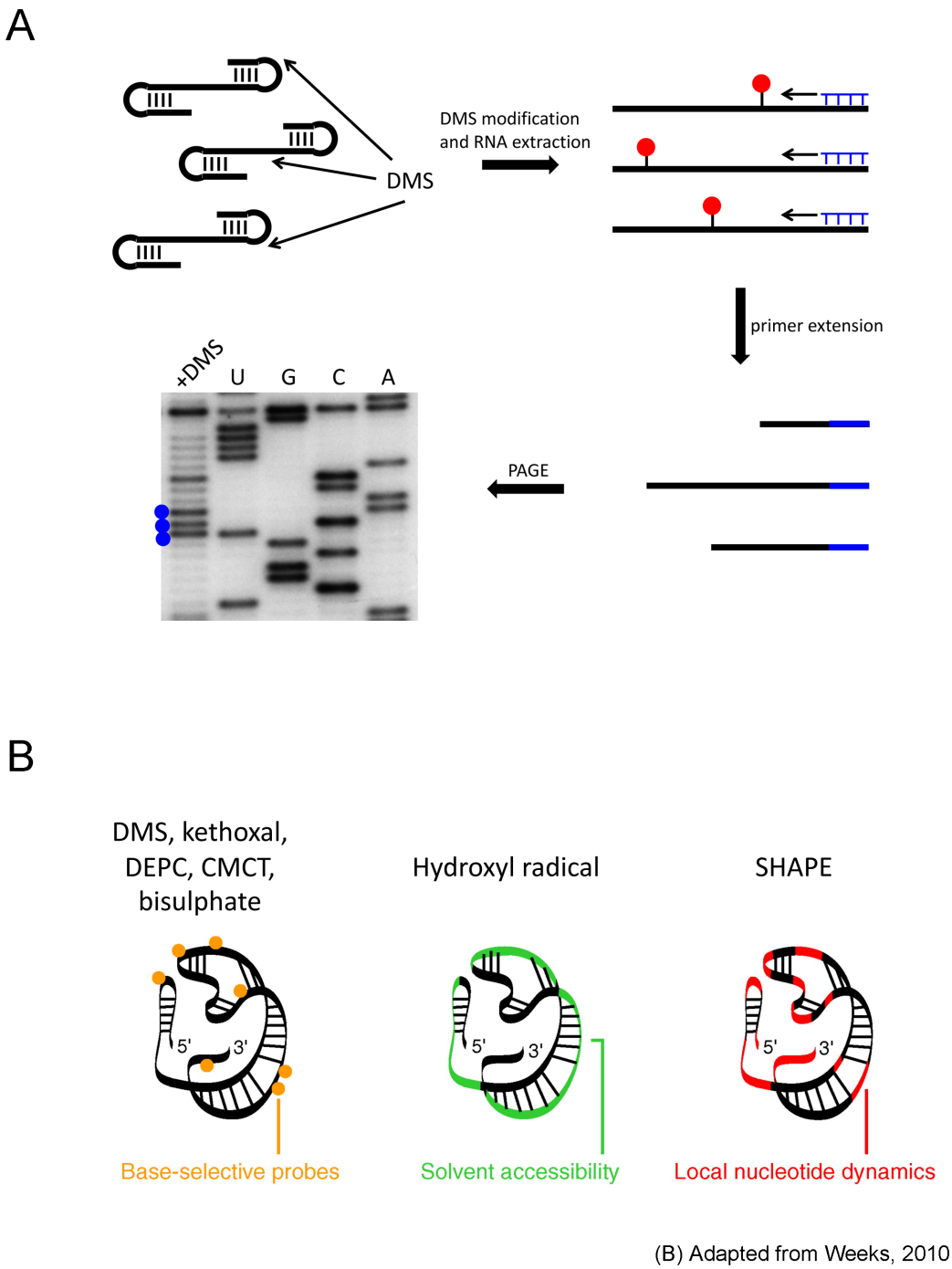
group and thus is not limited by base-specificity. Highly dynamic or flexible nucleotides are better able to adopt conformations that react with SHAPE reagents. Thus, interactions that constrain nucleotide dynamics, including base-pairing, reduce the reactivity of the 2'-hydroxyl group. Analyzing SHAPE reactivity by capillary electrophoresis, instead of traditional primer extension, has allowed complete interrogation of extremely long RNAs including the HIV-I genome and yeast rRNA (Wilkinson et al. 2008; Leshin et al. 2011).

While the approaches listed above have been invaluable for understanding how RNA folds, they are fairly low-throughput in nature. Primer extension and polyacrylamide gel electrophoresis only allow analysis of ~150 nt per oligonucleotide primer. Thus, 40-60 different oligonucleotides would be necessary to assay the entire length of especially long RNAs, such as rRNA. Assaying nucleotide modifications by capillary electrophoresis has somewhat alleviated this problem, but interrogating the entire length of rRNA still requires at least 20 different oligonucleotide primers (Leshin et al. 2011). A number of approaches have begun utilizing next-generation sequencing in an effort to increase the throughput of these assays. FragSeq and parallel analysis of RNA structure (PARS) utilize high-throughput sequencing to assay RNAs cleaved by single-stranded and double-stranded RNases *in vitro* (Kertesz et al. 2010; Underwood et al. 2010). In a similar manner, SHAPE-Seq has been employed to assay the structure of RNAs *in vitro* (Lucks et al. 2011). Limitations to these and the above approaches will be discussed in detail in Chapter 4.

To better understand the structure of RNAs, I have worked with the McManus group at Carnegie Mellon University to develop a high-throughput technique to assay the structure of RNAs probed *in vivo*. Our technique, called Mod-seq, combines *in vivo* DMS probing and next-generation sequencing to simultaneously assay the structure of the entire

transcriptome. The approach and applications of this technique will be discussed in Chapter 4.

FIGURE 10



(B) Adapted from Weeks, 2010

Figure 10: Chemical probing of RNA secondary structure

(A) Overview of RNA structure probing using chemical probes and primer extension. RNA is modified by small molecules, chemicals, or enzymes (e.g. DMS). Modifications (red) are then detected by primer extension using a fluorescently labeled or radiolabeled oligonucleotide (blue) and visualized either by capillary electrophoresis or PAGE (shown). (B) Classes of RNA structural information obtained using various chemical probes.

1.6.6 Recent insights into *in vivo* pre-rRNA folding during ribosome biogenesis

Many of the techniques described above have been used to investigate the structure and dynamics of mature ribosomes assembled *in vitro* (Moazed et al. 1986; Stern et al. 1989; Powers and Noller 1995; Culver 2003; Adilakshmi et al. 2005). However, only in the last five years have these techniques been employed to study rRNA folding in eukaryotes *in vivo*. A number of factors make studying pre-rRNA folding *in vivo* a daunting task. A major challenge is differentiating the structure of pre-rRNAs from mature rRNAs. This problem has been partially solved by designing oligonucleotide primers for primer extension that hybridize within pre-rRNA spacer sequences not present in mature rRNAs (Fig. 4). However, because primer extension and PAGE analysis only allows interrogation of ~150 nucleotides, the ability to assay the structures of what will become the mature rRNAs is limited by how far a primer extension reaction can extend "out of the spacers" and "into the sequences of mature rRNAs". Another challenge is the heterogeneous nature of pre-rRNAs. Most of the spacer sequences used as primer binding sites are present in more than one consecutive pre-rRNA intermediate. Furthermore, these intermediates are present in dynamic RNPs and thus each intermediate may be present in more than one conformation. Thus, these assays reflect the ensemble structure of pre-rRNAs, making data analysis more difficult. Nevertheless, a number of recent studies have begun looking at how pre-rRNAs fold during assembly, primarily in mutants that block a particular step in the biogenesis process. By comparing the structure of pre-rRNAs from wild-type cells to those in mutants, we are beginning to understand the transitions that these molecules undergo during biogenesis, protein factors that contribute to these transitions, and effects on pre-rRNA

processing when such transitions do not occur. Here I will briefly highlight three recent examples of *in vivo* pre-rRNA structure probing in yeast.

1.6.6.1 The U3 snoRNA is required for proper folding of pre-18S rRNA

Co-transcriptional processing and modification of pre-rRNAs requires a number of small nucleolar RNP complexes (snoRNPs). These complexes are directed to their target sites, by small nucleolar RNAs (snoRNAs) that base-pair with sequences in pre-rRNAs. The U3 snoRNP has previously been shown to be required for early steps in pre-rRNA processing and was proposed to play a role in structuring 18S rRNA (Hughes and Ares 1991; Hughes 1996; Henras et al. 2008). Using a combination of genetics and *in vivo* chemical probing, the Baserga group showed that depletion of U3 snoRNA results in misfolding of pre-rRNAs, particularly within the 5' ETS (Dutca et al. 2011). Furthermore, they found a previously uncharacterized interaction between the 3' end of the U3 snoRNA and the 5' ETS of pre-rRNA, highlighting the ability of this approach to not only detect structural changes, but also identify novel base-pairing interactions.

1.6.6.2 A conformational switch regulates pre-rRNA cleavage by Nob1

As described in section 1.2, the last processing step of 18S rRNA maturation involves removal of the remainder of ITS1 by endonucleolytic cleavage at the D site. It had long been suspected that the assembly factor Nob1 was the endonuclease required for this cleavage (Fatica et al. 2003a). Nob1 was shown to bind 18S rRNA both *in vitro* and *in vivo*, and recombinant Nob1 exhibited weak RNA cleavage activity *in vitro* (Lamanna and Karbstein 2009; Pertschy et al. 2009). More recent work from Lamanna and Karbstein

showed that Nob1 is indeed the nuclease that cleaves the D site, and that this cleavage is regulated by a conformational change within 18S rRNA (Lamanna and Karbstein 2009; Lamanna and Karbstein 2010). Using a combination of *in vitro* and *in vivo* structure probing, they showed that sequences within ITS1 base-pair with 18S rRNA in early assembly intermediates, but cleavage of the A_2 site results in a conformational switch resulting in the formation of decoding site of 18S rRNA. During this conformational switch, the D site is brought into close proximity to Nob1, facilitating its cleavage and final maturation of 18S rRNA. This work highlights the highly cooperative nature of pre-rRNA folding, protein binding, and pre-rRNA processing.

1.6.6.3 A subcomplex of assembly factors are required for proper folding of ITS2

The spacer sequence ITS2 is removed through a series of endo- and exonucleolytic digestions that eventually give rise to mature 5.8S and 25S rRNAs. This spacer was previously shown to be essential for ribosome assembly; its absence blocks processing of 27S pre-rRNAs, suggesting it is required for processing steps upstream of its removal (van der Sande et al. 1992). Chemical probing and phylogenetic analysis suggested that ITS2 can fold into at least two stable conformations (Yeh and Lee 1990). In one conformation, called the hairpin model, ITS2 is highly base-paired and folds into a series of extended helices. The other conformation, referred to as the ring model, predicts that ITS2 folds into a more open conformation with a series of short hairpins surrounding a central, single-stranded core. These predictions were supported by making mutations within ITS2 predicted to shift the equilibrium from one structure to the other (Cote et al. 2002). This analysis suggested that ITS2 forms the open ring conformation early in assembly, and later refolds to form the

hairpin structure. While this still has yet to be definitively proven, recent work from our laboratory and others work has supported these ideas. Relatively new RNA-protein cross-linking approaches have shown that the assembly factors Cic1, Nop15, and Rlp7 bind within ITS2 (Granneman et al. 2011)(Dembowski et al., accepted). *In vivo* DMS probing revealed that in the absence of these proteins, ITS2 becomes misfolded, adopting a conformation that resembles the hairpin structure. These studies suggest that these proteins may function early in assembly to maintain ITS2 in the ring conformatation , and support the model that ITS2 is dynamic and undergoes refolding during assembly. However, DMS probing is not sufficient to definitively differentiate between the two structures. Thus, further analysis of this potential conformational switch is needed. The dynamics of ITS2 will be discussed further in Chapter 2 and Appendix 5.5.

CHAPTER 2: Ribosome assembly factors Pwp1 and Nop12 aid folding of 5.8S rRNA during ribosome biogenesis in *Saccharomyces cerevisiae*

2.1 Introduction

Numerous studies have shown that subsets of AFs can be isolated as subcomplexes (Xue et al. 2000; Harnpicharnchai et al. 2001; Milkereit et al. 2001; Granneman et al. 2003; Milkereit et al. 2003; Dosil and Bustelo 2004; Krogan et al. 2004; Nissan et al. 2004; Miles et al. 2005; Karbstein and Doudna 2006; Lebreton et al. 2006b; Rashid et al. 2006; Rosado et al. 2007; Zhang et al. 2007; Merl et al. 2010; Hierlmeier et al. 2012; Talkish et al. 2012). Interestingly, proteins within a subcomplex are often required for the same steps of pre-rRNA processing, suggesting that they function together during ribosome biogenesis to achieve a common goal. One subcomplex that functions in assembly of the 60S subunit in *Saccharomyces cerevisiae* is composed of the AFs Brx1, Ebp2, Nop12, and Pwp1 and r-proteins, L8 and L15 (referred to as the Pwp1 subcomplex). High-speed centrifugation, followed by coimmunoprecipitation (co-IP) using epitope tagged Nop12 or Pwp1, revealed that these proteins interact in a stable complex that can be isolated independent of pre-ribosomes (Krogan et al. 2004; Zhang et al. 2004). Furthermore, Brx1, Ebp2, Nop12 and L8 have all been shown to be required for processing of $27SA_2$ and $27SA_3$ pre-rRNAs. (Poll et al. 2009; Granneman et al. 2011; Jakovljevic et al. 2012; Shimoji et al. 2012).

In the mature 60S subunit, r-proteins L8 and L15 closely interact with each other as well as with the ITS2-proximal stem (helix 10), a conserved helix formed by base-pairing between the 3' end of 5.8S rRNA and the 5' end of 25S rRNA (Fig. 11) (Ben-Shem et al. 2011). These two rRNA ends are generated upon the removal of Internal Transcribed

Spacer 2 (ITS2) during processing of 27SB pre-rRNA. It was recently reported that Nop12 can be UV crosslinked within the ITS2-proximal stem, as well as a nearby stretch of 5.8S rRNA (helix 8) (Fig. 11)(Granneman et al. 2011). This result, as well as the known location of L8 and L15 in mature 60S subunits, suggests that this complex binds within or near the ITS2-proximal stem and may play a role in folding rRNA and structuring this essential neighborhood.

Most of what we know about RNA folding during ribosome assembly has emerged from *in vitro* studies of bacterial ribosomes (Nierhaus 1991; Culver 2003; Woodson 2008; Sykes and Williamson 2009; Shajani et al. 2011; Woodson 2012). Only recently have investigations initiated on how rRNA folds in eukaryotes, *in vivo* (Lamanna and Karbstein 2010; Dutca et al. 2011; Granneman et al. 2011; Babiano et al. 2012; Dembowski et al. 2013). Our lab and others have shown that depletion of proteins that bind to ITS2 causes ITS2 to refold prematurely, suggesting that these proteins help regulate the structure of this spacer (Granneman et al. 2011) (Dembowski et al., in press). However, these proteins are required for the removal of ITS1 and generation of the 5' end of 5.8S rRNA (Dunbar et al. 2000; Gadal et al. 2002; Fatica et al. 2003b). In mature ribosomes the 5' end of 5.8S rRNA is ~160Å from the ITS2-proximal stem suggesting long-range coupling between removal of ITS1 and removal of ITS2. By binding to the ITS2-proximal stem, the Pwp1 subcomplex appears to be located in the pre-ribosome at a position to enable long-range communication between these two spacers (Fig. 11).

Our laboratory has recently characterized the essential Pwp1 subcomplex proteins Ebp2, Brx1, and r-protein L8, and established a hierarchy of association between these proteins and other factors required for $27SA_3$ pre-rRNA processing (Sahasranaman et al.

2011; Jakovljevic et al. 2012; Shimoji et al. 2012). To address the role of the Pwp1 subcomplex in forming the ITS2-proximal stem and structuring the surrounding rRNA, we focused on the less characterized proteins Nop12 and Pwp1. Interestingly, Both Nop12 and Pwp1 are nonessential proteins (Duronio et al. 1992; Wu et al. 2001). Because of this, we rationalized that the changes observed in their absences would be minimal, but highly specific. Nop12 contains a classic RNA recognition motif (RRM) and Pwp1 contains a WD40 motif, examples of which have been recently shown to bind RNA (Lau et al. 2009). Here we show that like other members of the Pwp1 subcomplex, Pwp1 functions in $27SA_2$ and $27SA_3$ pre-rRNA processing. Additionally, we have further defined the association hierarchy between the Pwp1 subcomplex and other A_3 factors. Most importantly, Both Nop12 and Pwp1 are required for proper folding of 5.8S rRNA and the ITS2 proximal stem. In the absence of both proteins, helices in the 3' half of 5.8S rRNA do not stably form, and in the absence of Nop12 helix 5 is folded into an alternative, unproductive helix.

FIGURE 11

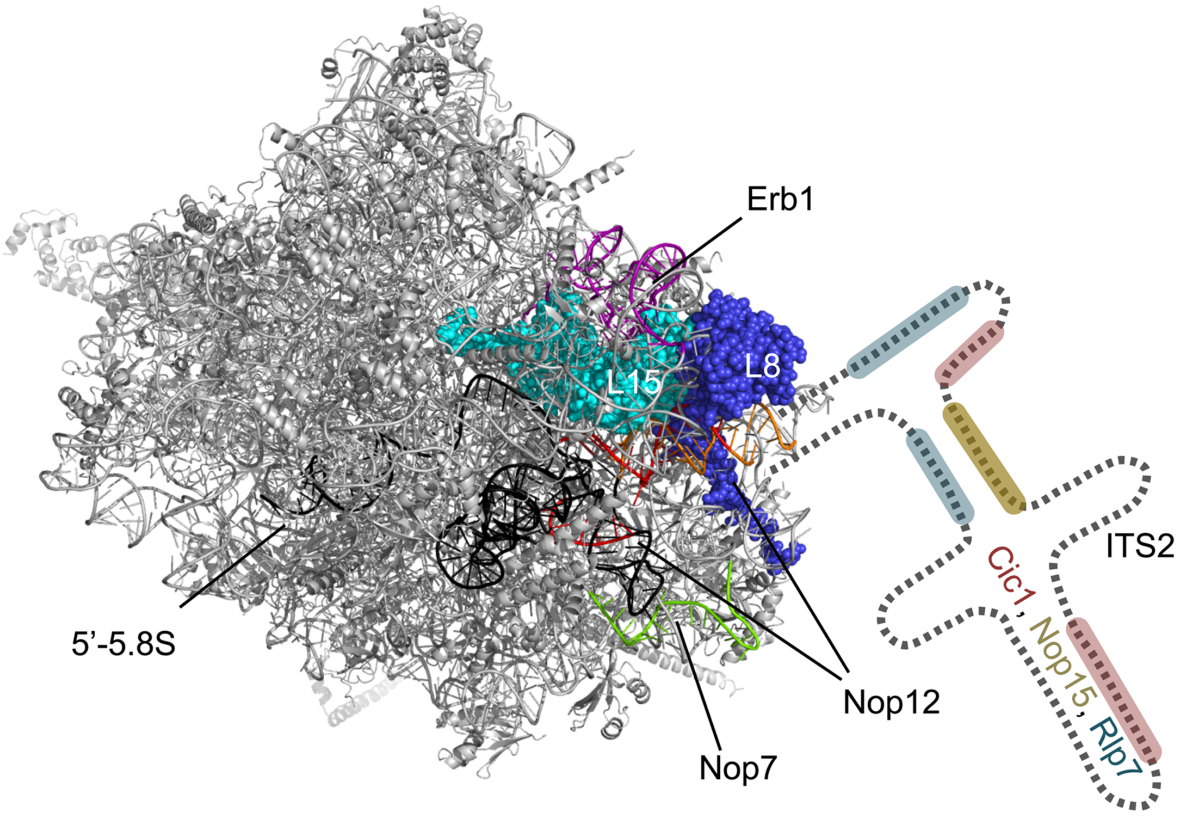


Figure 11: The Pwp1 subcomplex associates with pre-ribosomes near the ITS2-proximal stem

Shown is the crystal structure of the *Saccharomyces cerevisiae* 60S subunit viewed from the solvent accessible side (28) (PDB: 3U5H, 3U5I). 5.8S rRNA is shown in black. The ITS2-proximal stem is shown in orange. R-proteins L8 and L15 are colored dark blue and light blue, respectively. Sequences of rRNA cross- linked to Nop12, Nop7, and Erb1 are shown in red, green, and purple, respectively (25). ITS2 is represented by the dashed grey line to indicate the approximate locations of Cic1, Nop15, and Rlp7.

2.2 Results

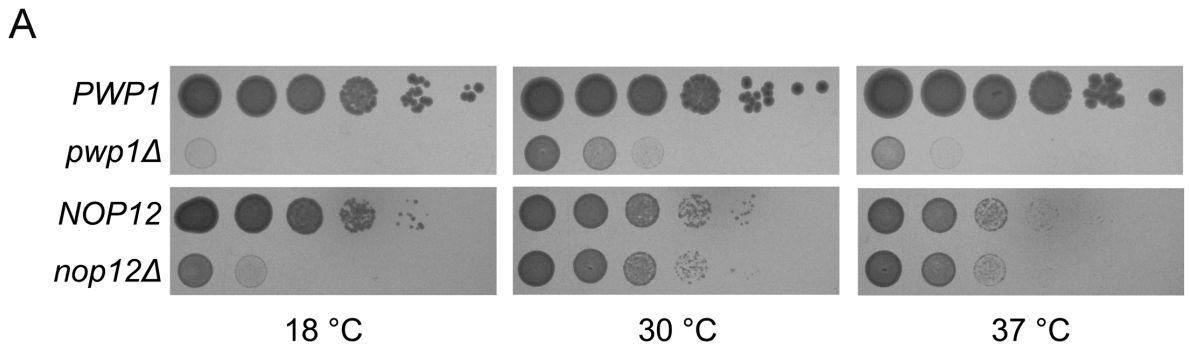
2.2.1 Pwp1 is nonessential and functions in 60S subunit biogenesis

Previously, Nop12 was shown to be a nonessential protein, although deletion causes cold sensitivity and blocks large subunit pre-rRNA processing (Wu et al. 2001; Granneman et al. 2011). Large-scale surveys of the yeast genome reported Pwp1 as an essential protein (Giaever et al. 2002), yet closer inspection by Duronio and co-workers showed that a strain containing an insertion in the *PWP1* gene was viable, although slow growing (Duronio et al. 1992). To clarify this, we precisely replaced the *PWP1* ORF with *HIS3* in diploid W303 yeast. Upon sporulation and dissection of tetrads, we recovered four viable spores, two of which were extremely slow growing (data not shown). This confirmed previous results that Pwp1 is nonessential. Although viable, *pwp1Δ* cells had doubling times ~8 fold longer compared to the wild-type spores and were cold-sensitive, causing lethality at 18 °C (Fig. 12A).

To test the role of Pwp1 in ribosome assembly, we assayed the amounts of mature ribosomes (by sucrose gradient centrifugation) in wild-type and *pwp1Δ* strains, at 30 °C and the non-permissive temperature of 18 °C. We also assayed the levels of mature ribosomes in a strain conditional for expression of Pwp1, in which the promoter of the *PWP1* gene was replaced with the *GAL1* promoter and thus repressed in glucose-containing medium (Fig. 12B). In all cases, the amounts of free 60S subunits relative to 40S subunits were decreased and halfmer polyribosomes were present (Fig. 13A-F). The decrease in ratio of 60S subunits to 40S subunits was exacerbated in the *pwp1Δ* strain shifted to 18 °C, consistent with the cold-sensitivity (Fig. 13C and 13D). Interestingly, an extra peak was

present in the *pwp1Δ* strain, sedimenting near the 43S peak (Fig. 13B and 13D). This has been previously observed in other ribosome assembly mutants defective in propagating the killer toxin-encoding M1 satellite double-stranded RNA of the L-A virus (Ohtake and Wickner 1995). Together, these results show that like Nop12, Pwp1 is a nonessential protein that functions in 60S ribosome biogenesis, deletion of which causes cold-sensitivity.

FIGURE 12


A
PWP1
pwp1Δ
NOP12
nop12Δ
18 °C
30 °C
37 °C

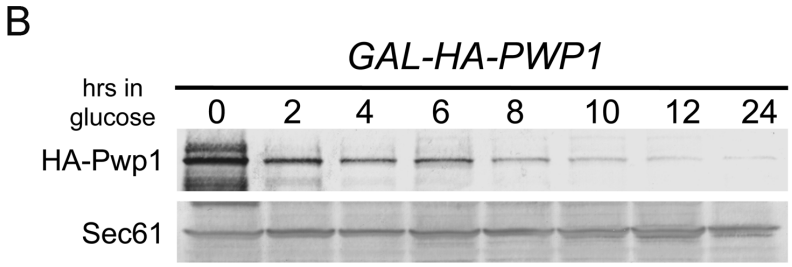

B
GAL-HA-PWP1
hrs in glucose
0
2
4
6
8
10
12
24
HA-Pwp1
Sec61

Figure 12: *PWP1* is non-essential and its deletion confers cold-sensitivity.

(A) Growth of the *pwp1Δ* and *nop12Δ* deletion strains. (B) Depletion of HA-Pwp1 upon shifting the *GAL-HA-PWP1* strain to glucose-containing medium. Sec61 serves as a loading control.

FIGURE 13

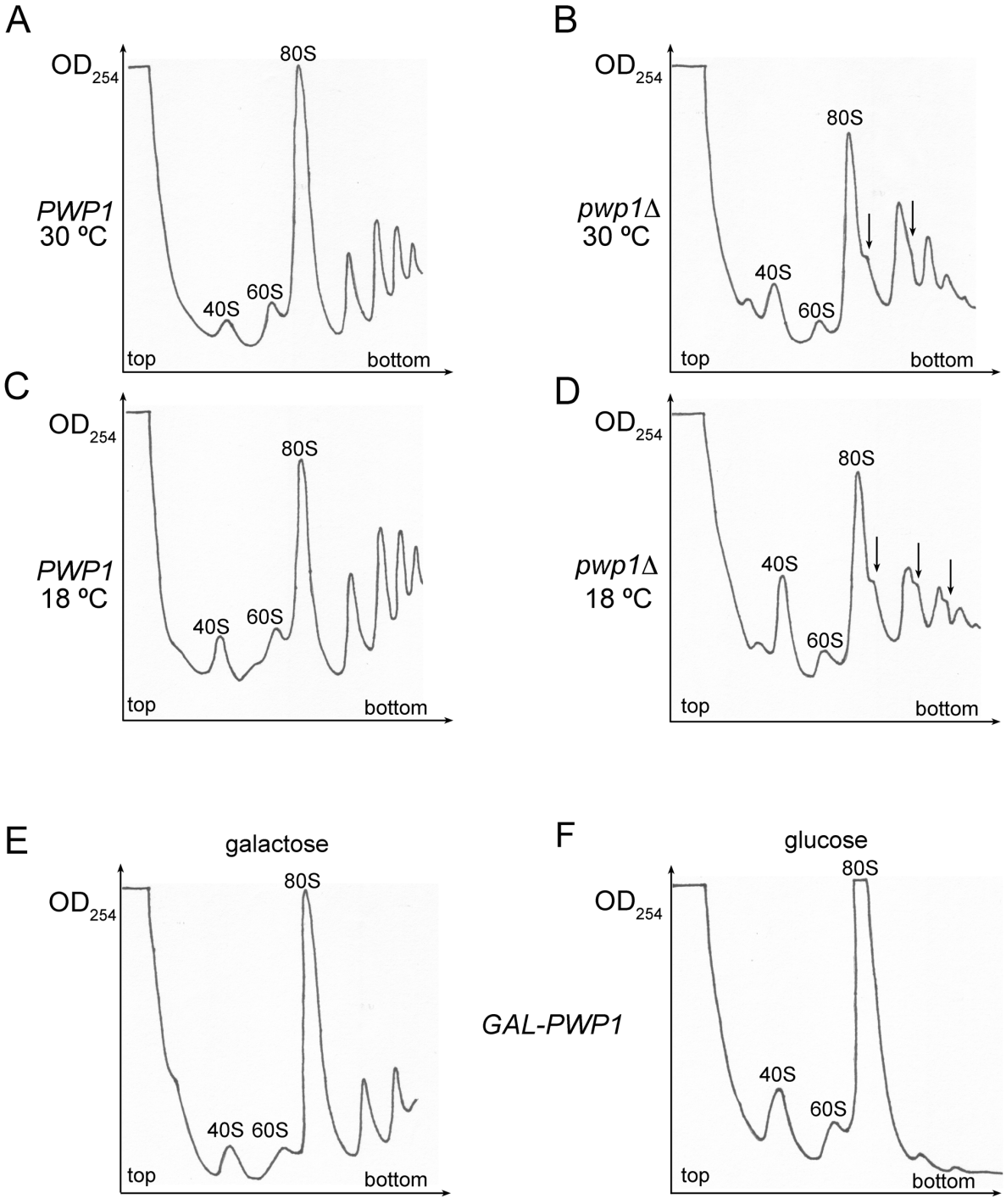

A
OD254
80S
PWP1
30 ºC
40S
60S
top
bottom
B
OD254
80S
pwp1Δ
30 ºC
40S
60S
top
bottom
C
OD254
80S
PWP1
18 ºC
40S
60S
top
bottom
D
OD254
80S
pwp1Δ
18 ºC
40S
60S
top
bottom
E
galactose
OD254
80S
40S 60S
top
bottom
F
glucose
OD254
80S
GAL-PWP1
40S
60S
top
bottom

Figure 13: Deletion of Pwp1 affects production of 60S ribosomal subunits.

Polysome profiles of wild-type and *pwp1Δ* strains grown at either 30 °C (A and B) or shifted to 18 °C for 4 hours (C and D). (E and F) Polysome profiles of the *GAL-HA-PWP1* strain either grown in YEPGal (E) or shifted to YEPGlu (F) for 16 hours. Halfmer polyribosomes (polysomes containing a 43S initiation complex bound to an AUG start codon in mRNA without a corresponding 60S subunit) are indicated by vertical arrows.

2.2.2 Pwp1 is important for efficient processing of $27SA_2$ and $27SA_3$ pre-rRNAs

Recently it was shown that Nop12 is required for processing of $27SA_3$ pre-rRNA (Granneman et al. 2011). To determine what step in production of 60S ribosomal subunits Pwp1 functions, we assayed pre-rRNA processing in wild-type cells and *pwp1Δ* cells grown at either 30 °C, or shifted to 18 °C or 37 °C for four hours. We also examined pre-rRNA processing in the *GAL-PWP1* strain either grown at 30 °C in YEPGal, or shifted to YEPGlu for 16 hours to deplete Pwp1. As controls, we compared the defects observed in the absence of Pwp1 to the pre-rRNA processing defects observed in the absence Nop12 and another A_3 factor, Rlp7 (Dunbar et al. 2000; Wu et al. 2001; Gadal et al. 2002). Deletion or depletion of *PWP1* resulted in similar pre-rRNA processing defects as deletion of *NOP12* or depletion of Rlp7 (Fig. 14). Consistent with the extreme slow growth phenotype of the *pwp1Δ* strain, the intensity of the pre-rRNA processing defect in the absence of Pwp1 was nearly identical to that in the absence of the essential A_3 factor Rlp7, and stronger than that in the absence of Nop12. Furthermore, the observed effects on pre-rRNA processing in the absence of Pwp1 were exacerbated when *pwp1Δ* cells were grown at 18 °C, consistent with the cold-sensitive growth phenotype.

The absence of Pwp1 resulted in a marked reduction in the levels of 25S rRNA relative to 18S rRNA (Fig. 14A, lanes 7-14). Northern blotting and primer extension revealed an accumulation of 35S, 33S/32S, $27SA_2$, $27SA_3$, and $27SB_L$ pre-rRNAs (Fig. 14A and B, lanes 7-14). The accumulation of $27SA_3$ pre-rRNA was accompanied by a corresponding decrease in $27SB_s$ pre-rRNA, suggesting that either $27SA_3$ pre-rRNA is not being processed, or $27SB_s$ pre-rRNA is being turned over. Additionally, we observed a decrease in 7S pre-rRNAs and 5.8S rRNA (data not shown). We also observed an

accumulation of 23S pre-rRNA, consistent with a delay in cleavage at sites A_0, A_1, and A_2 (Fig. 14A and B, lanes 7-14). A delay in these initial cleavage events was also evident by a decrease in 20S pre-rRNA. Because 18S rRNA levels are relatively unaffected, it is likely that the 23S pre-rRNA generated in the absence of Pwp1 can be processed into 18S rRNA.

To better discern the effects on pre-rRNA processing in the absence of Pwp1, we assayed pre-rRNA synthesis and turnover kinetics by pulse-chase analysis. In wild-type cells at both 30 °C and 18 °C, nascent pre-rRNAs are rapidly converted into 27SA, 27SB, and 20S pre-rRNAs, and these are ultimately processed to 25S and 18S rRNAs. In contrast, deletion of *PWP1* results in a delay in both the formation and processing of pre-rRNA intermediates and mature rRNAs (Fig. 14C and 14D). Levels of 25S rRNA from the *pwp1Δ* strain grown at 30 °C were lower than those in wild-type cells, while 18S rRNA appeared to be relatively unaffected. This was accompanied by an accumulation of 35S, 27SA, and 27SB pre-rRNAs relative to wild-type (Fig. 14C). There was also a slight accumulation of 23S pre-rRNA and a mild delay in processing of 20S pre-rRNA. Interestingly, at 18 °C, deletion of *PWP1* causes 27S pre-rRNAs to be turned over, and thus results in no 25S rRNA being produced (Fig. 14D). This is not simply a result of a failure to incorporate label into the RNA at 18 °C because we observed the formation of 20S pre-rRNA and 18S rRNA, although at slightly lower amounts. These results are strikingly similar to pulse-chase analyses upon depletion of r-protein L8, a member of the same subcomplex, or of other essential A_3 factors or r-proteins that are required for $27SA_2$ and $27SA_3$ processing (Dunbar et al. 2000; Gadal et al. 2002; Jakovljevic et al. 2012; Dembowski et al. 2013).

Taken together, these results demonstrate that Pwp1, like other subcomplex members, participates in early steps of 60S subunit biogenesis. Pwp1 functions in

processing of $27SA_2$ and $27SA_3$ pre-rRNAs. Consistent with an early block in pre-rRNA processing, fluorescence microscopy revealed a nucleolar accumulation of 66S pre-ribosomes in the absence of Pwp1 (Fig. 15). Similar to the deletion of *NOP12*, the effects on pre-rRNA processing are most evident when *pwp1Δ* cells are grown in the cold. Because both Nop12 and Pwp1 have domains proposed to bind RNA, the cold-sensitive phenotype suggests that in the absence of these proteins, pre-rRNAs may be misfolded or unable to undergo a conformational switch (Guthrie et al. 1969; Dammel and Noller 1993). In the case of Pwp1 this may lead to turnover of misassembled pre-ribosomes.

FIGURE 14

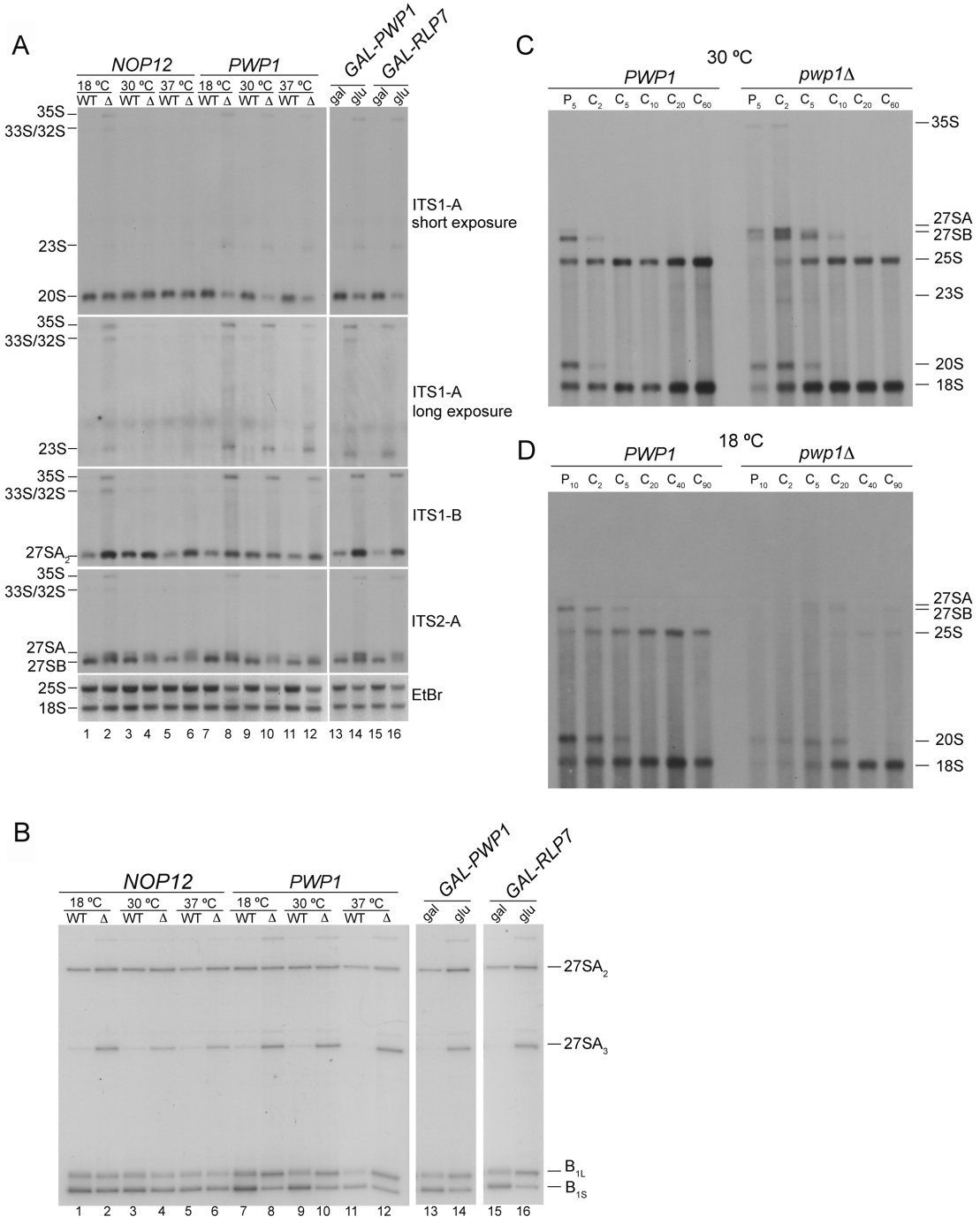

A
NOP12
PWP1
GAL-PWP1
GAL-RLP7
18 ºC
30 ºC
37 ºC
WT Δ
gal glu
35S
33S/32S
23S
20S
27SA2
27SA
27SB
25S
18S
ITS1-A
short exposure
ITS1-A
long exposure
ITS1-B
ITS2-A
EtBr
1 2 3 4 5 6 7 8 9 10 11 12 13 14 15 16
C
30 ºC
PWP1
pwp1Δ
P5 C2 C5 C10 C20 C60
35S
27SA
27SB
25S
23S
20S
18S
D
18 ºC
PWP1
pwp1Δ
P10 C2 C5 C20 C40 C90
27SA
27SB
25S
20S
18S
B
NOP12
PWP1
GAL-PWP1
GAL-RLP7
18 ºC
30 ºC
37 ºC
WT Δ
gal glu
27SA2
27SA3
B1L
B1S
1 2 3 4 5 6 7 8 9 10 11 12 13 14 15 16

Figure 14: Pwp1 functions in processing of $27SA_2$ and $27SA_3$ pre-rRNAs.

(A and B) Steady-state levels of pre-rRNAs and rRNAs extracted from wild-type, *pwp1Δ*, *GAL-HA-PWP1*, *nop12Δ*, and *GAL-HA-RLP7* strains assayed by northern blotting (A) and primer extension (B). The *nop12Δ* and *GAL-HA-RLP7* strains serves as controls of previously characterized mutants defective in processing $27SA_3$ pre-rRNA. Due to overexposure, 20S pre-rRNA was cropped from the "ITS1-A, long exposure" panel in (A) for clarity. B_{1S} and B_{1L} in (B) refer to the 5' end of $27SB_S$+$7S_S$ and $27SB_L$+$7S_L$, respectively. (C and D) Kinetics of synthesis and turnover of pre-rRNAs extracted from wild-type and *pwp1Δ* strains assayed by pulse-chase. Strains were grown at 30 °C (C) or shifted to 18°C for 4 hours (D).

FIGURE 15

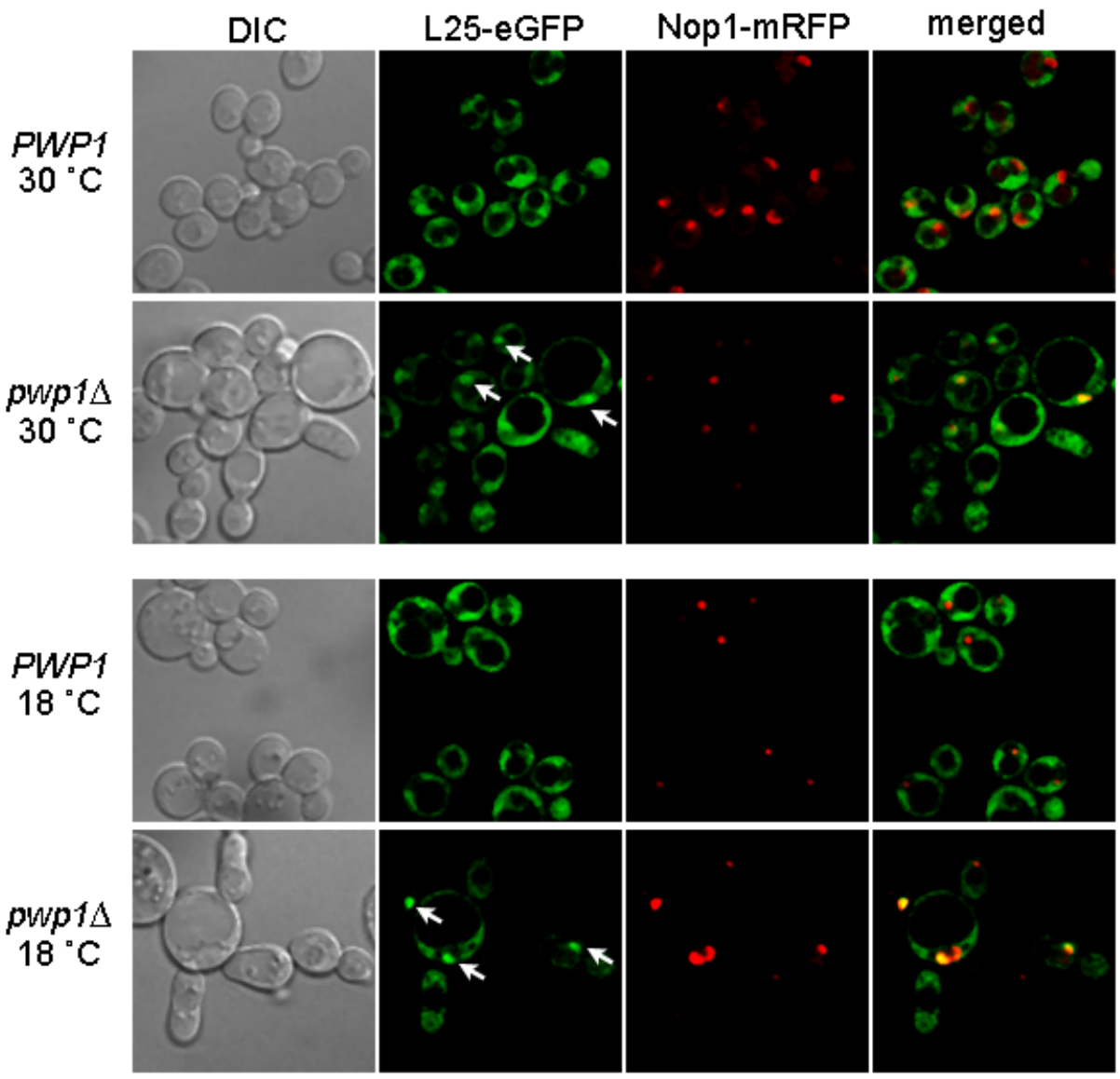

DIC
L25-eGFP
Nop1-mRFP
merged
PWP1
30 ˚C
pwp1Δ
30 ˚C
PWP1
18 ˚C
pwp1Δ
18 ˚C

Figure 15: Pre-ribosomes accumulate in the nucleolus in the absence of Pwp1

Wild-type and *pwp1Δ* strains were transformed with a plasmid co-expressing L25-eGFP and Nop1-mRFP (nucleolar marker). Cells were grown in C-ura medium at either 30 °C or shifted to 18 °C for four hours. The localization of L25-eGFP and Nop1-mRFP were assayed by fluorescence microscopy. Arrows point to nucleolar accumulation of L25-eGFP

2.2.3 Pwp1 associates with 90S pre-ribosomes and is exported to the cytoplasm.

Previous work from our laboratory and others have shown Ebp2, Brx1, Nop12, and r-protein L8 associate with pre-ribosomes during early steps of 60S subunit assembly and co-IP early 66S pre-rRNA intermediates (Granneman et al. 2011; Jakovljevic et al. 2012; Shimoji et al. 2012). To better understand when Pwp1 associates with pre-ribosomes, we TAP-tagged Pwp1 and purified pre-ribosomes. As a control, we also purified pre-ribosomes using Nop12-TAP. Like Nop12, Pwp1 associates with pre-ribosomes early in assembly; it co-IPed 35S, 27SA, 27SB, and 7S pre-rRNAs above background amounts from an untagged strain (Fig. 16A). Pwp1 also co-IPed appreciable amounts of mature 5.8S rRNA, suggesting that Pwp1 is associated with pre-ribosomes exported to the cytoplasm.

As an orthogonal approach to map the timing of association of Pwp1, we purified pre-ribosomes using the TAP-tagged AFs Ssf1 (nucleolar), Arx1 (nucloplasmic), and Lsg1 (cytoplasmic), and assayed by western blotting for the presence of HA-tagged Pwp1 (Fatica et al. 2002; Nissan et al. 2002). All three TAP-tagged proteins co-IPed Pwp1-HA, corroborating the results that Pwp1-TAP co-purifies the earliest pre-rRNA intermediate, as well as mature 5.8S rRNA (Fig. 16B). Thus, we conclude that like other members of the Pwp1 subcomplex, Pwp1 associates with pre-ribosomes early during biogenesis and remains associated until pre-ribosomes are exported from the nucleus to the cytoplasm.

FIGURE 16

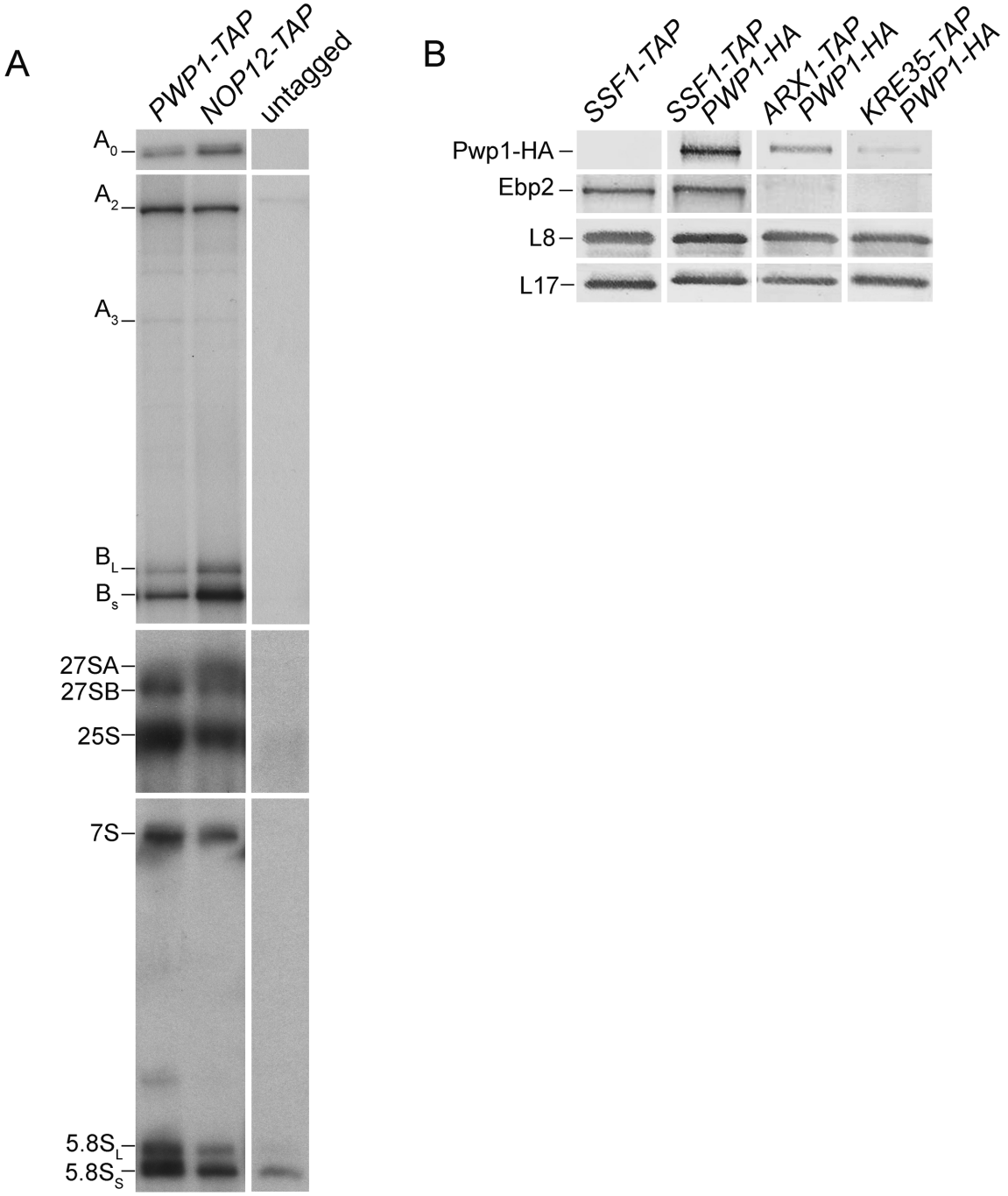

A
PWP1-TAP
NOP12-TAP
untagged
A0
A2
A3
BL
Bs
27SA
27SB
25S
7S
5.8SL
5.8SS
B
SSF1-TAP
SSF1-TAP PWP1-HA
ARX1-TAP PWP1-HA
KRE35-TAP PWP1-HA
Pwp1-HA
Ebp2
L8
L17

Figure 16: Pwp1 associates with pre-ribosomes in the nucleolus and is exported to the cytoplasm.

(A) Pre-rRNAs and rRNAs that co-immunoprecipitate with *PWP1-TAP* and *NOP12-TAP* (control) detected by primer extension and northern blotting. Detected pre-rRNAs, rRNAs, and pre-rRNA 5' ends are indicated. B_{1S} and B_{1L} refer to the 5' end of $27SB_S$+$7S_S$ and $27SB_L$+$7S_L$, respectively. (B) Western blotting analysis for the presence of Pwp1-HA in pre-ribosomes purified using TAP-tagged Ssf1 (nucleolar), Arx1 (nuclear), or Lsg1 (cytoplasmic). L17 serves as a loading control.

2.2.4 Pwp1 is important for stable association with pre-ribosomes of assembly factors required for 27SA$_3$ pre-rRNA processing.

Work from our lab has established a hierarchy in which the Pwp1 subcomplex members Ebp2 and Brx1 are required for stable association of six interdependent A$_3$ factors (Nop7, Erb1, Ytm1, Cic1, Rlp7, and Nop15), which in turn are necessary for stable association of two DEAD-box proteins (DBPs), Has1 and Drs1 (Sahasranaman et al. 2011; Jakovljevic et al. 2012; Dembowski et al. 2013). To better understand the relationship between association of Pwp1 and assembly of other proteins required for this step in biogenesis, we investigated changes in pre-ribosome composition in the absence of Pwp1. Because the extreme slow growth phenotype of the *pwp1Δ* strain made it difficult to grow large volumes of cells at sufficient density, pre-ribosomes were affinity-purified from an Rpf2-TAP strain conditional for expression of Pwp1 (as described above). After shifting cells for 16 hours to glucose-containing media, HA-Pwp1 was undetectable by western blotting (Fig. 17B and Fig. 12B).

Pre-ribosome constituents were resolved by SDS-PAGE and visualized by silver-staining (Fig. 17A). Previous mass spectrometry analysis from our lab has identified many of the polypeptides present in each of the gel bands (Zhang et al. 2007). Interestingly, depletion of Pwp1 results in a characteristic pattern of silver-stained bands similar to depletion of other A$_3$ factors (Fig. 18) (Sahasranaman et al. 2011; Jakovljevic et al. 2012; Shimoji et al. 2012). Specifically, there was an observable decrease in gel bands corresponding to the interdependent A$_3$ factors Erb1, Nop7, Ytm1, Cic1, Rlp7, and Nop15 (Fig. 17A, asterisks), suggesting that Pwp1 is important for stable association of these six interdependent proteins.

Western blotting confirmed that in the absence of Pwp1, Nop7 and Cic1 fail to stably associate with pre-ribosomes (Fig. 17B). Consistent with this, we observed a decrease in the DEAD box protein Has1. Additionally, levels of several AFs (Tif6, Rlp24, Nog1, Nsa2, Nog2) and r-proteins (L17) that function in the next step of ribosome biogenesis, processing of 27SB pre-rRNA, were decreased (Fig. 17B, B factors) (Basu et al. 2001; Saveanu et al. 2001; Saveanu et al. 2003; Lebreton et al. 2006a; Gamalinda et al. 2013). These proteins have all been shown to be dependent on the A_3 factors to stably bind pre-ribosomes (Sahasranaman et al. 2011; Jakovljevic et al. 2012; Dembowski et al. 2013)(J. Talkish, unpublished data). In summary, Pwp1 is important for stable association of a group of interdependent A_3 factors that function in the same step of pre-rRNA processing, as well as B factors that function in the following step.

To begin to understand the interdependence of the six proteins in the Pwp1 subcomplex, we used available antibodies to assay changes in the levels of Ebp2 and r-protein L8 in pre-ribosomes purified in the presence or absence of Pwp1. Western blotting revealed that upon depletion of Pwp1, both Ebp2 and L8 associated with pre-ribosomes at wild-type levels (Fig. 17B). We also wanted to test for changes in the levels of Nop12, but were unable to obtain positive transformants after numerous attempts to Myc-tag Nop12 in the *GAL-HA-PWP1* strain. It is likely that Nop12 fails to associate with particles in the absence of Pwp1 because *in vivo* chemical probing of pre-rRNA structure in the absence of Pwp1 revealed many of the same changes in RNA structure as those in a *nop12Δ* strain (see below, Fig. 19). Furthermore, many of the changes in the absence of Pwp1 were at or near the known Nop12 binding site, likely reflecting the failure of Nop12 to associate with pre-ribosomes. These results indicate that Pwp1 is not required to recruit the subcomplex

protein Ebp2 and L8, and suggests a hierarchy in which Pwp1, like Ebp2 and L8, stably associates with pre-ribosomes prior to the interdependent A_3 factors (Sahasranaman et al. 2011; Jakovljevic et al. 2012; Shimoji et al. 2012).

FIGURE 17

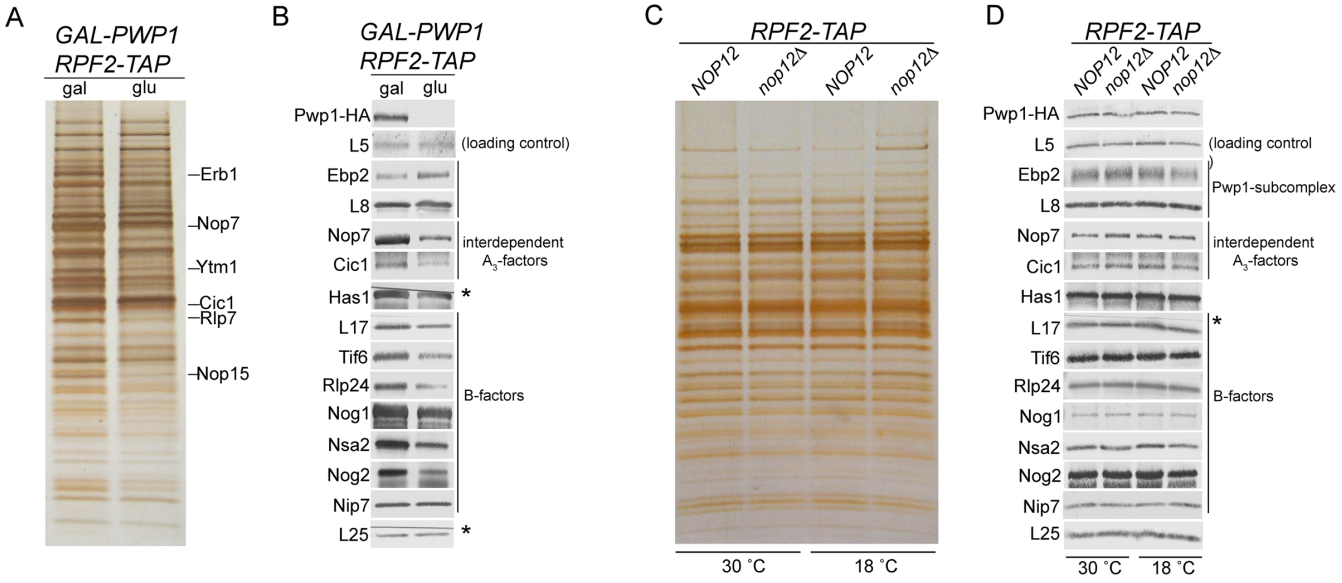

A
GAL-PWP1
RPF2-TAP
gal
glu
Erb1
Nop7
Ytm1
Cic1
Rlp7
Nop15
B
GAL-PWP1
RPF2-TAP
gal
glu
Pwp1-HA
L5
(loading control)
Ebp2
L8
Nop7
Cic1
interdependent
A3-factors
Has1
*
L17
Tif6
Rlp24
B-factors
Nog1
Nsa2
Nog2
Nip7
L25
*
C
RPF2-TAP
NOP12
nop12Δ
NOP12
nop12Δ
30 ˚C
18 ˚C
D
RPF2-TAP
NOP12
nop12Δ
NOP12
nop12Δ
Pwp1-HA
L5
(loading control
Ebp2
L8
Pwp1-subcomplex
Nop7
Cic1
interdependent
A3-factors
Has1
L17
*
Tif6
Rlp24
B-factors
Nog1
Nsa2
Nog2
Nip7
L25
30 ˚C
18 ˚C

Figure 17: Changes in composition of pre-ribosomes in the absence of Pwp1 and Nop12.

(A) Protein constituents of pre-ribosome components purified from the *GAL-HA-PWP1 RPF2-TAP* strain, grown in YEPGal, or shifted to YEPGlu for 16 hours, were resolved by SDS-PAGE and visualized by silver-staining. Stained polypeptide bands of the interdependent A_3 factors are indicated. (B) Pre-ribosome constituents purified in (A) were assayed by western blotting. (C) Pre-ribosomes were purified from wild-type and *nop12Δ* strains using Rpf2-TAP from cells either grown at 30 °C or shifted to 18 °C for four hours. Pre-ribosome constituents were resolved by SDS-PAGE and visualized by silver-staining. (D) Pre-ribosomes purified in (C) were assayed by western blotting. Cuts in the nitrocellulose membrane are indicated with an asterisk (B and D).

2.2.5 The composition of pre-ribosomes is largely unaffected in the absence of Nop12

To investigate changes in pre-ribosome composition in the absence of Nop12, we purified pre-ribosomes from wild-type and *nop12Δ* strains grown at either 30 °C or shifted to 18°C for four hours. SDS-PAGE and silver-staining revealed that pre-ribosomes are largely intact in the absence of Nop12 (Fig. 17C), as the pattern of silver-stained gel bands is clearly different from the that observed in the absence of Pwp1 or other essential A_3 factors (Fig. 17A and Fig. 18). Western blotting confirmed that, even upon shifting the *nop12Δ* strain to 18 °C, there were no significant changes in the levels of the interdependent A_3 factors or the DBP Has1 (Fig. 17D). This is especially interesting because to our knowledge, this is the first example of a ribosome assembly mutant in which the known A_3 factors are associated with pre-ribosomes, but $27SA_3$ pre-rRNA is not efficiently processed. Additionally, we observed no significant changes in the levels of the B factors tested.

To test the requirement of Nop12 for association of other members of the Pwp1 subcomplex, we also examined the levels of Ebp2, Pwp1-HA, and r-protein L8 by western blotting. We observed no changes in the levels of these proteins, even from pre-ribosomes purified from *nop12Δ* cells shifted to 18 °C (Fig. 17D). These results suggest that the Ebp2, Pwp1, and L8 either associate with pre-ribosomes prior to Nop12, or that their association is independent of Nop12.

Taken together, these data suggest that Nop12, although important for processing of $27SA_3$ pre-rRNA, is not directly involved in recruiting other proteins that function during this step of ribosome biogenesis. In the absence of Nop12 at 18 °C, processing of $27SA_3$ pre-rRNA is blocked at levels comparable to the absence of the essential A_3 factors (Fig. 14A and 14B), yet the protein composition of pre-ribosomes is largely unaffected. Furthermore,

this is the first example of a strong block in $27SA_3$ processing that does not lead to significant turnover of pre-rRNAs (data not shown)(Wu et al. 2001). This suggests that the observed defects in pre-rRNA processing in the absence of Nop12 are not due to an incomplete complement of proteins, but rather the pre-rRNA may not be in a conformation to facilitate efficient removal of ITS1.

2.2.6 Pwp1 and Nop12 are not dependent on the A_3 factors for stable association with pre-ribosomes.

It was previously shown that the Pwp1 subcomplex members Ebp2, Brx1, and L8 were able to stably associate with pre-ribosomes in the absence of the interdependent A_3 factors (Sahasranaman et al. 2011). To test the requirement of these proteins for stable binding of Pwp1 and Nop12, we HA-tagged Pwp1 and Myc-tagged Nop12 in an Rpf2-TAP strain conditional for expression of the A_3 factor Rlp7. Upon depletion of Rlp7, SDS-PAGE and silver-staining of affinity purified pre-ribosomes revealed the characteristic pattern of gel bands seen upon depletion of any one of the A_3 factors (Fig. 18, asterisks). Western blotting demonstrated that in the absence of Rlp7, both Pwp1 and Nop12 remain stably associated with pre-ribosomes (Fig. 18). The observed increase of Pwp1 and Nop12 in the absence of Rlp7 most likely represents the enrichment of early pre-ribosomes, and thus these two proteins.

Together, these and the above data suggest a hierarchy of association in which the Pwp1 subcomplex associates with pre-ribosomes prior to stable binding of the interdependent A_3 factors. Association of Nop12 occurs independently of the other A_3 factors; Nop12 is able to associate in the absence of these proteins and conversely, they

stably associate in the absence of Nop12. However, Pwp1 is important for stable recruitment into pre-ribosomes of the interdependent A_3 factors.

FIGURE 18

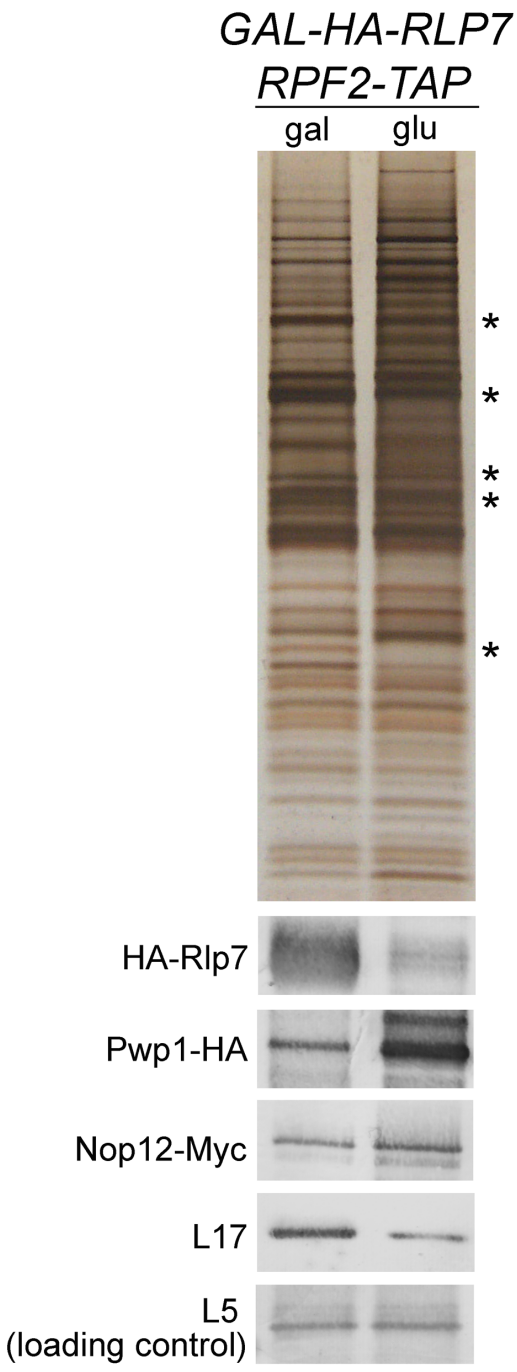

GAL-HA-RLP7
RPF2-TAP
gal
glu
*
*
*
*
*
HA-Rlp7
Pwp1-HA
Nop12-Myc
L17
L5
(loading control)

Figure 18: Pwp1 and Nop12 are not dependent on the interdependent A_3 factors for association with pre-ribosomes.

Pre-ribosome components purified from the *GAL-RLP7 RPF2-TAP PWP1-HA* strain or *GAL-RLP7 RPF2-TAP NOP12-13MYC* strain, were resolved by SDS-PAGE and visualized by silver-staining or subjected to western analysis after transferring to nitrocellulose membrane. R-protein L5 serves as a loading control. Pwp1-HA and Nop12-Myc were detected with anti-HA antibody (12CA5) and anti-myc antibody (9e10), respectively.

2.2.7 Pwp1 and Nop12 are important for proper folding of of 5.8S rRNA.

Pwp1 and Nop12 both contain domains predicted to bind RNA, and Nop12 was shown to crosslink helices 8 and 10 (ITS2-proximal stem) of 5.8S rRNA (Duronio et al. 1992; Wu et al. 2001; Granneman et al. 2011). Furthermore, the absence of both of these proteins results in cold-sensitivity, a phenotype often associated with ribonucleoprotein particles (RNPs) in which the RNA is misfolded or unable to undergo a structural transition (Guthrie et al. 1969; Dammel and Noller 1993). Thus, we hypothesized that these two proteins might be important for structuring 5.8S rRNA and neighboring domain I of 25S rRNA. To investigate this, we used the small chemical dimethylsulfate (DMS) to perform *in vivo* structure probing of pre-rRNAs in the presence or absence of Pwp1 and Nop12 (Wells et al. 2000; Liebeg and Waldsich 2009). DMS methylates the nitrogenous rings of adenines and cytosines in a manner that impedes reverse transcriptase, which can be visualized as primer extension stops (Stern et al. 1988). The extent of methylation is dependent upon the environment of each base: nucleotides that are base-paired, folded into a complex structures, or protected by proteins exhibit low DMS reactivity, whereas unpaired, solvent-accessible bases exhibit high DMS reactivity. To address the role that Pwp1 and Nop12 play in structuring 5.8S rRNA, we treated wild-type, *pwp1Δ*, and *nop12Δ* cells with DMS at 30 °C and 18 °C. The modified RNA was then assayed by primer extension with an oligonucleotide complementary to the 5' half of ITS2. Using an oligonucleotide in ITS2 ensures that we are assaying the structure of 5.8S rRNA sequences in pre-rRNAs and not mature 5.8S rRNA.

Deletion of Pwp1 at both 30 °C and 18 °C resulted in differential DMS reactivity of a number of nucleotides in the 3' half of pre-5.8S rRNA (Fig. 19A, 19C, and 19D). These were

highly specific to this RNP neighborhood as analysis of ITS2 revealed no changes in DMS reactivity (data not shown). The majority of modifications were the same in the absence of Pwp1 at both 30 °C and 18 °C, however there were a greater number of changes at 18 °C, consistent with the cold sensitive phenotype of the *pwp1Δ* strain. The majority of differentially modified nucleotides exhibited increased modification and lie in single-stranded regions, likely reflecting the footprint of Pwp1, Nop12, and/or the other A_3 factors and r-proteins that do not stably associate in the absence of Pwp1. A number of these increased modifications occurred at or near the Nop12 crosslinking site, suggesting Nop12 also fails to associate with pre-ribosomes in the absence of Pwp1 (Fig. 19C and 19D). We also observed increased modification of nucleotides within helices 5 (A2904, A2903), 7 (A2953), and the ITS2-proximal stem (A3010) suggesting at least two possibilities: i) Pwp1 aids in forming these structures during assembly and in its absence these helices form less stably, or ii) deletion of Pwp1 impedes assembly at a step before these helices stably form and their absence enriches for a population of intermediates prior to the formation of these helices. However, because a number of other assembly factors are diminished from pre-ribosomes in the absence of Pwp1, it is difficult to differentiate direct from indirect effects. We also observed a few nucleotides with decreased modification suggesting these nucleotides potentially become base-paired in the absence of Pwp1.

Because pre-ribosomes are largely intact in the absence of Nop12, the observed DMS modification patterns in its absence should be highly specific. Similar to the absence of Pwp1, deletion of Nop12 resulted in increased modification of nucleotides at or near the Nop12 crosslinking sites, and within helices 5, 7, and the ITS2-proximal stem (Fig. 19B, 19C, and 19D). Interestingly, we observed nucleotides with decreased reactivity to DMS

(A2970 and C2971 in helix 8), but only at 18 °C. We also observed decreased DMS modification of nucleotides A2902, A2940, and C2960, indicating that these nucleotides are becoming more protected, possibly through base-pairing. In mature 60S subunits, A2902 is single-stranded and immediately 5' of helix 5 of 5.8S rRNA. Helix 5 is three base-pairs in length and is formed by pairing of G2903, A2904, and A2905 (Fig. 19C and 19D, green) with U2963, U2962, and U2961 (Fig. 19C and 19D, orange), respectively. Interestingly, this sequence (GAA), composing the 5' half of helix 5, is repeated immediately 5' of helix 5 (referred to as GAA*). G2900, A2901, and A2902 (Fig. 19C and 19D, purple) have the potential to base-pair with U2963, U2962, and U2961, respectively. This would also allow the formation of three additional interactions between U2899-G2964, G2903-C2960, and A2904-U2959, resulting in a helix extended by three base-pairs. The observed pattern of DMS modification at 18 °C suggests that in the absence of Nop12, an extended helix 5 is formed by base-pairing of GAA* to U2963, U2962, and U2961.

Together, our data suggest the following: i) In the absence of both proteins at 30 °C, helix 5 is not stably formed, as evident by increased DMS modification of A2903 and A2904 (Fig. 20, left). ii) In the absence of Nop12 at 18 °C, an alternative, yet unproductive helix 5 is formed by pairing of GAA* to the 3' UUU. This accounts for the decreased DMS modification we observe for A2902 and C2960, and the increased modification of A2904 (Fig. 20, right). Although we observed nucleotides with decreased modification in the absence of Pwp1 at both 30 °C and 18 °C, they were not entirely consistent with an alternative helix 5. One potential reason is that the formation of this alternative helix requires stable association of the interdependent A_3 factors. Alternatively, this alternative

helix might not be as evident due to the extensive turnover of pre-rRNAs in the absence of Pwp1 at 18°C.

FIGURE 19

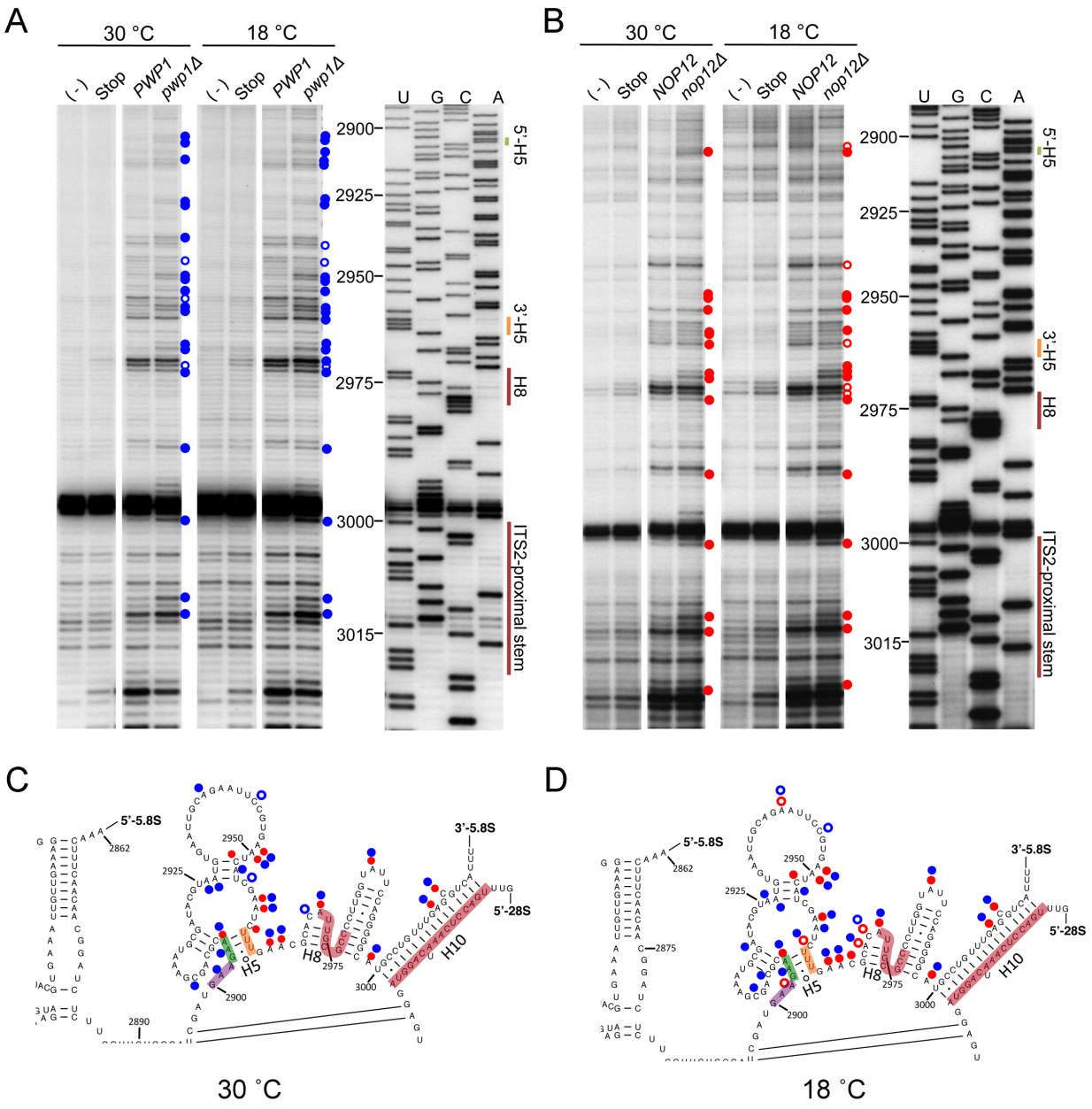

A
30 °C
18 °C
(-)
Stop
PWP1
pwp1Δ
U G C A
2900
2925
2950
2975
3000
3015
5'-H5
3'-H5
H8
ITS2-proximal stem
B
30 °C
18 °C
(-)
Stop
NOP12
nop12Δ
U G C A
2900
2925
2950
2975
3000
3015
5'-H5
3'-H5
H8
ITS2-proximal stem
C
5'-5.8S
3'-5.8S
5'-28S
H5
H8
H10
30 ˚C
D
5'-5.8S
3'-5.8S
5'-28S
H5
H8
H10
18 ˚C

Figure 19: Pwp1 and Nop12 are important for proper folding of 5.8S rRNA.

(A and B) *in vivo* DMS probing of wild-type, *pwp1Δ*, and *nop12Δ* strains visualized by primer extension using an oligonucleotide complimentary to the 5' half of ITS2. Corresponding sequencing lanes (U, G, C, A) with nucleotide positions are shown. Controls include a no DMS control (-) and a Stop control in which β-mercaptoethanol is added to cells prior to DMS. Nucleotides with enhanced DMS modification in the absence of Nop12 and Pwp1 are indicated with solid red and blue circles, respectively. Nucleotides with decreased DMS modification in the absence of Nop12 and Pwp1 are represented with red and blue hollow circles, respectively. (B and C) Changes in nucleotide reactivity at 30 °C (B) and 18 °C (C) are indicated on the secondary structure of 5.8S rRNA as described in (A) (U. Texas). The Nop12 crosslinking sites are highlighted in red. The 5' and 3' halves of helix 5 are highlighted in green and orange, respectively. Nucleotides that have the potential to form an alternative helix 5 are shown in purple.

FIGURE 20

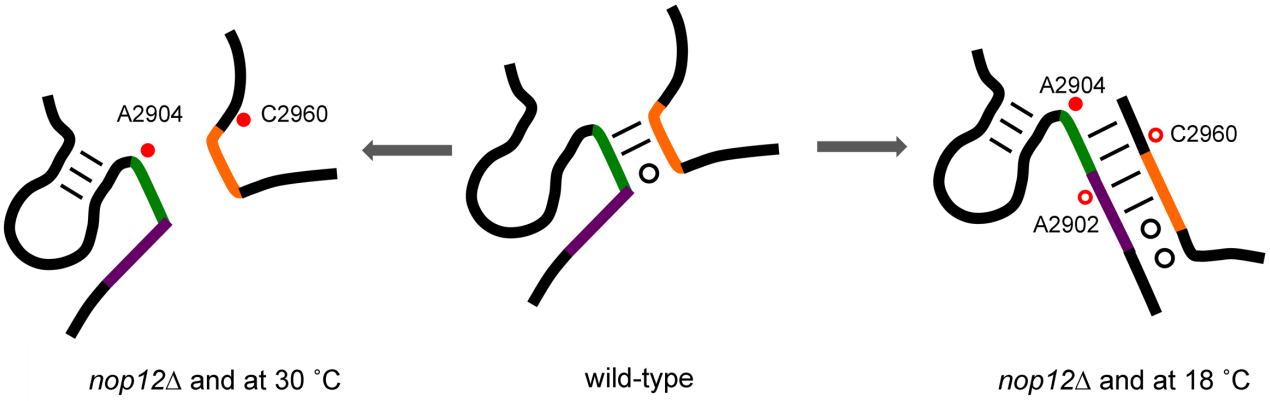

A2904
C2960
A2904
C2960
A2902
*nop12*Δ and at 30 ˚C
wild-type
*nop12*Δ and at 18 ˚C

Figure 20: Helix 5 of 5.8S rRNA is misfolded in the absence of Pwp1 and Nop12.

Model of structural changes that occur in helix 5 in the absence of Nop12 and Pwp1 at 30 °C and 18 °C. In wild-type cells, helix 5 is formed by base-pairing between sequences in green and orange (middle). In the absence of Nop12 and Pwp1, at 30 °C, helix 5 is not stably formed as evident by increased DMS modification of A2904 (left). Decreased modification of A2902 and C2960 indicated that in the absence of Nop12 and Pwp1 at 18 °C, an alternative helix 5 is formed between the upstream GAA* (purple) and the 3' UUU (orange)(right). Changes in DMS reactivity are shown as described in Figure 19.

2.3 Discussion

Processing of $27SA_2$ and $27SA_3$ pre-rRNAs, and subsequent generation of the 5' end of 5.8S rRNA, requires at least 12 AFs and 10 r-proteins (Dunbar et al. 2000; Pestov et al. 2001; Wu et al. 2001; Adams et al. 2002; Gadal et al. 2002; Oeffinger et al. 2002; Fatica et al. 2003b; Oeffinger and Tollervey 2003; Miles et al. 2005; Poll et al. 2009; Jakovljevic et al. 2012; Shimoji et al. 2012)(M. Gamalinda, submitted). Numerous physical and genetic interactions exist among these proteins, suggesting that they function in a highly cooperative manner to form pre-ribosomes competent to undergo removal of ITS1. At least 12 of these proteins can be isolated in one of three subcomplexes. These include (i) the Pwp1 subcomplex (Krogan et al. 2004; Zhang et al. 2004), (ii) the Nop7 subcomplex composed of Nop7, Erb1, and Ytm1 (Miles et al. 2005), and (iii) the ITS2 subcomplex containing Cic1, Nop15, and Rlp7 (J. Dembowski, submitted)

Isolation of assembly subcomplexes was initially achieved by affinity purifying AFs under conditions that disrupt interactions within the pre-ribosome (Harnpicharnchai et al. 2001; Horsey et al. 2004; Miles et al. 2005). These subcomplexes are thought to represent the most stable interactions between AFs and r-proteins, and thus are thought to reflect groups of proteins that function cooperatively during ribosome biogenesis. At least nine subcomplexes function in construction of 60S ribosomal subunits (Xue et al. 2000; Harnpicharnchai et al. 2001; Milkereit et al. 2001; Krogan et al. 2004; Nissan et al. 2004; Zhang et al. 2004; Miles et al. 2005; Lebreton et al. 2006b; Rosado et al. 2007; Zhang et al. 2007; Merl et al. 2010; Hierlmeier et al. 2012; Talkish et al. 2012). High-speed centrifugation of whole cell extracts, followed by affinity purification, or sedimentation of whole cell extracts on sucrose gradients and subsequent isolation of subcomplexes from

light fractions showed that some subcomplexes exist independently of pre-ribosomes. Consistent with this, recent work from the Milkereit group showed that subcomplexes could be isolated upon shutting down transcription of rDNA, and thus independently of nascent pre-ribosomes (Merl et al. 2010). By assembling *en bloc*, subcomplexes are thought to function as discrete building blocks, minimizing complexity and ensuring efficient assembly of these highly complex RNPs.

Work from our lab has shown that three of these subcomplexes assemble into pre-ribosomes in a coordinated and hierarchical manner. We have previously shown that: (i) binding of Ebp2 is required for association of Brx1 (Shimoji et al. 2012), (ii) both Ebp2 and Brx1 are required for binding of r-protein L8 (Shimoji et al. 2012), (iii) L8 is required for binding of the interdependent A_3 factors Nop7, Erb1, Ytm1, Cic1, Nop15, and Rlp7 (Jakovljevic et al. 2012), (iv) and all of the aforementioned proteins are required for stable association of the DBPs Drs1 and Has1 (Sahasranaman et al. 2011; Dembowski et al. 2013). In the absence of any of these proteins, ITS1 is not removed and pre-ribosomes are unstable and turned over.

Here we have begun to analyze the function of the previously uncharacterized AF Pwp1, and further characterized the A_3 factor Nop12. We show that like Nop12, Pwp1 is a non-essential protein that functions in production of 60S ribosomal subunits. Although cells are viable in the absence of Pwp1, their growth is severely compromised at 30 °C and they are inviable at low temperatures. Like other members of the Pwp1 subcomplex, Pwp1 associates with pre-ribosomes early in biogenesis and is necessary for efficient processing of $27SA_2$ and $27SA_3$ pre-rRNAs. We have been able to further refine the association hierarchy of proteins that function in this step of assembly by showing that Pwp1 is

upstream of the interdependent A_3 factors; Pwp1 is important for stable association of these proteins, but not vice versa. Nop12 however, does not play an active role in recruiting other A_3 factors. Last, we show that Nop12 and Pwp1 are required for proper folding of 5.8S rRNA and the ITS2 proximal stem. In the absence of these proteins, particularly when cells are grown at low temperature, 5.8S rRNA sequences within pre-rRNAs are misfolded and $27SA_3$ pre-rRNA is unable to be efficiently processed.

In most of our assays, deletion of Pwp1 results in the same phenotype as deletion of Nop12, only stronger. The *nop12Δ* strain behaves like a traditional cold-sensitive mutant, growing at nearly wild-type rates at 30 °C but much more slowly when cells are shifted to 18 °C. However, deletion of Pwp1, although non-lethal, results in an extremely slow growth phenotype at 30 °C, and lethality at 18 °C. Pwp1 is a WD-40 protein, whereas Nop12 is an RRM-containing RNA binding protein (Duronio et al. 1992; Wu et al. 2001). Pwp1, through its WD-40 motif, may participate in a greater number of interactions with the interdependent A_3 factors. Thus, in the absence of Pwp1, one might expect greater perturbations in pre-ribosome structure and thus stronger assembly defects and growth phenotypes. Consistent with this, examination of pre-ribosomes revealed no changes in the interdependent A_3 factors in the absence of Nop12, but decreased association of those proteins in the absence of Pwp1. Our recent investigations of A_3 factors show that pre-rRNAs are rapidly turned over in their absence, however it was unclear if this results from a failure to process $27SA_3$ pre-rRNA or the A_3 factors failing to stably associate with pre-ribosomes (Sahasranaman et al. 2011; Jakovljevic et al. 2012; Dembowski et al. 2013). Interestingly, pre-rRNAs are not turned over in the absence of Nop12 (Wu et al. 2001)(data

not shown), suggesting that turnover is a result of an incomplete set of assembly factors, and not simply due to unprocessed $27SA_3$ pre-rRNA.

High-resolution crystal structures of the yeast ribosome, as well as newly developed protein-RNA crosslinking approaches, indicate that the Pwp1, Nop7, and ITS2 subcomplexes bind pre-ribosomes adjacent to each other, near domain I of 25S/5.8S rRNA and ITS2 (Fig. 11). Using UV crosslinking and analysis of cDNA (CRAC), it was shown that Nop12 crosslinks to pre-rRNA sequences within the ITS2-proximal stem as well as helix 8 at the 5' end of 5.8S rRNA (Granneman et al. 2011). This is in close proximity to the binding sites of r-proteins L8 and L15 in mature 60S subunits (Ben-Shem et al. 2011). Two-hybrid interactions between Ebp2-Brx1 and Ebp2-Nop12 suggest that Brx1 and Ebp2 also occupy this neighborhood (Shimoji et al. 2012). The Nop7 subcomplex is thought to lie adjacent to the Pwp1 subcomplex. CRAC analysis revealed that Erb1 and Nop7 crosslink to sequences in domain I and domain III of 25S rRNA, respectively (Granneman et al. 2011). Last, Cic1, Nop15, and Rlp7 crosslink to sequences in ITS2 and the ITS2 proximal stem (Granneman et al. 2011; Babiano et al. 2013)(J. Dembowski, submitted). Thus, these three subcomplexes are positioned near each other within pre-ribosomes, occupying mostly domain I of 5.8S/25S rRNA and ITS2 (Fig. 11).

Interestingly, these proteins associate with pre-ribosomes near the 3' end of 5.8S rRNA, yet they are necessary for the removal of ITS1 and generation of the 5' end of 5.8S rRNA (Fig. 11). In mature 60S subunits, the 5' end of 5.8S rRNA is situated ~160Å from the 3' end. Depletion of the AFs that cluster around the 3' end of 5.8S rRNA and/or bind to ITS2 causes ITS2 to misfold, but results in a failure to remove ITS1 (Dunbar et al. 2000; Gadal et al. 2002; Fatica et al. 2003b; Oeffinger and Tollervey 2003; Granneman et al. 2011)

(J. Dembowski, submitted). These results highlight two key principles that drive processing of $27SA_3$ pre-rRNA: 1) Proper folding of ITS2 is at least in part a prerequisite for removal of ITS1, and 2) There is long-range communication between the removal of ITS1 and subsequent formation of the 5' end of 5.8S rRNA, and removal of ITS2 and generation of the 3' end of 5.8S rRNA.

Pioneering studies of bacterial ribosome biogenesis from Nomura and coworkers used genetic screens to identify cold-sensitive mutants defective in ribosome assembly *in vivo* (Guthrie et al. 1969). They rationalized that because *in vitro* assembly requires heating the reaction at an intermediate step, presumably to cause structural rearrangements of the assembling particle, ribosome assembly *in vivo* would also be temperature dependent. Thus, defects in ribosome assembly might be exacerbated at low temperatures. The temperature dependent nature of ribosome assembly, as well as other RNP particles, reflects the ability of RNA to fold into a myriad of secondary and tertiary structures. As RNA folds, it samples a number of different conformations as it transitions to its native, functional state (Woodson 2010). Many of these conformations are nonfunctional and represent kinetic traps that must be overcome. At low temperature, greater amounts of energy are needed for an RNA to transition from one conformer to the next, increasing the likelihood that it will fall into a kinetic trap. During ribosome biogenesis, these kinetic traps and energy barriers are thought to be overcome in part by AFs and r-proteins (Culver 2003; Shajani et al. 2011).

Analysis of pre-ribosomal particles in the absence of Nop12 revealed few changes in their composition. This is in contrast to depletion of Pwp1 or the essential, interdependent A_3 factors that cause a number of changes in pre-ribosome composition. The

interdependent nature of the A_3 factors often makes it difficult to tease apart direct from indirect effects, making RNA structure probing studies difficult to interpret. Although non-essential, deletion of Nop12, especially in the cold, results in the accumulation of unprocessed $27SA_3$ pre-rRNAs to a similar extent as depletion of the essential A_3 factors (compare to *GAL-RLP7*). Because the composition of pre-ribosomes appears to be unaffected when Nop12 is not present in pre-ribosomes, any changes in RNA structure should be highly specific to the absence of Nop12. Thus, our data suggest that the defects observed in $27SA_3$ pre-rRNA processing in the absence of Nop12 are not due to an incomplete inventory of AFs and r-proteins, but rather are due to misfolded RNA.

In this study we show that Pwp1 and Nop12 function to assist in folding 5.8S rRNA. *In* vivo structure probing of pre-rRNAs revealed that in the absence of these proteins, 5.8S sequences in pre-rRNAs are misfolded. The changes we observed in pre-rRNA structure are highly specific to the absence of Pwp1 and/or Nop12 and appear to be localized to the RNP neighborhood in which they bind. Of particular interest is helix 5. In mature 60S subunits, this three base-pair helix is generated by base pairing of a 5' AAG to a 3' UUU. Our results suggest that in the absence of Pwp1 and Nop12, at 30 °C, helix 5 is not stably formed. This was evident by increased DMS accessibility to A2904 of the 5' half of helix 5. However, in the absence of Nop12 at 18 °C, our DMS probing data are consistent with the formation of an alternative helix 5. This alternative helix 5 is generated by base pairing of an AAG (AAG*), repeated immediately upstream of the AAG that composes helix 5, to the 3' UUU. Base-pairing of the AAG* to the 3' UUU would allow the original AAG to participate in additional base-pairs, resulting in an alternative helix 5 that is extended by three base-pairs. These results are reminiscent of work from Dammel and Noller which showed that a

mutation in 16S rRNA that confers cold-sensitivity is due to competition between two helices, only one of which is productive (Dammel and Noller 1993). What remains to be determined is whether the alternative helix 5 is an on-pathway folding intermediate that is normally resolved with the assistance of Nop12, or whether this is simply a kinetic trap that occurs at low temperature. In mature subunits, helix 5 is in close proximity to a number of r-proteins surrounding the polypeptide exit tunnel. R-proteins L17, L26, L35, and L37 fail to stably associate with pre-ribosomes in the absence of the interdependent A_3 factors (Sahasranaman et al. 2011). These proteins associate with pre-ribosomes early during assembly, but are not stably incorporated into pre-ribosomes until after removal of ITS1. Rearrangement of pre-rRNA structures during $27SA_3$ processing might allow these r-proteins to participate in greater number of protein-RNA interactions and thus integrate more tightly into the ribosome structure. Thus, a more interesting possibility is that the alternative helix 5 is a normally occurring structure that is refolded before or during $27SA_3$ processing to form the helix 5 observed in the mature 60S subunits, and to help tighten the association of the surrounding r-proteins. Our working hypothesis is that during and immediately after removal of ITS1, 5.8S rRNA undergoes a series of conformational changes. These conformational changes achieve two goals; i) efficient removal of ITS1 (and possibly ITS2) and ii) stable integration of the r-proteins surrounding the exit tunnel.

The complex network of interactions among the A_3 factors, as well as their known locations within the pre-ribosome suggest long range communication between the 5' and 3' ends of 5.8S rRNA. Because the removal of spacer sequences is an irreversible process, their excision from pre-rRNAs is thought to act as checkpoints during ribosome biogenesis. By coupling the removal of two spacers (ITS1 and ITS2), the cell may have evolved

additional layers of regulation, ensuring that both spacers are competent for removal before the first spacer is excised. Our *in vivo* RNA structure probing data show that relatively small perturbations in rRNA structure are sufficient to disrupt pre-rRNA processing and spacer removal. This is not surprising since RNA folding is inherently cooperative, ensuring that RNAs proceed down a smooth folding landscape to form their native structures (Dill and Chan 1997; Pan et al. 1997; Chauhan et al. 2009; Shajani et al. 2011). We speculate that the long-range communication between the two ends of 5.8S rRNA is facilitated by an intricate network of protein-protein and protein-RNA interactions between the Pwp1, Nop7, and the ITS2 subcomplexes. The absence of Nop12 and Pwp1 results in a weakening, but not complete loss, of some of these interactions and a breakdown in communication between the 5' and 3' ends of 5.8S rRNA. Although the number of changes observed in the secondary structure of pre-rRNAs was small in the absence of Nop12 and Pwp1, we believe these changes are highly specific and could have profound consequences on the stability of tertiary interactions within 5.8S rRNA. *In vitro* folding studies of ribozymes have shown that the loss of a single base-pair or disruption of a single tertiary interaction can have drastic results and cause global misfolding of RNA (Silverman et al. 1999; Chauhan and Woodson 2008; Chauhan et al. 2009).

2.4 Materials and Methods

Construction of yeast strains

Yeast strains used in this study were derived from JWY6147, W303, or S288C and are listed in Table 5. *nop12Δ* and *pwp1Δ* strains were constructed as described in (Longtine et al. 1998). PCR products containing the *HIS3* gene and sequences complementary to either

NOP12 or *PWP1* were transformed into diploid W303 and transformants were screened on selective media lacking histidine. Correct integration of the *HIS3* gene at the *NOP12* and *PWP1* loci was verified by PCR. Diploids were sporulated and tetrads were dissected. Individual spores were screened for the ability to grow on c-his media and correct gene disruptions were verified by PCR.

A yeast strain conditional for Pwp1 expression was constructed as described in Longtine *et al*. (1998). Briefly, sequences containing the selectable marker *KANMX6* , plus the *GAL1* promotor sequence followed by an ATG and sequences encoding 3HA were amplified by PCR. PCR products were transformed, as described in Rigaut *et al*. (1999), into JWY6147 and transformants were screened for their ability to grow on selective media containing galactose. $G418^r$ transformats were screened for correct integration of the *GAL1* promotor and 3HA tag by western blotting with anti-HA sera.

Yeast strains expressing C-terminal TAP-tagged Rpf2, 13Myc-tagged Nop12, and 3HA-tagged Pwp1 were constructed by PCR of a selectable marker (TAP, *URA3*; 13Myc and 3HA, *KANMX6*) and transformation as previously described (Longtine et al. 1998; Rigaut et al. 1999). Transformants that grew on selective media were screened for correct integration of the PCR product and expression of the tagged protein by SDS-PAGE and western blotting.

Growth of yeast strains

Unless otherwise indicated, strains were grown in either YEPGlu (2% dextrose, 2% peptone, and 1% yeast extract) or YEPGal (2% glactose, 2% peptone, and 1% yeast extract) at 30 °C. *nop12Δ* and *pwp1Δ* strains were grown at the permissive temperature of 30 °C

and then shifted to either 18 °C or 37 °C for 4 hours. *GAL-HA3-PWP1* and *GAL-HA3-RLP7* strains were grown in liquid YEPGal, pelleted by centrifugation, susupended in YEPGlu, and grown for indicated times to deplete Pwp1 and Rlp7. Growth of the *GAL-HA3-PWP1* strain and depletion of Pwp1 was assessed by growth in liquid YEPGal or YEPGlu. Cells were continually diluted to ensure exponential growth and growth was monitored with a Genesis 20 spectrophotometer (Thermo Fisher Scientific). Aliquots were taken at indicated time points and assayed by SDS-PAGE and western blotting against 3HA-Pwp1. An antibody against Sec61 serves as a loading control. Growth of the *nop12Δ* and *pwp1Δ* strains was assessed at 18 °C, 30 °C, and 37 °C by spotting serial dilutions (undiluted to 1:100,000) of liquid cultures on solid YEPGlu medium.

RNA analysis

RNA from whole cell lysates was extracted and assayed by northern blotting, primer extension, and pulse-chase as previously described (Horsey et al. 2004). Pulse-chase analysis was performed using [^{3}H-methyl]-methionine. For northern blotting and primer extension, RNA was quantified using a Nano Drop 2000C spectrophotometer (Thermo Fisher Scientific). 5 ug of RNA was used in each lane or reverse transcription reaction.

Protein extraction, SDS-PAGE, and western blot analysis

Proteins in whole cell extracts were prepared for gel electrophoresis by dissolving in SDS sample buffer as previously described (Ausubel et al. 1994). Proteins were recovered from eluates during affinity purification by precipitation with 10% TCA and suspended in SDS sample buffer. Proteins were resolved by electrophoresis on 4%-20% Tris-Glycine Novex

gels (Invitrogen). To assay Nog2 by western blotting, 4%-12% Bis-Tris gels (Invitrogen) were used, since Nog2 co-migrates with IgG on 4%-20% Tris-Glycine gels. Proteins from whole cell extracts and affinity-purified pre-ribosomes were assayed by western blotting as previously described (Ausubel et al. 1994). To enable detection of multiple proteins from a single blot and to conserve antiserum, after electroblotting, nitrocellulose membranes were cut based on the known mobility of the proteins of interest. Visible cuts in the membrane are indicated with asterisks in the figures. TAP-tagged proteins were detected using alkaline phosphatase conjugated to IgG (Pierce). Mouse monoclonal antibodies 12CA5 (Roche) and 9e10 (Developmental Studies Hybridoma Bank) were used to detect HA-tagged and Myc-tagged proteins, respectively. Otherwise, antibodies specific to r-proteins or AFs were used. AP-conjugated anti-mouse or anti-rabbit secondary antibodies (Promega) were used, and proteins were visualized by colorimetric detection using NBT and BCIP (Promega).

Affinity purification of pre-ribosomes

Ribosome assembly intermediates were affinity-purified from whole cell extracts with magnetic Dynabeads (Invitrogen), using TAP-tagged Rpf2, as previously described (Sahasranaman et al. 2011). Rpf2 associates with pre-ribosomes early during biogenesis, with 35S or $27SA_2$ pre-rRNA, and is present in each consecutive 66S intermediate. Furthermore, association with pre-ribosomes of Rpf2 is not affected upon depletion of other proteins required for $27SA_2$ or $27SA_3$ pre-rRNA processing.

Sucrose gradient assays of ribosomes and polyribosomes

Pre-ribosomes, ribosomes, and polyribosomes were fractionated from 40 OD_{254} units of whole cell extracts on 7%-47%(w/v) sucrose gradients as previously described (Deshmukh et al. 1993), with the following modifications. Cycloheximide (5 mg) was added to cultures twenty minutes before harvesting cells. A Teledyne ISCO Foxy R1 density gradient fractionator was used to fractionate and analyze gradients.

In vivo DMS probing

In vivo structure probing using dimethyl sulfate (DMS) was performed as previously described (Babiano et al. 2012). Briefly, 10 ml of cells were grown in YEPGlu to an OD_{610} of 0.4 and incubated with 200 µl of a fresh dilution (1:4 vol/vol in 95% ethanol) of DMS (Sigma-Aldrich) for 2 min. Reactions were quenched by placing the tubes on ice and adding of 5 ml of water-saturated isoamyl alcohol and 5 ml of 0.6M β-mercaptoethanol. Cells were pelleted, washed again in 0.6M β-mercaptoethanol, and RNA was immediately phenol extracted.

Nucleotide modifications were assayed by primer extension with Transcriptor reverse transcriptase (Roche) and oligonucleotides complementary to ITS2 as previously described in Liebeg and Waldsich (2009) with the following changes. For each reaction, 2.5 µl (3 µg) of whole-cell RNA was incubated with 1 µl (0.2 µM) of ^{32}P-labeled primer and 1 µl of 4.5x hybridization buffer (225 mM Hepes pH 7.0; 450 mM KCl) at 95 °C for 5 minutes. Reactions were then cooled to the annealing temperature of 54 °C for 20 minutes. 15 µl of pre-warmed (54 °C) extension mix containing 4 µl of 5X hybridization buffer (Roche Applied Science) (250 mM Tris-HCl; 150 mM KCl; 40 mM $MgCl_2$, pH is approximately 8.5), 2.0 µl 2.5 mM dNTP mixture, 1.0 µl 0.1 mM DTT, 0.5 µl (20U) RNasin (Promega), 0.5 µl

(10U) Transcriptor Reverse Trascriptase (Roche Applied Science), and 7.5 µl of nuclease free water was added to each reaction. For sequencing reactions, 2 µl of the appropriate ddNTP (10 mM) (Roche Applied Science) was also added. Reactions were incubated at 54 °C for one hour. RNA was degraded by the addition of 3 µl 1M NaOH to each reaction and incubation at 55 °C for one hour. Reactions were neutralized by the addition of 3 µl 1.0 M HCl. cDNAs were precipitated with 1 µl of glycogen (10 mg/ml), 1 µl 0.5 M EDTA pH 8.0, 2.8 µl 3.0 M NaOAc pH 5.0, and 84 µl of ethanol. Following ethanol precipitation, dried cDNA pellets were resuspended in 6 µl of 1X loading dye (45% formamide; 0.01 M EDTA pH 8.0), resolved on 6% polyacrylamide/7M urea gels, and visualized by autoradiography. Oligonucleotide sequences are available in Table 6.

Fluorescence microscopy

Export of pre-ribosomes to the cytoplasm was assayed by monitoring the cellular localization of r-protein L25-eGFP as previously described in Babiano *et al*. (2012). Wild-type and *pwp1Δ* strains were transformed with pRS316 plasmid constructs co-expressing the nucleolar marker mRFP-Nop1 and L25-eGFP (Ulbrich et al. 2009). Cells were imaged using a Carl Zeiss LSM-510 META UV DuoScan inverted spectral confocal microscope and analyzed using ImageJ (Schneider et al. 2012).

ACKNOWLEDGEMENTS

I would like to thank the following people for generously providing antibodies: Jesús de la Cruz and Patrick Linder (Has1), Janine Maddock (Nog1), David Goldfarb (Nip7), Cosmin Saveanu and Micheline Fromont-Racine (Tif6, Rlp24, Nsa2 and Nog2), Michael McAlear

(Ebp2), Arlen Johnson (rpL8), Sabine Rospert (rpL17), Katja Siegers (rpL25), Elizabeth Tosta (Cic1). I would also like to thank Ed Hurt for providing the L25 eGFP Nop1-mRFP plasmid and Haibing Teng of the Molecular Biology Imaging Center at Carnegie Mellon University for training and assistance with microscopy.

CHAPTER 3: Disruption of ribosome biogenesis in yeast blocks co-transcriptional pre-rRNA processing and affects the global hierarchy of ribosome biogenesis

PREAMBLE

This chapter focuses on two different but related stories. My thesis work began by investigating the role of the DEAD-box protein Drs1 during ribosome assembly. Our initial hypothesis was that Drs1, through ATP hydrolysis, releases assembly factors from pre-ribosomes. We arrived at this hypothesis after purifying pre-ribosomes in the absence of Drs1 and observing enrichment of a number of assembly factors associated with these particles. Many of these assembly factors were known to be released from pre-ribosomes during the steps of assembly in which Drs1 functions. However, we came to realize our hypothesis was not proven by these results and thus I subsequently switched to a different project: investigating the roles of the assembly factors Nop12 and Pwp1 (Chapter 2). While studying these factors, new views emerged about ribosome assembly, primarily that early steps of pre-rRNA processing occur co-transcriptionally. In light of these new ideas, I reinterpreted much of the data I generated regarding Drs1, and came to the conclusion that in the absence of Drs1, early pre-rRNA processing steps switch from primarily occurring co-transcriptionally to occurring post-transcriptionally. Here we present data that indicates that when this occurs, the overall hierarchy of ribosome biogenesis changes. Because post-transcriptional processing does occur a fraction of the time in wild-type cells, this work supports *in vitro* analyses showing that ribosome assembly can occur through multiple, different, parallel pathways.

Work from our lab on a number of different assembly mutants suggests that this effect is not necessarily specific to Drs1, but rather due to disruption of 60S subunit biogenesis. Our working hypothesis is that disruption of ribosome biogenesis leads to decreased cell growth and division, resulting in a shift from co- to post-transcriptional pre-rRNA processing. Here I will initially summarize my investigations of Drs1 and then present data supporting our new hypothesis.

3.1 INTRODUCTION

The principles learned about hierarchical assembly of bacterial ribosomes *in vitro* have largely framed the way ribosome assembly is studied in eukaryotes *in vivo*. Purification of pre-ribosomal intermediates revealed that there is a global hierarchy of association of assembly factors with pre-ribosomes (Nissan et al. 2002). Some assembly factors associate with pre-ribosomes very early in assembly, others that associate during middle steps of assembly, those that bind to pre-rRNPs at the end of assembly, and a few that are present in particles throughout assembly. The hierarchical association of these factors, and the subsequent irreversible removal of spacer sequences from pre-rRNA, is thought to provide directionality to ribosome biogenesis, thus ensuring that assembly occurs in the proper order, and that late steps of assembly do not occur prematurely (Strunk and Karbstein 2009).

Recently, a number of studies have shown that in addition to hierarchical assembly between steps of biogenesis (early, middle, and late pre-ribosome intermediates), there is a more refined hierarchy of association within each step. As discussed in Chapter 2, Brx1 and Ebp2 are two assembly factors required for processing of 27SA pre-rRNAs. Both of these proteins associate early in assembly, with pre-ribosomes containing 35S and $27SA_2$ pre-rRNAs (Shimoji et al. 2012). A more careful analysis revealed a hierarchy in which Ebp2 associates with pre-ribosomes first and is necessary to recruit Brx1. Another example of hierarchical assembly is evident from recent work about a group of fourteen assembly factors required for 27SB pre-rRNA processing (Appendix 5.1). Most of these factors associate early with pre-ribosomes containing 35S or $27SA_2$ pre-rRNA (Saveanu et al. 2003; Graindorge et al. 2005; Saveanu et al. 2007; Zhang et al. 2007; Garcia-Gomez et al. 2011),

whereas two of these factors associate in the middle of assembly with pre-ribosomes containing 27SB pre-rRNA (Saveanu et al. 2001; Lebreton et al. 2006a). By systematically depleting each of these factors it was shown that even though the majority of them associate with early pre-ribosomes, they become more stably incorporated into pre-ribosomes in a hierarchical manner (Talkish et al. 2012). This presumably reflects changes in the pre-rRNA structure as these particles mature.

Traditionally, ribosome assembly is yeast has been portrayed as beginning with transcription of a 35S pre-rRNA and the formation of a 90S pre-ribosome in the nucleolus. The 35S pre-rRNA contains sequences for mature 18S, 5.8S, and 25S rRNAs as well as spacer sequences that are removed through a series of endo- and exonucleolytic cleavages (Woolford and Baserga, in press)(Fig. 3A and 4A). Cleavage of 35S pre-rRNA at the A_0, A_1, and A_2 sites separates the maturation of 43S pre-ribosomes from 66S pre-ribosomes. However, recent electron microscopy and rapid pulse-chase analyses have shown that in rapidly dividing yeast cells, ~70-80% of pre-rRNA transcripts are cleaved at the A_2 site before transcription of the pre-rRNA is completed (Osheim et al. 2004; Kos and Tollervey 2010). Thus, the majority of ribosome assembly actually initiates with 43S pre-ribosomes that contain 20S pre-rRNA and 66S pre-ribosomes that contain $27SA_2$ pre-rRNA (Fig. 3B and 4B).

Previously we showed that the DEAD-box protein (DBP) Drs1 functions in 60S subunit biogenesis and that missense mutations in Drs1 block 27SB pre-rRNA processing (Ripmaster et al. 1992; Adams et al. 2002). Here we show that depletion of Drs1 affects earlier steps of pre-rRNA processing, suggesting that Drs1 may function in more than one consecutive step of ribosome assembly. Furthermore, we show that Drs1 physically and

functionally interacts with a subcomplex of proteins containing the assembly factors Nop7, Erb1, and Ytm1. Depletion of this subcomplex results in a failure of Drs1 to associate with pre-ribosomes, suggesting Drs1 is physically recruited to pre-ribosomes by this group of proteins.

Most importantly, careful examination of the composition of pre-ribosomes upon depletion of Drs1 revealed a novel phenotype that we believe results from a shift from co-transcriptional pre-rRNA processing to post-transcriptional pre-rRNA processing. Disruption of co-transcriptional cleavage at the A_2 site, and transition to post-transcriptional cleavage, results in the formation of pre-ribosomal intermediates that contains both early- and late-associating assembly factors and r-proteins that do not coexist in the same particles when processing occurs co-transcriptionally. This was most evident by the fact that we see late-binding 66S assembly factors (Nog2, Arx1, and Lsg1) as well as late-associating 40S r-proteins (S3 and S20) associating with 35S pre-rRNA. Furthermore, we show that when cells are grown to high density, a greater fraction of pre-rRNA processing occurs post-transcriptionally, and follows an alternative pathway, expanding upon previously published data and highlighting the relationship between cell growth rates and ribosome biogenesis.

Together, these data show that the neighborhoods or binding sites of late associating assembly factors have the potential to also form very early in ribosome biogenesis, before pre-rRNA processing removes spacer sequences, thus changing the global hierarchy of ribosome biogenesis. Furthermore, this raises the question of how the sites for late associating proteins are created through cooperative and hierarchical protein-binding and RNA-folding events.

3.2 RESULTS

3.2.1 Drs1 is required for processing $27SA_2$ and $27SA_3$ pre-rRNAs

We previously showed that cold-sensitive *drs1* missense mutants block ribosome assembly, resulting in a deficit of 60S subunits, but not 40S subunits (Ripmaster et al. 1992). Pulse-chase analysis showed that upon shifting to the cold, *drs1* mutants accumulate 27SB pre-rRNA and do not produce 25S rRNA, but maturation of 18S was unaffected (Fig. 21) (Adams et al. 2002). Because the mutant Drs1 proteins are stable and can still assemble into pre-ribosomes (J. Talkish, data not shown), we wanted to test the effect on ribosome assembly of a *drs1* null mutant. To do so, we placed *DRS1* under control of the *GAL1* promoter. We assayed pre-rRNA processing upon depletion of Drs1 by northern blotting, primer extension, and pulse-chase analysis. Depletion of Drs1 results in a strong accumulation of $27SA_2$ and $27SA_3$ pre-rRNAs as early as 4 hours after shifting cells to YEPGlu (Fig. 22A, lane 2 and Fig. 22B), and a significant increase in 35S and 33S/32S pre-rRNAs at later time points (Fig. 22A, lanes 3 and 4 and Fig. 22C). Pulse-chase experiments showed that pre-rRNAs destined for the 60S subunit are either never made, or rapidly turned over. Furthermore, the 35S pre-rRNA that accumulates upon depletion of Drs1 can be processed to 18S rRNA, but pre-rRNAs that are normally processed to 5.8S rRNA and 25S rRNA are unstable. This was accompanied by a decrease in mature 25S rRNA (Fig. 22A and C). The decrease in 20S pre-rRNA suggests that 18S rRNA is generated through direct cleavage of 35S pre-rRNA at the A_3 site, and subsequent processing of 23S pre-rRNA (Fig. 22A and 22C). We conclude that depletion of Drs1 blocks processing of $27SA_2$ and $27SA_3$ pre-rRNAs, resulting in turnover of 66S pre-ribosomes. This is in contrast to *drs1* missense

mutants in which the subsequent step in assembly, processing of 27SB pre-rRNA, is blocked.

FIGURE 21

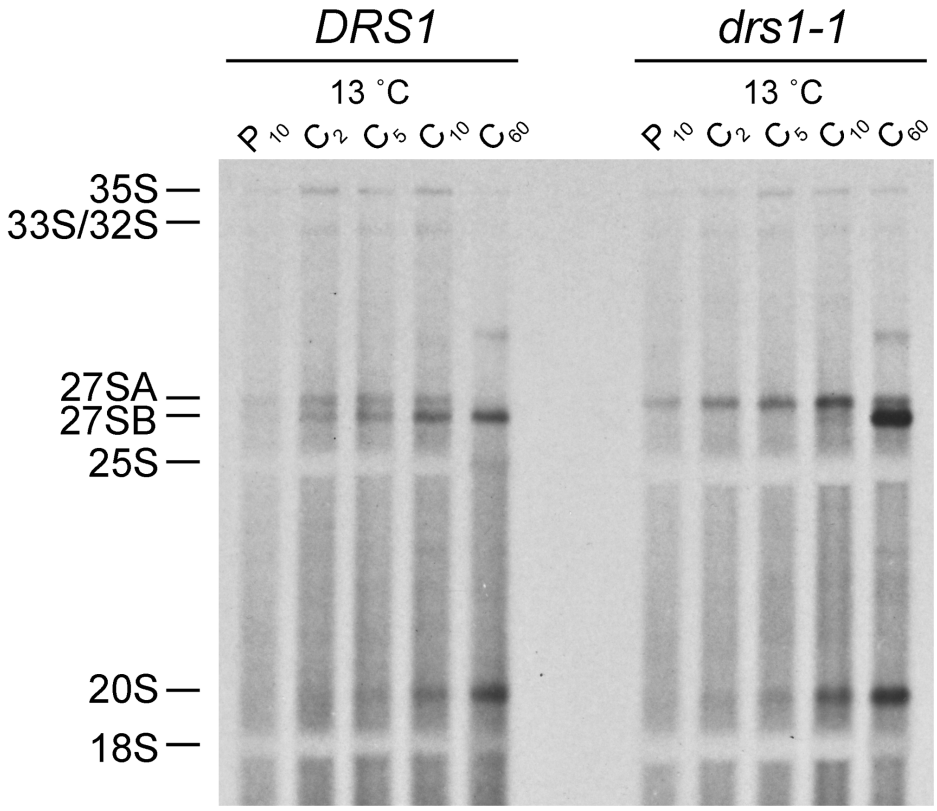

DRS1
drs1-1
13 ˚C
13 ˚C
P
10
C2
C5
C10
C60
P
10
C2
C5
C10
C60
35S
33S/32S
27SA
27SB
25S
20S
18S

Figure 21: *drs1* missense mutants block 27SB pre-rRNA processing.

To assay synthesis and turnover of pre-rRNA intermediates in the missense mutants, wild-type and *drs1-1* strains were grown in C-met media at 30 °C and subsequently shifted to the non-permissive temperature of 13 °C for 4 hours. Cells were pulse-labeled with [^{3}H methyl]-methionine for 10 minutes and chased with a molar excess of unlabeled methionine for 2, 5, 10, and 60 minutes. Total RNA was extracted and separated on a 1.2% agarose-6% formaldehyde gel.

FIGURE 22

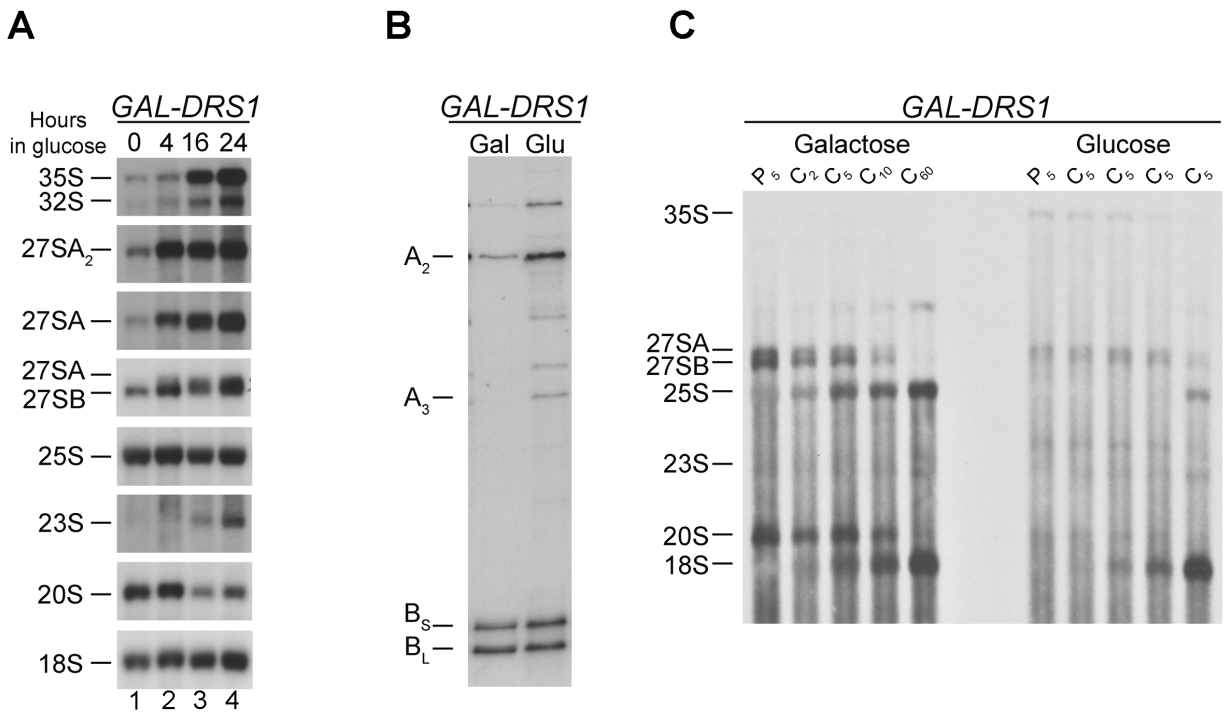

A
GAL-DRS1
Hours in glucose
0 4 16 24
35S
32S
27SA2
27SA
27SA
27SB
25S
23S
20S
18S
1 2 3 4
B
GAL-DRS1
Gal Glu
A2
A3
BS
BL
C
GAL-DRS1
Galactose
Glucose
35S
27SA
27SB
25S
23S
20S
18S

Figure 22: Depletion of Drs1 blocks $27SA_2$ and $27SA_3$ pre-rRNA processing

(A) To assay steady-state levels of pre-rRNAs in the absence of Drs1, the *GAL-HA-DRS1* strain was grown in YEPGal or shifted to YEPGlu media for the indicated time points. Total RNA was extracted from cells and separated on a 1.2% agarose-6% formaldehyde gel. Pre-rRNAs were assayed by northern blotting using oligonucleotide probes specific for each intermediate. (B) The steady-state levels of the 5' ends of 27S pre-rRNAs were assayed by primer extension. RNA was extracted from the *GAL-HA-DRS1* strain grown in YEPGal or shifted to YEPGlu for 16 hours. The oligonucleotide used for primer extension was complementary to sequences within ITS2. B_{1L} and B_{1S} represent the 5' end of $27SB_L$+$7S_L$ and $27SB_S$+$7S_S$ pre-rRNAs, respectively. (C) To assay synthesis and turnover of pre-rRNA intermediates in the absence of Drs1, the *GAL-HA-DRS1* strain was grown in C-met+Gal or shifted to C-met+Glu for 16 hours. Cells were pulse labeled with [^{3}H methyl]-methionine for 5 minutes and chased with a molar excess of unlabeled methionine for 2, 5, 10, and 60 minutes. Total RNA was extracted and separated on a 1.2% agarose-6% formaldehyde gel.

3.2.2 Association of Drs1 with pre-ribosomes requires the Nop7 subcomplex

A number of results of suggest that Drs1 functionally and physically interacts with the A_3-factors, specifically Nop7 or the Nop7 subcomplex: 1) Mutations in *NOP7* are synthetically lethal with *drs1* mutations, in an allele-specific manner (Adams et al. 2002). 2) Depletion of Drs1 results in a similar pre-rRNA processing phenotype as depletion of Nop7 or the other A_3-factors (Fig. 22). 3) Drs1 can be purified with the Nop7-subcomplex upon turning off transcription of rRNA and disrupting assembly of ribosomes (Merl et al. 2010). 4) Over expression of *DRS1* can suppress temperature-sensitive growth defects of *nop7* mutants (Fig. 23A). 5) Drs1 is dependent upon Nop7 to associate with pre-ribosomes, although Nop7 is not dependent on Drs1 (Fig. 23B and 23C). 6) Drs1 is part of a salt-stable Nop7-subcomplex (Fig. 23D). 7) Drs1 can bind the Nop7-subcomplex *in vitro* (Fig. 23E).

These data suggest that Drs1 interacts with the Nop7-subcomplex, possibly through direct interactions with Nop7. Drs1 is required for the same steps of pre-rRNA processing as Nop7, but appears to be recruited to pre-ribosomes only after the Nop7-subcomplex and other interdependent A_3-factors have associated.

FIGURE 23

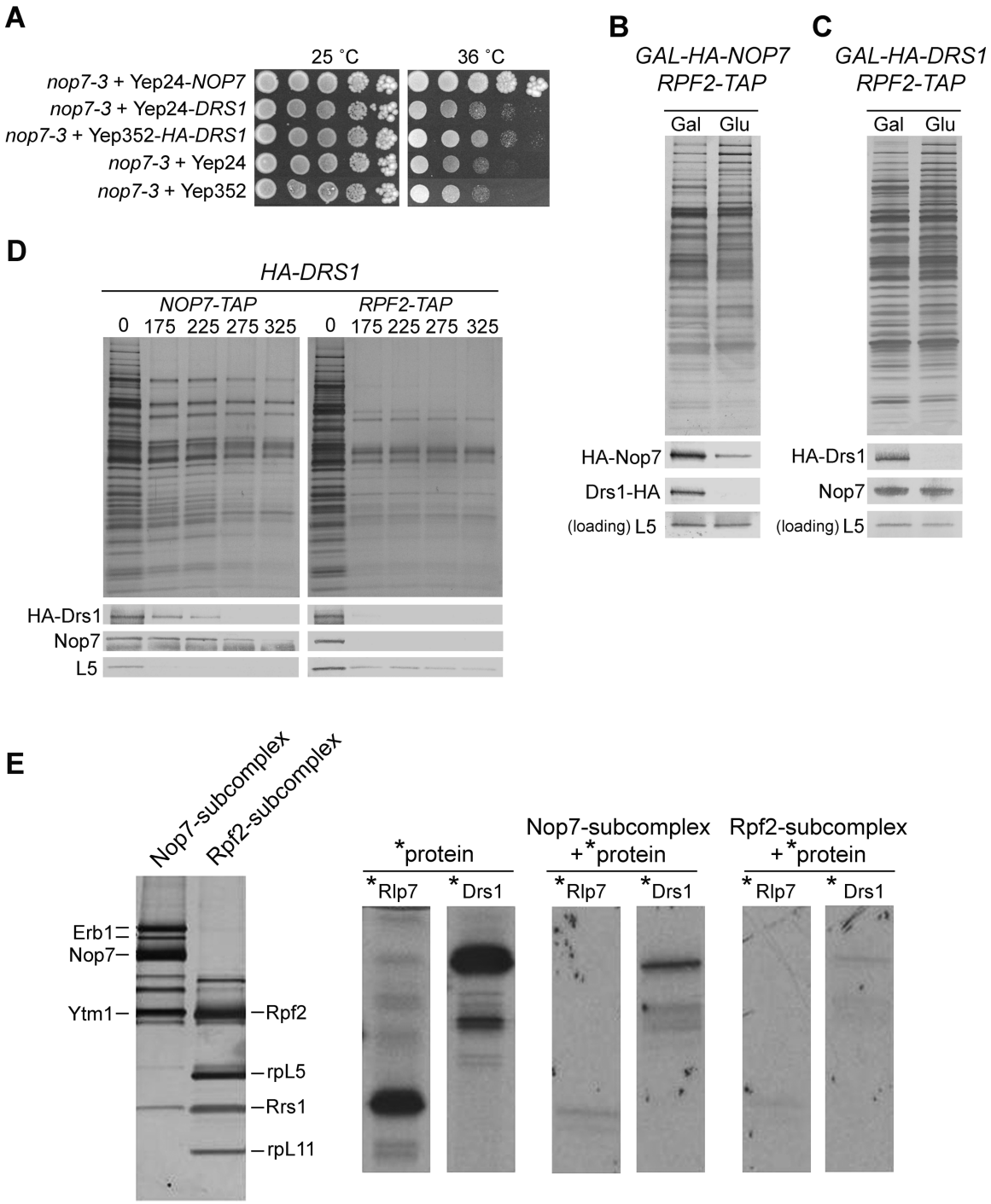

A
25 °C
36 °C
nop7-3 + Yep24-NOP7
nop7-3 + Yep24-DRS1
nop7-3 + Yep352-HA-DRS1
nop7-3 + Yep24
nop7-3 + Yep352
B
GAL-HA-NOP7
RPF2-TAP
Gal
Glu
HA-Nop7
Drs1-HA
(loading) L5
C
GAL-HA-DRS1
RPF2-TAP
Gal
Glu
HA-Drs1
Nop7
(loading) L5
D
HA-DRS1
NOP7-TAP
RPF2-TAP
0 175 225 275 325
0 175 225 275 325
HA-Drs1
Nop7
L5
E
Nop7-subcomplex
Rpf2-subcomplex
Erb1
Nop7
Ytm1
Rpf2
rpL5
Rrs1
rpL11
*protein
*Rlp7
*Drs1
Nop7-subcomplex +*protein
*Rlp7
*Drs1
Rpf2-subcomplex +*protein
*Rlp7
*Drs1

Figure 23: Drs1 functionally and physically interacts with the Nop7-subcomplex.

(A) Overexpression of Drs1 partially suppresses the temperature-sensitivity of the *nop7-3* strain at 36 °C. The *nop7-3* strain was transformed with high-copy vectors (Yep24 or Yep352) bearing *DRS1* or *NOP7* (positive control), or empty vectors (negative controls). Cells were grown to early log phase, serially diluted, spotted onto solid YEPGlu media, and incubated at 25 °C or 36 °C. (B) Nop7 is required for stable incorporation of Drs1 into pre-ribosomes. The *GAL-HA-NOP7 DRS1-HA RPF2-TAP* strain was grown in YEPGal or shifted to YEPGlu for 16 hours to deplete Nop7. Pre-ribosomes were affinity purified using Rpf2-TAP and visualized on 4-20% acrylamide gels by silver-staining. Western blots were performed using antibodies against specific proteins, or antibodies against specific epitope tags. Western blots against L5 serve as a loading control. (C) Drs1 is not required for stable association of Nop7 with pre-ribosomes. Pre-ribosomes were affinity purified from the *GAL-HA-DRS1 RPF2-TAP* strain grown in YEPGal or shifted to YEPGlu to deplete Drs1. Purified pre-ribosomes were visualized on 4-20% acrylamide gels by silver-staining. Western blots were performed as described in (B). (D) Pre-ribosomes were affinity purified from either the *GAL-HA-DRS1 NOP7-TAP* strain or the *GAL-HA-DRS1 RPF2-TAP* strain in the presence of increasing amounts of $MgCl_2$. Purified proteins were separated by SDS-PAGE and stained with silver for visualization. Western blots were performed to compare the amount of HA-Drs1 to L5 in each sample. (C) Whole-cell extracts from the *rrp1-1 NOP7-TAP* and *rrp1-1 RPF2-TAP* strains were subjected to high-speed centrifugation followed by affinity purification to purify the Nop7-subcomplex and Rpf2-subcomplex, respectively. Synthetic [^{35}S]-methionine labeled Drs1 or Rlp7 proteins (*) were incubated with the purified Nop7-subcomplex or Rpf2-subcomplex. Complexes were eluted, subjected

to SDS-PAGE, and visualized by autoradiography. 40% of the input [^{35}S] labeled protein in each assay (lanes 1 and 2) and 100% of the eluted complexes (lanes 3-6) are shown.

3.2.3 In the absence of Drs1, Nop7-containing pre-ribosomes are enriched for early associating 66S assembly factors and SSU components, but also late associating small subunit r-proteins.

To more thoroughly understand the relationship between Drs1 and the A_3-factors, and the pre-rRNA processing defect observed upon depletion of Drs1, we investigated how the composition of 66S pre-ribosomes changes in the absence of Drs1 using a combination of semi-quantitative iTRAQ mass spectrometry and western blotting. When 66S pre-ribosomes purified from wild-type cells and from Drs1-depleted cells were assayed by SDS-PAGE and silver-staining, we observed only a few changes in the number and intensity of polypeptide bands present (Fig. 24D). In support of this observation, iTRAQ mass spectrometry and western blotting showed that amounts of the majority of 60S assembly factors and r-proteins either did not change, or changed less than 2-fold in mutant pre-ribosomes (Fig. 24A and 24C). Consistent with an early block in 60S subunit assembly, we observed an accumulation of 66S assembly factors known to associate with pre-ribosomes early in assembly (Fig. 22A and 22D; Dbp2, Mak5, Nop4, Rrp5, Mak11, and Rrp15) and diminished amounts of 66S assembly factors thought to associate late in assembly (Nog2, Nsa2, Arx1, Rix1, and Drg1) (Nissan et al. 2002). This phenotype is often observed upon blocking early steps in ribosome biogenesis (Lebreton et al. 2008; Sahasranaman et al. 2011; Jakovljevic et al. 2012; Shimoji et al. 2012; Dembowski et al. 2013). We also saw a decrease of r-proteins L17, L19, L26, L35, and L37 (Fig. 24C and D). These r-proteins bind to domain I of 25S/5.8S rRNA, near the polypeptide exit tunnel, in close proximity to each other (Ben-Shem et al. 2011). As discussed in Chapter 2, these r-proteins have been observed to decrease in the absence of the A_3 factors or r-proteins that function in

processing of $27SA_3$ pre-rRNA. Many of the A_3 factors bind to domain I of rRNA (Granneman et al. 2011) and their absence is thought to result in a gross misfolding of rRNA domains I and III (Chapter 2) (Jakovljevic et al. 2012).

Last, we also observed a strong accumulation of small subunit r-proteins (Fig. 24C), 40S subunit assembly factors, and small subunit processome components (Fig. 24B) upon depletion of Drs1. Of the small subunit r-proteins that are enriched in Nop7-TAP particles, those that are most enriched are proteins that bind the 3' domain of 18S rRNA and whose bacterial homologues have been shown to be late, tertiary binders (S20 and S3) (Fig. 24E) (Mulder et al. 2010; Karbstein 2011). Whereas early steps of pre-rRNA processing occur co transcriptionally in yeast (Osheim et al. 2004; Kos and Tollervey 2010), r-proteins S3 and S20 are thought to associate with the assembling 40S subunit post-transcriptionally, or else after release of the nascent 43S pre-ribosome by cleavage at the A_2 site (Mulder et al. 2010; Strunk et al. 2011). Consistent with the late association, depletion of S3 or S20 affects late steps of 20S pre-rRNA processing as well as export of 20S-containing pre-ribosomes out of the nucleus (Ferreira-Cerca et al. 2005). Nop7, on the other hand, assembles into pre-ribosomes prior to A_2 cleavage, and thus should not be present in pre-ribosomes with r-proteins S3 and S20 when pre-rRNAs are processed co-transcriptionally (Harnpicharnchai et al. 2001; Granneman et al. 2011). Thus, the fact that we see significant enrichment of S3 and S20 in Nop7-TAP particles suggests that there is decreased cleavage at the A_2 site, and may reflect a shift from co-transcriptional to post-transcriptional pre-rRNA processing upon Drs1 depletion.

FIGURE 24 (continued on the next page)

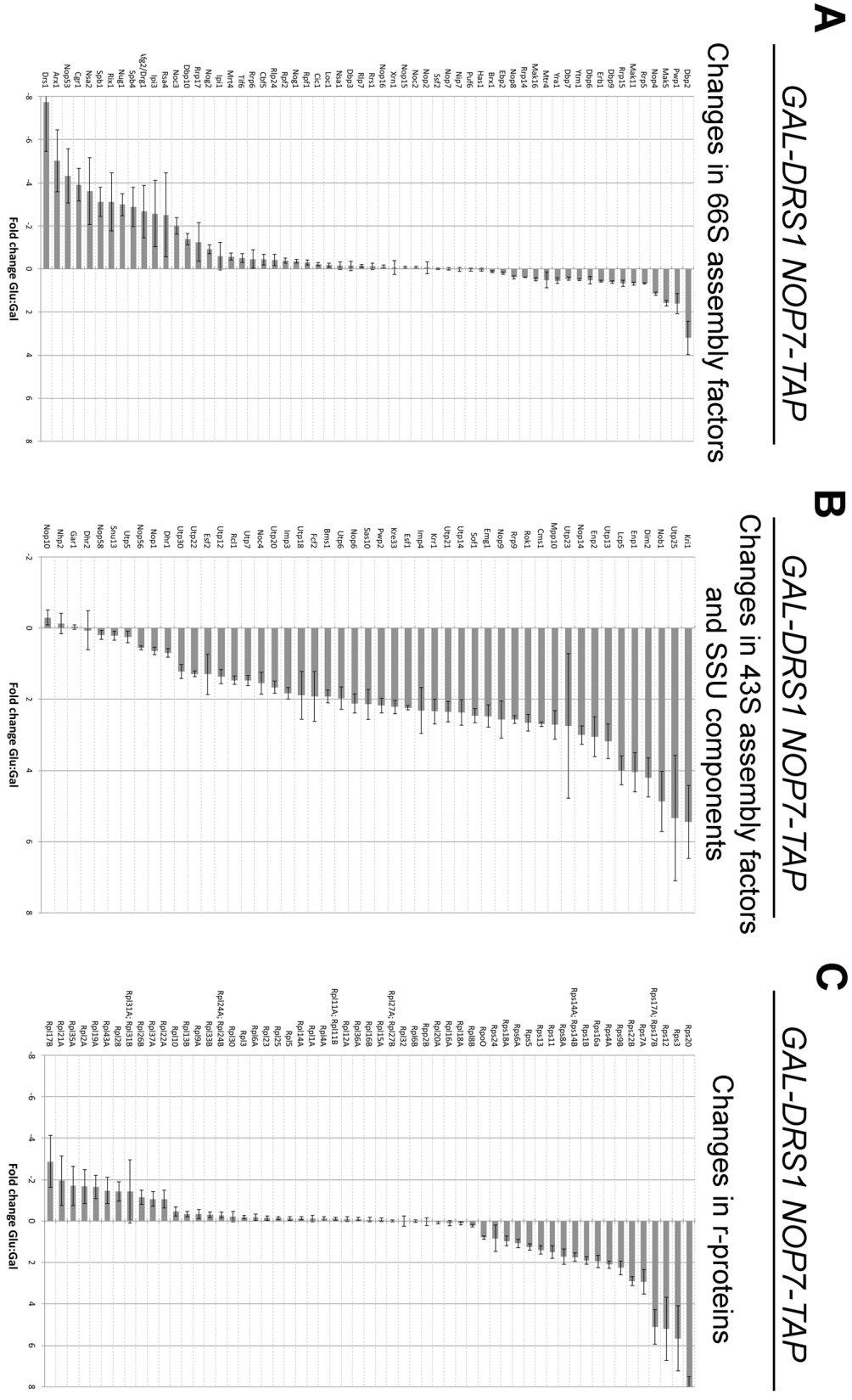


FIGURE 24 cont.

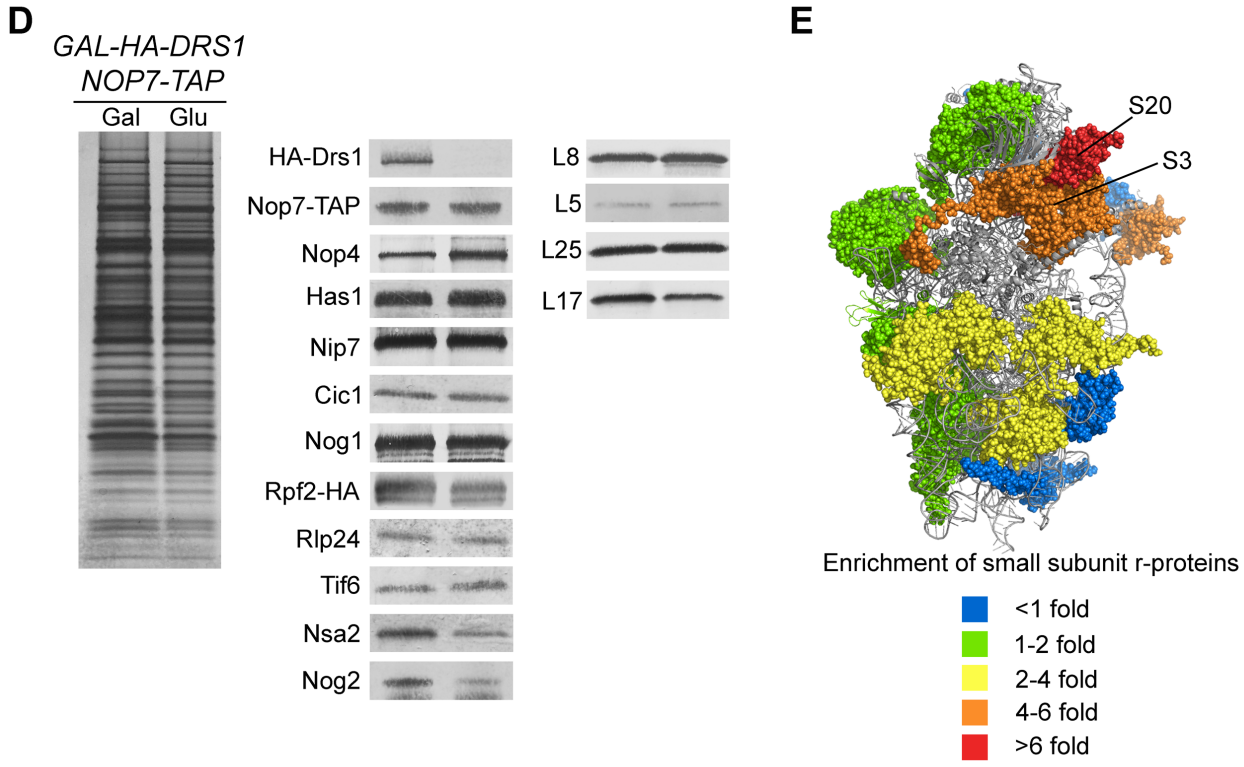


Figure 24: In the absence of Drs1, pre-ribosomes are enriched for early assembly factors and contain diminished amounts of late assembly factors.

(A-C) Pre-ribosomes were affinity purified from the *GAL-HA-DRS1 NOP7-TAP* strain grown in YEPGal or shifted to YEPGlu for 16 hours to deplete Drs1. Purified pre-ribosomes were assayed by semi-quantitative iTRAQ mass spectrometry to identify 60S assembly factors (A), 40S assembly factors and SSU components (B), and ribosomal proteins (C) and to compare relative amounts of each in wild-type and Drs1-depleted cells. Each data point shows the fold change of the respective protein upon depletion of Drs1. Error bars indicate the SEM. (D) To confirm iTRAQ results, pre-ribosomes were purified, separated by SDS-PAGE, and visualized by silver-staining. Western blots were performed against indicated proteins. (E) The crystal structure of the yeast 40S ribosomal subunit (PDB: 3U5F, 3U5G). R-proteins that are enriched in Nop7-TAP containing pre-ribosomes are highlighted. Colors indicate the fold-change observed for each r-protein. R-proteins S3 and S20 are most enriched upon Drs1 depletion and are indicated.

3.2.4 In the absence of Drs1, early 66S pre-ribosomes are enriched for late associating assembly factors.

In wild-type cells, Nop7 is associated with a number of consecutive 66S intermediates, and thus co-purifies a heterogeneous population of pre-ribosomes (Harnpicharnchai et al. 2001). Because upon depletion of Drs1 we observed a strong accumulation of small subunit r-proteins that are thought to associate with nascent ribosomes only after cleavage at the A_2 site, we wondered whether the decrease we observed in 66S assembly factors that associate after A_2 cleavage was an effect of Nop7-TAP being distributed among a different population of pre-ribosomes, containing earlier pre-rRNAs. Indeed, Nop7-TAP was associated with more 35S pre-rRNA upon Drs1 depletion. Furthermore, Nop7-TAP was associated with fewer pre-ribosomes containing 27SB pre-rRNA, most likely resulting from a combination of a block in pre-rRNA processing and enrichment of early pre-ribosomes (Fig. 25A).

Because Nop7-TAP is associated with an earlier subset of pre-ribosomes when Drs1 is depleted, we tested the effects of Drs1 depletion on the composition of early 66S intermediates. To do so, we purified pre-ribosomes from wild-type and Drs1-depleted cells using TAP-tagged Ssf1, an assembly factor present only in early pre-ribosomes (Fatica et al. 2002). In the course of our investigation we found that Ssf1-TAP pre-ribosomes become enriched with Nog2 in the absence of Drs1 (Fig. 25B). Nog2 associates with pre-ribosomes immediately before 27SB pre-rRNA is processed (Saveanu et al. 2001). However, a number of studies have convincingly shown that although both Ssf1 and Nog2 co-purify 27SB pre-rRNA, these two proteins are associated with mutually exclusive populations of pre-ribosomes (Saveanu et al. 2001; Kressler et al. 2008). The fact that we can detect Nog2 in

early pre-ribosomes suggests the following: 1) Late-associating assembly factors can still associate with pre-ribosomes in the absence of Drs1. This is evident by observing Nog2 in Ssf1-TAP particles. 2) However, their relative distribution between each of the consecutive particles changes. We believe this accounts for the "observed" decrease of Nog2 in Nop7-TAP particles. This will be discussed more in section 3.2.8.

FIGURE 25

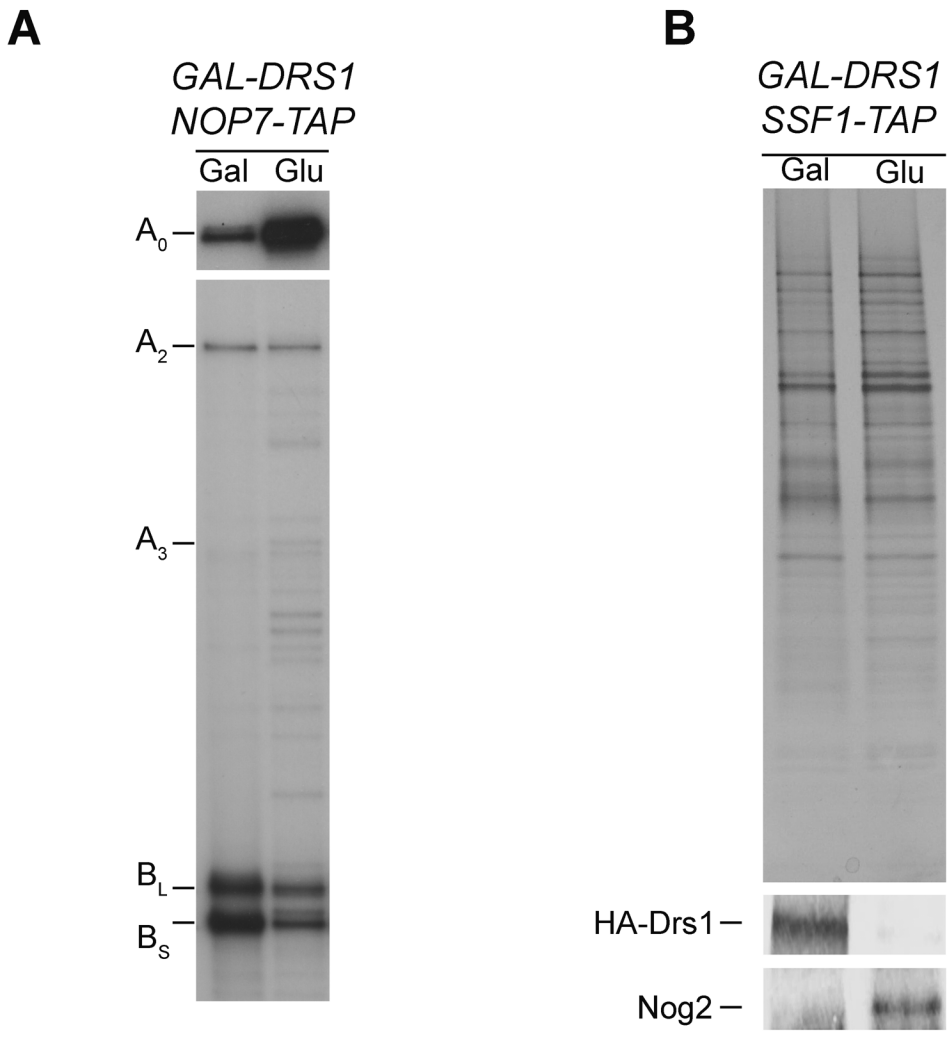

A
GAL-DRS1
NOP7-TAP
Gal
Glu
A0
A2
A3
BL
BS
B
GAL-DRS1
SSF1-TAP
Gal
Glu
HA-Drs1
Nog2

Figure 25: 60S assembly factors Nop7 and Nog2 are associated with a different subset of pre-ribosomes upon depletion of Drs1

(A) Pre-ribosomes were affinity purified, using Nop7-TAP, from the *GAL-HA-DRS1* strain grown in YEPGal or shifted to YEPGlu for 16 hours to deplete Drs1. RNA was extracted from purified pre-ribosomes and pre-rRNAs that copurified were detected by primer extension. An oligonucleotide complementary to the 5'-ETS was used to detect the 5' end of 35S pre-rRNA and an oligonucleotide complementary to ITS2 was used to detect the 5' ends of 27S pre-rRNAs. B_L and B_S represent the 5' end of $27SB_L$+$7S_L$ and $27SB_S$+$7S_S$ pre-rRNAs, respectively. (B) Depletion of Drs1 results in a population of pre-ribosomes that contain both Ssf1 and Nog2. Pre-ribosomes were affinity purified, using Ssf1-TAP, from the *GAL-HA-DRS1* strain grown in YEPGal or shifted to YEPGlu for 16 hours to deplete Drs1. Western blots were performed using antibodies against specific proteins, or antibodies against specific epitope tags.

3.2.5 In the absence of Drs1, late-associating 66S assembly factors and early associating 66S assembly factors are in the same pre-ribosome particles.

The data above suggest that in the absence of Drs1, a population of pre-ribosomes is generated that contain both 40S proteins (S3 and S20) and 60S proteins (Nog2) that normally only associate with pre-ribosomes after cleavage at the A_2 site has separated maturation of the 40S and 60S subunits. To further investigate this idea, we tested whether late-associating 66S assembly factors might behave similarly to r-proteins S3 and S20. If depletion of Drs1 really does affect co-transcriptional cleavage of the A_2 site, we might predict that late associating 66S assembly factors would co-purify early associating assembly factors upon Drs1 depletion. Indeed, examination of early pre-ribosomes purified using Ssf1-TAP suggested that late-associating 60S assembly factors, such as Nog2, might be assembling into early pre-ribosomal particles. To further investigate this idea, we TAP-tagged Nog2, Arx1, and Lsg1 in the *GAL-HA-DRS1* strain. Nog2 and Arx1 are primarily nucleoplasmic assembly factors, thought to associate with 66S pre-ribosomes only after 27SB pre-rRNA is generated (Saveanu et al. 2001; Nissan et al. 2002). Lsg1 has been shown to be cytoplasmic, and is one of the last assembly factors to associate with 66S pre-ribosomes (Nissan et al. 2002). We used each of these TAP-tagged assembly factors to purify pre-ribosomes from wild-type cells and cells in which Drs1 was depleted for 16 hours. As shown in Figure 26D (lanes 1, 3, and 5), late pre-ribosomes purified from wild-type cells expressing Drs1 are fairly simple particles, primarily composed of low-molecular weight r-proteins as well as a few assembly factors. However, when we depleted Drs1 we saw that Nog2-TAP, Arx1-TAP, and Lsg1-TAP purified more complex particles, enriched for high-molecular weight 66S factors (Fig. 26D, lanes 2, 4, and 6). In wild-type cells, these

high-molecular weight proteins assemble early and dissociate early from pre-ribosomes, before or immediately after these late TAP-tagged proteins join the nascent particle. This was consistent with our results that showed Nog2 is present in early Ssf1-TAP containing pre-ribosomes upon depletion of Drs1.

To investigate in more detail the changes in Nog2-TAP pre-ribosomes upon depletion of Drs1, we used iTRAQ mass spectrometry and western blotting (Fig. 26A-C and E). Many 66S assembly factors become enriched in Nog2-TAP pre-ribosomes when Drs1 is depleted, especially early assembly factors known to dissociate from pre-ribosomes during the same interval that Nog2 binds (Fig. 26A, 26D, and 26E). For example, we see strong enrichment of Ssf1, Npa1, and Rrp5. All three of these proteins have been reported to dissociate from pre-ribosomes before 27SB pre-rRNA is generated and before Nog2 binds the pre-ribosomes (Fatica et al. 2002; Nissan et al. 2002; Dez et al. 2004). Even more striking, we observed substantial enrichment of small subunit r-proteins as well as small subunit processome components and 40S assembly factors (Fig. 26B and 26C). Similar to our results with Nop7-TAP (Figure 24), we see that Nog2-TAP pre-ribosomes, purified from Drs1-depleted cells, are highly enriched for the late associating r-proteins S3 and S20 (Fig. 26C). Because Nog2 normally associates with pre-ribosomes only after A_2 cleavage has separated maturation of the 40S subunit from the 60S subunit, Nog2 should not be present in the same particles as proteins involved in maturation of 40S ribosomal subunits. Taken together, our results demonstrate that depletion of Drs1 results in the formation of pre-ribosomes that are enriched for both 40S r-proteins and 40S assembly factors, as well as late-associating 60S factors.

FIGURE 26 (continued on the next page)

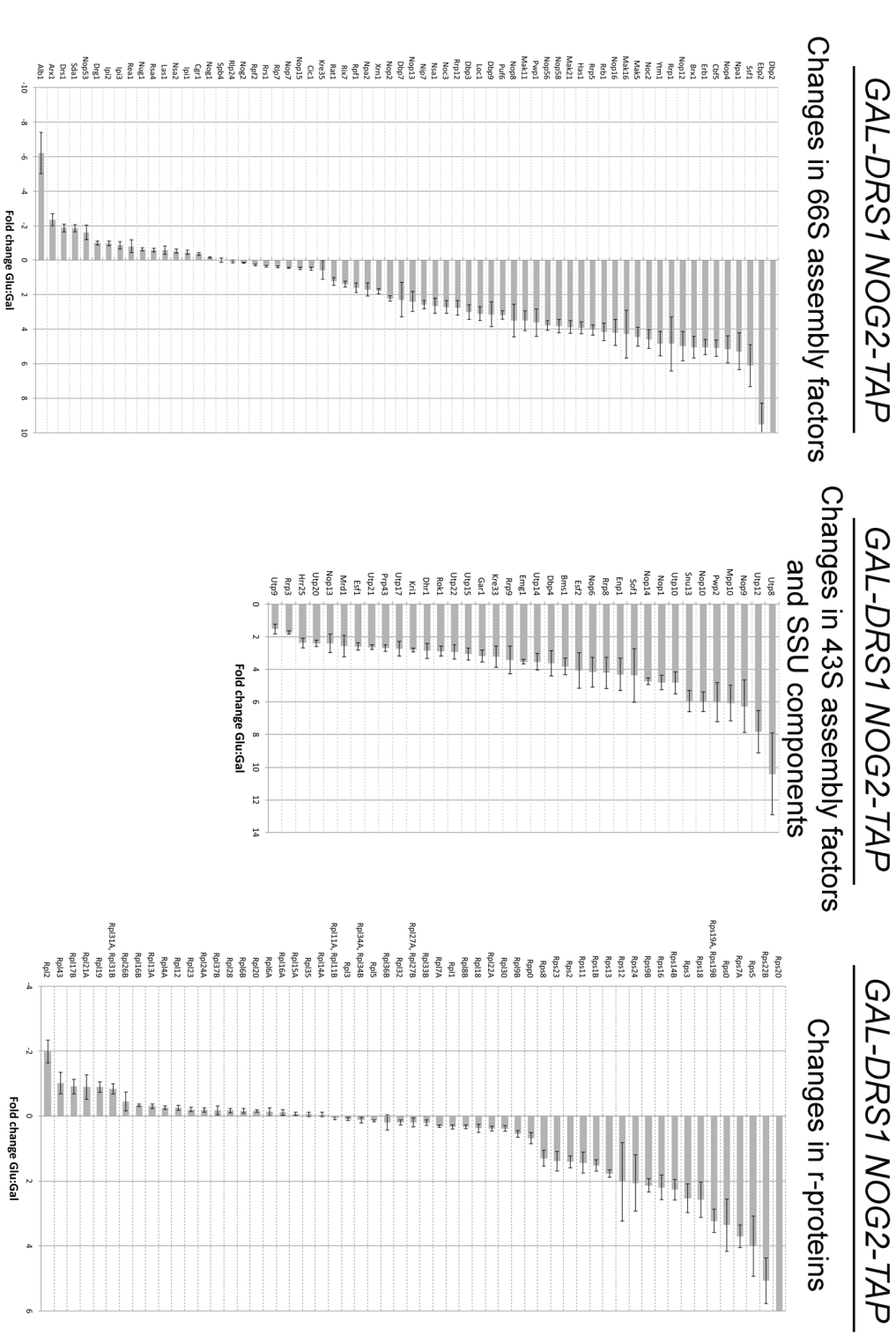


FIGURE 26 cont.

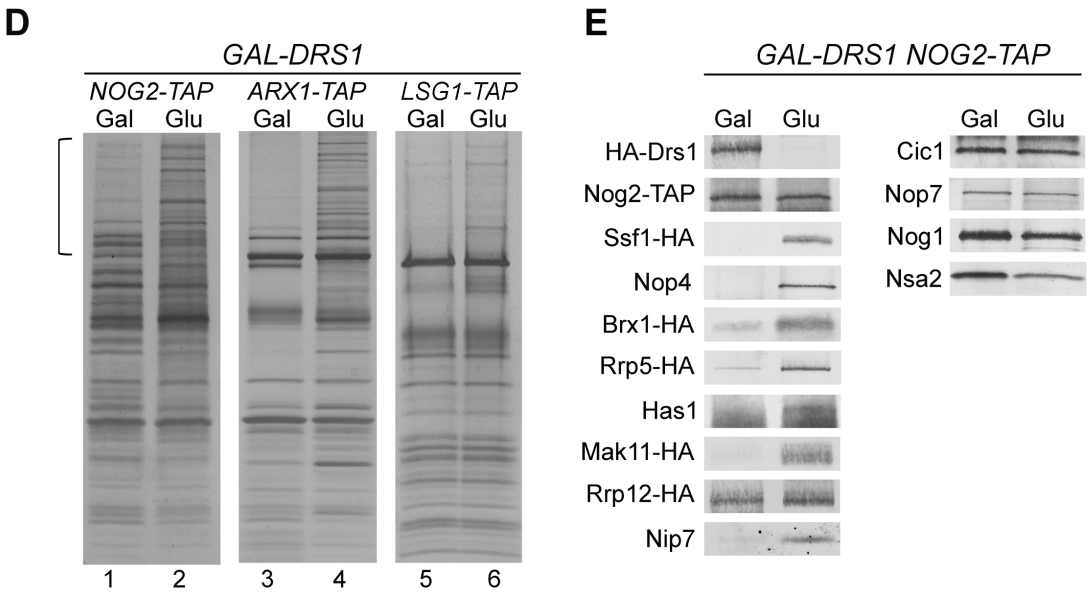


Figure 26: Late 60S pre-ribosomes are enriched for early assembly factors in the absence of Drs1.

(A-C) Pre-ribosomes were affinity purified from the *GAL-HA-DRS1 NOG2-TAP* strain grown in YEPGal or shifted to YEPGlu for 16 hours to deplete Drs1. Purified pre-ribosomes were assayed by iTRAQ mass spectrometry as described in Figure 24. Shown is the fold change in 60S assembly factors (A), 40S assembly factors and SSU components (B), and ribosomal proteins (C). Error bars indicate the SEM. (D) Pre-ribosomes were affinity-purified from the *GAL-HA-DRS1* strain grown in YEPGal or shifted to YEPGlu using Nog2-TAP, Arx1-TAP, or Lsg1-TAP. Purified pre-ribosomes were separated by SDS-PAGE and visualized by silver staining. The bracket indicates the enrichment of high molecular weight assembly factors that are known to be present in early 66S pre-ribosomes, but absent in late pre-ribosomes. (E) Western blotting was performed to confirm the *GAL-HA-DRS1 NOG2-TAP* iTRAQ data.

3.2.6 Late 66S assembly factors co-immunoprecipitate early pre-rRNAs in the absence of Drs1.

To more clearly delineate the effect of Drs1 depletion on the composition of pre-ribosomes, we assayed with what pre-rRNAs late assembly factors associate when Drs1 is absent. To test this we purified pre-ribosomes from wild-type and Drs1-depleted cells using Nog2-, Arx1-, and Lsg1-TAP and then assayed by primer extension what pre-rRNAs copurified with each assembly factor. As controls, we compared this to the pre-rRNAs copurified in a Nob1-TAP strain and the untagged parent strain. Nob1 associates with pre-ribosomes immediately prior to cleavage at the A_2 site, but after cleavage at sites A_0 and A_1 (Fatica et al. 2003a). Thus, we consider the signal observed for 35S pre-rRNA co-IPed with Nob1-TAP to be background amounts (Fig. 27A; lane 7). When pre-ribosomes and the pre-rRNAs contained within them were purified from cells in which Drs1 is expressed, Nog2-TAP and Arx1-TAP co-immunoprecipitate 27SB pre-rRNA, but not 35S, $27SA_2$, and $27SA_3$ pre-rRNAs, and Lsg1-TAP did not co-IP 35S or 27S pre-rRNAs (Fig. 27A; lanes 1, 3, and 5). Interestingly, upon depletion of Drs1, we observed that Nog2-, Arx1-, and Lsg1-TAP co-IPed above-background amounts of 35S, $27SA_2$, and $27SA_3$ pre-rRNAs (Fig. 27A; lanes 2, 4, and 6). Consistent with an early block in 27SA pre-rRNA processing we see that Nog2-TAP and Arx1-TAP co-IPed decreased amounts of 27SB pre-rRNA relative to 27SA pre-rRNA (Figure 27A; lanes 2 and 4). Thus, depletion of Drs1 results in Nog2, Arx1, and Lsg1 associating with a very different population of pre-ribosomal particles that contain early pre-rRNA intermediates compared to wild-type cells (Fig. 27B).

Together, our data indicate that depletion of Drs1 results in the formation of a population of pre-ribosomes that contain both early- and late-associating assembly factors,

which in wild-type cells are not found in the same particles. Interestingly, these mutant particles contain both 40S and 60S assembly factors and small subunit r-proteins that are thought to associate with pre-ribosomes only after A_2 cleavage has occurred. Because cleavage at the A_2 site separates maturation of 43S and 66S pre-ribosomes, these late associating proteins should not be found in the same particles. Most striking, upon depletion of Drs1, we observed that the late-associating 66S assembly factors Nog2, Arx1, and Lsg1 associate with pre-ribosomes containing 35S pre-rRNA. We believe this reflects a shift from co-transcriptional to post-transcriptional A_2 cleavage.

FIGURE 27

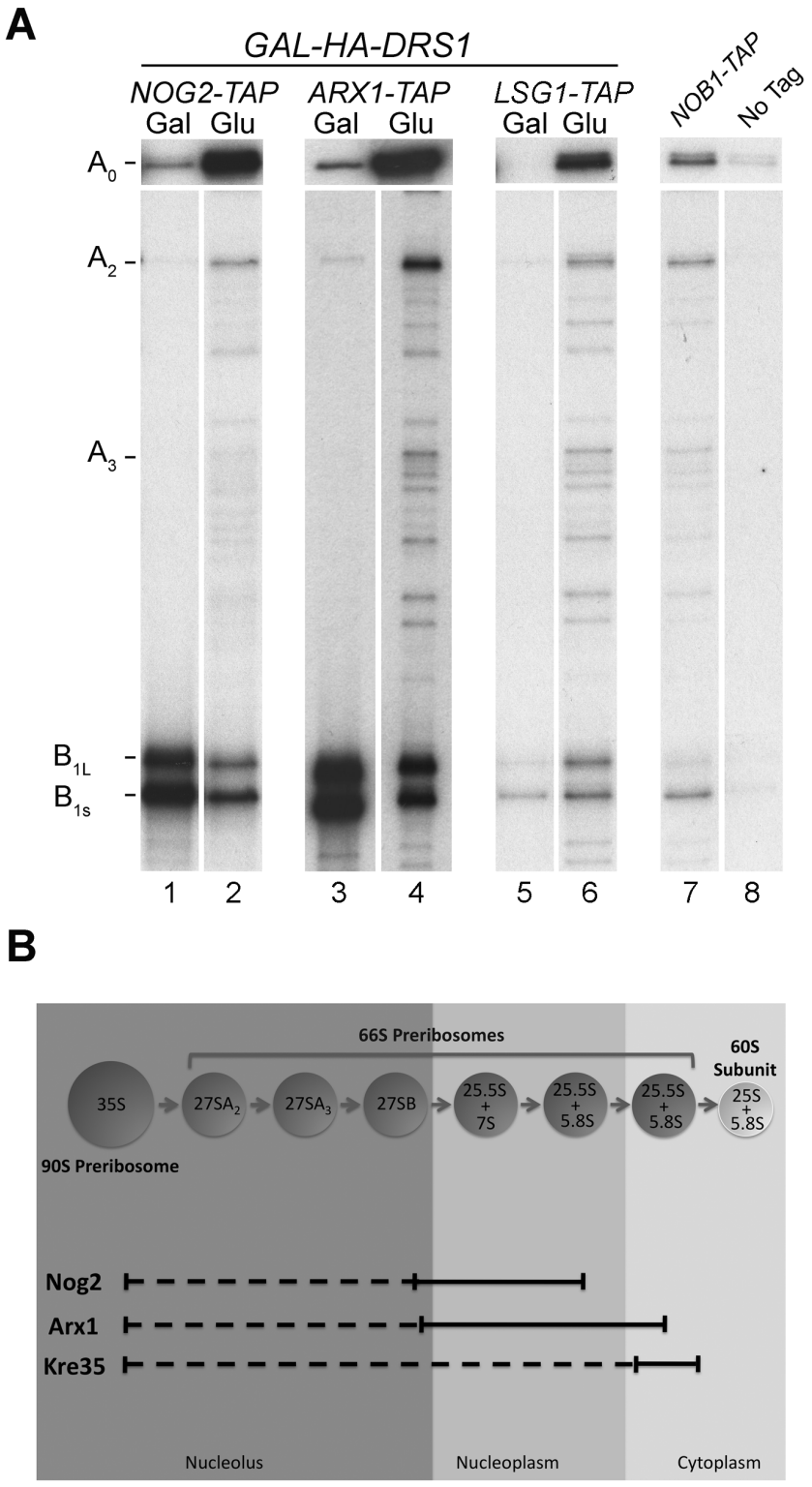

A
GAL-HA-DRS1
NOG2-TAP
Gal Glu
ARX1-TAP
Gal Glu
LSG1-TAP
Gal Glu
NOB1-TAP
No Tag
A0
A2
A3
B1L
B1s
1 2 3 4 5 6 7 8
B
66S Preribosomes
60S Subunit
35S
27SA2
27SA3
27SB
25.5S + 7S
25.5S + 5.8S
25.5S + 5.8S
25S + 5.8S
90S Preribosome
Nog2
Arx1
Kre35
Nucleolus
Nucleoplasm
Cytoplasm

Figure 27: In the absence of Drs1, late associating assembly factors copurify early pre-rRNA intermediates.

(A) Pre-ribosomes were affinity purified, using Nog2-TAP, Arx1-TAP, or Lsg1-TAP, from the *GAL-HA-DRS1* strain grown in YEPGal or shifted to YEPGlu for 16 hours to deplete Drs1. RNA was extracted from purified pre-ribosomes and pre-rRNAs that copurified were detected by primer extension. An oligonucleotide complementary to the 5'-ETS was used to detect the 5' end of 35S pre-rRNA and an oligonucleotide complementary to ITS2 was used to detect the 5' ends of 27S and 7S pre-rRNAs. B_{1L} and B_{1S} represent the 5' end of $27SB_L$+$7S_L$ and $27SB_S$+$7S_S$ pre-rRNAs, respectively. Nob1-TAP and the untagged parent strain serve as negative controls. (B) Model describing the timing of association of Nog2, Arx1, and Lsg1 in wild-type and Drs1-depleted cells. Spheres represent consecutive pre-ribosome intermediates. Solid lines indicate the pre-rRNAs associated with each assembly factor in wild-type cells. Dashed lines indicate the pre-rRNAs associated with each assembly factor in the absence of Drs1.

3.2.7 Nog2-containing pre-ribosomes are enriched with RNA polymerase I components upon depletion of Drs1.

Recently, a number of ribosome assembly factors were shown to co-purify with RNA polymerase I (Pol I), suggesting they are recruited to pre-ribosomes co-transcriptionally (Hierlmeier et al. 2012). Many of these factors, including Drs1, are proteins that associate with pre-ribosomes early in ribosome biogenesis. Late-associating proteins, such as Nog2, were not identified in a complex with Pol I, consistent with their binding of pre-ribosomes after the completion of transcription. In the course of our mass spectrometry analysis of pre-ribosomes isolated from cells when Drs1 is depleted, we identified subunits specific to Pol I (Rpa49 and Rpa135), but not Pol II or Pol III. When pre-ribosomes were depleted of Drs1 and purified using Nop7-TAP, no enrichment of Rpa49 and Rpa135 was seen (Fig. 28). Interestingly, when Drs1-depleted pre-ribosomes were purified using Nog2-TAP, Rpa49 and Rpa135 were enriched ~4.5 fold and 3.5 fold, respectively (Fig. 28). We believe these data reflect a shift from co- to post-transcriptional pre-rRNA processing. In wild-type cells, Nop7 is co-purified with Pol I, suggesting it normally associates with pre-ribosomes co-transcriptionally (Hierlmeier et al. 2012). Thus, we would predict that even upon a shift from co- to post-transcriptional pre-rRNA processing, Nop7 would still associate with pre-rRNAs co-transcriptionally, and not result in enrichment of Pol-I components with Nop7. Conversely, Nog2 normally associates only after transcription is finished. The fact that we see strong enrichment of Pol I subunits in pre-ribosomes purified using Nog2-TAP suggests that upon depletion of Drs1, Nog2 now associates with pre-ribosomes co-transcriptionally. These data, plus our finding that Nog2 can associate with 35S pre-rRNA upon depletion of Drs1 further strengthens our conclusion that depletion of Drs1, and subsequent disruption

of ribosome assembly, causes a shift from co- to post-transcriptional pre-rRNA processing. When this occurs, normally "late" associating assembly factors bind pre-ribosomes containing 35S pre-rRNA and the Pol I machinery (Fig. 29).

FIGURE 28

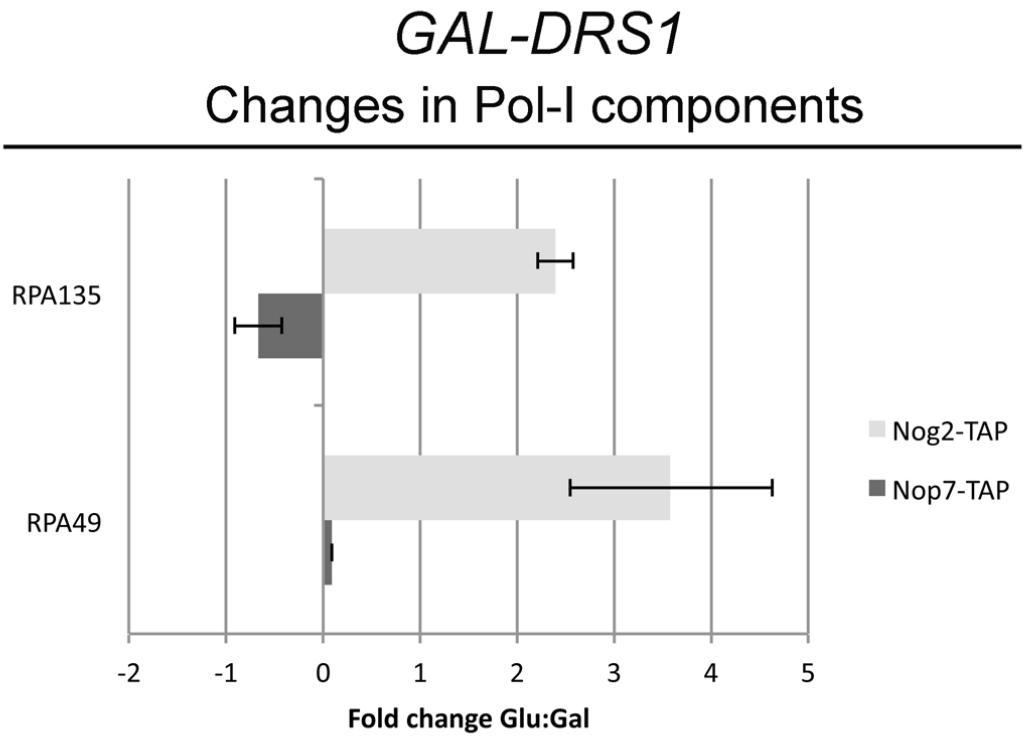

GAL-DRS1
Changes in Pol-I components
RPA135
RPA49
Nog2-TAP
Nop7-TAP
-2
-1
0
1
2
3
4
5
Fold change Glu:Gal

Figure 28: Nog2-containing pre-ribosomes are enriched with RNA polymerase I subunits upon depletion of Drs1.

Pre-ribosomes were affinity purified using either Nop7-TAP (dark grey bars) or Nog2-TAP (light grey bars) from the *GAL-HA-DRS1* strain grown in YEPGal or shifted to YEPGlu to deplete Drs1. Purified pre-ribosomes were assayed by iTRAQ mass spectrometry as described in Figure 24. Shown is the fold change in Pol-I subunits identified. Error bars indicate the SEM.

FIGURE 29

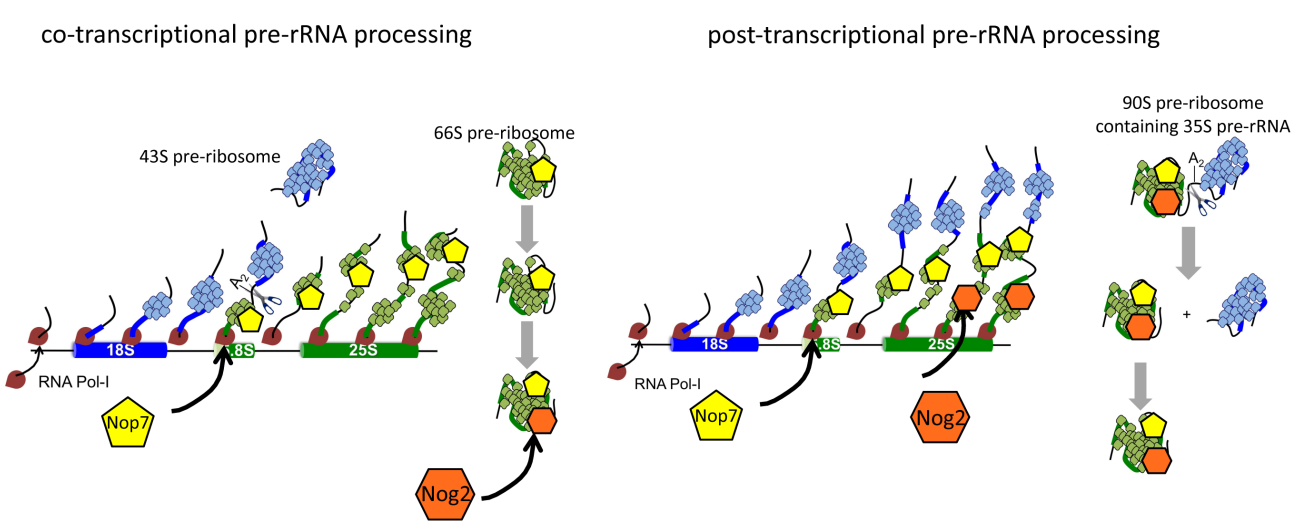

co-transcriptional pre-rRNA processing
post-transcriptional pre-rRNA processing
43S pre-ribosome
66S pre-ribosome
90S pre-ribosome
containing 35S pre-rRNA
18S
5.8S
25S
RNA Pol-I
Nop7
Nog2
A2

Figure 29: Depletion of Drs1 causes a shift from co-transcriptional pre-rRNA processing to post-transcriptional pre-rRNA processing.

In wild-type yeast cells, pre-rRNAs are synthesized by Pol I and cleaved at the A_2 site co-transcriptionally (left). This results in the formation of a 43S pre-ribosome containing 20S pre-rRNA (blue) and a 66S pre-ribosome containing $27SA_2$ pre-rRNA (green). The $27SA_2$ pre-rRNA is rapidly processed to 27SB pre-rRNA followed by the association of Nog2 (yellow). Upon depletion of Drs1, pre-rRNAs are processed post-transcriptionally generating 90S pre-ribosomes containing 35S pre-rRNA (right; blue/green). The enrichment of Pol-I subunits (red) and 35S pre-rRNA associated with Nog2-TAP containing pre-ribosomes indicates that Nog2 is able to associate with pre-ribosomes co-transcriptionally in the absence of Drs1.

3.2.8 ***Clarifying discrepancies in our data***

The results in sections 3.2.4-3.2.6 regarding the association of Nog2 appear to contradict themselves. In 3.2.4 we show that in the absence of Drs1, there is less Nog2 associated with Nop7-TAP containing pre-ribosomes. However, in 3.2.5 we show that Nog2 is present in early Ssf1-TAP containing pre-ribosomes and in 3.2.6 we show that pre-ribosomes purified using Nog2-TAP contain Nop7. Thus, all of our data suggest Nog2 can still associate with early particles, however we see decreased amounts of Nog2 when pre-ribosomes are purified using Nop7-TAP. In simpler terms, if Nog2 is really associating with 35S pre-rRNA in the absence of Drs1, then why do we see decreased amounts of Nog2 when pre-ribosomes are purified using Nop7-TAP?

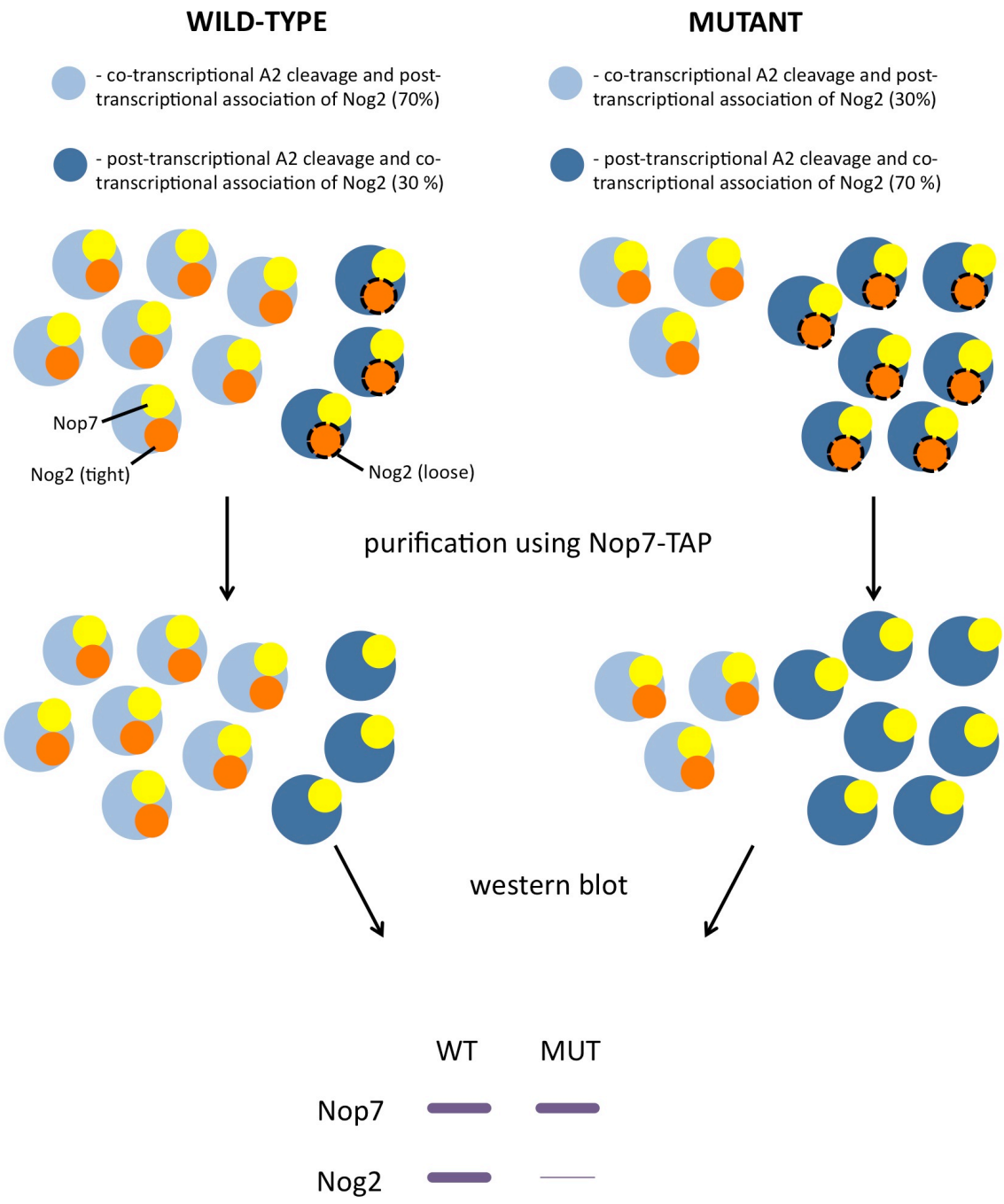
I think there are two issues here: a technical "loading" issue and a more relevant biological issue. The "loading" issue is actually less clear to me than potential biological issues. This is because it is still not entirely clear to us (the field) on how the proportion (of total intermediates) of each assembly intermediate changes relative to the others upon disruption of ribosome biogenesis. In a simplistic view, when we block assembly at a particular step, particles in the proceeding steps accumulate, and particles in the following steps are present in diminished amounts. However, in reality this situation is more complex and is accompanied by turnover of some intermediates (e.g. Fig 22C), alternative pathways of pre-rRNA processing (as shown in Fig. 22A and 22C, and Fig. 22), an overall decrease in ribosome production, and a shift from co- to post-transcriptional pre-rRNA processing. Thus, when we purify these particles from wild-type and mutant cells, and compare their constituents (by SDS-PAGE, western blotting, iTRAQ, etc.), we are really comparing two populations of pre-ribosomes, intermediates of which are distributed

differently among each population. In wild-type cells, the majority of Nog2 is associated with 27SB pre-rRNA, by far the most abundant intermediate. However, when we block assembly early, we prevent the formation of this long-lived intermediate, and thus lose a large fraction of pre-ribosomes that contain both Nop7 and Nog2. This could potentially account for the overall decrease we observe for Nog2 and other late proteins upon depletion of Drs1.

However, I think there is a more biologically relevant issue at play as well. For clarity purposes I will be a bit candid and in some places make extreme assumptions. If there is an equilibrium between co- and post-transcriptional cleavage in wild-type cells (say 70% occurs co-transcriptinally and 30% post-transcriptionally), then 70% of the time Nog2 enters post-transcriptionally and 30% of the time it enters co-transcriptionally and pulls down 35S (see Fig. 29 and Fig. 30). All of our data suggest that early protein binding events are less stable than later ones. We and others have shown that the affinities of some assembly factors and r-proteins for early pre-ribosomes are more sensitive to high salt concentrations, than those of later particles. Thus, there is a "tightening up effect" where some proteins become more stably integrated into the pre-ribosome structure as assembly progresses. Following this logic, one might expect that Nog2 has a low affinity for 35S pre-rRNA and a high affinity for 27SB pre-rRNA. Thus, when we purify pre-ribosomes with Nop7-TAP from wild-type cells, (say we purify 10 particles) 70% of Nop7 particles will have "tight" Nog2 and 30% would have "loose" Nog2. Let us be extreme and say when we do pull-downs with Nop7-TAP, our conditions are such that we lose 100% of the "loose" Nog2. Thus, out of 10 Nop7-TAP particles we pull down 7 Nog2s. In the mutant, we shift the equilibrium between co-transcriptional and post-transcriptional cleavage of the A_2 site

(lets say now only 30% is co-transcriptional and 70% is post-transcriptional) so now when we purify 10 Nop7 particles we only get 3 Nog2s. Furthermore, an early block in assembly would also prevent the formation of some of these later particles containing "tight" Nog2, further exacerbating the decrease (discussed above). Thus, the decrease of Nog2 we observe in Nop7-TAP particles might actually reflect: 1) the enrichment of early post-transcriptionally processed particles that contain both Nop7 and Nog2, but 2) Nog2 has a relatively low affinity for these early particles.

FIGURE 30


WILD-TYPE
- co-transcriptional A2 cleavage and post-transcriptional association of Nog2 (70%)
- post-transcriptional A2 cleavage and co-transcriptional association of Nog2 (30 %)
MUTANT
- co-transcriptional A2 cleavage and post-transcriptional association of Nog2 (30%)
- post-transcriptional A2 cleavage and co-transcriptional association of Nog2 (70 %)
Nop7
Nog2 (tight)
Nog2 (loose)
purification using Nop7-TAP
western blot
WT
MUT
Nop7
Nog2

3.2.9 Pre-rRNA processing is dependent on cell growth rates

Electron microscopy of actively transcribed rDNA revealed that when cells are rapidly dividing, a greater fraction of pre-rRNAs are processed co-transcriptionally (Osheim et al. 2004). However, when cells were grown to high density, nascent transcripts were more frequently processed post-transcriptionally. While establishing a link between cell growth rates and co- versus post-transcriptional pre-rRNA processing, these experiments did not address the order in which pre-rRNAs were processed in these two competing scenarios.

To better understand the relationship between cell growth rate and pre-rRNA processing, we extracted RNA from cells grown from OD_{610} 0.5 – 6.0 and assayed pre-rRNA processing by northern blotting (Fig. 32). We hypothesized that as cells reached high density we would observe an increase in 35S pre-rRNA relative to other intermediates.

Generally, we observed decreased steady state amounts of both pre-rRNAs and rRNAs as cells approached stationary phase, suggesting a global down-regulation in nascent ribosome production (Fig. 31 and Fig. 32). It is likely that the decrease of 25S and 18S rRNAs is due to a combination of decreased ribosome production and dilution of pre-existing ribosomes by cell division. Consistent with previous work from the Warner group, the decrease in pre-rRNAs occurred slightly prior to exit from exponential growth, suggesting cells regulate ribosome synthesis according to their "estimates" for the potential for growth (Ju and Warner 1994). At OD_{610} 2.0-4.0 cells were still rapidly dividing, however there was a significant decrease in the levels of $27SA_2$, 27SB, and 20S pre-rRNAs (Fig. 32, lanes 4 and 5). From OD_{610} 4.0-6.0, the steady-state levels of these intermediates remained largely the same, declining only slightly (Fig. 32, lanes 5-8).

Interestingly, as cell division approached stationary phase we observed a strong accumulation of 23S pre-rRNA coincident with the decrease in 20S pre-rRNA (Fig. 32, lanes 4 and 5). This intermediate, extending from the 5' end of the 35S pre-rRNA to the A_3 site, is generated by direct cleavage of the A_3 site prior to cleave at sites A_0, A_1, and A_2. This is thought to occur exclusively post-transcriptionally resulting in the generation of 23S pre-rRNA (5' product) and $27SA_3$ pre-rRNA (3' product). 23S pre-rRNA has been observed in a number of ribosome assembly mutants and has been suggested by some to be an aberrant intermediate. Work from our lab has shown 23S pre-rRNA accumulates in most mutants that block 60S assembly, but it can be processed to 18S rRNA and serves as an alternative route for maturation of the small subunit (Fig. 22C)(Jakovljevic et al. 2012). Because cells grown to high density remain viable, and normal pre-rRNA processing can be restored upon dilution of the culture with fresh media (Fig. 32, lane 9), it is likely that 23S pre-rRNA is a *bona fide* pre-rRNA processing intermediate. While we did not directly observe 35S in this experiment, a previous independent analysis showed accumulation of this post-transcriptionally derived intermediate relative to other pre-rRNAs as cell density increased (Fig. 33).

Together, these data confirm the previous electron microscopy analyses and show that as cells exit from exponential growth and approach stationary phase, a greater fraction of pre-rRNA processing occurs post-transcriptionally as evident by the accumulation of 35S pre-rRNA and 23S pre-rRNA. Our data suggest that when pre-rRNAs are processed post-transcriptionally, a large fraction of 35S pre-rRNA undergoes direct cleavage at the A_3 site, prior to cleavage at A_0, A_1, and A_2, resulting in 23S and $27SA_3$ pre-rRNAs. Thus, the accumulation of 23S pre-rRNA, and the corresponding decrease of 20S pre-rRNA, indicate

that nascent pre-rRNAs are processed through different pathways when pre-rRNA processing occurs post-transcriptionally.

**It should be noted that experiments are currently underway to more thoroughly investigate the effects of cell density on pre-rRNA processing. Specifically, I am repeating the experiments discussed in section 3.2.8 in an effort to visualize 35S, 23S, and 20S pre-rRNAs on the same northern blot. Furthermore, experiments are underway to test the effects of environmental stress on pre-rRNA processing. Pre-rRNA processing will be assayed under the following conditions: 1) heat-shock, 2) cold-shock, 3) TOR inhibition, 4) amino acid starvation, and 5) alternative carbon sources (ethanol, acetate, etc.). Upon completion of these experiments this work will be submitted to *Molecular Cell* for consideration.

FIGURE 31

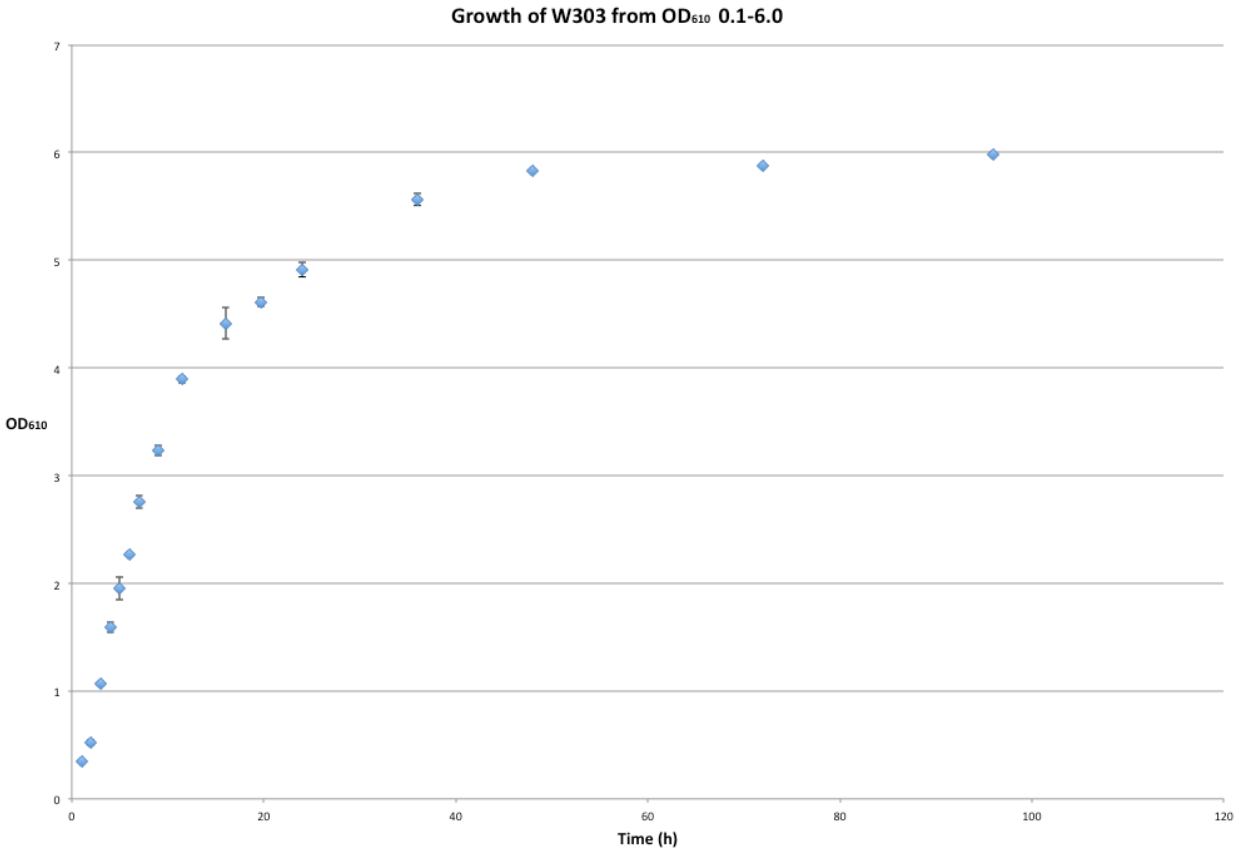

Growth of W303 from OD610 0.1-6.0
OD610
Time (h)
0
1
2
3
4
5
6
7
0
20
40
60
80
100
120

Figure 31: Growth of W303 from OD_{610} 0.1-6.0

Yeast strain W303 was grown in YEPGlu medium to increasing density. Aliquots of the culture were taken at indicated time-points and the OD_{610} was measured with a Genesis 20 spectrophotometer.

FIGURE 32

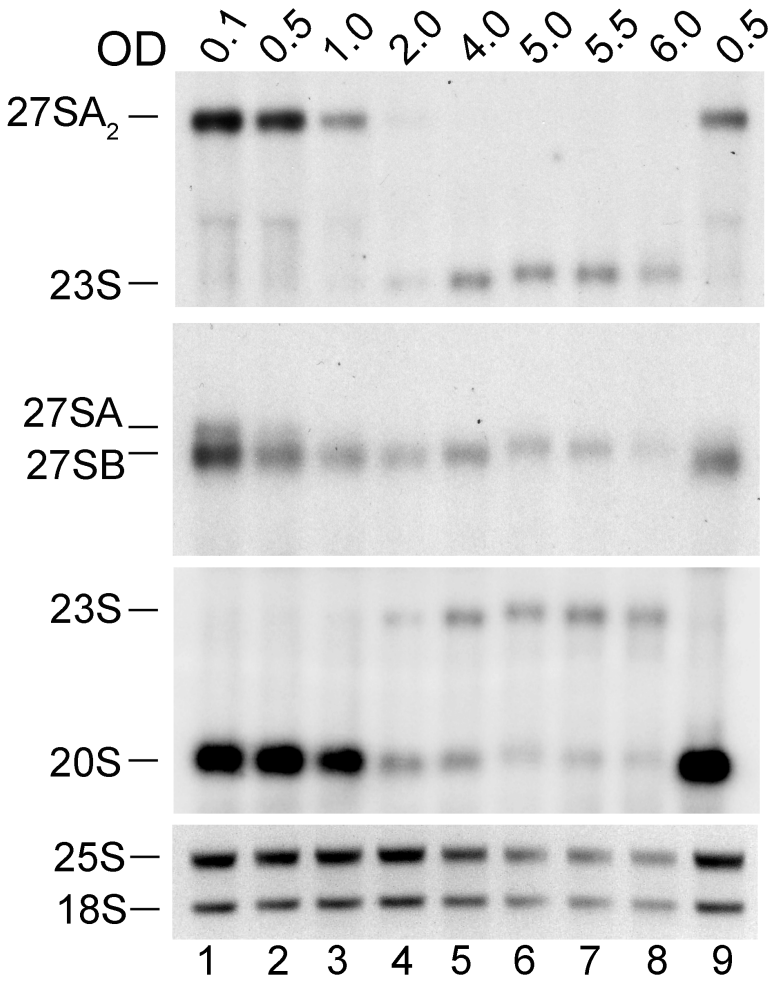
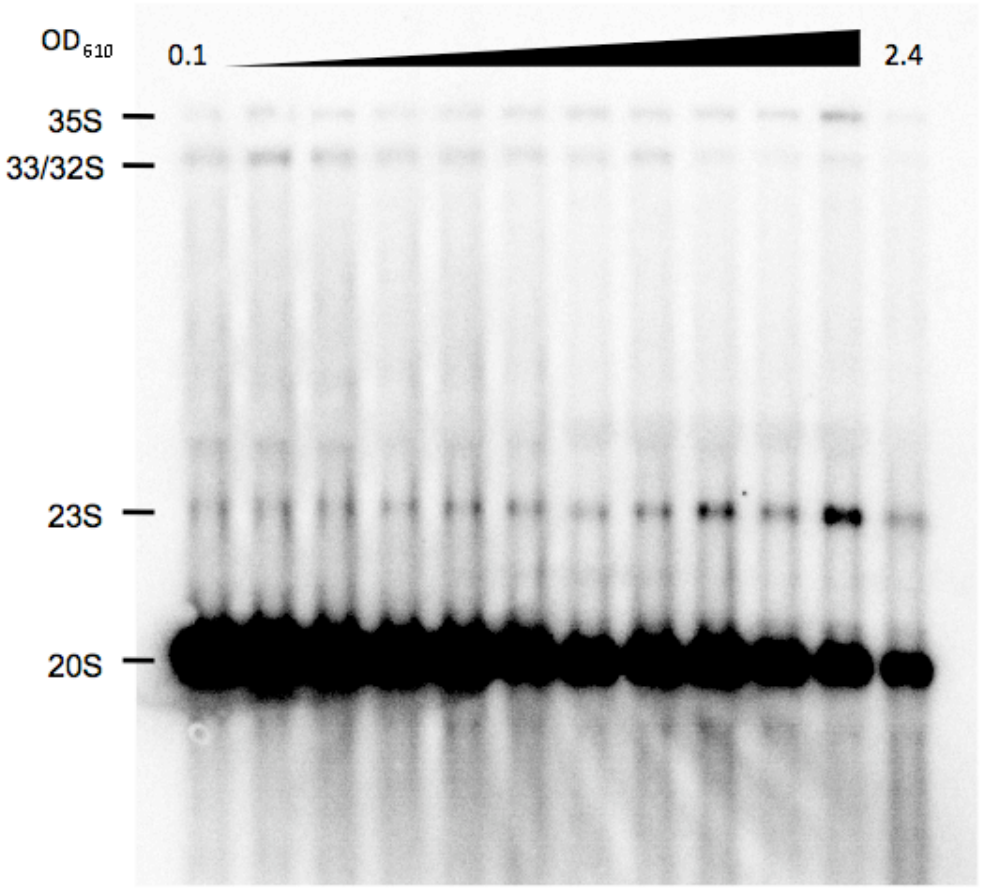

OD
0.1
0.5
1.0
2.0
4.0
5.0
5.5
6.0
0.5
27SA2
23S
27SA
27SB
23S
20S
25S
18S
1
2
3
4
5
6
7
8
9

Figure 32 (and 33): Pre-rRNA processing in cells grown to high density

Pre-rRNAs extracted from aliquots of cells at the indicated densities were assayed by northern blotting using oligonucleotides complimentary to ITS1 and ITS2. 25S and 18S rRNA was detected by staining with ethidium bromide. Lane 9 corresponds to cells that were diluted from OD_{610} = 6.0 to OD_{610} = 0.1, and then allowed to grow to OD_{610} = 0.5.

Pre-rRNAs assayed by northern blotting in Figure 33 (below) were extracted at the indicated densities from a different culture, grown independently of the culture described in Figures 31 and 32.

FIGURE 33



3.3 DISCUSSION

Previously, we showed that missense mutations in the DBP Drs1 cause cold-sensitivity and block processing of 27SB pre-rRNA (Fig. 21)(Ripmaster et al. 1992; Adams et al. 2002). Here we report that depletion of Drs1 affects earlier steps in 27S pre-rRNA processing, resulting in a different phenotype than that observed in *drs1* missense mutants. This highlights the necessity and benefit of looking at multiple different kinds of mutants, including missense mutants and null mutants.

Additionally, we provide evidence indicating that Drs1 can physically interact with the Nop7-subcomplex, and that Nop7 is required for association of Drs1 with pre-ribosomes. Last, we describe a previously unreported phenotype observed upon depletion of Drs1, in which a population of pre-ribosomes is produced that contains both early- and late-associating proteins, as well as early pre-rRNA intermediates. While initially confusing, we believe these results reflect that depletion of Drs1 causes a shift from co-transcriptional to post-transcriptional pre-rRNA processing. This work highlights and discusses novel ideas about ribosome assembly regarding the order and timing of pre-rRNA processing, and the overall hierarchy of protein association with nascent pre-ribosomal particles, and the effects on pre-rRNA processing when early steps of assembly occur post-transcriptionally.

Traditionally, many assembly factors were concluded to function in a particular step of ribosome biogenesis, based on pre-rRNAs that accumulate in a given mutant. Often, only one particular kind of mutant has been studied; either the original mutant isolated in a screen for defects in ribosome biogenesis, or a conditional null mutant. This has served the field of ribosome assembly well for initial classification of most of the proteins that function

in this complex processes. Nevertheless, it is becoming clear that many of these factors may function in more than one step of ribosome biogenesis, thus necessitating the need to assay ribosome assembly in more than one kind of assembly factor mutant.

Originally, Drs1 was classified as an assembly factor required for processing of 27SB pre-rRNA (Adams et al. 2002). This was based on pulse-chase analysis of *drs1* mutants that were isolated in our screens for cold-sensitive mutants defective in ribosome synthesis (Ripmaster et al. 1992). Here we show that depletion of Drs1 blocks processing of $27SA_2$ and $27SA_3$ pre-rRNAs (Fig. 22). The pre-rRNA processing defect observed upon depletion of Drs1 is earlier than that observed in the cold-sensitive missense mutants suggesting that Drs1 might function in more than one consecutive step of ribosome assembly. Sequencing of the original cold-sensitive *drs1* mutants revealed single amino acid changes, near the conserved motifs for RNA binding, ATP binding, or ATP hydrolysis. Furthermore, these original *drs1* mutant proteins are stable and able to associate with pre-ribosomes (data not shown). Thus, one possibility is that the physical presence of Drs1 is required for processing of 27SA pre-rRNAs, but a fully active form is necessary to proceed past the next step of pre-rRNA processing, cleavage of 27SB pre-rRNA at the C_2 site. Alternatively, the mutant *drs1* proteins may have enough activity to allow processing of 27SA pre-rRNA, but not enough to proceed past processing of 27SB pre-rRNA. A similar phenomenon for the DEAD-box protein Has1 has been described by Dr. Jill Dembowski in our lab (Dembowski et al. 2013).

We have shown that Drs1 physically and functionally interacts with the A_3 factor Nop7 (Fig. 23). Depletion of Nop7 results in a very similar pre-rRNA processing phenotype to depletion of Drs1, and Drs1 cannot assemble into pre-ribosomes when Nop7 is absent.

Furthermore, we show that Drs1 can physically interact *in vitro* with the Nop7-subcomplex. These data, plus previously observed genetic interactions, suggest Drs1 is recruited into pre-ribosomes by Nop7, strengthening the idea that Drs1 functions in processing of 27SA pre-rRNAs, in addition to 27SB pre-rRNA. Since depletion of Drs1 has no effect on the association of Nop7 with pre-ribosomes, and both proteins associate with pre-ribosomes early in assembly (data not shown), our data also begin to establish an order of assembly, suggesting Nop7 associates with pre-ribosomes before Drs1.

The Nop7-subcomplex is composed of the assembly factors Nop7, Erb1, and Ytm1 (Miles et al. 2005). Previously, it was shown that the mammalian homologues of these proteins (Pes1, Bop1, and WDR12) also form a stable subcomplex and are required for biogenesis of the large ribosomal subunit (Strezoska et al. 2002; Lapik et al. 2004; Holzel et al. 2005). Interestingly, overexpression of dominant mutant alleles, or siRNA-mediated knock-down of these proteins blocks processing of 32S pre-rRNA in mammalian cells. 32S pre-rRNA contains the sequences for 5.8S rRNA, ITS2, and 28S rRNA, and thus is the mammalian equivalent to yeast 27SB pre-rRNA. This is consistent with previous observations that cold-sensitive *drs1* mutants are defective in 27SB pre-rRNA processing, and solidifies our conclusion that Drs1 functions with the Nop7-subcomplex in processing of both 27SA and 27SB pre-rRNAs.

As discussed in Chapter 2, a number of the A_3-factor RNA-binding sites were determined by UV crosslinking (Granneman et al. 2011). Nop7 and Erb1 were shown to crosslink to domains III and I of 25S rRNA, respectively. When viewed using the crystal structure of the yeast 60S subunit, the RNA binding sites of Nop7 and Erb1 lie above and below the ITS2-proximal stem, a helix formed by the 5' end of 25S rRNA and the 3' end of

5.8S rRNA (refer to Fig. 11). Three other A_3-factors, Rlp7, Nop15, and Cic1, have been shown to bind within ITS2 (Granneman et al. 2011; Babiano et al. 2013). These proteins were originally classified as A_3 factors because their depletion results in an accumulation of $27SA_3$ pre-rRNA and reduction in the downstream product of $27SA_3$ processing, 27SB pre-rRNA. It still remains unclear whether the reduction in 27SB pre-rRNA upon depletion of the A_3-factors results from a failure to generate it, or because it is rapidly turned over when the A_3-factors are absent. The location of the A_3 factors, particularly Rlp7, Cic1, and Nop15 strongly suggests they may also play a role in either processing of 27SB pre-rRNA, or maintaining its stability after it is generated. The A_3 factors, including Drs1, may be precisely positioned within the assembling ribosome to first function in processing $27SA_3$ pre-rRNA to generate the 5' end of 5.8S rRNA, and then to function in processing of 27SB pre-rRNA to generate the 3' end of 5.8S rRNA. Furthermore, it is becoming increasingly clear that proper folding of ITS2 is a prerequisite for processing ITS1. It will be interesting to see if appropriate mutations in yeast Nop7, Erb1, and Ytm1 have similar pre-rRNA processing defects compared to mutations in mammalian Pes1, Bop1, and WDR12.

Recently, it was shown that cleavage at the A_2 site (and presumably the A_0 and A_1 site) predominantly occurs co-transcriptionally in yeast (Osheim et al. 2004; Kos and Tollervey 2010). Co-transcriptional cleavage at the A_2 site occurs ~70-80% of the time in rapidly dividing yeast cells. Thus, only ~20-30% of rRNA transcription results in a 35S pre-rRNA that is cleaved at the A_2 site post-transcriptionally. Furthermore, when yeast cells are grown to high OD_{600}, the frequency of co-transcriptional A_2 cleavage decreases dramatically, suggesting that co-transcriptional pre-rRNA processing is regulated by cell growth and division (Osheim et al. 2004). It was recently shown that pre-rRNA in *C.*

albicans is processed co-transcriptionally in rapidly dividing cells, but processed post-transcriptionally after cells undergo the diauxic shift (Pendrak and Roberts 2011). Kos and Tollervey predicted that 27SA pre-rRNA generated co-transcriptionally has a relatively short lifetime (~15 s) and is rapidly converted to 27SB pre-rRNA (Kos and Tollervey 2010). Conversely, 27SA pre-rRNA generated post-transcriptionally was predicted to have a much longer lifetime (~95 s). Thus, we would reason that more post-transcriptional cleavage at the A_2 site would result in greater steady state amounts of 35S and 27SA pre-rRNAs.

Depletion of Drs1, as well as the A_3-factors and other proteins that function early in the biogenesis of 60S subunits, results in the accumulation $27SA_3$ pre-rRNA and a subsequent decrease in $27SB_s$ pre-rRNA relative to $27SB_L$ pre-rRNA (Sahasranaman et al. 2011). Interestingly, many of these 66S assembly mutants are also accompanied by an increase of $27SA_2$ and 35S pre-rRNAs (Dunbar et al. 2000; Gadal et al. 2002; Fatica et al. 2003b; Oeffinger and Tollervey 2003). This phenotype is often attributed to the sequestration of early-functioning assembly factors on stalled 66S pre-ribosomes, causing early steps in pre-rRNA processing to be affected. An equally plausible scenario is that disruption of early steps of ribosome biogenesis causes a shift from co-transcriptional pre-rRNA processing to post-transcriptional pre-rRNA processing (Fig. 29). We believe that in our mutants, ribosome assembly is disrupted, leading to decreased cell growth, and thus a shift from co- to post-transcriptional pre-rRNA processing. This shift could account for the increased steady-state amounts of 35S and $27SA_2$ often observed in 66S assembly mutants, since more 35S pre-rRNA would be produced, and $27SA_2$ pre-rRNA is predicted to have a much longer lifetime when generated post-transcriptionally.

Here we directly confirmed the idea that cells grown to high density undergo a greater fraction of post-transcriptional pre-rRNA processing. By northern blotting we observed an enrichment of 35S pre-rRNA relative to other co-transcriptional intermediates (33S/32S pre-rRNA). A majority of post-transcriptionally produced 35S appeared to be directly cleaved at the A_3 site, resulting in the accumulation of 23S pre-rRNA. These results suggest that pre-rRNAs produced post-transcriptionally can mature through an alternative processing route. However, if this is the case, one might not expect to see the accumulation of $27SA_2$ as described above. One possibility is that post-transcriptionally derived 35S is not always cleaved directly at the A_3 site, but rather is in an equilibrium between cleavage of the A_2 site and A_3 site. When cleavage at the A_2 site occurs, the resulting $27SA_2$ pre-rRNA might have a longer lifetime than when generated co-transcriptionally. Alternatively, the predicted longer lifetime of 27S pre-rRNA could be attributed to $27SA_3$ pre-rRNA. The work done by Kos and Tollervey did not differentiate between $27SA_2$ and $27SA_3$ pre-rRNAs (Kos and Tollervey 2010).

Our results demonstrate that depletion of Drs1, and subsequent disruption of ribosome biogenesis, causes the formation of pre-ribosomes that contain both early- and late-associating assembly factors (Fig. 24). What is most striking about this phenotype is that pre-ribosomes contain both 40S and 60S factors that are thought to associate with pre-ribosomes only after A_2 cleavage has separated maturation of the large subunit from the small subunit. Upon depletion of Drs1 for 4 hours, we observed an accumulation of 27S pre-rRNA but little effect on processing of 35S or 33S/32S pre-rRNAs (Fig. 22). It was only at later time-points that an accumulation of 35S and 33S/32S pre-rRNAs was observed, suggesting that initial depletion of Drs1 does not affect cleavage at sites A_0, A_1, or A_2. We

believe that the later accumulation of 35S and 33S/32S does not reflect a defect in cleavage at the A_2 site, as but rather the shift from co- to post-transcriptional cleavage of the A_2 site. Furthermore, we see that Nog2, Arx1, and Lsg1 co-immunoprecipitate 35S pre-rRNA and are associated with increased amounts of Pol I components upon Drs1 depletion (Fig. 27A and Fig. 28). In rapidly dividing cells, co-transcriptional cleavage at the A_2 site prevents the formation of large amounts of 35S pre-rRNA. Once transcription is finished, the resulting $27SA_2$ molecule is rapidly converted to $27SA_3$ pre-rRNA and subsequently to 27SB pre-rRNA. These pre-rRNA processing steps may occur more rapidly than the folding and/or formation of the binding sites of Nog2, Arx1, and Lsg1. Thus, these proteins mainly associate with late 66S pre-ribosomes containing 27SB pre-rRNA (Fig. 29, left). Disruption of ribosome assembly, and subsequent shift from co- to post-transcriptional pre-rRNA processing would increase the amount of 35S pre-rRNA transcribed and the lifetime of 27SA pre-rRNA. This may provide a longer window of opportunity for the binding sites of normally "late" associating proteins to form within nascent transcripts and 35S and 27SA pre-rRNAs (Fig. 29, right).

Previous results suggest there is an underlying relationship between Pol I pausing and co-transcriptional cleavage at the A_2 site (El Hage et al. 2010). Electron microscopy and chromatin immunoprecipitation analysis of actively transcribed rDNA revealed a "pile-up" of Pol I over 18S rRNA and ITS1. Deletion of topoisomerase I and II exacerbated the pile-up suggesting that this was due to positive torsion forces and supercoiling of the rDNA in front of Pol I. Furthermore, loss of Top1 and Top2 resulted in the accumulation of aberrant pre-rRNAs with 5' ends corresponding to either the transcription start site, or the A_2 site. In yeast, cleavage of nascent transcripts generated by Pol II is essential to avoid

transcriptional "roadblocks" and for cell viability (Sigurdsson et al. 2010). Yeast may have evolved a similar mechanism for Pol I derived transcripts. In rapidly dividing yeast, co-transcriptional cleavage at the A_2 site may be necessary to accommodate the large number of polymerases actively transcribing rDNA. An interesting possibility is that fluctuations in Pol I pausing afford the pre-rRNA opportunities to sample a greater number of folding pathways, one of which leads to co-transcriptional cleavage.

3.4 MATERIALS AND METHODS

Construction and growth of yeast strains

Yeast strains used in this study were derived from JWY6147 and are listed in the strain list. Unless otherwise noted, yeast were grown at 30 °C in YEPGlu (2% dextrose, 2% peptone, and 1% yeast extract) or YEPGal (2% galactose, 2% peptone, and 1% yeast extract). Cells were harvested at mid-log phase, at 3-5x10^7 cells/ml, unless otherwise indicated.

Yeast strains conditional for expression of Drs1 were constructed as previously described (Longtine et al. 1998). Briefly, sequences containing the selectable marker *TRP1*, plus the *GAL1* promoter followed by an ATG and codons encoding three copies of the hemaglutinin (HA3) epitope were amplified by PCR. The PCR products were transformed into yeast and transformants were screened for correct integration of the *GAL1* promoter and HA tag by western blotting with anti-HA antisera. Strains containing the *GAL1* promoter fused with the *DRS1* ORF were grown at 30 °C in YEPGal to 3-5x10^7 cells/ml, or were grown in YEPGal and then shifted to YEPGlu for indicated times, to 3-5x10^7 cells/ml, to deplete Drs1 *in vivo*.

Yeast strains expressing C-terminal TAP-tagged proteins or C-terminal 3HA-tagged proteins were created by PCR of the tag sequences and a selectable marker (*URA3* for the TAP tag and *HIS3* or *kanMX6* for the 3HA tag), transformation, and selection as described in Rigaut *et al*. (1999) or Longtine *et al.* (1998) respectively.

Assaying pre-rRNA processing and turnover

Steady-state levels of pre-rRNAs and rRNAs were assayed by northern blotting and primer extension, and synthesis and turnover of pre-rRNAs were monitored by pulse-chase assays, as previously described (Horsey et al. 2004; Jakovljevic et al. 2012), with the following modifications. 5 µg of RNA was used for northern blotting and primer extension. Oligonucleotides used for northern blotting and primer extension are listed in the Oligonucleotide list. For pulse-chase assays, cells were pulse labeled with [^{3}H methyl]-methionine for 5 or 10 minutes and chased with a molar excess of unlabeled methionine for 2, 5, 10, and 60 minutes. Total RNA was extracted and equal counts per minute of each sample was loaded and separated on a 1.2% agarose-6% formaldehyde gel.

Affinity purification of pre-ribosomes

Ribosome assembly intermediates were affinity-purified from whole-cell extracts using magnetic Dynabeads (Invitrogen) as described in Sahasranaman *et al*. (2011). RNA enriched in these purified pre-ribosomes was extracted, as described in Sahasranaman *et al*. (2011), and was assayed by primer extension as described in Horsey *et al* (2004). To test the association of HA-Drs1 with the Nop7-subcomplex, pre-ribosomes were purified as described above with the following modification. After incubating whole-cell extracts with

magnetic Dynabeads, the beads were washed with buffer containing the indicated amounts of $MgCl_2$ prior to elution with TEV protease.

Protein extraction, SDS-PAGE, and western blot analysis

Proteins in whole cell extracts were prepared for gel electrophoresis as previously described in Ausubel *et al*. (1994). Proteins were isolated from affinity-purified pre-ribosomes by precipitation with 10% TCA, and were resuspended in SDS sample buffer. Proteins were resolved by SDS-PAGE on 4%-20% Tris-Glycine Novex precast gels (Invitrogen), and stained with silver by standard methods. Proteins from whole-cell extracts or from purified pre-ribosomes were assayed by western blot analysis. To enable detection of multiple different proteins on the same blot, after electroblotting, nitrocellulose membranes were cut into smaller pieces based on previously established mobility of different proteins. Each section of membrane was then probed with the appropriate antibody, developed, and the membrane reconstructed. TAP-tagged proteins were detected using alkaline phosphatase conjugated to IgG (Pierce). HA-tagged proteins were identified with mouse monoclonal antibody 12CA5. Myc-tagged proteins were identified with mouse monoclonal antibody 9e10 (Developmental Studies Hybridoma Bank). Otherwise, antibodies specific for r-proteins or ribosomal assembly factors were used. To assay Nog2 protein by western blotting, NuPage 4%-12% Bis-Tris gels (Invitrogen) were used, since Nog2 co-migrates with IgG on 4%-20% Novex gels. AP-conjugated anti-mouse or anti-rabbit secondary antibodies (Promega) were used, and colorimetric detection was performed using NBT and BCIP (Promega) to visual western blots.

Affinity purification of pre-ribosomes and analysis by iTRAQ mass spectrometry

For semi-quantitative iTRAQ mass spectrometry, pre-ribosomes were purified as described above. Pre-ribosomes were purified from 1 l of cell culture at 3-5x10^7 cells/ml. Purified pre-ribosomes were eluted from the IgG Dynabeads, precipitated with 10% TCA, and resuspended in 20 µl of 20 mM HEPES pH 7.4. iTRAQ labeling and quantification was performed as previously described in Jiang *et al*. (Jiang et al. 2007).

PyMOL

The PyMOL image of the structure of yeast the yeast 40S ribosomal subunit was generated using PDB files 3U5f and 3U5G.

High-copy suppressor screens

Mutations in *NOP7* were generated by error prone PCR. Plasmids containing the mutated genes were transformed into a *nop7Δ* strain harboring a plasmid containing wild-type *NOP7* and the *URA3* gene. Transformants were grown on solid 5-FOA medium to force loss of the *URA3* plasmid containing wild-type *NOP7.* Transformants were then screened for temperature-sensitive growth phenotypes at 36 °C. To test whether extra copies of *DRS1* could suppress the *nop7* mutants, *DRS1* was cloned into high-copy vectors Yep24 and Yep352 and transformed into *nop7* mutant strains. Suppression was assayed by spotting serial dilutions (1-, 10-, 100-, 1,000-, and 10,000-fold) on solid medium and incubating at 25 °C and 36 °C.

Subcomplex purification and *in vitro* pull-down assays

The Nop7-subcomplex and Rpf2-subcomplex were purified from *rrp1-1* mutant cell extracts as previously described (Miles et al. 2005). Pre-ribosomes are unstable in the *rrp1-1* mutant, allowing better purification of assembly subcomplexes. Instead of eluting from the calmodulin column, the subcomplexes were left on the beads after the initial wash and later used in pull-down assays.

[^{35}S]-methionine-labeled Drs1 and Rlp7 were synthesized *in vitro* using the TNT T7 Quick for PCR DNA kit (Promega). Pull-downs were performed as described in Miles *et al*. (2005) with the following modifications. 40% of each labeling reaction was incubated with the Nop7-subcomplex and Rpf2-subcomplex, still bound to the calmodulin column. After incubation at 4 °C for 2 hours, complexes were eluted from the calmodulin column, separated by SDS-PAGE, and visualized by autoradiography.

CHAPTER 4: Mod-seq: High-throughput sequencing for chemical probing of RNA structure

PREAMBLE

Over the last few years our lab has come to realize the importance of RNA folding during ribosome biogenesis and have begun assaying RNA structure in ribosome assembly mutants. Traditional RNA structure probing approaches are tedious, time-consuming, and labor intensive. Therefore, I was extremely excited when the McManus group approached us about collaborating to develop a method to assay RNA structure probing experiments by next-generation sequencing. This work was a collaboration in the truest sense: each person involved contributed through their particular area of expertise and the work was divided evenly among all. I contributed by performing *in vivo* DMS probing, primer extension and PAGE analysis, as well as preparing parts of the manuscript. I also played a large role in initially designing the "proof-of-principle" experiments and data interpretation. Gemma May performed sequencing library preparation and contributed to preparation of the manuscript. The general experimental design, data analysis, and manuscript preparation were done by Joel McManus. The work presented here is currently under consideration for publication in *RNA.*

I will be joining the McManus group for a short post-doctoral appointment upon completion of my tenure in the Woolford laboratory.

4.1 INTRODUCTION

To date, the RCSB Protein Data Bank, contains structures for ~83,000 proteins, compared to only ~1,000 RNAs (Berman et al. 2000). Thus, our knowledge of RNA structure at the atomic level is still in its infancy. However, classical "footprinting" approaches to understand RNA structure have revealed how these dynamic molecules can fold up into complex secondary and tertiary structures. As discussed in Chapter 1 (1.6.5), these techniques rely on small molecules, ions, or enzymes to cleave or modify the RNA, often in a solvent accessible manner (Peattie and Gilbert 1980; Ehresmann et al. 1987; Weeks 2010). Cleavages or modifications can then be detected using a radioactively labeled primer, reverse transcription, and PAGE analysis (Stern et al. 1988; Wells et al. 2000). While these approaches have been invaluable to gaining insight into the secondary and tertiary structures of RNAs, they are often labor intensive and time-consuming. The resolution of primer extension and SDS-PAGE analysis only allows interrogation of ~150 nucleotides per radiolabeled primer, and only a handful of RNAs can be investigated at a time. Furthermore, quantifying the signals on an autoradiograph can be extremely tedious even with the development of new software such as SAFA (Das et al. 2005).

New approaches have helped streamline investigating RNA secondary and tertiary structures. A relatively new approach to assaying RNA structure, Selective 2'-Hydroxyl Acylation and Primer Extension (SHAPE) measures nucleotide flexibility, providing structural information such as base-pairing and tertiary interactions (Merino et al. 2005). Combining SHAPE with fluorescently labeled oligonucleotides and capillary electrophoresis has allowed rapid interrogation of much longer RNAs, including *E. coli* and yeast ribosomal RNAs (Deigan et al. 2009; Leshin et al. 2011) and the HIV-I RNA genome (Wilkinson et al.

2008; Watts et al. 2009). Resolving the extension reactions by capillary electrophoresis (SHAPE-CE), in combination with automated sequencing and data analysis, allows approximately 600-700 nucleotides of a given RNA to be assayed per fluorescently labeled oligonucleotide. While this has greatly improved the speed and accuracy of obtaining and analyzing structure probing data, there are still limitations to this approach: 1) Analysis of data obtained by capillary electrophoresis is still relatively time-consuming. Data must be corrected for background, mobility shifts due to the different primers, and signal decay of longer read lengths. Then, the sequencing traces must be aligned, and the area under each nucleotide peak calculated. 2) Furthermore, because each nucleotide modification is detected by primer extensions initiating from the same site on the RNA of interest, complex modeling of polymerase drop-off is needed during data interpretation. 3) Last, because this approach uses oligonucleotides complementary to an RNA of interest, structure probing of long RNAs requires the use of more than one oligonucleotide, and only a limited number of RNAs can be assayed at a time.

In an effort to characterize the structures of multiple, different RNAs in a single experiment, recent approaches have begun utilizing next-generation sequencing to assay modifications or cleavages in RNA structure probing experiments. FragSeq and parallel analysis of RNA structure (PARS) rely on structure-specific nucleases that cleave either single-stranded or double-stranded RNAs (Kertesz et al. 2010; Underwood et al. 2010). While a significant step forward, these techniques are limited to *in vitro* analysis and only provide a low-resolution picture of RNA secondary structure. SHAPE-Seq combines SHAPE chemistry with deep sequencing technology to simultaneously assay nucleotide flexibility of multiple RNAs (Lucks et al. 2011). While providing higher resolution structure

information, SHAPE-Seq has been limited to the analysis of relatively short RNAs (~300 nts) transcribed *in vitro*.

To overcome the challenges listed above we have developed a new method called Mod-seq for assaying the *in vivo* structure of long RNAs by next-generation sequencing. This approach is applicable both *in vivo* and *in vitro*, and can be utilized with any small molecule, chemical, or enzyme that cleaves or modifies RNA and blocks processivity of reverse transcriptase. Using the small molecule dimethyl sulfate (DMS) and deep sequencing, we probed the entire yeast transcriptome in a single experiment. Mod-seq analysis of total cellular RNA generated secondary structure information for all four yeast rRNAs and 32 other highly abundant non-coding RNAs *in vivo*. Our approach produced DMS modification patterns consistent with the published structure of the yeast ribosome, highlighting the power of this technique to investigate the structure of especially long RNAs (Ben-Shem et al. 2011). To validate this technique, we assayed the structural changes that occur in 80S yeast ribosomes in a previously characterized *rpl26Δ* deletion mutant (Babiano et al. 2012). By combining *in vivo* DMS probing with deep sequencing, we were able to detect previously characterized structural changes in 5.8S and 25S rRNAs, and footprinted the L26 binding site. Thus, Mod-seq is sure to be a powerful new approach to understanding the dynamics and folding of long RNAs and complex RNA mixtures.

4.2 RESULTS

4.2.1 Overview of the Mod-seq strategy and pipeline

We sought a high-throughput method to probe long RNA structures *in vivo* to advance research in RNA biology. While DMS probing is a well-established, powerful approach to interrogate RNA structural characteristics in living cells, identifying the sites of DMS modification using traditional electrophoresis approaches is tedious and relatively slow. We developed a new method, called Mod-seq, to map RNA chemical modification using high-throughput sequencing (Fig. 34). Mod-seq introduces several features that allow high-throughput probing of long RNAs. Chemically treated RNA is randomly fragmented and an adapter oligonucleotide is ligated to 3' ends of RNA fragments. This 3' adapter serves as a universal primer-binding site for reverse transcription, allowing modification mapping on RNAs of any length. However, fragmentation of the RNA introduces another challenge; differentiating reverse transcriptase stops due to DMS modification from those that result from runoff of reverse transcriptase from the fragmented RNA ends. To solve this problem, a second adapter oligonucleotide is ligated to 5' ends of RNA fragments. RNA fragments containing the 5' adapter are enriched and converted to cDNA via reverse transcription using a primer containing a 5' phosphorylated end. Finally, cDNA products are circularized and PCR amplified to produce barcoded libraries for multiplexed high-throughput sequencing. High-throughput sequence reads that initiate with the 5' adapter indicate reverse transcriptase drop off at random fragment ends, while reads without the 5' adapter result from reverse transcriptase release at a modified nucleotide.

FIGURE 34

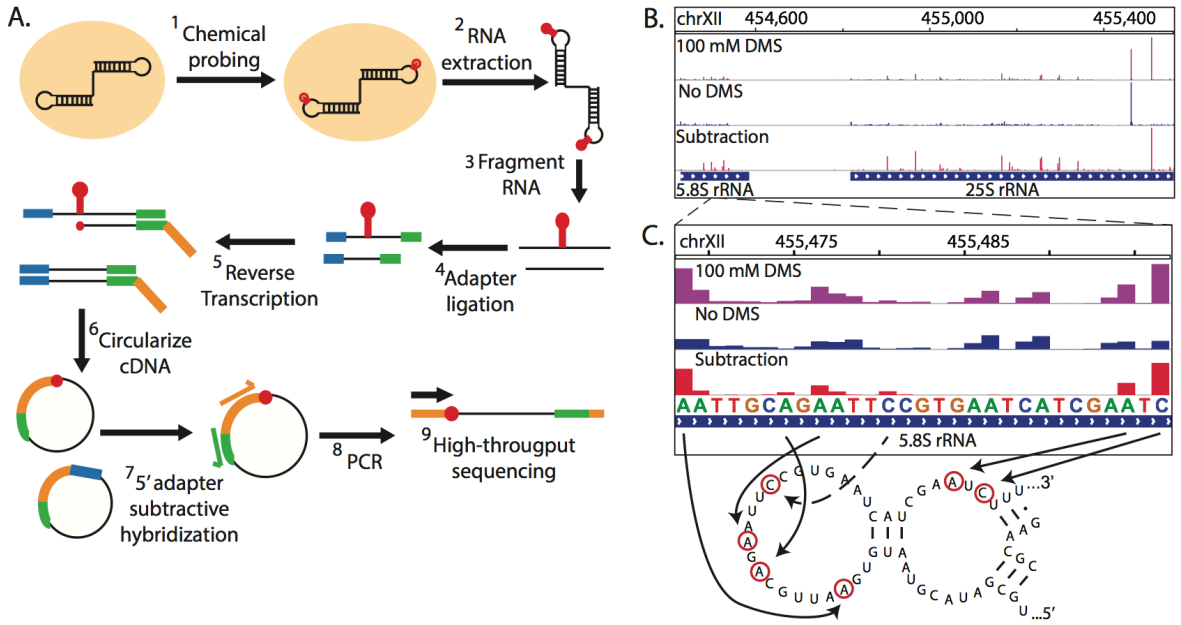

A.
1 Chemical probing
2 RNA extraction
3 Fragment RNA
4 Adapter ligation
5 Reverse Transcription
6 Circularize cDNA
7 5′ adapter subtractive hybridization
8 PCR
9 High-throughput sequencing
B.
chrXII 454,600 455,000 455,400
100 mM DMS
No DMS
Subtraction
5.8S rRNA
25S rRNA
C.
chrXII 455,475 455,485
100 mM DMS
No DMS
Subtraction
AATTGCAGAATTCCGTGAATCATCGAATC
5.8S rRNA
3′
5′

Figure 34: Mapping DMS modification sites with high-throughput sequencing

(A) RNA from DMS treated cells is randomly fragmented, ligated to specific 5' (blue) and 3' (green) adapter oligonucleotides and reverse transcribed. cDNA is circularized and products containing 5' adapter sequences are reduced via subtractive hybridization. Remaining cDNA products are PCR amplified to introduce Illumina library sequences. Each library is given a unique 6 nucleotide barcode and pooled for high-throughput sequencing. Reads containing the 5' adapter sequence are removed from further analysis. (B) Genome browser view (IGV) showing the number of 5' read ends from DMS treated (+, purple) and untreated (Neg, blue) samples. The peak in the "no DMS" sample corresponds to a known site of endogenous rRNA methylation. The difference between these plots is shown in red, after shifting peaks 1 nucleotide 5' to represent actual sites of chemical modification. (C) Enlarged genome browser view of structure probing on the 5.8S rRNA. Reverse transcriptase blocks due to DMS modification are mostly A and C nucleotides, and map to known single-stranded regions in 5.8S rRNA.

4.2.2 *In vivo* Mod-seq analysis of yeast rRNA

As proof-of-principle, we used Mod-seq to identify sites of *in vivo* DMS modification of yeast ribosomal RNA. Mod-seq libraries were prepared using RNA from DMS-treated (T) and control (C) cells. Libraries were sequenced to produce an average of 5.7 million reads from each of two replicate experiments (Table 2). We identified 606 nucleotides from 36 highly abundant non-coding RNAs (rRNA, tRNA, and snoRNA) with significantly more chemical modification after DMS treatment (Table 3). Mod-scores from significant sites ranged over more than three orders of magnitude, suggesting our approach is highly sensitive. The mod-scores for sites on scR1 (7S RNA of signal recognition particle) and rRNAs are depicted in Figures 35 and 36, respectively. Sites with high mod-scores are localized to regions of single-stranded RNA, and were consistent with traditional primer extension analysis (Fig. 37). DMS-specific reverse transcriptase stops were enriched at A residues, consistent with the known base-specificity of DMS (1.8-fold enrichment compared to genomic A frequency, Fisher's Exact Test, P = 2.1x10^-8). In addition, several robust reverse transcriptase stops were present in negative control experiments. These DMS-independent stops occurred at known endogenously modified rRNA nucleotides (Fig. 34B). We conclude that Mod-seq can successfully map chemically modified nucleotides on large RNAs from living cells.

TABLE 2

Numbers of high-throughput sequencing reads obtained for this study. Reads labeled "5' adapter" indicate RT run off from RNA fragment ends, while reads labeled "Mod-stop" indicate reads that lacked the 5' adapter sequence.

Sample	DMS Treatment	Total reads	5' adapter reads	Mod-stop reads
Wild-type Replicate 1	None	6,572,240	1,501,392	4,314,075
	100 mM	5,213,100	1,156,426	3,680,790
rpl26Δ Replicate 1	None	6,318,665	1,396,911	4,233,819
	100 mM	5,438,919	958,087	4,058,273
Wild-type Replicate 2	None	7,374,336	1,941,401	4,885,646
	100 mM	5,476,710	946,597	4,048,461
rpl26Δ Replicate 2	None	6,645,131	1,398,804	4,649,725
	100 mM	6,961,172	1,878,217	4,685,461

TABLE 3

Mod-seq identified sites of DMS-dependent modification in yeast total RNA. The number of sequence reads indicating modification at each site are shown (RT stops), as are the total number for the gene (Total RT stops). The enrichment ratio is the relative enrichment of RT stops at each position in RNA from DMS treated culture as compared to untreated culture. The results of statistical analysis are given, including both raw (CMH) and Benjamini-Hochberg corrected (B-H) p-values.

Gene	Position	Nucleotide	100 mM DMS Replicate 1		No DMS Replicate 1		100 mM DMS Replicate 2		No DMS Replicate 2		Enrichment Ratio (DMS / No DMS)	CMH P-values	B-H adjusted P-values	Mod-Score
			RT stops	Total RT stops	RT stops	Total RT stops	RT stops	Total RT stops	RT stops	Total RT stops				
ETS1	94	A	21	1085	4	930	11	779	1	586	5.29	0.000234859	0.041041581	2.99
ETS1	428	A	18	1085	2	930	11	779	1	586	7.91	0.000117724	0.027429797	2.98
ETS1	452	A	38	1085	4	930	14	779	0	586	8.65	8.13E-08	5.68E-05	3.25
ETS1	469	C	30	1085	4	930	11	779	0	586	6.82	6.35E-06	0.002220634	3.13
ETS1	581	A	20	1085	0	930	6	779	2	586	7.01	0.000351924	0.049198991	2.95
ITS1	5	A	27	944	12	1061	14	851	4	851	2.78	0.000553979	0.023315116	2.72
ITS1	10	A	51	944	14	1061	11	851	0	851	4.59	2.14E-08	2.57E-06	2.99
ITS1	13	A	47	944	13	1061	12	851	3	851	4.05	2.14E-07	1.93E-05	2.95
ITS1	74	A	28	944	0	1061	15	851	3	851	11.31	8.89E-09	1.60E-06	2.91
ITS1	133	A	12	944	0	1061	20	851	2	851	11.12	1.32E-06	9.54E-05	2.78
ITS1	154	A	17	944	0	1061	16	851	10	851	3.12	0.000935167	0.033666017	2.68
ITS1	155	A	48	944	37	1061	62	851	30	851	1.74	0.000582878	0.023315116	2.98
ITS1	293	A	11	944	0	1061	8	851	0	851	10.12	0.000278394	0.014317428	2.58
ITS2	2	C	30	1221	9	1027	13	1001	4	835	2.77	0.001337525	0.038621049	2.46
ITS2	5	C	97	1221	27	1027	61	1001	13	835	3.32	3.61E-12	4.17E-10	3.06
ITS2	52	G	26	1221	12	1027	33	1001	9	835	2.35	0.000892448	0.029450771	2.55
ITS2	70	A	54	1221	15	1027	22	1001	13	835	2.27	0.000240506	0.009259495	2.65
ITS2	149	A	36	1221	4	1027	22	1001	5	835	5.40	3.01E-07	1.74E-05	2.69
ITS2	159	A	30	1221	5	1027	18	1001	4	835	4.47	1.33E-05	0.000612368	2.59
ITS2	160	A	51	1221	1	1027	29	1001	4	835	13.37	7.28E-13	1.68E-10	2.89
NME1	97	T	44	322	0	265	33	364	2	293	20.76	1.35E-12	4.58E-10	3.57
RDN18	2	A	1797	603870	1011	717056	2266	545462	989	592258	2.30	2.78E-215	1.09E-213	2.56
RDN18	25	C	3342	603870	1588	717056	2568	545462	1506	592258	2.18	3.01E-282	1.47E-280	2.70
RDN18	40	A	317	603870	185	717056	266	545462	118	592258	2.20	5.59E-30	4.01E-29	1.70
RDN18	43	A	1310	603870	644	717056	949	545462	486	592258	2.28	3.78E-120	9.06E-119	2.30
RDN18	65	A	4654	603870	1081	717056	2711	545462	540	592258	5.23	0	0	2.97
RDN18	67	A	1200	603870	235	717056	918	545462	152	592258	6.26	1.56E-315	9.06E-314	2.44
RDN18	71	A	3520	603870	1444	717056	2274	545462	689	592258	3.12	0	0	2.79
RDN18	72	A	1972	603870	1570	717056	1418	545462	862	592258	1.60	1.13E-70	2.00E-69	2.29
RDN18	76	A	1211	603870	417	717056	765	545462	427	592258	2.67	8.66E-137	2.33E-135	2.29
RDN18	80	A	1242	603870	411	717056	1134	545462	273	592258	3.97	7.51E-257	3.22E-255	2.44
RDN18	84	A	719	603870	513	717056	741	545462	482	592258	1.67	4.96E-36	4.21E-35	1.96
RDN18	103	A	440	603870	266	717056	287	545462	182	592258	1.86	1.30E-25	7.96E-25	1.72
RDN18	104	A	1328	603870	712	717056	966	545462	508	592258	2.15	2.50E-108	5.56E-107	2.28
RDN18	135	A	529	603870	295	717056	549	545462	191	592258	2.53	7.87E-69	1.35E-67	2.01
RDN18	154	G	920	603870	477	717056	869	545462	340	592258	2.50	6.12E-111	1.39E-109	2.22
RDN18	176	C	2460	603870	976	717056	1189	545462	469	592258	2.91	7.72E-284	3.86E-282	2.57
RDN18	180	A	1010	603870	646	717056	698	545462	395	592258	1.88	1.02E-59	1.50E-58	2.09
RDN18	181	A	7445	603870	2472	717056	4672	545462	1042	592258	3.97	0	0	3.15
RDN18	188	A	801	603870	218	717056	524	545462	170	592258	3.91	4.37E-143	1.27E-141	2.19
RDN18	196	G	946	603870	552	717056	602	545462	322	592258	2.03	1.74E-65	2.77E-64	2.09
RDN18	198	A	964	603870	129	717056	418	545462	64	592258	8.26	5.29E-237	2.21E-235	2.28
RDN18	215	A	3859	603870	578	717056	1684	545462	245	592258	7.78	0	0	2.88
RDN18	228	G	909	603870	717	717056	883	545462	513	592258	1.66	2.28E-43	2.43E-42	2.05
RDN18	251	A	2642	603870	566	717056	1702	545462	548	592258	4.45	0	0	2.72
RDN18	266	A	3263	603870	1290	717056	2360	545462	894	592258	2.95	0	0	2.76
RDN18	271	A	373	603870	223	717056	495	545462	251	592258	2.07	1.53E-38	1.41E-37	1.85
RDN18	273	G	87	603870	34	717056	116	545462	57	592258	2.51	6.01E-14	2.14E-13	1.28
RDN18	274	G	97	603870	57	717056	212	545462	108	592258	2.09	6.61E-15	2.45E-14	1.41
RDN18	279	G	327	603870	194	717056	536	545462	361	592258	1.74	4.92E-25	2.93E-24	1.77
RDN18	281	G	360	603870	143	717056	561	545462	219	592258	2.86	3.72E-70	6.50E-69	1.98
RDN18	287	G	1224	603870	473	717056	1378	545462	538	592258	2.91	1.12E-200	4.22E-199	2.43
RDN18	288	A	257	603870	132	717056	446	545462	254	592258	2.04	1.72E-30	1.26E-29	1.76
RDN18	307	G	114	603870	67	717056	201	545462	142	592258	1.69	3.84E-09	1.03E-08	1.31
RDN18	312	A	2923	603870	735	717056	2309	545462	743	592258	4.03	0	0	2.79
RDN18	352	A	11642	603870	987	717056	5524	545462	653	592258	12.03	0	0	3.39
RDN18	359	A	2448	603870	827	717056	1397	545462	641	592258	3.00	3.59E-310	#NUM!	2.60
RDN18	369	A	323	603870	86	717056	318	545462	180	592258	2.71	2.52E-46	2.87E-45	1.80

TABLE 3 cont.

RDN18	412	A	3422	603870	699	717056	2312	545462	507	592258	5.44	0	0	0	2.86
RDN18	416	A	453	603870	175	717056	394	545462	175	592258	2.75	6.69E-62	1.04E-60	1.04E-60	1.93
RDN18	417	A	100	603870	51	717056	116	545462	74	592258	1.95	1.86E-09	5.14E-09	5.14E-09	1.22
RDN18	420	A	167	603870	88	717056	114	545462	52	592258	2.30	1.70E-16	7.05E-16	7.05E-16	1.39
RDN18	421	A	59	603870	34	717056	61	545462	49	592258	1.63	0.000647788	0.001054783	0.001054783	0.87
RDN18	452	A	1863	603870	693	717056	1328	545462	438	592258	3.23	7.23E-281	3.33E-279	3.33E-279	2.54
RDN18	455	C	634	603870	355	717056	455	545462	273	592258	1.98	6.49E-44	6.95E-43	6.95E-43	1.93
RDN18	492	A	1085	603870	542	717056	427	545462	273	592258	2.14	4.40E-72	7.84E-71	7.84E-71	2.10
RDN18	497	G	78	603870	52	717056	58	545462	25	592258	2.03	6.23E-07	1.39E-06	1.39E-06	1.03
RDN18	498	G	567	603870	389	717056	345	545462	148	592258	1.96	4.50E-36	3.84E-35	3.84E-35	1.84
RDN18	510	G	379	603870	330	717056	355	545462	223	592258	1.52	1.47E-13	5.16E-13	5.16E-13	1.59
RDN18	511	A	1003	603870	733	717056	701	545462	441	592258	1.66	9.66E-42	9.87E-41	9.87E-41	2.02
RDN18	515	A	1735	603870	120	717056	1303	545462	137	592258	13.44	0	0	0	2.64
RDN18	529	A	1355	603870	141	717056	1513	545462	265	592258	7.95	0	0	0	2.59
RDN18	534	A	27777	603870	1855	717056	14821	545462	1336	592258	15.30	0	0	0	3.79
RDN18	540	G	629	603870	306	717056	785	545462	435	592258	2.15	3.90E-67	6.56E-66	6.56E-66	2.08
RDN18	541	A	1993	603870	1001	717056	1008	545462	588	592258	2.17	8.42E-145	2.52E-143	2.52E-143	2.40
RDN18	542	A	1791	603870	307	717056	1758	545462	389	592258	5.77	0	0	0	2.66
RDN18	544	A	3362	603870	579	717056	2532	545462	819	592258	4.78	0	0	0	2.86
RDN18	554	C	1058	603870	349	717056	1031	545462	453	592258	2.95	1.46E-164	4.76E-163	4.76E-163	2.34
RDN18	579	A	1579	603870	730	717056	1325	545462	539	592258	2.61	2.07E-192	7.45E-191	7.45E-191	2.45
RDN18	605	A	185	603870	123	717056	238	545462	148	592258	1.76	1.97E-13	6.86E-13	6.86E-13	1.46
RDN18	643	G	61	603870	11	717056	179	545462	125	592258	1.94	3.32E-10	9.66E-10	9.66E-10	1.28
RDN18	648	G	316	603870	242	717056	649	545462	286	592258	2.06	9.48E-42	9.72E-41	9.72E-41	1.89
RDN18	652	G	78	603870	45	717056	206	545462	140	592258	1.71	1.37E-08	3.49E-08	3.49E-08	1.28
RDN18	655	G	46	603870	35	717056	92	545462	60	592258	1.63	0.000929211	0.000497638	0.000497638	0.93
RDN18	669	G	128	603870	86	717056	256	545462	164	592258	1.72	1.98E-11	6.33E-11	6.33E-11	1.41
RDN18	671	G	348	603870	189	717056	611	545462	333	592258	2.06	7.42E-42	7.67E-41	7.67E-41	1.89
RDN18	673	A	137	603870	124	717056	266	545462	168	592258	1.55	1.14E-08	2.94E-08	2.94E-08	1.36
RDN18	696	C	195	603870	56	717056	324	545462	104	592258	3.64	1.28E-52	1.66E-51	1.66E-51	1.77
RDN18	697	C	1155	603870	586	717056	1307	545462	633	592258	2.29	3.28E-130	8.31E-129	8.31E-129	2.34
RDN18	706	A	2096	603870	560	717056	1912	545462	394	592258	4.79	0	0	0	2.70
RDN18	707	A	308	603870	188	717056	383	545462	156	592258	2.28	1.86E-37	1.65E-36	1.65E-36	1.78
RDN18	714	G	1164	603870	712	717056	1643	545462	497	592258	2.64	5.90E-187	2.08E-185	2.08E-185	2.44
RDN18	722	G	92	603870	71	717056	112	545462	62	592258	1.74	6.54E-07	1.45E-06	1.45E-06	1.14
RDN18	730	G	132	603870	110	717056	219	545462	120	592258	1.72	1.28E-10	3.85E-10	3.85E-10	1.37
RDN18	733	A	1346	603870	647	717056	1002	545462	375	592258	2.63	4.23E-158	1.36E-156	1.36E-156	2.36
RDN18	734	A	1323	603870	319	717056	1385	545462	210	592258	5.84	0	0	0	2.55
RDN18	741	C	2656	603870	898	717056	1931	545462	512	592258	3.73	0	0	0	2.72
RDN18	756	A	2591	603870	1142	717056	2615	545462	710	592258	3.21	0	0	0	2.75
RDN18	771	A	760	603870	241	717056	557	545462	166	592258	3.70	5.55E-135	1.45E-133	1.45E-133	2.18
RDN18	780	A	1741	603870	986	717056	995	545462	417	592258	2.25	4.71E-141	1.32E-139	1.32E-139	2.37
RDN18	787	G	540	603870	405	717056	421	545462	114	592258	2.14	1.13E-45	1.49E-44	1.49E-44	1.90
RDN18	789	A	1527	603870	570	717056	670	545462	293	592258	2.94	5.83E-174	1.94E-172	1.94E-172	2.35
RDN18	803	A	2725	603870	1303	717056	1447	545462	443	592258	2.76	7.31E-301	3.99E-299	3.99E-299	2.62
RDN18	809	A	445	603870	175	717056	243	545462	106	592258	2.81	1.71E-52	2.20E-51	2.20E-51	1.84
RDN18	811	A	2178	603870	1387	717056	822	545462	601	592258	1.75	1.12E-84	2.09E-83	2.09E-83	2.29
RDN18	812	A	5846	603870	964	717056	2247	545462	557	592258	6.13	0	0	0	3.02
RDN18	816	G	2889	603870	1686	717056	2138	545462	1572	592258	1.76	1.40E-142	3.99E-141	3.99E-141	2.53
RDN18	824	G	726	603870	606	717056	538	545462	342	592258	1.53	3.59E-23	2.01E-22	2.01E-22	1.83
RDN18	853	G	2266	603870	1249	717056	2034	545462	650	592258	2.59	6.37E-280	2.80E-278	2.80E-278	2.62
RDN18	859	A	3650	603870	1686	717056	2243	545462	772	592258	2.76	0	0	0	2.77
RDN18	875	G	39	603870	15	717056	33	545462	32	592258	1.73	0.004035283	0.006044525	0.006044525	0.68
RDN18	885	G	411	603870	278	717056	225	545462	185	592258	1.58	6.60E-14	2.34E-13	2.34E-13	1.56
RDN18	904	G	527	603870	303	717056	398	545462	244	592258	1.93	2.80E-35	2.32E-34	2.32E-34	1.84
RDN18	929	A	2301	603870	608	717056	1080	545462	331	592258	4.15	0	0	0	2.60
RDN18	934	C	398	603870	182	717056	207	545462	174	592258	1.94	3.98E-24	2.28E-23	2.28E-23	1.66
RDN18	970	A	670	603870	142	717056	413	545462	121	592258	4.71	1.41E-136	3.73E-135	3.73E-135	2.13
RDN18	971	A	117	603870	56	717056	98	545462	74	592258	1.88	1.10E-08	2.85E-08	2.85E-08	1.20
RDN18	993	A	842	603870	103	717056	554	545462	112	592258	7.40	5.02E-227	2.05E-225	2.05E-225	2.28
RDN18	1005	A	372	603870	163	717056	360	545462	245	592258	2.03	1.54E-31	1.16E-30	1.16E-30	1.77
RDN18	1020	A	312	603870	188	717056	291	545462	150	592258	2.03	2.49E-26	1.56E-25	1.56E-25	1.68
RDN18	1030	A	226	603870	112	717056	324	545462	107	592258	2.84	3.50E-42	3.69E-41	3.69E-41	1.75
RDN18	1061	A	2126	603870	695	717056	1710	545462	446	592258	3.85	0	0	0	2.65

TABLE 3 cont.

RDN18	1062	A	487	603870	158	717056	486	545462	172	592258	3.34	6.58E-90	1.30E-88	2.03
RDN18	1091	A	581	603870	260	717056	223	545462	125	592258	2.41	1.09E-48	1.31E-47	1.86
RDN18	1116	A	769	603870	190	717056	444	545462	250	592258	3.14	5.93E-105	1.24E-103	2.11
RDN18	1126	G	53	603870	50	717056	65	545462	21	592258	1.90	2.09E-05	3.98E-05	0.94
RDN18	1139	A	857	603870	22	717056	387	545462	18	592258	35.67	2.20E-287	1.13E-285	2.28
RDN18	1140	G	28	603870	4	717056	16	545462	5	592258	5.57	2.23E-07	5.16E-07	0.75
RDN18	1193	A	5637	603870	1947	717056	2409	545462	867	592258	3.30	0	0	2.94
RDN18	1217	A	198	603870	48	717056	45	545462	18	592258	4.28	4.53E-30	3.27E-29	1.46
RDN18	1219	A	992	603870	155	717056	316	545462	96	592258	6.01	2.55E-194	9.35E-193	2.23
RDN18	1226	A	1017	603870	168	717056	396	545462	78	592258	6.64	3.38E-220	1.35E-218	2.27
RDN18	1227	A	293	603870	54	717056	101	545462	20	592258	6.17	2.03E-60	3.04E-59	1.71
RDN18	1246	C	23655	603870	557	717056	10658	545462	426	592258	40.03	0	0	3.72
RDN18	1247	T	200	603870	76	717056	151	545462	69	592258	2.76	1.04E-26	6.68E-26	1.54
RDN18	1263	G	62	603870	33	717056	49	545462	23	592258	2.27	4.42E-07	9.94E-07	0.99
RDN18	1265	G	873	603870	149	717056	857	545462	87	592258	8.38	3.94E-293	2.08E-291	2.38
RDN18	1319	A	2292	603870	507	717056	1716	545462	511	592258	4.48	0	0	2.69
RDN18	1325	A	3295	603870	1245	717056	1949	545462	779	592258	2.97	0	0	2.73
RDN18	1346	A	1628	603870	688	717056	959	545462	394	592258	2.75	6.99E-186	2.42E-184	2.41
RDN18	1360	A	1218	603870	728	717056	753	545462	493	592258	1.85	6.57E-66	1.06E-64	2.15
RDN18	1368	G	421	603870	298	717056	415	545462	292	592258	1.61	5.24E-19	2.45E-18	1.70
RDN18	1371	A	1094	603870	414	717056	936	545462	446	592258	2.68	1.15E-140	3.19E-139	2.30
RDN18	1383	G	403	603870	177	717056	361	545462	184	592258	2.40	1.52E-45	1.68E-44	1.84
RDN18	1384	A	27	603870	14	717056	23	545462	18	592258	1.77	0.014008678	0.019890775	0.54
RDN18	1385	G	26	603870	17	717056	24	545462	15	592258	1.67	0.030666123	0.041699437	0.47
RDN18	1402	G	276	603870	163	717056	274	545462	159	592258	1.94	9.32E-22	4.98E-21	1.62
RDN18	1419	G	262	603870	123	717056	289	545462	186	592258	2.01	1.14E-23	6.47E-23	1.64
RDN18	1421	A	2012	603870	661	717056	1525	545462	695	592258	2.97	1.46E-280	6.58E-279	2.57
RDN18	1427	A	69	603870	43	717056	154	545462	83	592258	1.98	6.23E-10	1.78E-09	1.25
RDN18	1428	G	181	603870	91	717056	270	545462	101	592258	2.65	1.04E-31	7.86E-31	1.65
RDN18	1460	A	141	603870	68	717056	183	545462	129	592258	1.85	5.99E-12	1.96E-11	1.37
RDN18	1472	C	211	603870	92	717056	163	545462	175	592258	1.58	7.77E-09	2.02E-08	1.34
RDN18	1474	G	1543	603870	1202	717056	1224	545462	789	592258	1.59	1.03E-56	1.45E-55	2.20
RDN18	1488	G	948	603870	373	717056	1049	545462	433	592258	2.81	7.42E-147	2.26E-145	2.31
RDN18	1490	C	942	603870	256	717056	629	545462	597	592258	2.08	3.91E-70	6.76E-69	2.11
RDN18	1492	A	2526	603870	1333	717056	3157	545462	1974	592258	1.94	6.82E-208	2.61E-206	2.64
RDN18	1493	A	585	603870	124	717056	871	545462	399	592258	3.11	2.28E-122	5.62E-121	2.19
RDN18	1503	A	476	603870	82	717056	505	545462	112	592258	5.72	3.53E-139	9.62E-138	2.10
RDN18	1507	G	472	603870	309	717056	634	545462	384	592258	1.80	9.14E-35	7.50E-34	1.89
RDN18	1521	G	1473	603870	214	717056	2562	545462	376	592258	7.67	0	0	2.74
RDN18	1556	A	1804	603870	1083	717056	2264	545462	1276	592258	1.95	1.33E-151	4.14E-150	2.50
RDN18	1572	G	101	603870	57	717056	131	545462	79	592258	1.92	9.34E-10	2.63E-09	1.25
RDN18	1593	A	247	603870	185	717056	396	545462	255	592258	1.64	5.94E-16	2.38E-15	1.60
RDN18	1638	G	190	603870	132	717056	302	545462	235	592258	1.50	2.92E-09	7.89E-09	1.42
RDN18	1640	C	128	603870	54	717056	145	545462	110	592258	1.87	1.30E-10	3.91E-10	1.31
RDN18	1651	A	295	603870	203	717056	329	545462	171	592258	1.90	4.00E-23	2.23E-22	1.67
RDN18	1679	G	26	603870	17	717056	32	545462	22	592258	1.68	0.015003095	0.021235694	0.57
RDN18	1681	A	8703	603870	655	717056	5423	545462	707	592258	11.82	0	0	3.31
RDN18	1689	A	252	603870	187	717056	215	545462	144	592258	1.61	2.97E-11	9.30E-11	1.44
RDN18	1701	A	1075	603870	533	717056	877	545462	713	592258	1.78	3.21E-58	4.54E-57	2.13
RDN18	1702	A	203	603870	74	717056	210	545462	177	592258	1.85	6.10E-15	2.28E-14	1.48
RDN18	1707	A	1243	603870	631	717056	877	545462	463	592258	2.22	1.53E-106	3.32E-105	2.26
RDN18	1712	A	377	603870	48	717056	313	545462	68	592258	6.74	6.80E-108	1.49E-106	1.96
RDN18	1715	G	53	603870	38	717056	52	545462	37	592258	1.59	0.002508305	0.003817632	0.79
RDN18	1721	A	1334	603870	330	717056	973	545462	246	592258	4.58	7.53E-282	3.56E-280	2.45
RDN18	1722	A	538	603870	328	717056	575	545462	358	592258	1.84	4.50E-37	3.97E-36	1.90
RDN18	1731	A	1752	603870	229	717056	1354	545462	254	592258	7.31	0	0	2.62
RDN18	1749	A	85	603870	19	717056	21	545462	8	592258	4.56	1.82E-14	6.55E-14	1.11
RDN18	1750	A	8	603870	3	717056	11	545462	3	592258	3.58	0.006742008	0.009893045	0.33
RDN18	1762	A	5	603870	0	717056	8	545462	3	592258	3.63	0.029352451	0.040034161	0.21
RDN25	6	A	131	1130039	59	1243362	191	1065093	102	1116960	2.14	1.11E-15	4.50E-15	1.43
RDN25	18	G	848	1130039	633	1243362	875	1065093	449	1116960	1.71	1.19E-44	1.27E-43	2.04
RDN25	30	G	492	1130039	123	1243362	589	1065093	100	1116960	5.21	4.47E-138	1.27E-136	2.13
RDN25	85	A	4243	1130039	324	1243362	3516	1065093	254	1116960	14.46	0	0	3.05
RDN25	115	A	1028	1130039	695	1243362	749	1065093	566	1116960	1.52	3.81E-30	2.76E-29	1.97

TABLE 3 cont.

RDN25	116	A	1480	1130039	989	1243362	1262	1065093	771	1116960	1.68	1.43E-65	2.21E-64	2.23	
RDN25	121	A	921	1130039	376	1243362	788	1065093	417	1116960	2.32	5.76E-90	1.13E-88	2.18	
RDN25	137	G	157	1130039	62	1243362	378	1065093	229	1116960	1.95	1.11E-20	5.76E-20	1.61	
RDN25	150	A	6000	1130039	656	1243362	4021	1065093	465	1116960	9.64	0	0	3.14	
RDN25	162	G	104	1130039	40	1243362	90	1065093	50	1116960	2.31	1.79E-11	5.69E-11	1.23	
RDN25	164	A	1005	1130039	580	1243362	570	1065093	312	1116960	1.91	1.91E-55	2.56E-54	2.06	
RDN25	165	A	145	1130039	56	1243362	136	1065093	43	1116960	3.06	1.48E-23	8.66E-23	1.47	
RDN25	204	A	147	1130039	68	1243362	134	1065093	125	1116960	1.56	2.00E-06	4.23E-06	1.20	
RDN25	206	G	3081	1130039	1514	1243362	1843	1065093	804	1116960	2.30	2.60E-252	1.21E-250	2.63	
RDN25	212	G	531	1130039	255	1243362	435	1065093	256	1116960	2.03	6.33E-40	5.98E-39	1.88	
RDN25	213	A	755	1130039	47	1243362	402	1065093	40	1116960	14.35	1.00E-220	3.88E-219	2.22	
RDN25	232	G	135	1130039	76	1243362	128	1065093	92	1116960	1.68	1.38E-07	3.19E-07	1.22	
RDN25	241	G	147	1130039	70	1243362	142	1065093	62	1116960	2.35	6.83E-17	2.97E-16	1.41	
RDN25	251	G	1264	1130039	561	1243362	845	1065093	478	1116960	2.19	1.62E-99	3.51E-98	2.25	
RDN25	253	A	1014	1130039	575	1243362	524	1065093	334	1116960	1.83	1.37E-48	1.58E-47	2.03	
RDN25	256	G	349	1130039	137	1243362	371	1065093	257	1116960	1.95	1.35E-27	9.02E-27	1.74	
RDN25	285	A	464	1130039	229	1243362	354	1065093	268	1116960	1.77	3.29E-24	1.98E-23	1.74	
RDN25	348	A	6270	1130039	2396	1243362	2248	1065093	817	1116960	2.88	0	0	2.93	
RDN25	365	A	1173	1130039	808	1243362	411	1065093	286	1116960	1.57	3.95E-31	2.95E-30	1.94	
RDN25	366	A	2805	1130039	564	1243362	802	1065093	316	1116960	4.45	0	0	2.63	
RDN25	372	A	1642	1130039	596	1243362	417	1065093	223	1116960	2.73	3.86E-142	1.11E-140	2.30	
RDN25	378	A	612	1130039	252	1243362	272	1065093	176	1116960	2.23	1.48E-44	1.57E-43	1.88	
RDN25	385	A	1445	1130039	974	1243362	735	1065093	459	1116960	1.65	1.25E-49	1.49E-48	2.12	
RDN25	390	G	568	1130039	304	1243362	388	1065093	157	1116960	2.24	3.61E-48	4.11E-47	1.91	
RDN25	402	A	416	1130039	155	1243362	271	1065093	105	1116960	2.85	4.68E-51	5.82E-50	1.84	
RDN25	423	A	90	1130039	30	1243362	69	1065093	49	1116960	2.16	1.36E-08	3.47E-08	1.12	
RDN25	436	A	116	1130039	78	1243362	121	1065093	70	1116960	1.72	2.08E-07	4.78E-07	1.19	
RDN25	437	G	4264	1130039	1142	1243362	3403	1065093	979	1116960	3.89	0	0	2.94	
RDN25	438	A	501	1130039	102	1243362	479	1065093	118	1116960	4.78	1.04E-118	2.61E-117	2.08	
RDN25	439	C	5189	1130039	1594	1243362	3904	1065093	2607	1116960	2.32	0	0	2.90	
RDN25	440	A	954	1130039	231	1243362	910	1065093	227	1116960	4.37	9.85E-210	3.64E-208	2.35	
RDN25	442	G	167	1130039	87	1243362	187	1065093	131	1116960	1.74	9.69E-11	2.91E-10	1.37	
RDN25	443	G	284	1130039	167	1243362	334	1065093	159	1116960	2.04	4.58E-26	2.92E-25	1.69	
RDN25	450	G	256	1130039	127	1243362	463	1065093	144	1116960	2.84	1.55E-52	2.02E-51	1.86	
RDN25	453	C	479	1130039	83	1243362	579	1065093	212	1116960	3.83	5.90E-107	1.33E-105	2.08	
RDN25	468	G	31	1130039	24	1243362	37	1065093	23	1116960	1.55	0.024806112	0.033419345	0.57	
RDN25	477	A	2606	1130039	612	1243362	2477	1065093	597	1116960	4.52	0	0	2.79	
RDN25	478	A	1171	1130039	656	1243362	1056	1065093	570	1116960	1.95	7.03E-82	1.30E-80	2.23	
RDN25	480	C	4647	1130039	1060	1243362	3206	1065093	1037	1116960	4.03	0	0	2.96	
RDN25	490	A	208	1130039	127	1243362	230	1065093	176	1116960	1.55	4.41E-09	1.16E-08	1.38	
RDN25	495	G	237	1130039	137	1243362	242	1065093	159	1116960	1.74	5.23E-14	1.94E-13	1.50	
RDN25	499	G	117	1130039	59	1243362	131	1065093	69	1116960	2.08	9.11E-12	2.96E-11	1.30	
RDN25	511	G	257	1130039	176	1243362	220	1065093	111	1116960	1.79	3.39E-15	1.34E-14	1.51	
RDN25	514	G	159	1130039	67	1243362	159	1065093	107	1116960	1.96	5.09E-13	1.79E-12	1.38	
RDN25	521	A	525	1130039	133	1243362	363	1065093	150	1116960	3.38	5.67E-80	1.02E-78	1.99	
RDN25	522	A	871	1130039	490	1243362	746	1065093	313	1116960	2.17	2.35E-75	4.02E-74	2.13	
RDN25	523	A	3264	1130039	615	1243362	2357	1065093	414	1116960	5.89	0	0	2.86	
RDN25	537	A	541	1130039	52	1243362	666	1065093	100	1116960	8.49	5.13E-196	1.80E-194	2.22	
RDN25	546	C	104	1130039	20	1243362	71	1065093	43	1116960	2.98	8.50E-15	3.30E-14	1.26	
RDN25	547	G	210	1130039	80	1243362	219	1065093	118	1116960	2.32	7.94E-24	4.72E-23	1.58	
RDN25	548	G	607	1130039	428	1243362	688	1065093	380	1116960	1.72	2.03E-34	1.66E-33	1.92	
RDN25	572	A	376	1130039	71	1243362	458	1065093	119	1116960	4.69	9.40E-100	2.05E-98	2.01	
RDN25	579	G	356	1130039	83	1243362	455	1065093	78	1116960	5.41	2.20E-106	4.95E-105	2.01	
RDN25	592	A	262	1130039	27	1243362	318	1065093	63	1116960	6.88	3.92E-87	7.53E-86	1.89	
RDN25	593	C	407	1130039	26	1243362	364	1065093	105	1116960	6.28	1.23E-110	2.86E-109	2.00	
RDN25	597	G	341	1130039	184	1243362	226	1065093	167	1116960	1.74	1.76E-16	7.52E-16	1.57	
RDN25	598	A	19	1130039	8	1243362	36	1065093	17	1116960	2.34	0.000416717	0.000687441	0.69	
RDN25	602	A	91	1130039	35	1243362	102	1065093	26	1116960	3.40	1.44E-18	6.85E-18	1.32	
RDN25	603	A	120	1130039	20	1243362	126	1065093	39	1116960	4.46	1.96E-29	1.39E-28	1.47	
RDN25	604	G	189	1130039	75	1243362	217	1065093	196	1116960	1.60	1.80E-09	4.86E-09	1.38	
RDN25	607	A	55	1130039	18	1243362	123	1065093	67	1116960	2.22	6.85E-10	1.92E-09	1.18	
RDN25	608	A	24	1130039	6	1243362	22	1065093	15	1116960	2.34	0.001297056	0.002033012	0.61	
RDN25	613	G	11	1130039	6	1243362	27	1065093	15	1116960	1.92	0.020347529	0.027731779	0.46	
RDN25	619	A	545	1130039	102	1243362	508	1065093	90	1116960	5.90	2.76E-145	8.07E-144	2.13	

TABLE 3 cont.

RDN25	621	A	410	1130039	153	1243362	442	1065093	169	1116960	2.84	2.70E-62	3.93E-61	1.93
RDN25	692	A	55979	1130039	1004	1243362	47306	1065093	928	1116960	57.51	0	0	4.20
RDN25	693	A	481	1130039	105	1243362	393	1065093	159	1116960	3.55	7.51E-83	1.42E-81	1.99
RDN25	697	A	860	1130039	452	1243362	671	1065093	288	1116960	2.23	1.90E-75	3.26E-74	2.12
RDN25	708	G	640	1130039	458	1243362	522	1065093	291	1116960	1.67	1.71E-28	1.17E-27	1.86
RDN25	710	A	286	1130039	190	1243362	234	1065093	177	1116960	1.52	5.69E-10	1.60E-09	1.44
RDN25	711	A	562	1130039	180	1243362	442	1065093	155	1116960	3.23	9.84E-86	1.88E-84	2.03
RDN25	718	G	617	1130039	363	1243362	480	1065093	395	1116960	1.56	4.42E-21	2.33E-20	1.78
RDN25	721	G	353	1130039	174	1243362	341	1065093	118	1116960	2.56	4.28E-44	4.47E-43	1.82
RDN25	734	C	1461	1130039	569	1243362	506	1065093	394	1116960	2.21	2.10E-95	4.39E-94	2.22
RDN25	735	A	1016	1130039	414	1243362	634	1065093	150	1116960	3.17	4.43E-137	1.23E-135	2.24
RDN25	736	A	377	1130039	102	1243362	194	1065093	56	1116960	3.91	5.23E-60	7.40E-59	1.82
RDN25	744	A	747	1130039	309	1243362	351	1065093	225	1116960	2.22	2.08E-54	2.75E-53	1.97
RDN25	761	A	7609	1130039	282	1243362	2820	1065093	271	1116960	20.36	0	0	3.19
RDN25	765	C	2079	1130039	925	1243362	703	1065093	569	1116960	2.02	1.44E-110	3.33E-109	2.33
RDN25	769	G	96	1130039	60	1243362	51	1065093	36	1116960	1.66	0.000133286	0.000233271	0.95
RDN25	771	A	963	1130039	432	1243362	513	1065093	323	1116960	2.11	1.97E-65	3.03E-64	2.08
RDN25	783	A	550	1130039	257	1243362	469	1065093	244	1116960	2.19	7.24E-49	8.48E-48	1.93
RDN25	784	A	582	1130039	76	1243362	434	1065093	80	1116960	7.01	2.16E-153	6.55E-152	2.13
RDN25	800	G	2645	1130039	254	1243362	1941	1065093	212	1116960	10.60	0	0	2.81
RDN25	845	G	521	1130039	241	1243362	605	1065093	243	1116960	2.50	9.32E-68	1.44E-66	2.02
RDN25	846	A	1986	1130039	291	1243362	1646	1065093	333	1116960	6.25	0	0	2.67
RDN25	848	A	1887	1130039	94	1243362	1807	1065093	167	1116960	15.15	0	0	2.73
RDN25	877	C	2815	1130039	133	1243362	1999	1065093	152	1116960	18.16	0	0	2.85
RDN25	882	A	452	1130039	192	1243362	246	1065093	181	1116960	2.02	6.59E-29	4.59E-28	1.73
RDN25	883	A	1849	1130039	786	1243362	1274	1065093	508	1116960	2.60	2.62E-198	9.28E-197	2.47
RDN25	887	G	860	1130039	245	1243362	688	1065093	332	1116960	2.88	2.61E-114	6.23E-113	2.19
RDN25	891	G	3049	1130039	1069	1243362	2074	1065093	589	1116960	3.34	0	0	2.74
RDN25	895	A	2000	1130039	622	1243362	1452	1065093	438	1116960	3.51	3.02E-318	1.63E-316	2.58
RDN25	959	C	6622	1130039	1131	1243362	2300	1065093	786	1116960	5.04	0	0	3.04
RDN25	978	G	400	1130039	203	1243362	344	1065093	189	1116960	2.04	2.26E-31	1.70E-30	1.77
RDN25	980	A	5927	1130039	906	1243362	2566	1065093	460	1116960	6.74	0	0	3.05
RDN25	1025	A	1841	1130039	746	1243362	1237	1065093	437	1116960	2.81	3.74E-218	1.41E-216	2.49
RDN25	1026	A	4443	1130039	1718	1243362	2886	1065093	994	1116960	2.92	0	0	2.87
RDN25	1027	A	1233	1130039	646	1243362	953	1065093	487	1116960	2.08	1.11E-92	2.28E-91	2.24
RDN25	1036	A	340	1130039	165	1243362	271	1065093	125	1116960	2.27	4.64E-32	3.54E-31	1.72
RDN25	1055	A	1068	1130039	412	1243362	373	1065093	165	1116960	2.71	1.16E-98	2.47E-97	2.15
RDN25	1064	A	322	1130039	145	1243362	223	1065093	123	1116960	2.19	5.46E-27	3.58E-26	1.66
RDN25	1079	A	11485	1130039	2270	1243362	4511	1065093	810	1116960	5.64	0	0	3.31
RDN25	1091	A	432	1130039	261	1243362	351	1065093	262	1116960	1.61	2.05E-17	9.20E-17	1.66
RDN25	1102	A	1249	1130039	197	1243362	581	1065093	176	1116960	5.30	2.73E-237	1.21E-235	2.36
RDN25	1103	A	174	1130039	66	1243362	84	1065093	84	1116960	1.85	1.31E-09	3.56E-09	1.26
RDN25	1105	A	161	1130039	115	1243362	109	1065093	78	1116960	1.51	1.34E-05	2.62E-05	1.15
RDN25	1106	G	159	1130039	110	1243362	117	1065093	74	1116960	1.62	4.26E-07	9.49E-07	1.21
RDN25	1136	A	1403	1130039	188	1243362	1105	1065093	348	1116960	5.01	1.03E-311	5.41E-310	2.49
RDN25	1145	G	241	1130039	112	1243362	307	1065093	254	1116960	1.60	2.76E-12	9.30E-12	1.51
RDN25	1157	G	1202	1130039	391	1243362	1189	1065093	321	1116960	3.61	1.04E-226	4.12E-225	2.43
RDN25	1159	A	681	1130039	103	1243362	862	1065093	119	1116960	7.45	4.15E-237	1.81E-235	2.32
RDN25	1200	A	439	1130039	194	1243362	277	1065093	168	1116960	2.13	3.47E-33	2.76E-32	1.77
RDN25	1209	G	1442	1130039	895	1243362	1049	1065093	583	1116960	1.82	4.61E-76	7.98E-75	2.24
RDN25	1219	C	8571	1130039	697	1243362	4008	1065093	903	1116960	8.46	0	0	3.23
RDN25	1221	A	286	1130039	124	1243362	319	1065093	285	1116960	1.58	6.32E-13	2.20E-12	1.54
RDN25	1225	A	7994	1130039	230	1243362	6526	1065093	354	1116960	26.67	0	0	3.33
RDN25	1244	A	481	1130039	171	1243362	447	1065093	204	1116960	2.66	7.89E-62	1.14E-60	1.95
RDN25	1245	A	1763	1130039	348	1243362	1141	1065093	324	1116960	4.66	0	0	2.55
RDN25	1270	A	7965	1130039	2142	1243362	4733	1065093	1940	1116960	3.35	0	0	3.14
RDN25	1271	A	1639	1130039	246	1243362	1509	1065093	485	1116960	4.61	0	0	2.58
RDN25	1273	A	6891	1130039	992	1243362	5423	1065093	1234	1116960	5.94	0	0	3.20
RDN25	1301	A	674	1130039	414	1243362	564	1065093	424	1116960	1.59	2.06E-25	1.29E-24	1.85
RDN25	1326	A	233	1130039	53	1243362	387	1065093	129	1116960	3.63	4.05E-60	5.77E-59	1.84
RDN25	1346	G	604	1130039	503	1243362	665	1065093	267	1116960	1.78	6.18E-37	5.29E-36	1.93
RDN25	1348	T	49	1130039	36	1243362	99	1065093	51	1116960	1.82	1.02E-05	2.01E-05	1.02
RDN25	1349	G	1678	1130039	434	1243362	1757	1065093	427	1116960	4.28	0	0	2.61
RDN25	1350	A	2477	1130039	473	1243362	2185	1065093	430	1116960	5.55	0	0	2.77

TABLE 3 cont.

RDN25	621	A	410	1130039	153	1243362	442	1065093	169	1116960	2.84	2.70E-62	3.93E-61	1.93
RDN25	692	A	55979	1130039	1004	1243362	47306	1065093	928	1116960	57.51	0	0	4.20
RDN25	693	A	481	1130039	105	1243362	393	1065093	159	1116960	3.55	7.51E-83	1.42E-81	1.99
RDN25	697	A	860	1130039	452	1243362	671	1065093	288	1116960	2.23	1.90E-75	3.26E-74	2.12
RDN25	708	G	640	1130039	458	1243362	522	1065093	291	1116960	1.67	1.71E-28	1.17E-27	1.86
RDN25	710	A	286	1130039	190	1243362	234	1065093	177	1116960	1.52	5.69E-10	1.60E-09	1.44
RDN25	711	A	562	1130039	180	1243362	442	1065093	155	1116960	3.23	9.84E-86	1.88E-84	2.03
RDN25	718	G	617	1130039	363	1243362	480	1065093	395	1116960	1.56	4.42E-21	2.33E-20	1.78
RDN25	721	G	353	1130039	174	1243362	341	1065093	118	1116960	2.56	4.28E-44	4.47E-43	1.82
RDN25	734	C	1461	1130039	569	1243362	506	1065093	394	1116960	2.21	2.10E-95	4.39E-94	2.22
RDN25	735	A	1016	1130039	414	1243362	634	1065093	150	1116960	3.17	4.43E-137	1.23E-135	2.24
RDN25	736	A	377	1130039	102	1243362	194	1065093	56	1116960	3.91	5.23E-60	7.40E-59	1.82
RDN25	744	A	747	1130039	309	1243362	351	1065093	225	1116960	2.22	2.08E-54	2.75E-53	1.97
RDN25	761	A	7609	1130039	282	1243362	2820	1065093	271	1116960	20.36	0	0	3.19
RDN25	765	C	2079	1130039	925	1243362	703	1065093	569	1116960	2.02	1.44E-110	3.33E-109	2.33
RDN25	769	G	96	1130039	60	1243362	51	1065093	36	1116960	1.66	0.000133286	0.000233271	0.95
RDN25	771	A	963	1130039	432	1243362	513	1065093	323	1116960	2.11	1.97E-65	3.03E-64	2.08
RDN25	783	A	550	1130039	257	1243362	469	1065093	244	1116960	2.19	7.24E-49	8.48E-48	1.93
RDN25	784	A	582	1130039	76	1243362	434	1065093	80	1116960	7.01	2.16E-153	6.55E-152	2.13
RDN25	800	G	2645	1130039	254	1243362	1941	1065093	212	1116960	10.60	0	0	2.81
RDN25	845	G	521	1130039	241	1243362	605	1065093	243	1116960	2.50	9.32E-68	1.44E-66	2.02
RDN25	846	A	1986	1130039	291	1243362	1646	1065093	333	1116960	6.25	0	0	2.67
RDN25	848	A	1887	1130039	94	1243362	1807	1065093	167	1116960	15.15	0	0	2.73
RDN25	877	C	2815	1130039	133	1243362	1999	1065093	152	1116960	18.16	0	0	2.85
RDN25	882	A	452	1130039	192	1243362	246	1065093	181	1116960	2.02	6.59E-29	4.59E-28	1.73
RDN25	883	A	1849	1130039	786	1243362	1274	1065093	508	1116960	2.60	2.62E-198	9.28E-197	2.47
RDN25	887	G	860	1130039	245	1243362	688	1065093	322	1116960	2.88	2.61E-114	6.23E-113	2.19
RDN25	891	G	3049	1130039	1069	1243362	2074	1065093	589	1116960	3.34	0	0	2.74
RDN25	895	A	2000	1130039	622	1243362	1452	1065093	438	1116960	3.51	3.02E-318	1.63E-316	2.58
RDN25	959	C	6622	1130039	1131	1243362	2300	1065093	786	1116960	5.04	0	0	3.04
RDN25	978	G	400	1130039	203	1243362	344	1065093	189	1116960	2.04	2.26E-31	1.70E-30	1.77
RDN25	980	A	5927	1130039	906	1243362	2566	1065093	460	1116960	6.74	0	0	3.05
RDN25	1025	A	1841	1130039	746	1243362	1237	1065093	437	1116960	2.81	3.74E-218	1.41E-216	2.49
RDN25	1026	A	4443	1130039	1718	1243362	2886	1065093	994	1116960	2.92	0	0	2.87
RDN25	1027	A	1233	1130039	646	1243362	953	1065093	487	1116960	2.08	1.11E-92	2.28E-91	2.24
RDN25	1036	A	340	1130039	165	1243362	271	1065093	125	1116960	2.27	4.64E-32	3.54E-31	1.72
RDN25	1055	A	1068	1130039	412	1243362	373	1065093	165	1116960	2.71	1.16E-98	2.47E-97	2.15
RDN25	1064	A	322	1130039	145	1243362	223	1065093	123	1116960	2.19	5.46E-27	3.58E-26	1.66
RDN25	1079	A	11485	1130039	2270	1243362	4511	1065093	810	1116960	5.64	0	0	3.31
RDN25	1091	A	432	1130039	261	1243362	351	1065093	262	1116960	1.61	2.05E-17	9.20E-17	1.66
RDN25	1102	A	1249	1130039	197	1243362	581	1065093	176	1116960	5.30	2.73E-237	1.21E-235	2.36
RDN25	1103	A	174	1130039	66	1243362	84	1065093	84	1116960	1.85	1.31E-09	3.56E-09	1.26
RDN25	1105	A	161	1130039	115	1243362	109	1065093	78	1116960	1.51	1.34E-05	2.62E-05	1.15
RDN25	1106	G	159	1130039	110	1243362	117	1065093	74	1116960	1.62	4.26E-07	9.49E-07	1.21
RDN25	1126	A	1403	1130039	188	1243362	1105	1065093	348	1116960	5.01	1.03E-311	5.41E-310	2.49
RDN25	1145	G	241	1130039	122	1243362	307	1065093	254	1116960	1.60	2.76E-12	9.30E-12	1.51
RDN25	1157	G	1202	1130039	391	1243362	1189	1065093	321	1116960	3.61	1.04E-226	4.12E-225	2.43
RDN25	1159	A	681	1130039	103	1243362	862	1065093	119	1116960	7.45	4.15E-237	1.81E-235	2.32
RDN25	1200	A	439	1130039	194	1243362	277	1065093	168	1116960	2.13	3.47E-33	2.76E-32	1.77
RDN25	1209	G	1442	1130039	895	1243362	1049	1065093	583	1116960	1.82	4.61E-76	7.98E-75	2.24
RDN25	1219	C	8571	1130039	697	1243362	4008	1065093	903	1116960	8.46	0	0	3.23
RDN25	1221	A	286	1130039	124	1243362	319	1065093	285	1116960	1.58	6.32E-13	2.20E-12	1.54
RDN25	1225	A	7994	1130039	230	1243362	6526	1065093	354	1116960	26.67	0	0	3.33
RDN25	1244	A	481	1130039	171	1243362	447	1065093	204	1116960	2.66	7.89E-62	1.14E-60	1.95
RDN25	1245	A	1763	1130039	348	1243362	1141	1065093	324	1116960	4.66	0	0	2.55
RDN25	1270	A	7965	1130039	2142	1243362	4733	1065093	1940	1116960	3.35	0	0	3.14
RDN25	1271	A	1639	1130039	246	1243362	1509	1065093	485	1116960	4.61	0	0	2.58
RDN25	1273	A	6891	1130039	992	1243362	5423	1065093	1234	1116960	5.94	0	0	3.20
RDN25	1301	A	674	1130039	414	1243362	564	1065093	424	1116960	1.59	2.06E-25	1.29E-24	1.85
RDN25	1326	A	233	1130039	53	1243362	387	1065093	129	1116960	3.63	4.05E-60	5.77E-59	1.84
RDN25	1346	G	604	1130039	503	1243362	665	1065093	267	1116960	1.78	6.18E-37	5.29E-36	1.93
RDN25	1348	T	49	1130039	36	1243362	99	1065093	51	1116960	1.82	1.02E-05	2.01E-05	1.02
RDN25	1349	G	1678	1130039	434	1243362	1757	1065093	427	1116960	4.28	0	0	2.61
RDN25	1350	A	2477	1130039	473	1243362	2185	1065093	430	1116960	5.55	0	0	2.77

TABLE 3 cont.

RDN25	1352	A	1082	1130039	217	1243362	1008	1065093	365	1116960	3.85	5.84E-211	2.18E-209	2.38	
RDN25	1354	G	554	1130039	410	1243362	667	1065093	375	1116960	1.67	1.34E-29	9.59E-29	1.88	
RDN25	1355	A	495	1130039	108	1243362	582	1065093	122	1116960	5.02	2.08E-134	5.69E-133	2.13	
RDN25	1363	A	118	1130039	62	1243362	135	1065093	89	1116960	1.29	1.06E-08	2.72E-08	1.24	
RDN25	1366	A	488	1130039	79	1243362	560	1065093	154	1116960	4.81	3.88E-127	1.03E-125	2.11	
RDN25	1375	G	162	1130039	18	1243362	205	1065093	32	1116960	7.85	6.86E-59	9.50E-58	1.70	
RDN25	1382	G	25	1130039	8	1243362	44	1065093	40	1116960	1.53	0.029228303	0.038817132	0.58	
RDN25	1383	G	1726	1130039	453	1243362	1471	1065093	483	1116960	3.67	7.74E-308	3.98E-306	2.56	
RDN25	1386	A	239	1130039	117	1243362	203	1065093	131	1116960	1.91	1.02E-16	4.41E-16	1.51	
RDN25	1391	C	46	1130039	20	1243362	56	1065093	45	1116960	1.68	0.00129383	0.002028892	0.81	
RDN25	1400	G	716	1130039	201	1243362	581	1065093	294	1116960	2.81	5.09E-93	1.05E-91	2.11	
RDN25	1401	A	192	1130039	70	1243362	136	1065093	102	1116960	2.05	9.23E-15	3.57E-14	1.41	
RDN25	1408	G	72	1130039	32	1243362	82	1065093	64	1116960	1.71	3.46E-05	6.50E-05	1.00	
RDN25	1409	G	811	1130039	350	1243362	541	1065093	370	1116960	2.02	1.28E-54	1.71E-53	2.02	
RDN25	1421	G	615	1130039	34	1243362	726	1065093	52	1116960	16.69	3.59E-261	1.72E-259	2.29	
RDN25	1449	A	88	1130039	30	1243362	18	1065093	9	1116960	2.96	1.88E-09	5.07E-09	1.03	
RDN25	1465	A	95	1130039	46	1243362	90	1065093	58	1116960	1.91	1.08E-07	2.54E-07	1.14	
RDN25	1481	A	175	1130039	108	1243362	136	1065093	103	1116960	1.59	2.26E-07	5.16E-07	1.25	
RDN25	1503	A	5079	1130039	1353	1243362	3582	1065093	940	1116960	4.07	0	0	3.00	
RDN25	1519	G	58	1130039	29	1243362	43	1065093	20	1116960	2.22	3.67E-06	7.56E-06	0.93	
RDN25	1520	G	190	1130039	115	1243362	191	1065093	118	1116960	1.76	9.05E-12	2.94E-11	1.41	
RDN25	1521	G	3206	1130039	678	1243362	3485	1065093	575	1116960	5.74	0	0	2.93	
RDN25	1539	A	569	1130039	234	1243362	543	1065093	439	1116960	1.77	2.64E-32	2.03E-31	1.88	
RDN25	1545	A	127	1130039	41	1243362	272	1065093	94	1116960	2.36	1.62E-17	7.32E-17	1.48	
RDN25	1557	A	141	1130039	85	1243362	81	1065093	69	1116960	1.56	2.68E-05	5.09E-05	1.09	
RDN25	1561	G	144	1130039	100	1243362	202	1065093	92	1116960	1.93	1.32E-13	4.81E-13	1.41	
RDN25	1566	A	962	1130039	502	1243362	1104	1065093	426	1116960	2.39	2.28E-114	5.48E-113	2.27	
RDN25	1571	A	542	1130039	169	1243362	695	1065093	207	1116960	3.52	4.27E-115	1.04E-113	2.14	
RDN25	1576	G	34	1130039	14	1243362	76	1065093	51	1116960	1.80	0.000330614	0.000191941	0.88	
RDN25	1577	G	136	1130039	65	1243362	212	1065093	95	1116960	2.32	1.41E-19	7.00E-19	1.49	
RDN25	1580	A	483	1130039	173	1243362	673	1065093	246	1116960	2.95	4.57E-88	8.81E-87	2.07	
RDN25	1583	A	1807	1130039	775	1243362	1274	1065093	660	1116960	2.31	1.33E-160	4.18E-159	2.43	
RDN25	1604	G	947	1130039	349	1243362	1142	1065093	560	1116960	2.46	3.44E-121	8.85E-120	2.28	
RDN25	1613	A	154	1130039	96	1243362	246	1065093	187	1116960	1.51	1.21E-07	2.82E-07	1.33	
RDN25	1619	A	494	1130039	310	1243362	541	1065093	416	1116960	1.53	1.36E-18	6.47E-18	1.75	
RDN25	1628	C	814	1130039	391	1243362	665	1065093	642	1116960	1.54	1.72E-26	1.11E-25	1.90	
RDN25	1652	G	46	1130039	23	1243362	118	1065093	69	1116960	1.89	8.50E-07	1.86E-06	1.08	
RDN25	1656	A	680	1130039	68	1243362	1067	1065093	135	1116960	9.18	2.80E-290	1.40E-288	2.38	
RDN25	1658	G	1105	1130039	687	1243362	1364	1065093	962	1116960	1.60	1.33E-50	1.63E-49	2.16	
RDN25	1674	G	43	1130039	21	1243362	38	1065093	29	1116960	1.74	0.002451015	0.003698831	0.73	
RDN25	1683	A	1118	1130039	621	1243362	1357	1065093	713	1116960	1.99	1.86E-94	3.87E-93	2.28	
RDN25	1704	A	2376	1130039	613	1243362	2473	1065093	882	1116960	3.48	0	0	2.73	
RDN25	1731	A	235	1130039	66	1243362	212	1065093	130	1116960	2.44	5.74E-27	3.75E-26	1.61	
RDN25	1741	A	819	1130039	150	1243362	1606	1065093	421	1116960	4.52	2.32E-277	1.14E-275	2.47	
RDN25	1757	A	280	1130039	105	1243362	196	1065093	133	1116960	1.51	1.33E-06	2.98E-06	1.24	
RDN25	1758	G	139	1130039	83	1243362	515	1065093	247	1116960	2.36	3.45E-50	4.19E-49	1.88	
RDN25	1760	A	1610	1130039	174	1243362	2658	1065093	356	1116960	8.59	0	0	2.77	
RDN25	1761	C	1805	1130039	181	1243362	1897	1065093	443	1116960	6.34	0	0	2.68	
RDN25	1769	G	55	1130039	44	1243362	103	1065093	56	1116960	1.69	4.49E-05	8.32E-05	1.00	
RDN25	1770	G	83	1130039	72	1243362	144	1065093	79	1116960	1.61	6.38E-06	1.28E-05	1.13	
RDN25	1775	G	53	1130039	27	1243362	137	1065093	86	1116960	1.79	9.96E-07	2.17E-06	1.12	
RDN25	1776	G	214	1130039	116	1243362	461	1065093	252	1116960	1.95	9.39E-26	5.96E-25	1.71	
RDN25	1789	G	58	1130039	36	1243362	91	1065093	58	1116960	1.69	6.85E-05	0.000123773	0.98	
RDN25	1809	A	669	1130039	213	1243362	759	1065093	203	1116960	3.69	1.09E-138	3.12E-137	2.21	
RDN25	1811	G	94	1130039	26	1243362	139	1065093	58	1116960	2.96	5.46E-19	2.64E-18	1.38	
RDN25	1813	A	4489	1130039	1251	1243362	3559	1065093	908	1116960	4.02	0	0	2.97	
RDN25	1814	A	2656	1130039	819	1243362	2176	1065093	674	1116960	3.48	0	0	2.73	
RDN25	1842	A	464	1130039	336	1243362	419	1065093	214	1116960	1.73	2.36E-24	1.42E-23	1.76	
RDN25	1847	A	1301	1130039	245	1243362	688	1065093	217	1116960	4.64	1.81E-235	7.58E-234	2.38	
RDN25	1879	A	3182	1130039	750	1243362	999	1065093	273	1116960	4.44	0	0	2.70	
RDN25	1887	A	818	1130039	311	1243362	438	1065093	198	1116960	2.67	6.15E-84	1.17E-82	2.08	
RDN25	1913	A	116	1130039	51	1243362	82	1065093	69	1116960	1.77	6.70E-07	1.48E-06	1.13	
RDN25	1928	G	75	1130039	30	1243362	46	1065093	42	1116960	1.81	7.20E-05	0.000130029	0.92	
RDN25	1929	G	1266	1130039	980	1243362	701	1065093	430	1116960	1.51	1.48E-32	1.15E-31	2.01	

TABLE 3 cont.

RDN25	1930	A	4416	1130039	866	1243362	1803	1065093	449	1116960	5.12	0	0	2.89
RDN25	1932	A	756	1130039	180	1243362	401	1065093	149	1116960	3.80	1.01E-116	2.49E-115	2.12
RDN25	1933	A	163	1130039	21	1243362	80	1065093	26	1116960	5.57	7.86E-34	6.31E-33	1.49
RDN25	1952	G	60	1130039	29	1243362	60	1065093	40	1116960	1.86	3.76E-05	7.05E-05	0.94
RDN25	1953	G	342	1130039	153	1243362	325	1065093	161	1116960	2.28	3.83E-35	3.17E-34	1.76
RDN25	1957	G	461	1130039	273	1243362	468	1065093	326	1116960	1.66	1.11E-22	6.35E-22	1.76
RDN25	1969	G	1636	1130039	573	1243362	1174	1065093	519	1116960	2.77	1.65E-195	5.71E-194	2.44
RDN25	1974	A	514	1130039	64	1243362	522	1065093	100	1116960	6.77	2.22E-153	6.66E-152	2.14
RDN25	1979	G	79	1130039	24	1243362	111	1065093	54	1116960	2.60	2.40E-13	8.60E-13	1.26
RDN25	1983	G	30	1130039	17	1243362	56	1065093	35	1116960	1.76	0.00144212	0.002247932	0.77
RDN25	1984	C	51	1130039	24	1243362	57	1065093	45	1116960	1.67	0.000933828	0.00148355	0.83
RDN25	1985	G	260	1130039	68	1243362	311	1065093	79	1116960	4.16	8.40E-63	1.24E-61	1.83
RDN25	1987	G	111	1130039	79	1243362	96	1065093	51	1116960	1.72	1.38E-06	2.96E-06	1.12
RDN25	1991	G	144	1130039	56	1243362	154	1065093	76	1116960	2.42	3.73E-18	1.74E-17	1.43
RDN25	1993	G	18	1130039	18	1243362	58	1065093	23	1116960	1.98	0.000497615	0.000812604	0.77
RDN25	1994	G	570	1130039	267	1243362	657	1065093	247	1116960	2.56	8.80E-77	1.54E-75	2.06
RDN25	1995	A	362	1130039	98	1243362	515	1065093	55	1116960	6.17	1.26E-123	3.27E-122	2.06
RDN25	1998	G	88	1130039	50	1243362	141	1065093	96	1116960	1.67	1.13E-06	2.44E-06	1.16
RDN25	2003	G	493	1130039	143	1243362	738	1065093	398	1116960	2.42	2.14E-70	3.42E-69	2.05
RDN25	2012	G	147	1130039	66	1243362	358	1065093	210	1116960	1.94	2.07E-19	1.02E-18	1.58
RDN25	2022	G	83	1130039	31	1243362	125	1065093	94	1116960	1.77	3.78E-07	8.48E-07	1.15
RDN25	2024	G	34	1130039	17	1243362	122	1065093	74	1116960	1.82	6.02E-06	1.21E-05	1.04
RDN25	2025	G	785	1130039	530	1243362	1100	1065093	536	1116960	1.90	2.49E-64	3.79E-63	2.14
RDN25	2026	A	451	1130039	116	1243362	987	1065093	179	1116960	5.20	7.17E-182	2.41E-180	2.26
RDN25	2035	G	149	1130039	38	1243362	304	1065093	93	1116960	3.68	7.72E-45	8.35E-44	1.71
RDN25	2042	G	1553	1130039	718	1243362	2089	1065093	887	1116960	2.43	2.11E-205	7.69E-204	2.52
RDN25	2049	A	273	1130039	67	1243362	498	1065093	156	1116960	3.68	2.45E-75	4.16E-74	1.94
RDN25	2058	G	533	1130039	266	1243362	758	1065093	542	1116960	1.71	2.40E-33	1.91E-32	1.92
RDN25	2062	G	426	1130039	361	1243362	646	1065093	336	1116960	1.65	4.41E-25	2.73E-24	1.82
RDN25	2088	A	2405	1130039	583	1243362	2339	1065093	418	1116960	5.10	0	0	2.77
RDN25	2089	A	1064	1130039	500	1243362	896	1065093	353	1116960	2.48	2.26E-115	5.52E-114	2.26
RDN25	2092	A	1713	1130039	657	1243362	1024	1065093	479	1116960	2.60	7.10E-174	2.30E-172	2.41
RDN25	2093	A	130	1130039	37	1243362	117	1065093	91	1116960	2.06	1.13E-11	4.29E-11	1.30
RDN25	2095	G	654	1130039	369	1243362	540	1065093	264	1116960	2.03	6.50E-49	7.66E-48	1.97
RDN25	2099	A	1346	1130039	370	1243362	1253	1065093	321	1116960	4.05	1.42E-273	6.87E-272	2.48
RDN25	2100	A	545	1130039	61	1243362	634	1065093	98	1116960	7.94	1.14E-186	3.86E-185	2.20
RDN25	2105	G	303	1130039	162	1243362	481	1065093	192	1116960	2.37	1.17E-43	1.21E-42	1.85
RDN25	2113	A	130	1130039	46	1243362	234	1065093	92	1116960	2.81	4.83E-27	3.18E-26	1.56
RDN25	2118	C	296	1130039	150	1243362	395	1065093	283	1116960	1.70	1.55E-18	7.35E-18	1.65
RDN25	2123	G	11	1130039	2	1243362	18	1065093	9	1116960	2.80	0.003862694	0.005709119	0.46
RDN25	2124	G	66	1130039	42	1243362	146	1065093	79	1116960	1.87	3.58E-08	8.76E-08	1.19
RDN25	2166	A	1211	1130039	528	1243362	960	1065093	421	1116960	2.46	1.09E-126	2.86E-125	2.30
RDN25	2198	A	1217	1130039	65	1243362	1218	1065093	112	1116960	14.73	0	0	2.55
RDN25	2206	G	328	1130039	183	1243362	398	1065093	252	1116960	1.79	3.47E-22	1.94E-21	1.70
RDN25	2207	A	960	1130039	534	1243362	759	1065093	454	1116960	1.87	2.31E-57	3.18E-56	2.09
RDN25	2208	A	241	1130039	103	1243362	287	1065093	176	1116960	2.02	2.98E-22	1.68E-21	1.62
RDN25	2215	A	572	1130039	144	1243362	563	1065093	161	1116960	3.99	3.36E-119	8.51E-118	2.12
RDN25	2220	A	157	1130039	75	1243362	148	1065093	66	1116960	2.33	2.08E-17	9.29E-17	1.43
RDN25	2222	A	345	1130039	113	1243362	300	1065093	250	1116960	1.90	2.35E-23	1.37E-22	1.68
RDN25	2257	C	3280	1130039	445	1243362	5066	1065093	860	1116960	6.83	0	0	3.04
RDN25	2272	G	161	1130039	126	1243362	331	1065093	192	1116960	1.65	2.56E-12	8.61E-12	1.48
RDN25	2284	C	279	1130039	114	1243362	457	1065093	332	1116960	1.76	2.07E-21	1.11E-20	1.70
RDN25	2357	A	8621	1130039	760	1243362	8372	1065093	771	1116960	11.92	0	0	3.38
RDN25	2386	A	8219	1130039	1173	1243362	5075	1065093	865	1116960	7.04	0	0	3.25
RDN25	2398	A	1545	1130039	414	1243362	771	1065093	207	1116960	4.04	5.19E-245	2.35E-243	2.43
RDN25	2401	A	1989	1130039	151	1243362	1090	1065093	148	1116960	11.10	0	0	2.64
RDN25	2404	A	1298	1130039	138	1243362	917	1065093	112	1116960	9.55	0	0	2.49
RDN25	2412	G	412	1130039	147	1243362	272	1065093	81	1116960	3.24	2.65E-59	3.68E-58	1.86
RDN25	2458	A	4566	1130039	2166	1243362	2280	1065093	1227	1116960	2.18	1.40E-317	7.42E-316	2.76
RDN25	2477	G	627	1130039	265	1243362	642	1065093	380	1116960	2.11	4.52E-56	6.08E-55	2.01
RDN25	2478	C	647	1130039	199	1243362	397	1065093	174	1116960	3.02	1.57E-82	2.94E-81	2.03
RDN25	2479	C	1326	1130039	326	1243362	839	1065093	230	1116960	4.20	1.52E-236	6.54E-235	2.41
RDN25	2480	A	798	1130039	250	1243362	737	1065093	169	1116960	3.95	6.98E-159	2.15E-157	2.25
RDN25	2486	A	2561	1130039	547	1243362	2187	1065093	548	1116960	4.66	0	0	2.76

TABLE 3 cont.

RDN25	2502	A	316	1130039	126	1243362	273	1065093	78	1116960	3.11	7.28E-49	8.49E-48	1.79
RDN25	2523	A	225	1130039	87	1243362	225	1065093	67	1116960	3.14	4.48E-38	3.97E-37	1.68
RDN25	2530	G	121	1130039	92	1243362	142	1065093	83	1116960	1.61	9.50E-07	2.07E-06	1.19
RDN25	2531	C	522	1130039	204	1243362	324	1065093	223	1116960	2.13	5.61E-39	5.09E-38	1.84
RDN25	2539	C	2440	1130039	1704	1243362	2587	1065093	1872	1116960	1.51	1.03E-79	1.89E-78	2.42
RDN25	2554	A	254	1130039	187	1243362	254	1065093	120	1116960	1.78	7.63E-16	3.13E-15	1.54
RDN25	2556	C	1827	1130039	594	1243362	1069	1065093	631	1116960	2.55	4.55E-178	1.50E-176	2.43
RDN25	2557	A	1303	1130039	796	1243362	983	1065093	603	1116960	1.76	7.08E-64	1.06E-62	2.18
RDN25	2562	A	82	1130039	26	1243362	71	1065093	50	1116960	2.16	2.75E-08	6.80E-08	1.10
RDN25	2569	A	2831	1130039	657	1243362	1573	1065093	445	1116960	4.32	0	0	2.72
RDN25	2580	A	1291	1130039	611	1243362	689	1065093	468	1116960	1.98	9.18E-76	1.58E-74	2.18
RDN25	2593	A	45	1130039	8	1243362	23	1065093	27	1116960	2.08	0.000420283	0.000705151	0.74
RDN25	2638	C	416	1130039	43	1243362	344	1065093	68	1116960	7.34	1.63E-117	4.03E-116	2.01
RDN25	2640	A	905	1130039	522	1243362	495	1065093	254	1116960	1.95	3.19E-52	4.14E-51	2.02
RDN25	2667	A	1813	1130039	315	1243362	1359	1065093	368	1116960	4.99	0	0	2.59
RDN25	2675	C	2313	1130039	533	1243362	1514	1065093	508	1116960	3.96	0	0	2.65
RDN25	2678	A	921	1130039	214	1243362	864	1065093	262	1116960	4.02	9.67E-188	3.32E-186	2.32
RDN25	2679	A	1532	1130039	699	1243362	1299	1065093	617	1116960	2.31	1.15E-147	3.41E-146	2.40
RDN25	2680	A	8167	1130039	701	1243362	7245	1065093	569	1116960	13.06	0	0	3.34
RDN25	2683	T	235	1130039	157	1243362	325	1065093	228	1116960	1.56	2.08E-11	6.57E-11	1.49
RDN25	2689	A	647	1130039	66	1243362	555	1065093	37	1116960	12.59	3.66E-221	1.43E-219	2.23
RDN25	2702	A	1038	1130039	272	1243362	492	1065093	331	1116960	2.73	9.82E-106	2.19E-104	2.18
RDN25	2720	G	664	1130039	382	1243362	494	1065093	327	1116960	1.76	4.40E-33	3.49E-32	1.89
RDN25	2764	C	611	1130039	42	1243362	580	1065093	39	1116960	15.81	2.73E-230	1.12E-228	2.24
RDN25	2769	A	90	1130039	46	1243362	96	1065093	68	1116960	1.25	2.57E-06	5.39E-06	1.09
RDN25	2772	C	238	1130039	22	1243362	173	1065093	40	1116960	7.11	1.85E-63	2.76E-62	1.74
RDN25	2787	G	164	1130039	144	1243362	290	1065093	124	1116960	1.82	6.05E-15	2.37E-14	1.50
RDN25	2821	C	201	1130039	29	1243362	250	1065093	170	1116960	2.41	1.36E-26	8.83E-26	1.61
RDN25	2838	A	334	1130039	42	1243362	443	1065093	83	1116960	6.64	4.27E-114	1.01E-112	2.01
RDN25	2847	A	1814	1130039	149	1243362	1867	1065093	262	1116960	9.59	0	0	2.71
RDN25	2872	A	180	1130039	85	1243362	458	1065093	289	1116960	1.81	2.79E-20	1.41E-19	1.65
RDN25	2946	A	14922	1130039	175	1243362	16504	1065093	201	1116960	89.65	0	0	3.68
RDN25	2947	G	361	1130039	155	1243362	430	1065093	217	1116960	2.28	3.64E-41	3.57E-40	1.84
RDN25	3003	G	77	1130039	61	1243362	117	1065093	57	1116960	1.76	1.20E-06	2.59E-06	1.11
RDN25	3006	A	18273	1130039	545	1243362	10768	1065093	324	1116960	36.12	0	0	3.64
RDN25	3007	T	240	1130039	79	1243362	114	1065093	62	1116960	2.71	2.25E-25	1.41E-24	1.54
RDN25	3021	A	227	1130039	109	1243362	312	1065093	126	1116960	2.46	2.19E-32	1.69E-31	1.70
RDN25	3022	G	564	1130039	268	1243362	616	1065093	406	1116960	1.87	6.61E-40	6.23E-39	1.93
RDN25	3027	A	138	1130039	54	1243362	193	1065093	125	1116960	1.97	1.08E-13	3.95E-13	1.41
RDN25	3072	C	796	1130039	166	1243362	868	1065093	297	1116960	3.85	5.17E-168	1.64E-166	2.28
RDN25	3074	G	149	1130039	80	1243362	256	1065093	141	1116960	1.96	4.20E-16	1.76E-15	1.49
RDN25	3106	A	102	1130039	64	1243362	97	1065093	78	1116960	1.50	0.000224701	0.000383154	1.02
RDN25	3114	A	179	1130039	110	1243362	211	1065093	108	1116960	1.92	5.86E-15	2.30E-14	1.46
RDN25	3117	C	375	1130039	63	1243362	308	1065093	109	1116960	4.26	1.80E-76	3.13E-75	1.91
RDN25	3141	A	7179	1130039	891	1243362	4392	1065093	543	1116960	8.72	0	0	3.20
RDN25	3142	A	134	1130039	57	1243362	145	1065093	74	1116960	2.28	1.59E-15	6.29E-15	1.39
RDN25	3143	C	221	1130039	93	1243362	186	1065093	143	1116960	1.85	2.77E-14	1.04E-13	1.46
RDN25	3146	G	98	1130039	43	1243362	125	1065093	51	1116960	2.54	5.85E-15	2.30E-14	1.32
RDN25	3170	A	1104	1130039	509	1243362	624	1065093	240	1116960	2.50	1.10E-103	2.43E-102	2.20
RDN25	3174	A	317	1130039	117	1243362	353	1065093	166	1116960	2.54	5.10E-42	5.09E-41	1.80
RDN25	3180	A	88	1130039	40	1243362	106	1065093	79	1116960	1.74	1.76E-06	3.73E-06	1.11
RDN25	3181	C	290	1130039	62	1243362	235	1065093	69	1116960	4.31	1.10E-59	1.55E-58	1.79
RDN25	3183	A	2339	1130039	762	1243362	1391	1065093	548	1116960	3.07	1.03E-296	5.23E-295	2.59
RDN25	3188	G	258	1130039	113	1243362	375	1065093	144	1116960	2.64	4.94E-42	4.97E-41	1.78
RDN25	3199	G	189	1130039	121	1243362	250	1065093	125	1116960	1.91	1.63E-16	6.95E-16	1.51
RDN25	3202	G	2087	1130039	1221	1243362	1577	1065093	670	1116960	2.09	4.46E-156	1.37E-154	2.47
RDN25	3205	G	212	1130039	93	1243362	246	1065093	123	1116960	2.27	2.25E-24	1.36E-23	1.60
RDN25	3209	A	1718	1130039	626	1243362	1401	1065093	530	1116960	2.90	1.04E-230	4.32E-229	2.50
RDN25	3218	A	110	1130039	60	1243362	152	1065093	56	1116960	2.42	4.12E-16	1.73E-15	1.38
RDN25	3226	A	3630	1130039	1816	1243362	2152	1065093	1272	1116960	2.02	1.27E-227	5.08E-226	2.65
RDN25	3228	C	95	1130039	61	1243362	102	1065093	59	1116960	1.76	9.34E-07	2.03E-06	1.12
RDN25	3239	G	184	1130039	75	1243362	205	1065093	81	1116960	2.68	5.01E-27	3.29E-26	1.58
RDN25	3244	A	383	1130039	263	1243362	553	1065093	265	1116960	1.90	5.96E-33	4.69E-32	1.84
RDN25	3245	A	1190	1130039	83	1243362	1362	1065093	73	1116960	17.57	0	0	2.57

TABLE 3 cont.

RDN25	3254	G	732	1130039	352	1243362	699	1065093	239	1116960	2.61	9.36E-92	1.89E-90	2.13	
RDN25	3268	A	3339	1130039	1100	1243362	1768	1065093	541	1116960	3.37	0	0	2.74	
RDN25	3305	A	816	1130039	353	1243362	661	1065093	335	1116960	2.31	1.19E-77	2.12E-76	2.11	
RDN25	3316	A	311	1130039	142	1243362	458	1065093	191	1116960	2.47	6.21E-46	6.75E-45	1.85	
RDN25	3318	G	332	1130039	194	1243362	487	1065093	264	1116960	1.91	1.61E-29	1.15E-28	1.78	
RDN25	3335	A	712	1130039	148	1243362	1219	1065093	558	1116960	2.91	4.82E-143	1.40E-141	2.29	
RDN25	3336	A	3941	1130039	261	1243362	8084	1065093	612	1116960	14.66	0	0	3.24	
RDN25	3337	G	169	1130039	85	1243362	385	1065093	218	1116960	1.94	3.46E-21	1.84E-20	1.62	
RDN25	3345	G	153	1130039	163	1243362	269	1065093	124	1116960	1.58	2.63E-09	7.01E-09	1.38	
RDN25	3354	T	1	1130039	3	1243362	16	1065093	3	1116960	3.01	0.026413283	0.035415915	0.25	
RDN25	3362	A	1	1130039	2	1243362	13	1065093	2	1116960	3.72	0.025086864	0.033770778	0.20	
RDN5	42	C	57859	111376	3631	66784	46359	120884	5010	103111	8.61	0	0	3.68	
RDN5	72	C	137	111376	24	66784	32	120884	5	103111	3.73	2.78E-12	5.46E-12	0.82	
RDN5	73	G	143	111376	7	66784	25	120884	11	103111	6.31	2.97E-16	6.14E-16	0.87	
RDN5	75	G	86	111376	27	66784	23	120884	9	103111	1.97	0.000451318	0.000752197	0.49	
RDN5	85	G	4	111376	4	66784	42	120884	14	103111	2.07	0.009704799	0.015737513	0.04	
RDN5	92	C	8	111376	3	66784	22	120884	7	103111	2.32	0.025794671	0.040199488	-0.07	
RDN58	44	A	250	47534	112	46073	428	82911	295	74663	1.54	6.45E-12	2.11E-11	1.46	
RDN58	53	A	3011	47534	985	46073	3560	82911	1026	74663	3.05	0	0	2.72	
RDN58	54	A	786	47534	198	46073	1060	82911	455	74663	2.62	5.92E-106	1.55E-104	2.14	
RDN58	71	A	3260	47534	924	46073	4522	82911	1206	74663	3.39	0	0	2.82	
RDN58	77	A	237	47534	96	46073	522	82911	309	74663	1.72	5.11E-19	2.51E-18	1.59	
RDN58	79	A	1524	47534	783	46073	3037	82911	1487	74663	1.86	1.89E-128	5.94E-127	2.40	
RDN58	83	C	312	47534	71	46073	510	82911	326	74663	1.90	9.32E-27	6.37E-26	1.67	
RDN58	97	A	1733	47534	759	46073	3865	82911	1261	74663	2.57	1.54E-301	6.03E-300	2.62	
RDN58	99	C	3566	47534	779	46073	6624	82911	1568	74663	4.01	0	0	2.96	
RDN58	109	A	68	47534	1	46073	14	82911	3	74663	19.21	5.91E-16	2.32E-15	0.97	
RDN58	117	C	1	47534	1	46073	12	82911	0	74663	5.97	0.016350659	0.027021616	0.16	
RDN58	120	C	7	47534	3	46073	33	82911	13	74663	2.28	0.006263772	0.010806728	0.44	
SCR1	8	A	81	4695	24	2963	65	4275	35	3715	1.84	0.000100184	0.002087835	2.59	
SCR1	30	A	16	4695	3	2963	13	4275	3	3715	3.55	0.004474845	0.043903077	2.09	
SCR1	37	G	10	4695	0	2963	12	4275	2	3715	5.61	0.003270642	0.034775603	2.05	
SCR1	59	A	48	4695	22	2963	79	4275	30	3715	1.87	0.000147443	0.002845104	2.52	
SCR1	101	A	80	4695	0	2963	101	4275	16	3715	8.50	1.59E-22	1.65E-20	2.97	
SCR1	112	C	90	4695	14	2963	92	4275	33	3715	2.96	1.31E-11	8.56E-10	2.84	
SCR1	145	G	19	4695	4	2963	23	4275	7	3715	2.91	0.001623423	0.019669984	2.20	
SCR1	214	G	5	4695	0	2963	14	4275	1	3715	7.35	0.002787321	0.031569435	2.01	
SCR1	225	A	60	4695	17	2963	57	4275	13	3715	2.86	1.11E-07	5.24E-06	2.65	
SCR1	227	A	61	4695	22	2963	59	4275	14	3715	2.43	1.73E-06	6.92E-05	2.62	
SCR1	236	A	50	4695	11	2963	29	4275	6	3715	3.30	3.56E-06	0.000132652	2.51	
SCR1	273	A	180	4695	10	2963	187	4275	20	3715	9.30	1.02E-44	1.78E-42	3.28	
SCR1	364	A	293	4695	17	2963	178	4275	6	3715	14.43	5.48E-61	1.43E-58	3.41	
SCR1	400	A	65	4695	5	2963	35	4275	4	3715	7.96	3.82E-12	3.32E-10	2.71	
SCR1	402	A	618	4695	36	2963	181	4275	24	3715	9.20	1.92E-85	9.99E-83	3.62	
SCR1	413	A	174	4695	21	2963	59	4275	6	3715	5.90	8.87E-23	1.16E-20	3.06	
SCR1	421	A	16	4695	0	2963	4	4275	1	3715	7.01	0.005359432	0.048142487	2.03	
SCR1	448	G	15	4695	0	2963	15	4275	0	3715	11.13	6.68E-05	0.001580938	2.24	
SCR1	475	A	84	4695	27	2963	6	4275	2	3715	2.00	0.001341447	0.016640332	2.47	
snR11	104	C	20	381	4	326	18	374	4	297	3.92	0.000336532	0.043244399	2.98	
snR11	174	T	27	381	3	326	18	374	2	297	7.47	1.61E-06	0.000413229	3.12	
snR17a	230	C	17	745	0	715	26	562	4	488	7.72	7.81E-07	0.00038188	3.16	
snR17a	273	A	11	745	0	715	17	562	0	488	12.70	2.00E-05	0.003267718	3.02	
snR17a	286	C	21	745	2	715	14	562	0	488	10.79	2.05E-06	0.000501381	3.09	
snR17a	339	T	22	745	3	715	4	562	0	488	6.11	0.000266458	0.026059597	2.93	
snR17a	340	A	27	745	4	715	8	562	3	488	4.63	9.29E-05	0.011356557	3.01	
snR190	31	C	31	364	7	439	6	369	4	314	3.66	9.43E-05	0.00891458	2.83	
snR190	44	A	32	364	1	439	13	369	0	314	23.49	2.95E-10	5.58E-08	3.06	
snR3	21	C	19	179	0	131	18	211	4	176	5.87	8.91E-05	0.017192094	3.12	
snR3	126	C	8	179	1	131	16	211	1	176	9.47	0.000469078	0.045265993	3.03	
snR30	98	C	31	1259	2	908	15	1176	3	1029	7.23	2.59E-06	0.000522782	2.99	
snR30	152	T	19	1259	1	908	11	1176	2	1029	7.94	0.000127929	0.012899552	2.81	
snR30	196	C	27	1259	6	908	17	1176	3	1029	3.79	0.000166331	0.013380095	2.91	
snR30	201	A	42	1259	8	908	25	1176	4	1029	4.32	7.36E-07	0.000222758	3.11	
snR30	254	C	23	1259	3	908	16	1176	1	1029	7.52	1.14E-05	0.001721196	2.93	

TABLE 3 cont.

snR30	504	T	16	1259	3	908	22	1176	5	1029	3.85	0.000369229	0.024820412	2.84
snR30	546	A	15	1259	0	908	16	1176	2	1029	8.35	6.48E-05	0.007844414	2.85
snR30	547	C	29	1259	1	908	29	1176	6	1029	6.80	1.08E-07	6.52E-05	3.09
snR37	322	A	25	296	2	384	28	374	7	398	6.71	3.17E-09	1.22E-06	3.42
snR52	26	A	29	199	12	230	18	122	3	119	3.45	4.41E-05	0.002005544	2.97
snR73	33	C	25	51	0	57	14	32	0	21	17.57	1.07E-06	0.000112369	3.69
tD(GUC)D	4	G	7	151	4	283	17	320	12	630	2.92	0.001211 13	0.028663403	2.38
tD(GUC)D	20	G	9	151	9	283	59	320	34	630	3.07	1.81E-08	1.28E-06	2.84
tD(GUC)J1	17	T	5	133	2	303	22	374	12	612	3.32	0.000265075	0.006273438	2.43
tE(CUC)D	19	C	8	131	6	292	64	447	69	963	2.08	2.58E-05	0.001832906	2.66
tE(CUC)I	5	G	24	469	29	971	71	1299	110	3072	1.57	0.001134354	0.013423189	2.14
tE(CUC)I	18	T	4	469	11	971	63	1299	78	3072	1.75	0.000760295	0.013423189	2.05
tE(CUC)I	19	A	30	469	33	971	144	1299	226	3072	1.56	1.57E-05	0.000556285	2.39
tE(CUC)I	26	C	13	469	3	971	4	1299	7	3072	3.77	0.000988344	0.013423189	1.71
tE(UUC)B	19	A	21	358	31	832	101	873	119	1807	1.72	2.19E-05	0.001558344	2.48
tG(GCC)D2	18	A	33	563	52	1361	166	2051	332	6242	1.52	3.47E-06	0.000242606	2.25
tG(GCC)P1	17	T	6	543	12	1361	52	2022	87	6205	1.75	0.000911795	0.031912818	1.82
tG(UCC)G	6	T	32	282	25	634	95	1458	199	4211	1.57	9.86E-05	0.006998412	2.28
tG(UCC)G	17	T	5	282	20	634	70	1458	101	4211	1.73	0.0002865	0.010170738	2.11
tL(CAA)A	71	C	20	118	10	270	2	82	2	113	3.85	0.000207875	0.023489907	2.95
tL(UAA)B1	39	C	100	924	19	1498	4	463	4	972	7.52	8.68E-23	7.20E-21	2.74
tL(UAA)J	39	A	27	280	5	461	5	121	0	230	8.99	1.59E-08	1.32E-06	2.78
tS(UGA)I	30	C	11	3980	15	12907	20	5082	18	15796	2.97	9.98E-06	0.000404112	1.26
tS(UGA)P	38	C	12	4054	2	12802	4	5188	0	15751	14.57	1.08E-07	8.72E-06	1.07
YDR278C	59	C	8	433	6	1053	64	1584	69	3282	2.02	2.74E-05	0.008679434	2.77
YGL086W	163	A	8	321	0	346	15	325	1	314	11.62	7.31E-05	0.011334079	3.09
YLR110C	109	A	13	445	1	571	21	619	12	939	3.84	2.85E-05	0.01141144	2.97
YLR110C	330	C	12	445	0	571	6	619	2	939	8.39	0.000153431	0.030762967	2.80
YLR154C-G	5	G	24	8220	16	7654	63	12017	34	12388	1.74	0.002110234	0.007312207	1.43
YLR154C-G	9	A	339	8220	32	7654	540	12017	51	12388	10.50	3.24E-140	2.42E-138	2.77
YLR154C-G	36	A	603	8220	330	7654	723	12017	354	12388	1.91	3.94E-42	1.47E-40	2.67
YLR154C-G	57	A	1194	8220	301	7654	1233	12017	423	12388	3.30	2.15E-181	3.20E-179	3.10
YLR154C-G	84	A	132	8220	30	7654	109	12017	73	12388	2.31	6.44E-13	1.20E-11	2.00
YLR154C-G	94	A	415	8220	76	7654	782	12017	220	12388	4.05	2.63E-115	1.30E-113	2.82
YMR013W-A	29	C	25	40	0	36	14	21	0	13	15.28	1.45E-05	0.001158211	3.71

FIGURE 35

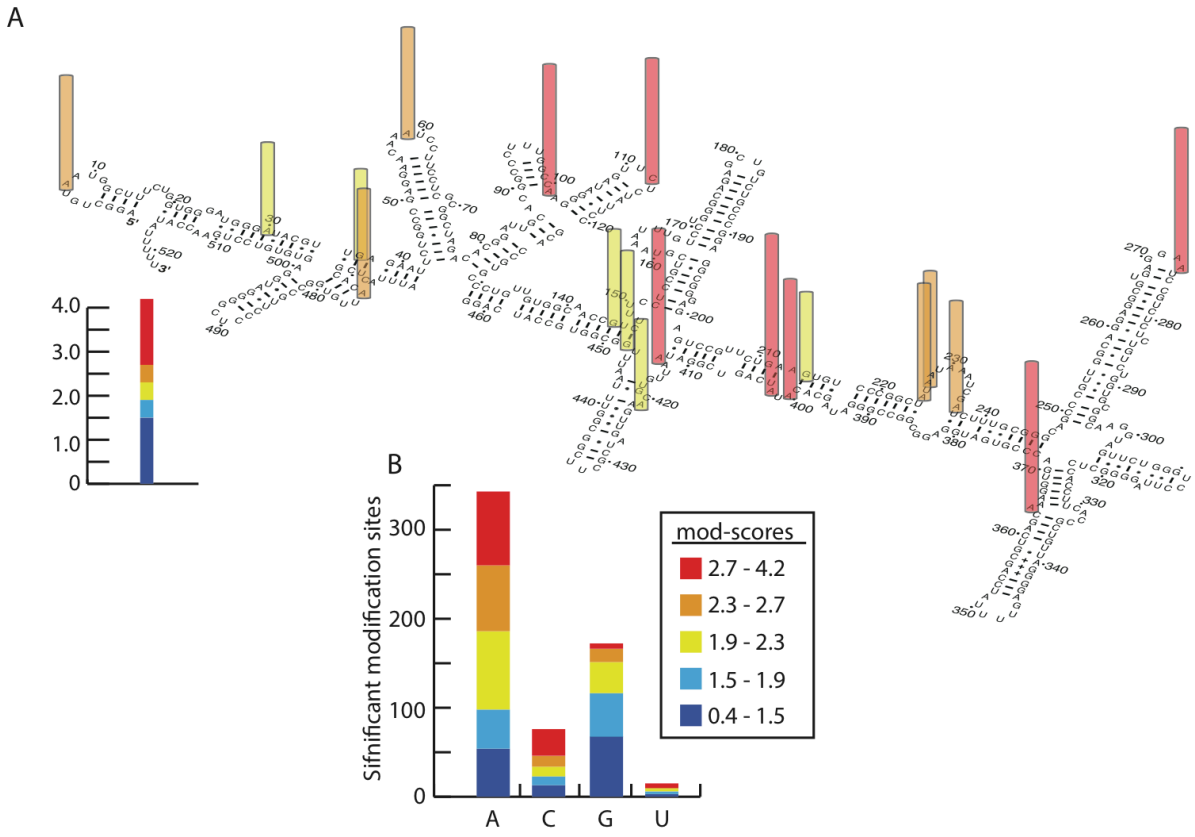

A
4.0
3.0
2.0
1.0
0
B
Sifnificant modification sites
300
200
100
0
A
C
G
U
mod-scores
2.7 - 4.2
2.3 - 2.7
1.9 - 2.3
1.5 - 1.9
0.4 - 1.5

Figure 35: Sites of *in vivo* DMS modification of scR1 detected by Mod-seq

(A) Example of Mod-seq sites on the 522 nucleotide long SRP RNA (SCR1). Nucleotides with significantly enriched sites of DMS modification are shown with colored bars depicting relative modification strength (mod-score). Sites with high mod-scores (orange and red) are exclusively located at As and Cs in single stranded regions. Mid-range mod-scores included significant modification of 4 Gs located in internal bulges and multi-helix junctions. (B) Nucleotide composition of significant modification sites. The bargraph shows the number of significant modifications at each of the four RNA nucleotide bases. Bars are colored to represent the distribution of mod-scores for each nucleotide. Sites with high mod-scores are almost exclusively A and C, while significantly modified Gs have smaller enrichment scores.

FIGURE 36 (continued on the following pages)

Figure S1-A. Secondary structure model of 5.8S and the 5′ end of 25S rRNAs.

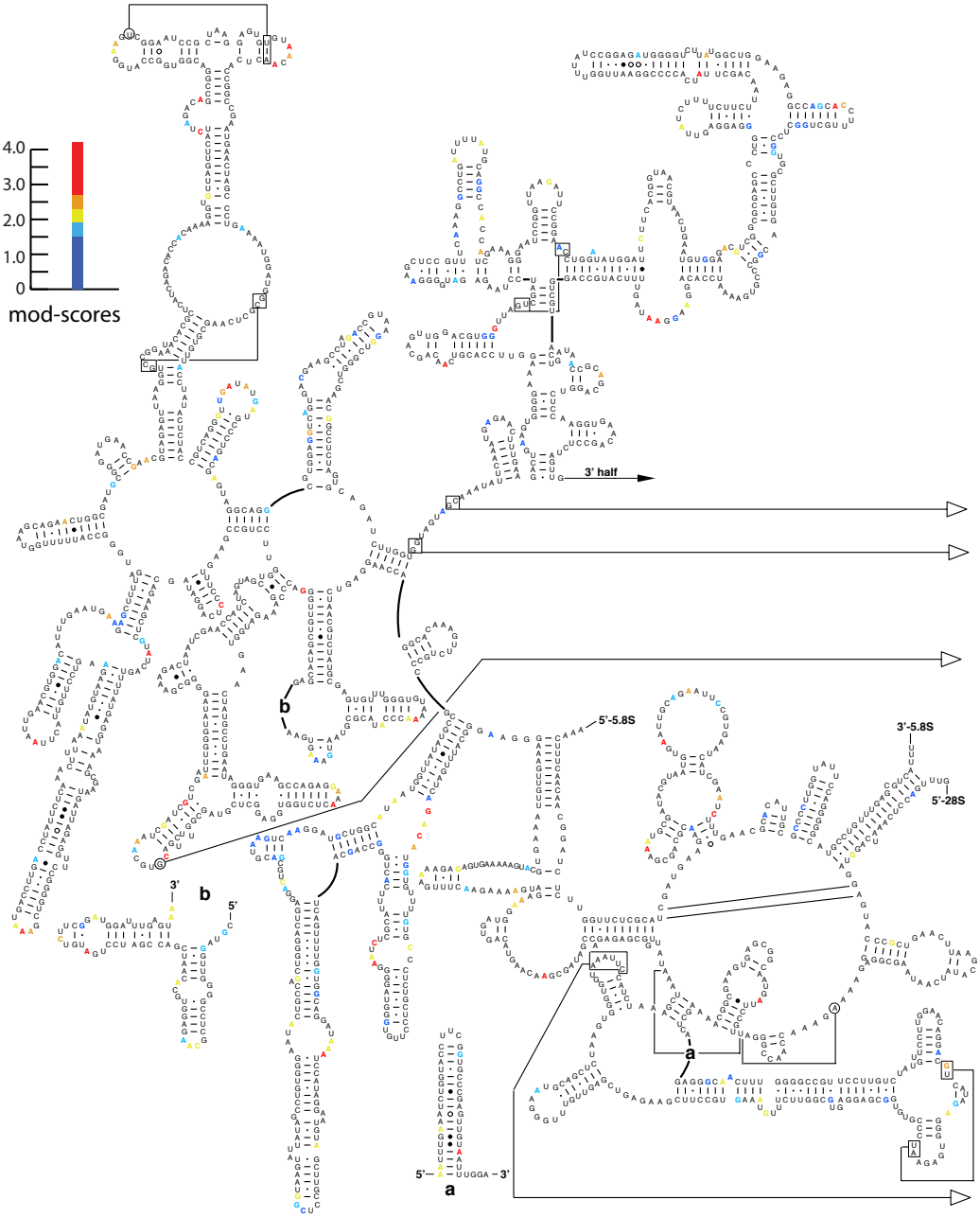


FIGURE 36 cont.

Figure S1-B. Secondary structure model of the 3' end of 25S rRNA.

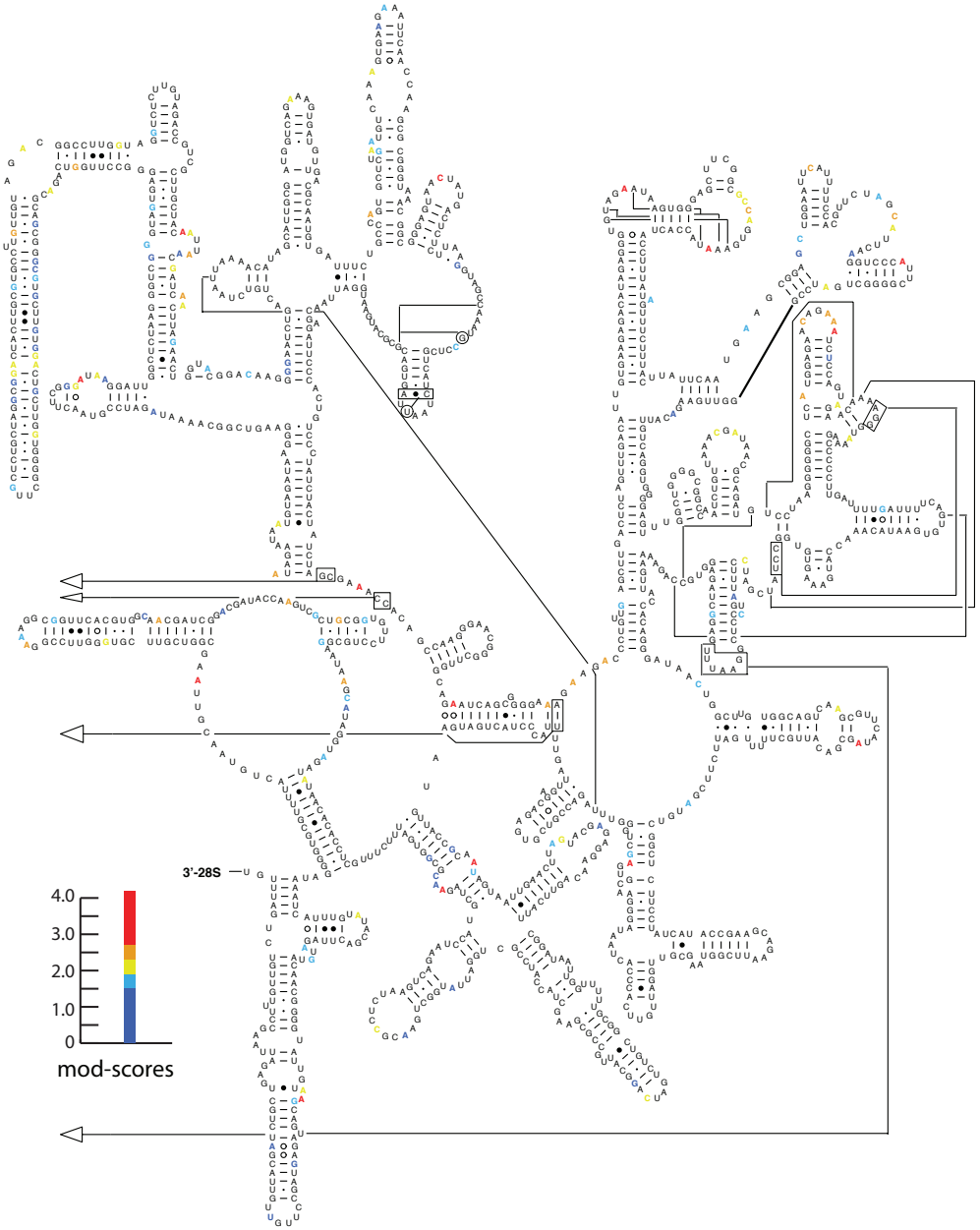


FIGURE 36 cont.

Figure S1-C Secondary structure model of the 18S rRNA.

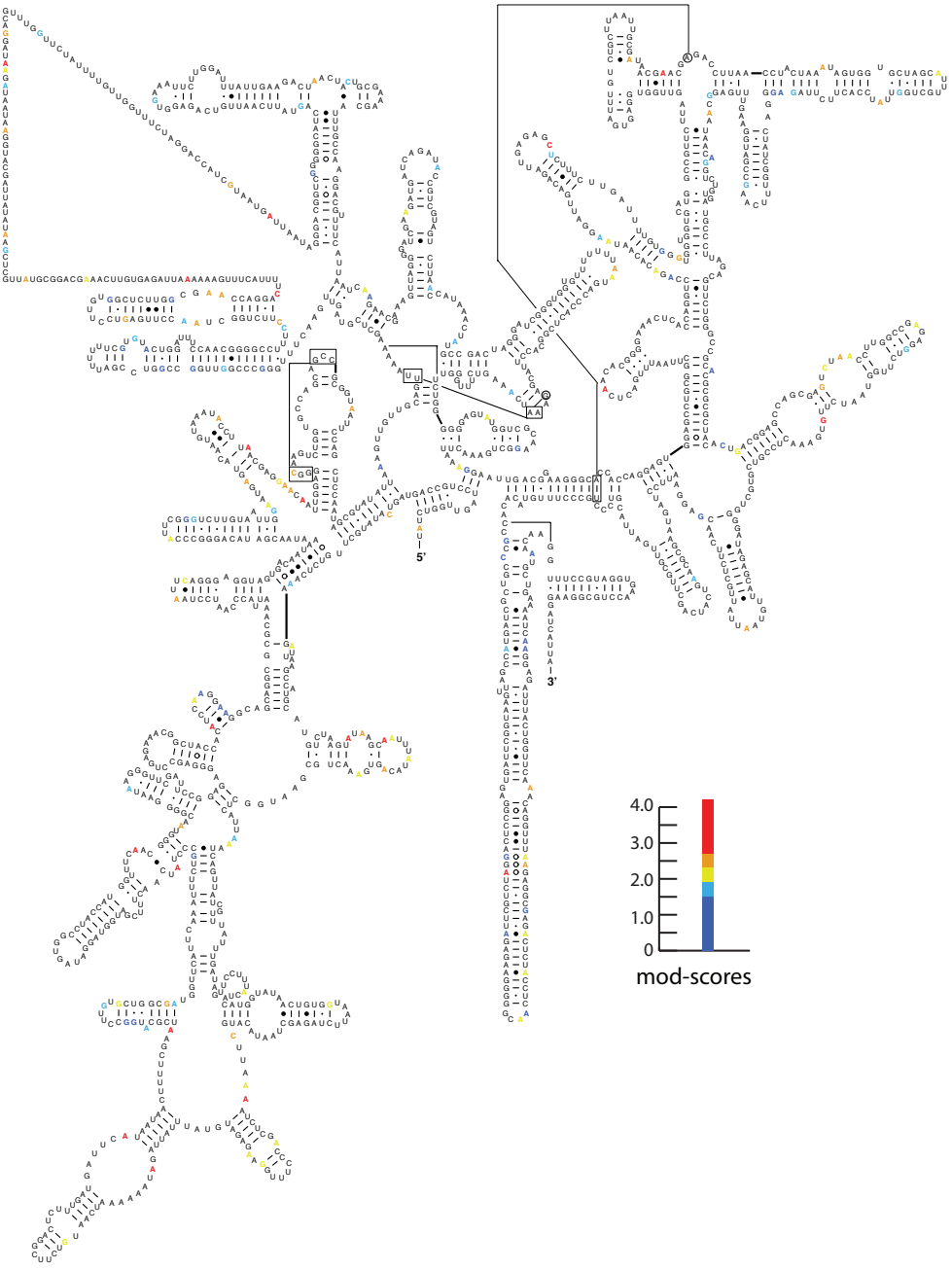


Figure 36: Modified nucleotides in rRNA detected by Mod-seq

Secondary structure model of 25S, 18S, and 5.8S with significantly modified residues identified by Mod-seq. Mod-scores of significantly modified nucleotides are shown using color coding for 5.8S and the 5' end of 25S rRNAs, the 3' end of 25S rRNA, and 18S rRNA.

FIGURE 37

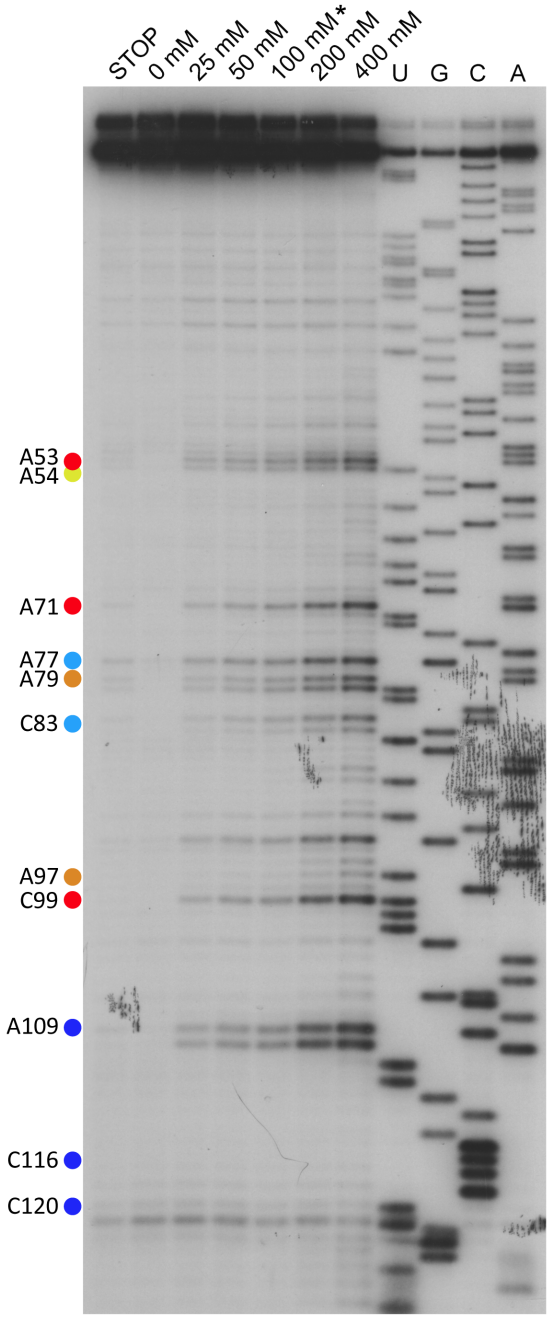

STOP
0 mM
25 mM
50 mM
100 mM*
200 mM
400 mM
U
G
C
A
A53
A54
A71
A77
A79
C83
A97
C99
A109
C116
C120

Figure 37: Sites of *in vivo* DMS modification of 5.8S rRNA identified by primer extension and PAGE analysis.

Cells were treated with a range of DMS concentrations. The asterisk indicates the concentration of DMS utilized in Mod-seq experiments. For comparison, mod-scores of modified nucleotides identified by Mod-seq are indicated. The "STOP" reaction serves as a control for the effectiveness of DMS quenching.

4.2.3 Detection of modified guanines by Mod-seq

Treatment with DMS methylates N1 of adenine and, to a lesser extent, N3 of cytosine. These modifications lead to termination of reverse transcription by disrupting base pairing with incoming nucleotides. Position N7 of guanines is also methylated, however the resulting modification (7mG) is thought to have little effect on reverse transcription, because the added methyl group is not on the base pairing face. Traditional approaches for detecting this modification require cleavage of the RNA backbone by reduction with sodium borohydride and treatment with analine (Stern et al. 1988) (Wells et al. 2000). However, several studies have reported rare increases in reverse transcription termination at G residues upon treatment with DMS (Wells et al. 2000). This has previously been interpreted as resulting from rare methylation at position N1, which may occur on enol-tautomers of guanosine (Moazed and Noller 1986). Surprisingly, we found that nearly one third of significant modifications mapped to G residues (Fig. 35B). However, G modifications have a weaker effect on reverse transcription termination. Over ninety percent of sites in the highest quintile of mod-scores are A or C residues, with few G residues. In contrast, G residues make up roughly half of the sites in the lower two quintiles. Modified U residues were rarely identified, comprising only two percent of all significant sites.

4.2.4 Detection of RBP binding sites and RNP structural changes by Mod-seq

We next determined the efficacy of using Mod-seq to map the binding site of an RNA binding protein (RBP) *in vivo*. We used ribosomal protein L26 as a test case, as deletion of L26 has little effect on growth in rich media (Babiano et al. 2012) and its binding site on the

ribosome is well known from the crystal structure model (Ben-Shem et al. 2011). Thus, we predicted that in its absence the number of observed changes would be minimal, but highly specific. Mod-seq was performed in duplicate experiments on an L26 deletion strain. We identified 58 nucleotides with significantly more modification in *rpl26Δ* than in wildtype; however most of these sites have mod-scores less than 1.0 (Table 4). Viewed on rRNA secondary structure, L26-sensitive sites of DMS probing are concentrated on the base-pairing interface of 5.8S and 25S rRNAs, localized primarily to domain I of rRNA (Fig. 38). These sites form a cluster of nucleotides around the L26 protein in the yeast ribosome crystal structure (Fig. 39). Importantly, these results also indicate reduced base-pairing in helices 4 and 24 in 25S-5.8S rRNA suggesting that the absence of L26, although tolerated, results in subtle structural changes in the neighborhood in which it binds. Thus, we conclude that Mod-seq is an effective method to map specific binding sites of RBPs.

It is interesting to note that we also observed differentially modified nucleotides outside of the L26 neighborhood. While most of these nucleotides had relatively low mod-scores, they may indicate subtle changes in the overall structure or dynamics of ribosomes in the absence of L26. A number of these modifications cluster around the two interfaces of the 40S and 60S ribosomal subunits (Fig. 40A). During translation, translocation of proteins into or across membranes requires the signal recognition particle. Cryo-EM of SRP bound to ribosomes revealed that the Alu-domain contacts the ribosome near the subunit interfaces at the elongation factor binding site, whereas the S-domain binds ribosomes at the polypeptide exit tunnel, near the L26 binding site (Fig. 40B) (Halic et al. 2004). An interesting possibility is that the some of the subtle changes we observe in nucleotide

reactivity are due to reduced affinity of SRP for the translating ribosome, or slight changes in the dynamics of these two RNPs during translation and translocation.

TABLE 4 (continued on the following page)

Table S3. Ribosomal RNA positions with increased DMS-dependent modification in the *rpl26Δ* strain. The number of sequence reads indicating modification at each site are shown (RT stops), as are the total number for the gene (Total RT stops). The enrichment ratio is the relative enrichment of RT stops at each position in RNA from DMS treated culture as compared to untreated culture. The results of statistical analysis are given, including both raw (CMH) and Benjamini-Hochberg corrected (B-H) p-values.

Gene	Position	100 mM DMS *rpl26A* 1		100 mM DMS Wild-type 1		100 mM DMS *rpl26A* 2		100 mM DMS Wild-type 2		Enrichment Ratio (DMS /	CMH P-values	B-H adjusted P-values	Mod-Score
		RT stops	Total RT stops	RT stops	Total RT stops	RT stops	Total RT stops	RT stops	Total RT stops				
RDN18	152	32	823711	8	603870	21	623406	12	545462	2.12	0.00530733	0.03897096	0.54
RDN18	333	90	823711	37	603870	115	623406	71	545462	1.55	0.00027061	0.00412569	0.93
RDN18	337	58	823711	23	603870	86	623406	49	545462	1.64	0.0007005	0.00810127	0.82
RDN18	356	69	823711	24	603870	62	623406	43	545462	1.58	0.00286441	0.0246559	0.76
RDN18	448	60	823711	29	603870	81	623406	43	545462	1.59	0.00150679	0.0148973	0.80
RDN18	596	88	823711	28	603870	59	623406	35	545462	1.86	4.26E-05	0.00091144	0.92
RDN18	753	200	823711	86	603870	61	623406	44	545462	1.55	5.58E-05	0.00113979	1.08
RDN18	770	173	823711	59	603870	120	623406	80	545462	1.68	4.71E-07	1.80E-05	1.17
RDN18	777	155	823711	46	603870	74	623406	61	545462	1.69	8.32E-06	0.00022012	1.07
RDN18	1121	24	823711	11	603870	53	623406	22	545462	1.93	0.00177432	0.01688887	0.64
RDN18	1198	28	823711	12	603870	29	623406	9	545462	2.16	0.00269879	0.02379961	0.58
RDN18	1228	74	823711	30	603870	20	623406	11	545462	1.75	0.00320242	0.02647421	0.72
RDN18	1242	103	823711	28	603870	53	623406	33	545462	2.02	3.17E-06	9.49E-05	0.99
RDN25	189	277	1355767	138	1130039	236	1175271	159	1065093	1.50	2.66E-08	8.75E-07	1.36
RDN25	202	40	1355767	13	1130039	64	1175271	34	1065093	1.95	0.00015573	0.00180449	0.82
RDN25	221	2564	1355767	338	1130039	1425	1175271	362	1065093	4.92	0	0	2.63
RDN25	231	268	1355767	145	1130039	182	1175271	114	1065093	1.50	2.05E-07	5.57E-06	1.31
RDN25	306	108	1355767	55	1130039	122	1175271	78	1065093	1.51	0.00017341	0.00195592	1.01
RDN25	319	135	1355767	53	1130039	44	1175271	42	1065093	1.62	0.00018459	0.00205472	0.97
RDN25	336	115	1355767	28	1130039	52	1175271	45	1065093	1.98	1.11E-06	2.51E-05	1.05
RDN25	351	681	1355767	145	1130039	146	1175271	78	1065093	3.16	1.12E-57	4.77E-55	1.88
RDN25	352	188	1355767	75	1130039	49	1175271	55	1065093	1.56	5.52E-05	0.00076137	1.07
RDN25	373	394	1355767	185	1130039	134	1175271	92	1065093	1.63	4.47E-11	2.37E-09	1.45
RDN25	375	61	1355767	31	1130039	47	1175271	30	1065093	1.53	0.00900662	0.04726042	0.70
RDN25	376	506	1355767	245	1130039	195	1175271	136	1065093	1.57	8.56E-13	5.70E-11	1.55
RDN25	388	204	1355767	104	1130039	178	1175271	112	1065093	1.54	4.81E-07	1.24E-05	1.25
RDN25	394	1301	1355767	589	1130039	511	1175271	318	1065093	1.71	2.25E-40	6.96E-38	2.01
RDN25	647	135	1355767	86	1130039	215	1175271	110	1065093	1.56	5.26E-07	1.34E-05	1.22
RDN25	660	71	1355767	39	1130039	47	1175271	28	1065093	1.52	0.00739869	0.04104338	0.74
RDN25	684	17	1355767	5	1130039	9	1175271	2	1065093	3.18	0.00693443	0.03936854	0.38
RDN25	1184	56	1355767	22	1130039	112	1175271	76	1065093	1.52	0.00121173	0.00943538	0.87
RDN25	1335	66	1355767	28	1130039	190	1175271	121	1065093	1.53	4.30E-05	0.00061382	1.05
RDN25	1345	101	1355767	46	1130039	89	1175271	64	1065093	1.50	0.00076613	0.00660152	0.93
RDN25	1390	106	1355767	40	1130039	92	1175271	50	1065093	1.91	2.96E-07	7.85E-06	1.10
RDN25	1413	98	1355767	37	1130039	72	1175271	59	1065093	1.54	0.00084335	0.00712251	0.90
RDN25	1798	76	1355767	33	1130039	125	1175271	80	1065093	1.57	0.00015035	0.00176012	0.98
RDN25	1837	52	1355767	18	1130039	38	1175271	21	1065093	2.00	0.00032174	0.00326066	0.78
RDN25	1866	132	1355767	59	1130039	130	1175271	85	1065093	1.59	9.32E-06	0.00016832	1.11
RDN25	1881	85	1355767	27	1130039	40	1175271	31	1065093	1.86	0.00010425	0.00129176	0.89
RDN25	1891	76	1355767	35	1130039	60	1175271	40	1065093	1.57	0.00189274	0.01367206	0.82
RDN25	1895	282	1355767	138	1130039	164	1175271	108	1065093	1.56	1.88E-08	6.38E-07	1.34
RDN25	1897	38	1355767	15	1130039	20	1175271	9	1065093	2.08	0.00303256	0.01992038	0.61
RDN25	1901	91	1355767	31	1130039	50	1175271	38	1065093	1.77	0.00011937	0.00143704	0.92
RDN25	2625	16	1355767	17	1130039	43	1175271	11	1065093	1.84	0.00888703	0.0468501	0.55
RDN25	2915	25	1355767	5	1130039	34	1175271	22	1065093	1.93	0.00581184	0.03418452	0.57
RDN25	2924	16	1355767	2	1130039	42	1175271	21	1065093	2.25	0.00112223	0.00881941	0.63
RDN25	3161	40	1355767	20	1130039	97	1175271	60	1065093	1.52	0.00357602	0.02269272	0.78
RDN25	3163	84	1355767	52	1130039	97	1175271	46	1065093	1.61	0.00017086	0.00193361	0.96
RDN25	3265	59	1355767	26	1130039	41	1175271	24	1065093	1.73	0.00181779	0.01324332	0.75
RDN25	3302	90	1355767	30	1130039	48	1175271	43	1065093	1.64	0.00078726	0.00674937	0.86
RDN5	84	0	122607	3	111376	4	137136	17	120884	0.22	0.00188002	0.00980882	0.07
RDN5	88	1	122607	7	111376	4	137136	15	120884	0.20	0.00070101	0.00382367	0.04
RDN5	89	0	122607	2	111376	10	137136	24	120884	0.37	0.00731239	0.02924958	0.05
RDN58	48	581	74878	201	47534	407	94795	268	82911	1.56	2.68E-15	2.34E-14	1.54
RDN58	52	509	74878	142	47534	288	94795	189	82911	1.77	3.98E-18	4.46E-17	1.53

TABLE 4 cont.

RDN58	83	880	74878	312	47534	775	94795	510	82911	1.52	2.29E-22	3.59E-21	1.73
RDN58	88	4544	74878	521	47534	5981	94795	1399	82911	4.28	0	0	2.87
RDN58	89	7138	74878	1211	47534	7766	94795	2355	82911	3.20	0	0	2.98

FIGURE 38 (continued on the following pages)

Figure S3-A. Secondary structure model of 5.8S and the 5′ end of 25S rRNAs.

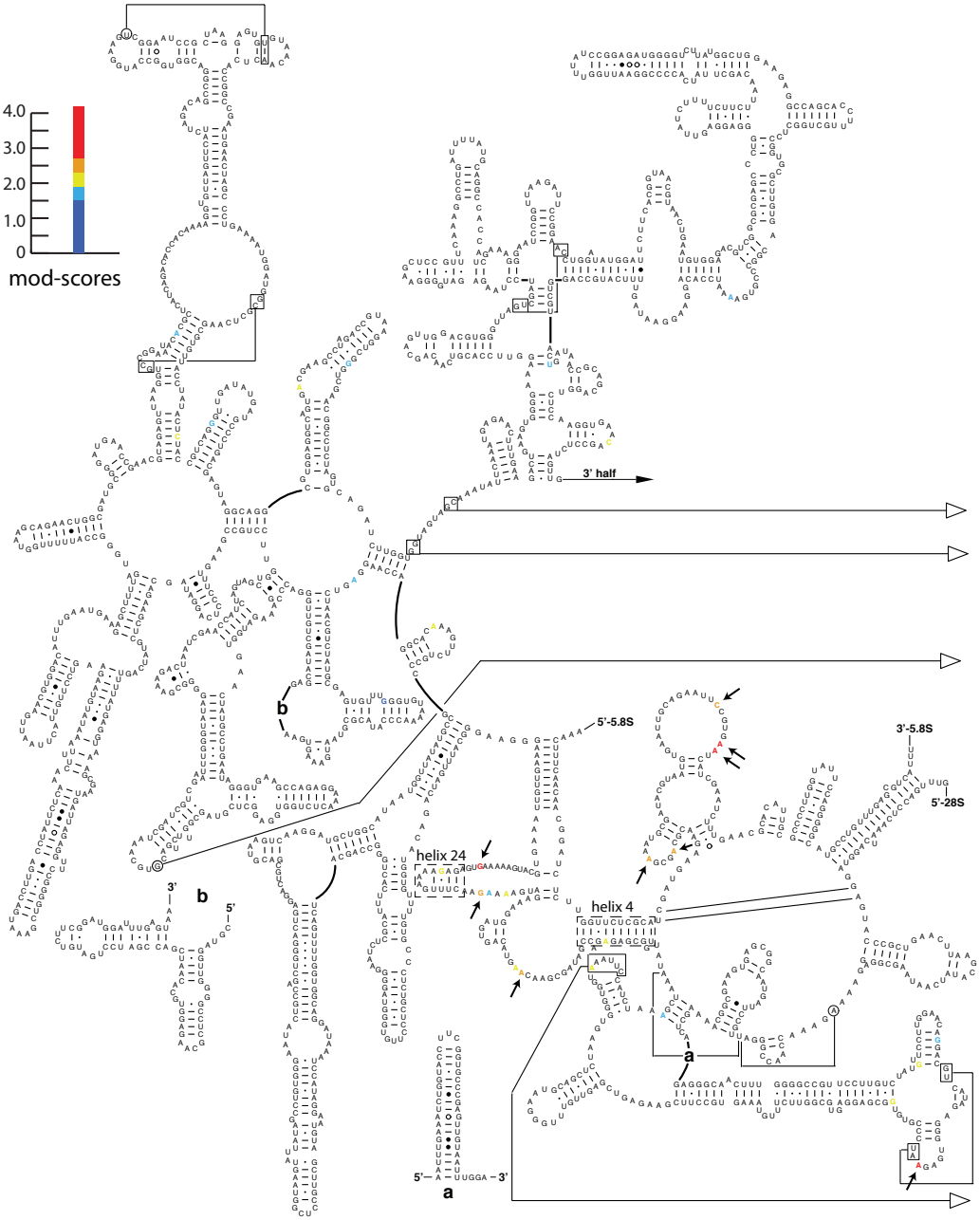


FIGURE 38 cont.

Figure S3-B. Secondary structure model of the 3' end of 25S rRNA.

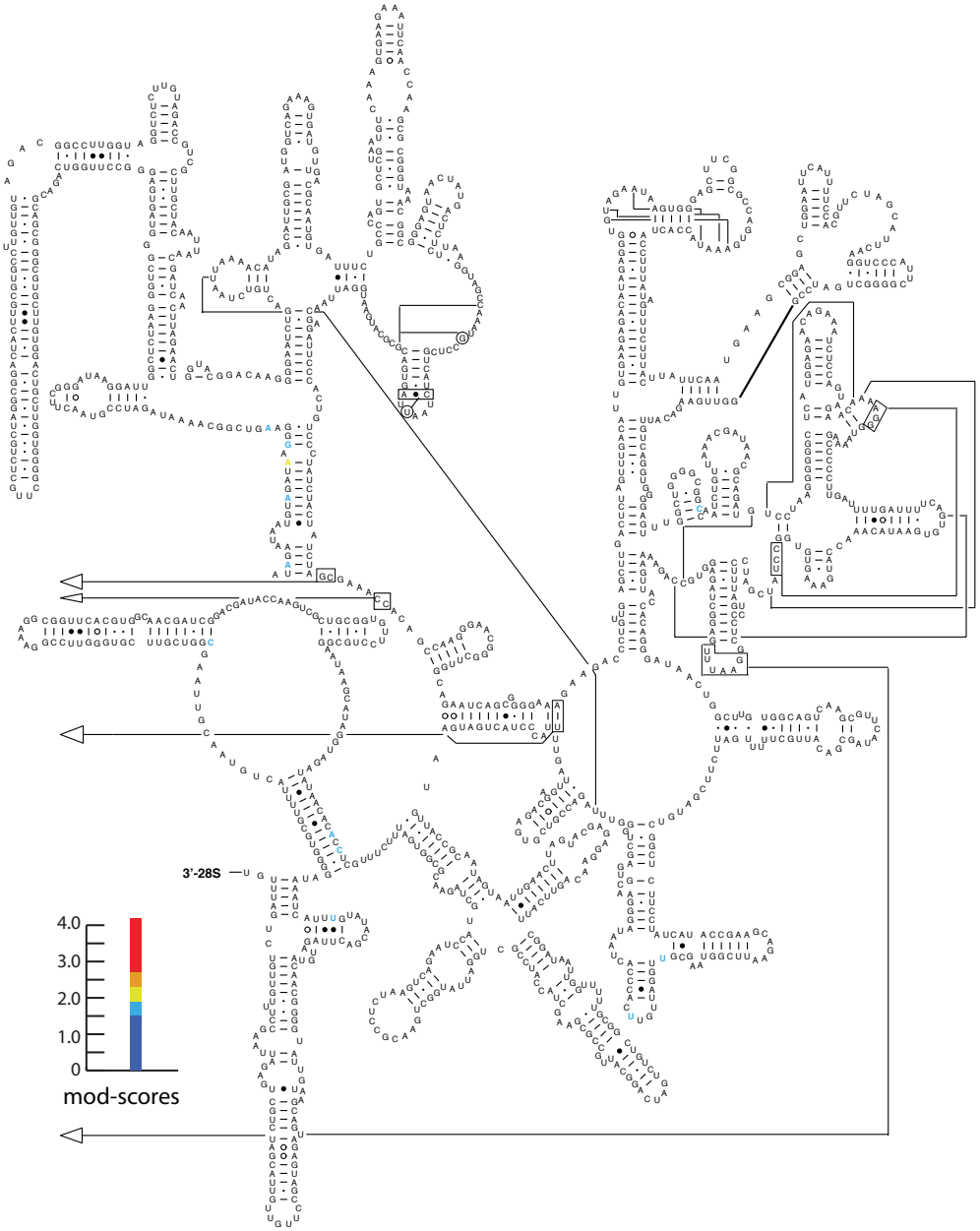


FIGURE 38 cont.

Figure S3-C Secondary structure model of the 18S rRNA.

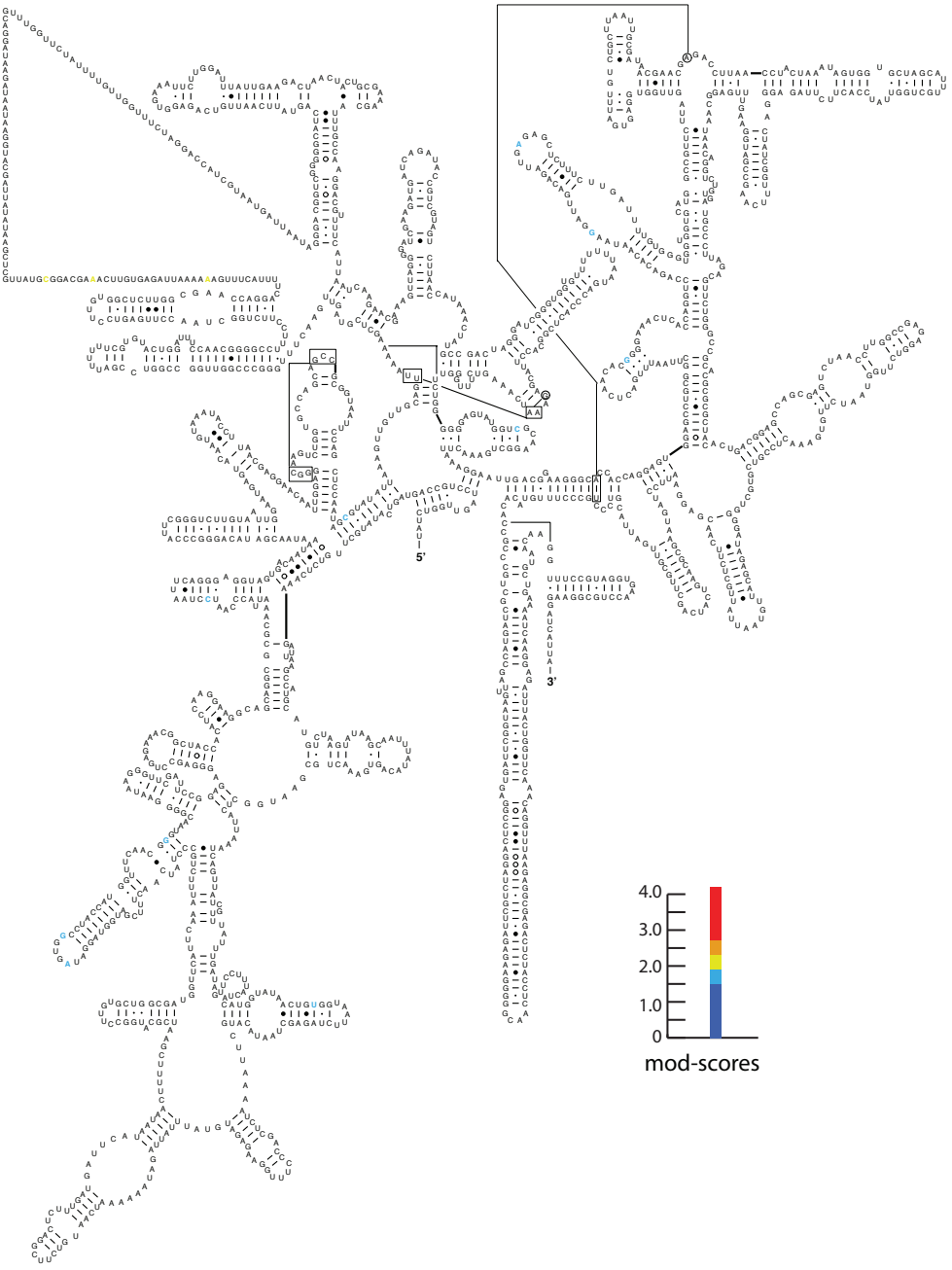


Figure 38: Differentially modified nucleotides in the absence of r-protein L26 detected by Mod-seq.

Secondary structure model of 25S, 18S, and 5.8S showing nucleotides with significantly more modification in the *rpl26Δ* strain, compared to wildtype (BY4741). Mod-scores of significantly modified nucleotides are shown using color coding for 5.8S and the 5' end of 25S rRNAs, the 3' end of 25S rRNA, and 18S rRNA. The most prominent differences are indicated with arrows, and cluster around the protein binding site in the 5.8S and 25S rRNAs.

FIGURE 39

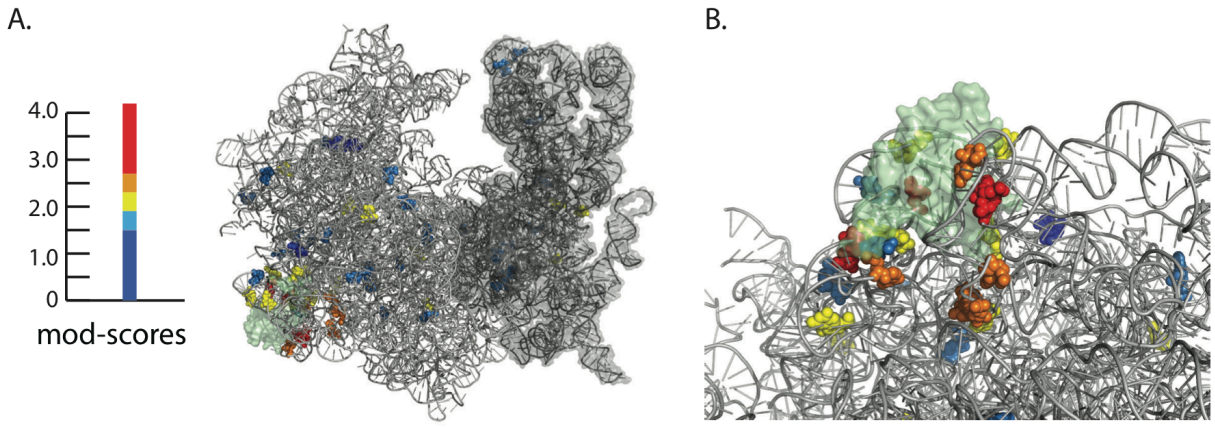
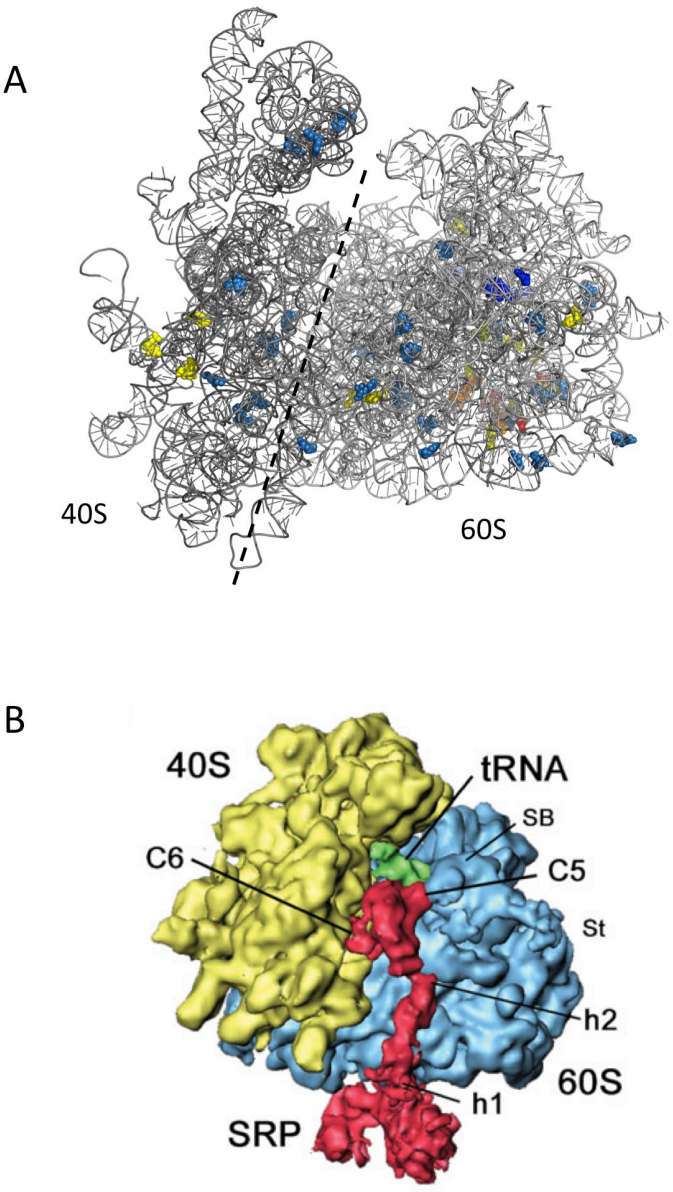


Figure 39: rRNA structural changes in the absence of r-protein L26 detected by Mod-seq.

Views of the x-ray crystal structure model of the yeast 80S ribosome generated with pymol (PDB: 3U5F, 3U5G, 3U5H, 3U5I). (A) The large (left) and small (right) subunits are shown in different shades of grey. Ribosomal protein L26 is shown in a transparent surface rendering. Nucleotides with increased modification by DMS in the absence of L26 protein in vivo are shown in colors representing their mod-scores. (B) Magnified views showing residues with the largest differences in DMS sensitivity (red and orange nucleotides). These nucleotides cluster around the site of L26 binding.

FIGURE 40



(B) Halic *et al.* 2004

Figure 40: Differentially modified nucleotides in the absence of L26 localize near the SRP binding site

(A) Shown is the crystal structure of the 80S yeast ribosome with differentially modified nucleotides colored according to their mod-score. The dashed line indicates the subunit interfaces. (B) Cryo-EM map of mammalian SRP bound to 80S ribosomes. The 40S and 60S subunits are shown in yellow and blue, respectively. SRP is red. The Alu domain of SRP can be seen contacting the 60S subunit near the subunit interface.

4.2.5 Mod-seq provides secondary structure information for pre-rRNAs

Although beyond the scope of the initial development of Mod-seq, we also obtained structural information about pre-rRNAs. In wild-type cells we observed modification of nucleotides in the 5' ETS, ITS1, and ITS2; however the number of sequencing reads was low due to the fact that pre-rRNAs are present in much lower abundance than mature rRNAs and other ncRNAs. I have previously assayed *in vivo* modification of ITS2 (Appendix 5.5) by primer extension and PAGE, and the results obtained by Mod-seq are in good agreement, identifying some of the "strongest" modifications (Fig. 41). Thus, Mod-seq will be a powerful tool for assaying structural changes in pre-ribosomes, but will require prior enrichment of pre-rRNAs. Strategies to enrich for pre-rRNAs will be discussed in the Appendix (5.7).

FIGURE 41

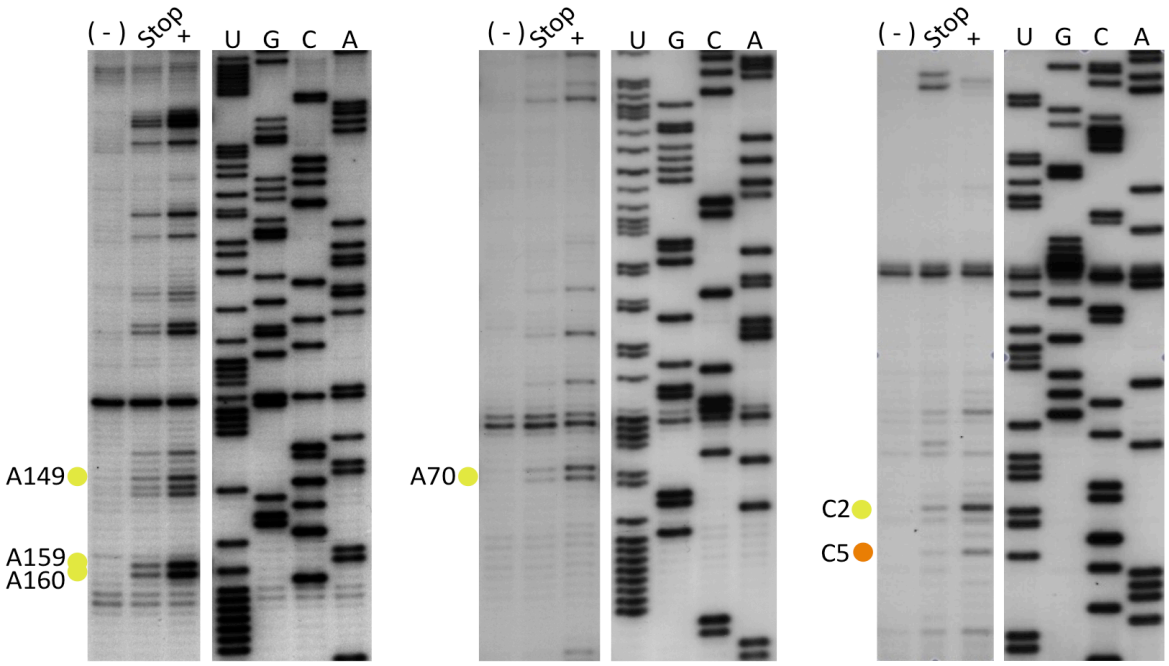


Figure 41: Mod-seq analysis of pre-rRNAs

Shown are representative gels of nucleotides in ITS2 modified *in vivo* with DMS and visualized by primer extension and PAGE. Modified nucleotides detected by Mod-seq are indicated with colored circles representing their mod-scores. The "STOP" reaction serves as a control for the effectiveness of DMS quenching.

4.3 DISCUSSION

Mod-seq differs from prior approaches in that it can be used both *in vivo* or *in vitro*, and can be applied to RNAs of any length. Random fragmentation of cellular RNA ensures that reverse transcription will initiate at random positions, alleviating the need for complex reverse transcriptase stop probability modeling. However, random fragmentation introduces a problem - differentiating reverse transcriptase stops due to chemical modification from those resulting from run off of random fragment ends. We solved this problem by ligating 5' adapters to our RNA before reverse transcription. High-throughput sequence reads that initiate with the 5' adapter indicate reverse transcriptase drop off at random fragment ends, while reads without the adapter result from reverse transcriptase release at a modified nucleotide. We used Mod-seq to map significant sites of DMS modification simultaneously on 36 non-coding RNAs *in vivo*. Identified modification sites were consistent with known secondary structure models from these RNAs. Finally, we show that comparing Mod-seq results in the presence and absence of an RNA-binding protein can reveal its binding site and resulting structural changes in its absence.

We found that many DMS-dependent sites of modification were located at guanosines. Although guanosine sites have lower mod scores, we suggest they likely represent legitimate sites of modification for the following reasons. First, false-positive sites should be equally likely to occur at U or G residues, yet we see very few DMS dependent termination sites at Us. Second, some of the rRNA nucleotides with increased modification in the *rpl26Δ* strain that are footprinted to the L26 binding site are Gs, and were previously observed when assayed with radiolabeled primer extension (Babiano et al. 2012). Finally, methylation of guanosine N7 (m7G) is known to occur more rapidly than

that of As and Cs (Lawley and Brookes 1963). Several factors could make Mod-seq more sensitive to m7G, as compared to traditional approaches relying on primer extension and gel electrophoresis. For example, m7G could cause a subtle increase in the probability of reverse transcriptase termination only detectable with deep sequencing. Another possibility is that this modification may increase the probability of RNA fragmentation or impede ligation of 5' linkers by RNA ligase 1.

4.3.1 Applications of Mod-seq

Recent advances in sequencing technologies and the Encyclopedia of DNA Elements (ENCODE) project have revealed that a much greater fraction of the genome is transcribed than previously thought. RNA-seq analysis showed that 62% of genomic bases are transcribed into RNA, but only 5% of these bases are within exons of protein coding genes (Djebali et al. 2012). Thus, a large fraction of the transcriptome is represented as either introns or intergenic non-coding RNAs. Among others, these include RNAs that function in splicing (snRNAs), translation (micro-RNAs) and protein synthesis (rRNAs, tRNAs, snoRNAs, RNase-P, SRP-7S), as well as a relatively new class, the long non-coding RNAs (lncRNAs). Although these RNAs do not encode proteins, they play key roles in regulating gene expression and are therefore indispensible for life.

We envision many applications for Mod-seq, as this method is suitable for RNA of any length. Selective removal of rRNA before library preparation would allow genome-wide probing of mRNA structure *in vivo*. In alternative splicing, splice site selection can be dictated by the secondary structure of the pre-mRNA. Sequestration of splice sites or *cis*-regulatory sequences into complex secondary structures has been shown to inhibit

splicing. In fact, many alternative splice sites are enriched for conserved secondary structures; suggesting a strong relationship between secondary structures, splice site selection, and alternative splicing (Shepard and Hertel 2008). Conversely, folding of pre-mRNA has also been shown to aid in splicing, by bringing distal regulatory sequences in close proximity to each other (Buratti and Baralle 2004; Warf and Berglund 2010; McManus and Graveley 2011). Thus, a deeper knowledge of pre-mRNA structure will allow a better understanding of the mechanisms that govern alternative splicing.

For more targeted studies, oligonucleotides can be used to purify RNAs of interest prior to sequencing library preparation. This strategy would be applicable to understanding the dynamics and assembly of large RNP complexes such as the ribosome and the spliceosome. By targeting pre-rRNAs and snRNAs, either from wild-type cells, or mutants blocked at various stages of assembly, one can visualize structural changes in these RNPs over time.

This approach will also greatly advance our understanding of lncRNAs, some of which are longer than ribosomal RNAs. These are RNAs >200 nucleotides (not including classical non-coding RNAs such as rRNA, snRNAs, telomerase-associated RNA, etc.), that do not act as templates for protein synthesis. The ENCODE project predicts human cells express at least 15,000 different lncRNAs. The exact mechanism of how many of these RNAs function still remains a mystery, but lncRNAs have been shown to participate in regulating transcription, splicing, translation, the cell-cycle, and diseases such as cancer (Rinn and Chang 2012) (Yoon et al. 2012). Even less is know about the overall structure and architecture of lncRNAs. Do lncRNAs fold into complex three-dimensional structures similar to rRNA? Are lncRNAs present in large RNP complexes, bound by numerous

proteins? How does folding of lncRNAs regulate their activity and function? Only recently has the first experimentally derived structure of a lncRNA (steroid receptor RNA activator) been determined (Novikova et al. 2012). This comprehensive analysis used a combination of DMS, RNase V1, in-line, and SHAPE probing and revealed that this ~1 kb RNA is highly structured with domain architectures reminiscent of rRNAs. However, analysis of the probing data by capillary electrophoresis required at least 5-10 different oligonucleotide primers (for each of the four structure probing approaches). Thus, Mod-seq is sure to streamline this process in future analyses of other lncRNAs.

Precise footprinting of protein binding sites, as demonstrated here with ribosomal protein L26, is also possible. Thus, Mod-seq could be utilized for transcriptome-wide mapping of RBP binding sites *in vivo*. Furthermore, applying Mod-seq with SHAPE reagents, either *in vitro* or *in vivo*, would provide a powerful approach to interrogating RNA tertiary structure (Spitale et al. 2012). Last, in the absence of DMS, we observed reverse transcriptase termination sites at nucleotides with known endogenous modifications (e.g. m1A, at positions 645 in 25S rRNA), suggesting that Mod-seq could be used to identify naturally occurring modifications. More sequencing depth will likely be needed for such genome-wide applications. However, the ever-decreasing cost of high-throughput sequencing makes these studies approachable to labs of any size.

4.4 MATERIALS AND METHODS

Growth of Yeast Strains, DMS Probing, and RNA extraction

All strains were grown at 30 °C in liquid YEPD media (2% dextrose, 2% peptone, and 1% yeast extract). DMS probing was performed as previously described with the following modifications (Wells *et al*. 2000). 10 ml cultures of WT (BY4741; *MATa his3Δ1 leu2Δ0 met15Δ0 ura3Δ0*) (Euroscarf) and *rpl26Δ* (JWY9670; *MATa his3Δ1 leu2Δ0 met15Δ0 ura3Δ0 RPL26A::*kanMX4 *RPL26B::*kanMK4) (Babiano *et al*. 2012) strains were grown to mid-logarithmic phase, at 3-5 X 10^7 cells/ml. 400 µl of freshly diluted DMS (1:4 vol/vol in 95% ethanol) (Sigma-Aldrich) was added to the cells to a final concentration of 100 mM. Cells were incubated with shaking at 30 °C for 2 minutes. The DMS reactions were quenched by placing the cultures on ice and adding 5 ml of ice-cold 0.6M β-mercaptoethanol and water-saturated isoamyl alcohol. Cells were pelleted by centrifugation at 5000 x *g* for 5 minutes. Cell pellets were resuspended and washed in 5 ml of ice-cold 0.6M β-mercaptoethanol and centrifuged again. Total RNA was immediately phenol-extracted from the cell pellets, ethanol precipitated, and resuspended in RNase-free water as previously described (Horsey *et al*. 2004). "No DMS" controls were treated the same as the experimental samples except for the addition of DMS. "Stop" controls were treated the same as the experimental samples except that DMS was not added until after the addition of 5 ml of 0.6M β-mercaptoethanol and water-saturated isoamyl alcohol. "Stop" controls serve as a measure of how effectively the DMS reactions were quenched.

Primer extension and PAGE

DMS modifications were assayed by primer extension with radiolabeled oligonucleotides as described in Liebeg and Waldsich (2009) with the following changes. For each reaction, 2.5 µl (500 ng) of whole-cell RNA was incubated with 1 µl (0.2 µM) of ^{32}P-labeled primer (5´ AAATGACGCTCAAACAGGCATGC 3´), and 1 µl of 4.5x hybridization buffer (225 mM Hepes pH 7.0; 450 mM KCl) at 95 °C for 5 minutes. Reactions were then cooled to the annealing temperature of 54 °C for 20 minutes. 15 µl of pre-warmed (54 °C) extension mix containing 4 µl of 5X hybridization buffer (Roche Applied Science) (250 mM Tris-HCl; 150 mM KCl; 40 mM $MgCl_2$, pH is approximately 8.5), 2.0 µl 2.5 mM dNTP mixture, 1.0 µl 0.1 mM DTT, 0.5 µl (20U) RNasin (Promega), 0.5 µl (10U) Transcriptor Reverse Trascriptase (Roche Applied Science), and 7.5 µl of nuclease free water was added to each reaction. For sequencing reactions, 2 µl of the appropriate ddNTP (10 mM) (Roche Applied Science) was also added. Reactions were incubated at 54 °C for one hour. RNA was degraded by the addition of 3 µl 1M NaOH to each reaction and incubation at 55 °C for one hour. Reactions were neutralized by the addition of 3 µl 1.0 M HCl. cDNAs were precipitated with 1 µl of glycogen (10 mg/ml), 1 µl 0.5 M EDTA pH 8.0, 2.8 µl 3.0 M NaOAc pH 5.0, and 84 µl of ethanol. Following ethanol precipitation, dried cDNA pellets were resuspended in 6 µl of 1X loading dye (45% formamide; 0.01 M EDTA pH 8.0), resolved on 6% polyacrylamide/7M urea gels, and visualized by autoradiography.

Library preparation

Total RNA (3 µg) was randomly fragmented using RNA Fragmentation Reagents (Ambion®) for 3 minutes at 70°C in a 20 µl reaction. The fragmented RNA was purified using a RNA Clean & Concentrator™-5 column (Zymo Research) using the manufacturer's >

17 nucleotide long protocol, and resuspended in 15.5 µl of nuclease free water. The RNA fragments were phosphatase-treated to remove 2'-3' cyclic phosphate groups by incubating with 15U of T4 Polynucleotide Kinase (PNK) (New England Biolabs) with 20U of SUPERase-In™(Life Technologies) for one hour at 37°C in a 20 µl reaction. RNA fragments were then 5' phosphorylated by adding 12.5 µl of nuclease free water, 2 µl 10X T4 PNK buffer, 15U T4 PNK, and ATP to a concentration of 1 mM, and incubating at 37°C for one hour. The RNA fragments were purified using a RNA Clean & Concentrator™-5 column and resuspended in 11.75 µl of nuclease free water.

The end prepared RNA fragments were ligated to 500ng of universal miRNA cloning linker (5′ rAppCTGTAGGCACCATCAAT–NH2 3′) (New England Biolabs). RNA fragments and linker were heated at 80 °C for 2 minutes and then placing on ice to disrupt secondary structures, and incubated overnight at 16 °C in a 20 µl reaction containing 12.5% PEG 8000, 10% DMSO, 20U SUPERase-IN™, 200U T4 RNA Ligase 2 truncated (New England Biolabs), and 1X T4 RNA ligase reaction buffer (NEB). The RNA was purified using a RNA Clean & Concentrator™-5 column (Zymo Research) using the manufacturer's > 200 nucleotide long protocol, and resuspended in 10 µl of nuclease free water. The RNA was then ligated at it's 5' end to the 5' linker (5' End Acceptor Oligonucleotide 17.93R, 5' ATCGTaggcaccugaaa 3', (Lau et al. 2001)) where uppercase is DNA and lowercase is RNA. To reduce secondary structure, the 5' linker was incubated at 70°C for 2 minutes and placed immediately on ice. The RNA and 5' linker were incubated at 22°C overnight in a 30 µl reaction containing 10% DMSO, 1X Quick Ligase Buffer (NEB), 20U SUPERase-IN™, and 15U T4 RNA ligase 1 (NEB). The RNA was purified using a RNA Clean & Concentrator™-5 column (Zymo Research, >200nt protocol) and resuspended in 26 µl of nuclease free water.

RNA fragments with ligated 5' linkers were selectively enriched using a biotinylated oligonucleotide (5' TTTCAGGTGCCTACGAT 3' – Biotin-TEG) complimentary to the 5' linker. The RNA and 0.67 μM oligonucleotide were denatured in a 30 μl reaction at 90°C for 90 seconds in 1.3X SSC. The RNA and oligonucleotide were then annealed by cooling from 37°C to room temperature at 3°C per minute in a thermocycler, and bound to streptavidin beads (Dynabeads MyOne C1, Life Technologies) according to the manufacturers instructions. To elute bound RNA from the beads, the sample was resuspended in 12 μl of TE, heated to 80°C for 2 minutes, immediately placed on a magnet, and all of the supernatant was removed.

The RNA was reverse transcribed using Superscript® II Reverse Transcriptase at 50°C according to the manufacturers instructions. The reverse transcription primer (5′-(Phos) AGATCGGAAGAGCGTCGTGTAGGGAAAGAGTGTAGATCTCGGTGGTCGC-(SpC18)-CACTCA-(SpC18)-TTCAGACGTGTGCTCTTCCGATCTATTGATGGTGCCTACAG-3′) as described in (Ingolia et al. 2012) is complimentary to the Universal miRNA cloning linker (NEB) and also contains sequence complimentary to Illumina™ forward and reverse PCR primers. After reverse transcription, the RNA template was destroyed by adding NaOH to a concentration of 100mM and incubating the reaction at 98°C for 20 minutes. The cDNA was ethanol precipitated and resuspended in 10 μl TE. Fragments in the size range of 150-330 base pairs were extracted from an 8% denaturing urea gel and resuspended in 15 μl of TE.

The size selected cDNA fragments were circularized by incubating with 100U CircLigase™ ssDNA Ligase (Epicentre) at 60°C for 1.5 hours according to the manufacturers instructions. Because the reverse transcription terminates at DMS modified bases, cDNA that contains the 5' linker would not have contained a DMS modified base. In order to

enrich for cDNA that contain information on DMS stops, the cDNA was first annealed a biotinylated oligonucleotide complimentary to the 5' linker cDNA sequence (Biotin – TEG – 5'ATCGTAGGCACCTGAAA3') and then sequences containing the 5' linker sequence were removed using streptavidin beads (Dynabeads MyOne C1, Life Technologies) according to the manufacturers instructions. The remaining cDNA was ethanol precipitated and resuspended in 20 µl TE.

The cDNA was amplified by PCR using forward and reverse primers containing sequences specific to the Ion Torrent™ (Life Technologies) sequencing platform. The reverse primer (5' CCTCTCTATGGGCAGTCGGTGATCCGATCTATTGATGGTGCCTACAG 3') was universal whereas the forward primer (5'-CCATCTCATCCCTGCGTGTCTCCGACTCAG -(6nt barcode)- CTACACGACGCTCTTCCGATCT-3') contained a 6 nucleotide barcode specific to each sample. In a 20 µl reaction, 1 µl of cDNA template, 0.5µM each forward and reverse primer, 0.5mM dNTPs, 0.4U Phusion® DNA polymerase (Finnzymes), and 1X Phusion HF buffer, were cycled for 12 rounds using an annealing temperature of 64°C. The libraries were purified and eluted in 10 µl TE using a MinElute PCR purification column (Qiagen) according to the manufactures instructions. The libraries were assessed and quantified using a Agilent 2200 TapeStation System. Libraries were pooled and sequenced on and Illumina HiSeq 2000 at the University of Southern California Epigenome Center.

Data Analysis

Sequence reads were first processed to remove 5' and 3' adapter sequences using cutadapt (Martin 2011). Reads matching the 5' adapter (adapter reads) result from reverse transcription termination at random fragment ends and were removed from further

analyses. Reads lacking the 5' adapter (mod-reads) were aligned to the current yeast genome sequence (SacCer3) using bowtie (version 0.12.8; (Langmead et al. 2009)). Reverse transcriptase can sometimes add untemplated nucleotides to cDNA 3' ends. Mod-read alignments often had mismatches at their 5' ends corresponding to these untemplated nucleotides. We corrected these mismatches by trimming them from the alignment files using a custom perl script. Aligned mod-reads were mapped to annotated genes using the intersectBed program from bedtools. Gene-mapped reads from treatment and control samples were then combined into tables containing the number of read 5' ends mapping to each nucleotide of each gene.

The resulting data were further analyzed to identify sites significantly enriched in treatment sample reverse transcriptase stops using a custom program in R. All tests of statistical significance were performed in R (version 2.15.2). Cochran-Mantel-Haenszel tests were used to estimate the odds ratios of enrichment. Resulting P-values were corrected using the Benjamini-Hochberg method (Benjamini et al. 2001). Mod-scores were also calculated in R. For a given nucleotide position (n), the Mod-score (M_n) is defined as:

$$M_n = Log_{10}\left[\left(\left(T_n / \sum T\right) * 100 - \left(C_n / \sum C\right) * 100\right) * l\right]$$

where T_n and C_n represent the number of RT stops at a particular nucleotide, and ΣT and ΣC represent the sum of all stops in treatment (T) and control (C) samples, respectively, and (l) denotes the length of the RNA. Mod-scores were mapped to rRNA secondary structure models (Cannone et al. 2002) by modification of previously described programs (Leshin et al. 2011).

Data access

High-throughput sequencing data have been submitted to NCBI Short Read Archive under accession number SRP029192. Genome-browser track files (bedGraph) are available upon request.

Acknowledgements

We are grateful to members of the McManus and Woolford labs for helpful comments and discussions. We would also like to thank the De la Cruz lab at the Universidad de Sevilla for providing the *l26Δ* strain. This work was supported by a grant from the National Institutes of Health laboratory (RO1 GM28301-32) to JLW, and start-up funding provided by the Department of Biological Sciences at Carnegie Mellon University to CJM.

CHAPTER 5: APPENDIX

5.1 Hierarchical Recruitment into Nascent Ribosomes of Assembly Factors Required for 27SB pre-rRNA Processing in *Saccharomyces cerevisiae*

**I worked on this project with Jingyu Zhang as a rotation student in the lab. When Jingyu graduated in 2008, I took over and completed the remainder of this work. Some of this data is already presented in Jingyu's thesis, but our model has been slightly refined. This work was published in *Nucleic Acids Research* in February, 2013.

INTRODUCTION

Eukaryotic ribosome biogenesis initiates in the nucleolus, where ribosomal RNA (rRNA) is transcribed, folded, bound by ribosomal proteins (r-proteins) and assembly factors, modified, and processed to begin to form mature ribosomal subunits. Subsequent steps in maturation of pre-ribosomal particles (pre-rRNPs) occur upon their release from the nucleolus to the nucleoplasm and finally, upon export to the cytoplasm. This assembly pathway requires a dynamic series of remodeling steps in which protein-protein, RNA-protein, and RNA-RNA interactions are established, disrupted, and reconfigured (Venema and Tollervey 1999; Henras et al. 2008; Staley and Woolford 2009; Kressler et al. 2010; Panse and Johnson 2010; Karbstein 2011).

Ribosome biogenesis is best studied in the yeast *Saccharomyces cerevisiae*, where more than 200 phylogenetically conserved *trans*-acting ribosome assembly factors have been discovered (Henras et al. 2008; Kressler et al. 2010). Genetic analyses led to the

discovery of many of these factors, and pinpointed specific steps in ribosomal precursor RNA (pre-rRNA) processing for which each of these proteins is required (Fig. 4). Affinity purifications of pre-ribosomes containing pre-rRNA processing intermediates enabled identification of many other assembly factors and determined with which pre-rRNAs each factor associates. While this approach establishes a timeline of association of factors with nascent ribosomes, assembly no doubt involves more steps than those defined by the known pre-rRNA processing reactions. Thus we need to understand recruitment at higher resolution.

Having discovered most of the factors required for ribosome biogenesis, it is now critical to determine how these molecules facilitate rearrangement of pre-rRNAs and pre-rRNPs. Transitions between different conformations may create the structures necessary for protein binding, pre-rRNA processing, and export from the nucleus to produce functional ribosomes. To understand these rearrangements, we are studying one specific step in assembly, processing of 27SB pre-rRNA to generate 25.5S and 7S pre-rRNAs. The clearest landmark for this processing step is endonucleolytic cleavage at the C_2 site of ITS2 (Internal Transcribed Spacer 2) (Fig. 4). This step is thought to require major conformational rearrangements of pre-rRNAs and pre-rRNPs. For example, structural and mutational analysis supports two possible secondary structures of the ITS2 RNA, the "ring structure" (Joseph et al. 1999), and the "hairpin structure" (Yeh et al. 1990). Processing of 27SB pre-rRNA may be an important control point in ribosome biogenesis; nascent ribosomes are released from the nucleolus into the nucleoplasm once this step is completed (Gadal et al. 2002).

Of the approximately 75 different assembly factors reproducibly found in 66S precursors to 60S ribosomal subunits (Table 1), fourteen assembly factors, hereafter referred to as the "B-factors", have been shown to be necessary for processing of 27SB pre-rRNA (Ripmaster et al. 1992; Hong et al. 1997; Zanchin et al. 1997; de la Cruz et al. 1998; Burger et al. 2000; Tsuno et al. 2000; Basu et al. 2001; Saveanu et al. 2001; Morita et al. 2002; Wehner and Baserga 2002; Kallstrom et al. 2003; Saveanu et al. 2003; Emery et al. 2004; Lebreton et al. 2006a; Saveanu et al. 2007; Zhang et al. 2007; Garcia-Gomez et al. 2011). Yeast strains mutant for each of these B-factors exhibit a diagnostic pre-rRNA processing phenotype-increased amounts of 27SB pre-rRNA relative to $27SA_2$ and $27SA_3$ pre-rRNAs, indicating a failure to cleave the C_2 site within ITS2 (Fig. 4). The B-factors fall into several functional categories: RNA binding proteins Tif6, Nip7, Rpf2, Rlp24, and Nsa2, GTPases Nog1 and Nog2, DEAD box proteins (DBPs)/ATPases Spb4, Dbp10, Drs1, and Has1, and the scaffolding protein Mak11. Nop2 is thought to function as an RNA methyltransferase and Rrs1 has no predicted function. Because Drs1 and Has1 appear to also function during earlier steps of pre-rRNA processing, (Ripmaster et al. 1992; Emery et al. 2004) we have not included them in this study. This work focuses on the order by which these B-factors are recruited into nascent ribosomes, by systematically examining their interdependence for assembly into pre-rRNPs. Defining the recruiting pathway for the proteins involved in this step in assembly will enable identification of cofactors that function with each B-factor and the substrates on which they act. These are important steps to more precisely determine the roles of these proteins in ribosome assembly.

Fromont-Racine and colleagues showed that Mak11, Rlp24, Nog1, and Nsa2 form a network of genetic and physical interactions to generate a recruiting pathway ending with

Nog2 (Saveanu et al. 2001; Saveanu et al. 2003; Lebreton et al. 2006a; Saveanu et al. 2007; Lebreton et al. 2008). They showed that Nsa2 and Nog2 associate with pre-ribosomes only after 27SB pre-rRNA is generated and that Nsa2 is required to recruit Nog2. Here we show that all B-factor proteins are required to recruit Nog2. Interestingly, we found that only a subset of the B-factors are required to recruit Nsa2, and that Nsa2 alone is not sufficient to recruit Nog2.

We further define the order in which the B-factors bind to pre-ribosomes, by assaying their association in yeast strains depleted of each protein. We show that a newly defined subcomplex containing Nop2 and Nip7 is necessary for the stable incorporation of the previously characterized Rpf2 subcomplex containing the assembly factors Rpf2 and Rrs1 and the ribosomal proteins (r-proteins) L5 and L11 (Zhang et al. 2007). The Rpf2 subcomplex is required for association of the DBP Spb4, which is necessary, but not sufficient to load the GTPase Nog2 into nascent ribosomes. Furthermore, we found the Nop2/Nip7 subcomplex is necessary for stable association of Rlp24, Nog1, and Tif6 with pre-ribosomes. Dbp10 also seems to be important for the recruitment of Rlp24; it is involved in association of Rlp24 with pre-ribosomes, but is not necessary for recruiting Rpf2, Tif6, or the Nop2/Nip7 subcomplex. Taken together, our data lead to a recruitment model in which the B-factors assemble into nascent ribosomes in a hierarchical manner via two largely independent linear recruiting pathways that converge on Nog2. Lastly, we also identified a means by which this step in ribosome biogenesis is regulated in concert with cell growth via the TOR protein kinase pathway.

RESULTS

Pre-ribosomes are largely intact in the absence of B-factors.

To determine the interdependence of B-factors for assembly into pre-ribosomes, we assayed association of these proteins with pre-rRNPs in the absence of each B-factor. Because this is a first attempt to understand the order in which all B-factors assemble and there are few if any missense alleles for each of the genes encoding these proteins, we chose to assay interdependence in conditional null strains. To do so, we replaced the promoter of each B-factor gene with the *GAL1* promoter. In galactose, the *GAL1* promoter is active, but in the presence of glucose, *GAL1* is repressed. We used TAP-tagged assembly factor Nop7 to affinity-purify pre-ribosomes from these strains containing or lacking each B-factor. Nop7 is present in 90S particles as well as each of the 66S pre-RNPs, but does not depend on B-factors for association with pre-ribosomes (data not shown), and is not known to be required for processing of 27SB pre-rRNA (Harnpicharnchai et al. 2001). In addition, the population of pre-rRNAs with which Nop7 is associated does not change significantly in the absence of the B-factors. Thus, any changes that we observe in any B-factor mutant most likely would not result from Nop7 failing to associate with pre-ribosomes or being associated with a different population of assembly intermediates.

Pre-ribosome were purified upon depletion of each of nine B-factors and pre-ribosomal proteins were resolved by SDS-PAGE (Fig. 42). Typically we observed changes in the levels of 4-8 assembly factors associated with pre-ribosomes in each of the B-factor mutants. Many of these changes were the same in each mutant, but there were observable differences. The fact that we see only a small number of changes in each mutant suggests that pre-ribosomes are largely intact. In contrast, depletion of proteins that block the

preceding step in ribosome assembly, processing of $27SA_3$ pre-rRNA, causes a greater number of changes in pre-ribosome composition (Fig. 42, A_3 factor control). The proteins required for this earlier step are interdependent for their association with pre-ribosomes, and in their absence pre-ribosomes are unstable and turned over (Sahasranaman et al. 2011). Thus, the phenotype that we observe in B-factor mutants is specific to blocking this step of assembly, and is different from that seen when previous steps are blocked.

FIGURE 42

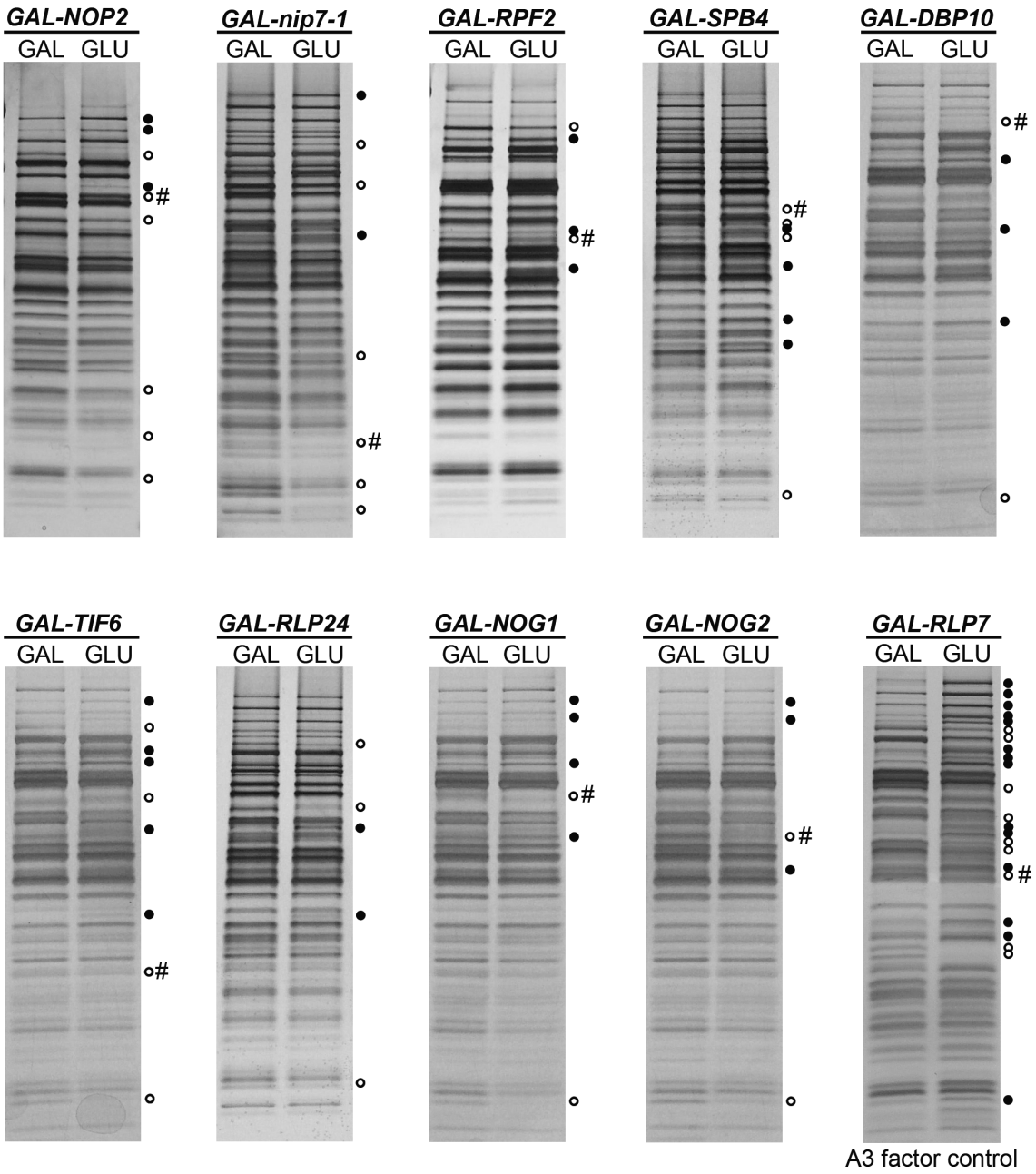

GAL-NOP2
GAL GLU
GAL-nip7-1
GAL GLU
GAL-RPF2
GAL GLU
GAL-SPB4
GAL GLU
GAL-DBP10
GAL GLU
GAL-TIF6
GAL GLU
GAL-RLP24
GAL GLU
GAL-NOG1
GAL GLU
GAL-NOG2
GAL GLU
GAL-RLP7
GAL GLU
A3 factor control

Figure 42: Depletion of B-factors causes few changes in the SDS-PAGE profile of proteins contained in pre-ribosomes.

Nine of the twelve B-factors necessary for processing of 27SB pre-rRNA were individually depleted using the conditional *GAL* promoter. TAP-tagged ribosome assembly factor Nop7 was used to purify 90S and 66S pre-ribosomes from yeast grown in YEPGal (left lane in each pair), and from strains grown in YEPGal and shifted to YEPGlu for 16h to deplete each B-factor (right lane in each pair). Proteins present in purified pre-ribosomes were separated by SDS-PAGE and stained with silver. TAP-tagged Rpf2 was used to purify pre-ribosomes from the *GAL-RLP7* strain in which Rlp7 was depleted. Rlp7 is required for processing of $27SA_3$ pre-rRNA. Thus, this strain serves as a control to demonstrate specificity of the gel profiles for B- factor-depleted strains. Silver-stained bands that increased in the absence of each assembly factor are indicated with solid circles. Bands that decreased are indicated with hollow circles. When able to be identified, the protein under control of the *GAL* promoter is indicated with #.

Nog2 is the last B-factor to associate with pre-ribosomes and is dependent on the other B-factors.

Previously two sets of interacting assembly factors, the Rpf2 subcomplex, as well as Rlp24, Mak11, and Nog1, were shown to be required to recruit Nog2 to pre-ribosomes (Saveanu et al. 2003; Saveanu et al. 2007; Zhang et al. 2007). These proteins assemble into early pre-ribosomal particles containing 35S or $27SA_2$ pre-rRNAs. However, these proteins do not appear to be required for subunit maturation until much later, for processing of 27SB pre-rRNA within 66S pre-rRNPs. In contrast, Nog2 assembles into pre-ribosomes just before 27SB pre-rRNA is cleaved at the C_2 site (Saveanu et al. 2001). Thus, the B-factors may serve as a recruiting scaffold or help create pre-rRNP structures in early precursor particles, to enable proper loading of Nog2 and other B-factors.

To test the requirement of the other B-factors for the recruitment of Nog2 into pre-ribosomes, we assayed levels of Nog2 in pre-ribosomes purified from strains in which each B-factor was depleted. Consistent with previous results, we saw that the levels of Nog2, associated with pre-ribosomes, were severely decreased, and in some cases undetectable, in the absence of Rpf2, Rlp24, and Nog1 (Fig. 43A). In addition, we saw that Nog2 levels were strongly diminished in pre-ribosomes in the absence of Nop2, Nip7, Spb4, Tif6, or Dbp10. This was not simply a result of protein turnover, as Nog2 was stable in whole-cell extracts upon depletion of other B-factors (Fig. 44A). Thus, all of the known B-factors are required to recruit, and/or maintain stable association of Nog2 with pre-ribosomes.

Because Nog2 assembles into pre-ribosomes after 27SB pre-rRNA is generated, whereas the other B-factors assemble earlier (excluding Nsa2), we reasoned that Nog2 would not be required to recruit these proteins. Semiquantitative assays of pre-ribosomes

in Nog2-depleted yeast using SILAC mass spectrometry suggested that few changes occur in its absence (Lebreton et al. 2008). To test this idea in more detail, we assayed by western blotting for the presence of eight other B-factor proteins in pre-ribosomes when Nog2 was depleted (Fig. 43B). We observed no changes in the level of these proteins in pre-ribosomes, consistent with Nog2 associating with pre-ribosomes after the other B-factors.

FIGURE 43

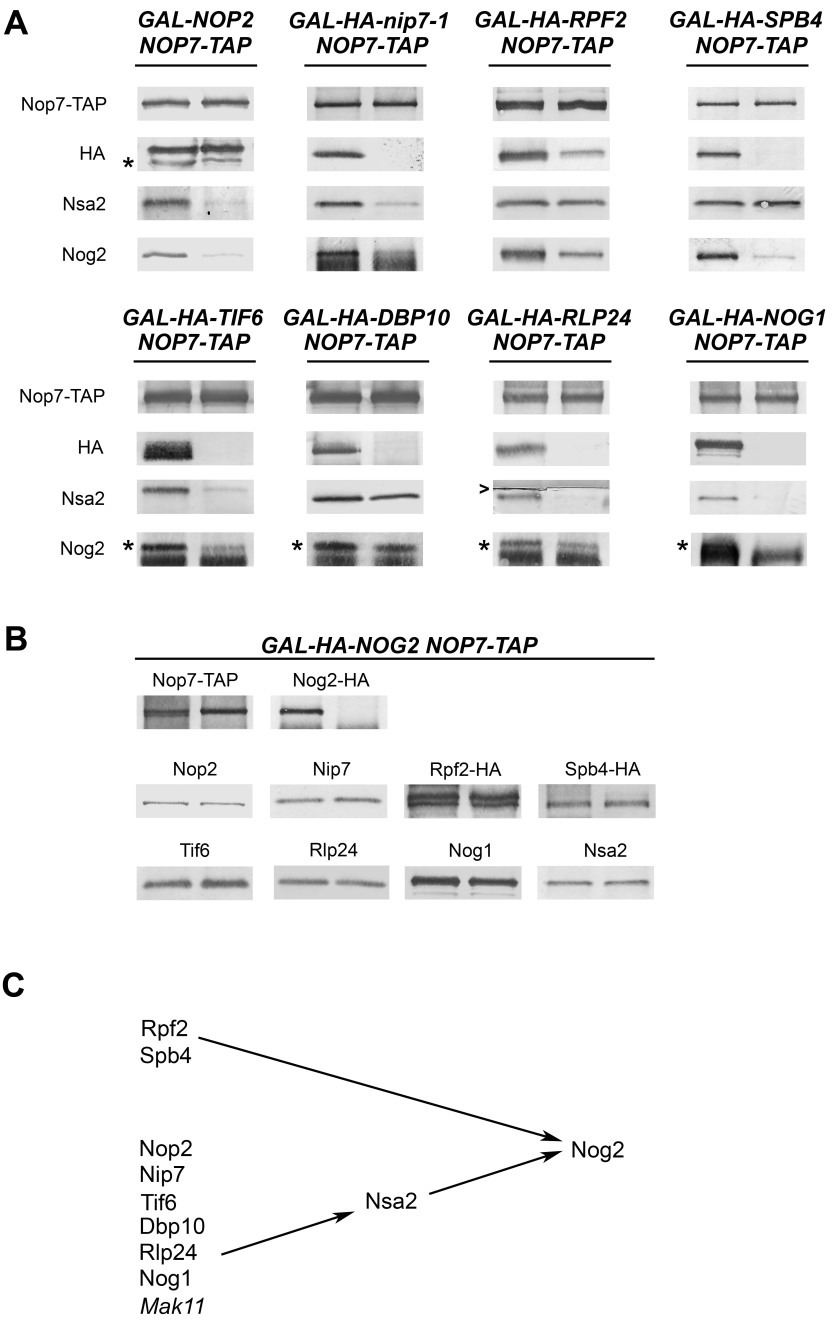

A
GAL-NOP2 NOP7-TAP
GAL-HA-nip7-1 NOP7-TAP
GAL-HA-RPF2 NOP7-TAP
GAL-HA-SPB4 NOP7-TAP
Nop7-TAP
HA
Nsa2
Nog2
GAL-HA-TIF6 NOP7-TAP
GAL-HA-DBP10 NOP7-TAP
GAL-HA-RLP24 NOP7-TAP
GAL-HA-NOG1 NOP7-TAP
B
GAL-HA-NOG2 NOP7-TAP
Nop7-TAP
Nog2-HA
Nop2
Nip7
Rpf2-HA
Spb4-HA
Tif6
Rlp24
Nog1
Nsa2
C
Rpf2
Spb4
Nop2
Nip7
Tif6
Dbp10
Rlp24
Nog1
Mak11
Nsa2
Nog2

Figure 43: All of the B-factors are necessary to recruit Nog2 to pre-ribosomes; only a subset of B-factors are required to recruit Nsa2 into pre-ribosomes.

(A) Changes in the levels of pre-ribosome-associated Nsa2 and Nog2 in the absence of each of the B-factors. Pre-ribosomes were purified from cells grown in YEPGal, or shifted to YEPGlu to deplete each B-factor. Proteins from pre-rRNPs were resolved by SDS-PAGE, and assayed by western blotting. In each pair of samples shown in this figure and in Figures 45, 47, 48, and 49, protein from the undepleted strain is on the left and protein from the depleted strain is on the right. In this blot and all subsequent blots, where two bands are detected, the *bona fide* protein is indicated with an asterisk. Nop7-TAP serves as the loading control. (B) Nog2 is not required to recruit any of the B-factors. Proteins in pre-ribosomes purified from *GAL-NOG2* yeast grown in YEPGal, or shifted to YEPGlu to deplete Nog2 were assayed by western blotting. Nop7-TAP serves as a loading control. Each pair of samples is shown as described in Figure 43A. (C) All of the B-factors are required to recruit Nog2 to pre-ribosomes. A subset of B-factors is required to recruit Nsa2 and Nog2.

FIGURE 44

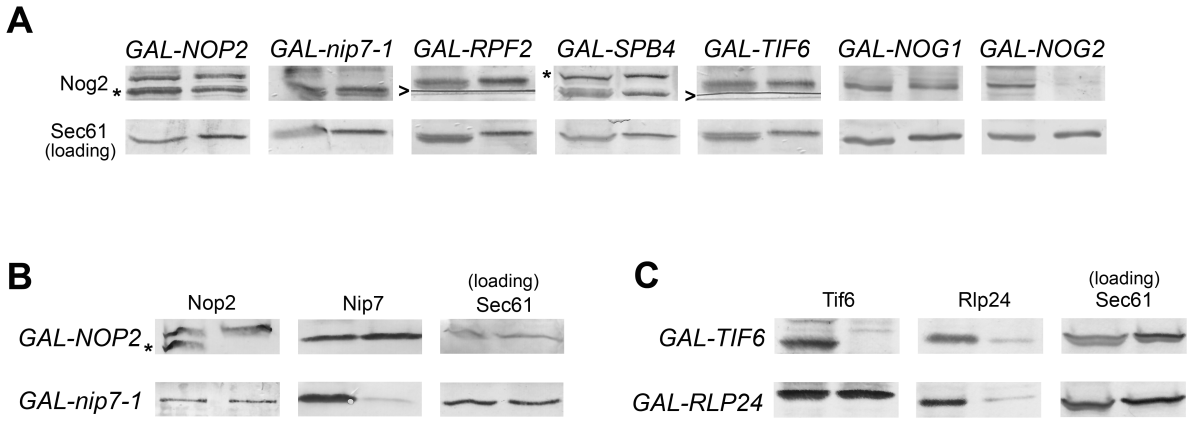

A
GAL-NOP2
GAL-nip7-1
GAL-RPF2
GAL-SPB4
GAL-TIF6
GAL-NOG1
GAL-NOG2
Nog2
Sec61
(loading)
B
Nop2
Nip7
(loading)
Sec61
GAL-NOP2
GAL-nip7-1
C
Tif6
Rlp24
(loading)
Sec61
GAL-TIF6
GAL-RLP24

Figure 44: Stability of the B-factors in the absence of others.

(A) Nog2 is stable in the absence of the B-factors. Whole cell extracts from cells depleted of each of the B factors were assayed by SDS-PAGE and western blotting for amount of Nog2. Sec61 serves as a loading control. (B) Nop2 and Nip7 are stable in the absence of each other. Whole cell extracts from Nop2 or Nip7-depleted yeast were assayed by SDS-PAGE and western blotting for amounts of Nop2 and Nip7. Sec61 serves as a loading control. (C) Upon depletion of Tif6, Rlp24 is unstable, but not vice versa. Levels of Rlp24 and Tif6 present in whole cell extracts of strains in which Rlp24 or Tif6 were depleted were examined by western blotting. Sec61 serves as a loading control.

Nsa2 is recruited to pre-ribosomes by a subset of B-factors.

Like Nog2, Nsa2 assembles into pre-ribosomes only after 27SB pre-rRNA is generated (Lebreton et al. 2006a). Nsa2 depends on the B-factors Rlp24, Mak11, and Nog1, and its recruitment is a prerequisite for association of Nog2 (Lebreton et al. 2006a; Saveanu et al. 2007). We therefore tested the association of Nsa2 with pre-ribosomes in the absence of the eight remaining B-factors (Fig. 43A). Western blotting showed that Nsa2 fails to associate with pre-ribosomes in the absence of Nop2, Nip7, Tif6, Dbp10, Rlp24, and Nog1. However, Nsa2 did not depend on the Rpf2 subcomplex or the DBP Sbp4. Thus, there are B-factor mutants in which both Nsa2 and Nog2 fail to associate with pre-ribosomes as well as mutants in which only Nog2 fails to associate. These results show that Nsa2 alone is not sufficient to recruit Nog2 to pre-ribosomes and that recruitment of Nog2 requires the concerted assembly of additional proteins. Since Nog2 is the last B-factor recruited to pre-ribosomes, it may use GTP hydrolysis as a signal or trigger for cleavage of 27SB pre-rRNA at the C2 site. Thus its recruitment may be highly regulated by the cooperation of a number of assembly factors to ensure that cleavage of the C2 site does not occur prematurely. Thus, our results, with those of the Fromont-Racine group, describe a recruiting pathway among the B-factor proteins that culminates with the association of the GTPase Nog2 (Fig. 43C).

The Rpf2 subcomplex is required to recruit Spb4 into pre-ribosomes and Spb4 is required for subsequent recruitment of Nog2.

We next tested the interdependence of the B-factors that associate with pre-ribosomes before Nsa2 and Nog2. To do so, we assayed their association with pre-ribosomes when each of the other B-factors was depleted. We began by investigating the requirement of the

Rpf2 subcomplex for association of other B-factors. Previous work showed that Rpf2, Rrs1, L5, and L11 are mutually interdependent for assembly of the subcomplex and association with the pre-ribosome (Zhang et al. 2007). Thus, depleting Rpf2 is analogous to depleting the entire Rpf2 subcomplex. To test whether the Rpf2 subcomplex is required to load any of the other B-factors into nascent ribosomes, we assayed the amounts of B-factors in purified pre-ribosomes when Rpf2 was depleted. Levels of Nog2 and HA-tagged Spb4 in pre-ribosomes were significantly decreased when Rpf2 was depleted, but amounts of Nog1, Nop2-HA, Nip7, Nsa2, and Tif6-HA remained largely the same (Fig. 43A and 45A). There was a reproducible but very slight decrease of Rlp24. These results, plus our previous experiments with Rpf2 depletions (Fig. 43A) and (Zhang et al. 2007)), suggest that association of Spb4 with pre-ribosomes occurs early during assembly and depends on the Rpf2 subcomplex. Conversely, Spb4 recruits Nog2 much later.

We then tested whether the other B-factors depend on Spb4 to associate with pre-ribosomes. To do so we assayed their association upon depletion of Spb4. Of eight B-factors, only Nog2 was decreased (Fig. 43A and 45B). We did not directly test the association of Dbp10 in the absence of Spb4. Since Nsa2 depends on Dbp10 (Fig 43A and 43C), and Nsa2 does not change in the absence of Spb4, we infer that Dbp10 does not depend on Spb4. We conclude that the Rpf2 subcomplex is necessary for association of Spb4 with pre-ribosomes and that Spb4 recruits Nog2 (Fig. 45C). No other B-factors depend on Rpf2, Spb4, or Nog2 for association with pre-ribosomes.

FIGURE 45

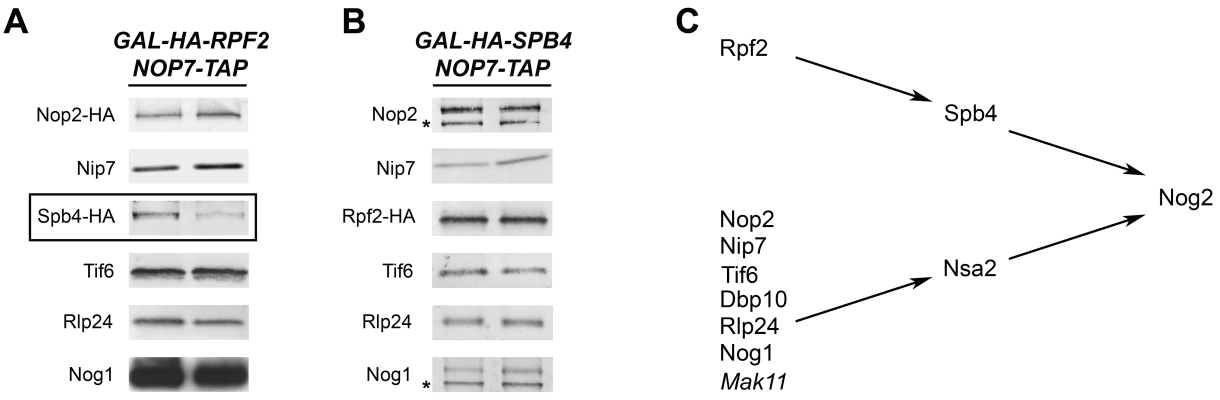

A
GAL-HA-RPF2
NOP7-TAP
Nop2-HA
Nip7
Spb4-HA
Tif6
Rlp24
Nog1
B
GAL-HA-SPB4
NOP7-TAP
Nop2 *
Nip7
Rpf2-HA
Tif6
Rlp24
Nog1 *
C
Rpf2
Spb4
Nog2
Nop2
Nip7
Tif6
Dbp10
Rlp24
Nog1
Mak11
Nsa2

Figure 45: Spb4 depends on Rpf2 to dock with pre-ribosomes.

(A) Rpf2 is necessary to load Spb4 and into nascent ribosomes. Pre-ribosomes were purified from a *GAL-RPF2* strain grown in YEPGal, or shifted to YEPGlu to deplete Rpf2. Pre-ribosomes were purified from whole cell lysates of undepleted and depleted cells using TAP-tagged Nop7. Proteins from pre-rRNPs were resolved by SDS-PAGE, and assayed by western blotting. Each pair of samples is shown as described in Figure 43A. Western blots showing the depletion of Rpf2 from preribosomes, and the Nop7-TAP loading control are shown in Figure 3A. B-factors that decrease in the absence of Rpf2 are boxed. (B) No other B-factors are recruited into pre-ribosomes by Spb4. Proteins in pre-ribosomes purified from *GAL-SPB4* yeast grown in YEPGal or shifted to YEPGlu to deplete Spb4 were assayed by western blotting. Each pair of samples is shown as described in Figure 43A. Western blots showing the depletion of Spb4 from preribosomes, and the Nop7-TAP loading control are shown in Figure 43A. (C) Hierarchy for recruiting Rpf2, Spb4, and Nog2 into pre-ribosomes.

Nop2 and Nip7 form a subcomplex important for recruitment of the other B-factors into pre-ribosomes.

Previously Nop2 and Nip7 were found to be necessary for processing of 27SB pre-rRNA (Hong et al. 1997; Zanchin et al. 1997). Both proteins cosedimented with 66S pre-ribosomes when whole cell extracts were fractionated by sucrose gradient centrifugation (Fig. 46), and both are commonly found in affinity-purified 66S pre-ribosomes (Table 1). To investigate Nop2 and Nip7 in more detail, we TAP-tagged each of them and assayed which pre-ribosomal proteins copurified with them.

When affinity purification was carried out with whole cell extracts from a Nip7-TAP strain, large amounts of Nop2 copurified with Nip7-TAP, and much smaller amounts of other pre-ribosomal proteins were present (Fig. 47, lane 3). This may be caused by the C-terminal TAP-tag interfering with the C-terminal PUA RNA binding domain of Nip7, weakening its association with pre-ribosomes, but not with Nop2. Consistent with this potentially deleterious effect of the TAP-tag on Nip7, we observed that the *NIP7-TAP* strain grew more slowly than wild-type, untagged *NIP7* strains (data not shown). In addition, extracts prepared from the *NIP7-TAP* strain contain halfmer polyribosomes (Fig 46B), indicative of a defect in production or function of 60S subunits (Helser et al. 1981; Rotenberg et al. 1988). Affinity purification of Nop2-TAP using whole cell extracts revealed the typical SDS-PAGE profile of proteins present in early and middle 66S pre-rRNPs (Fig 47A, lane1 and Table 1). However, when whole cell extracts from a *NOP2-TAP* strain were subjected to high-speed centrifugation, to pellet ribosomes and pre-ribosomes before affinity purification with Nop2-TAP, primarily Nop2 and Nip7 were recovered (Fig. 47A,

lane 2). Taken together, these results demonstrate that Nop2 and Nip7 are tightly associated and form a heteromeric subcomplex.

Another indication that Nop2 and Nip7 form a subcomplex is the observation that both proteins were detected in fractions 3-5 near the top of gradients (as well as in fractions containing 66S pre-ribosomes), when wild-type whole cell extracts were subjected to centrifugation (Fig. 46A). Furthermore, much greater amounts of both Nop2 and Nip7-TAP sedimented near the top of gradients when *NIP7-TAP* extracts were subjected to centrifugation (Fig. 46B).

Since Nip7 and Nop2 form a subcomplex, we assayed whether they depend on each other to assemble into pre-ribosomes, as well as whether any other B-factors depend on either of them. Indeed, Nop2 was not present in pre-ribosomes purified from strains in which Nip7 was depleted (Fig. 47B). Likewise, pre-ribosomes from Nop2-depleted cells contained diminished amounts of Nip7 (Fig. 47C). In both Nop2 and Nip7-depleted strains, decreased amounts of Rpf2, Tif6, Rlp24, Nog1, Nsa2, and Nog2 were associated with pre-ribosomes (Fig. 43A, 47B, and 47C). Spb4, Mak11, Rrs1, and Dbp10 were not tested. We assume that when Rpf2 is absent, both Rrs1 and Spb4 are also unable to assemble into pre-rRNPs (Fig. 45A and (Zhang et al. 2007)). The inability of Nop2 or Nip7 to assemble with pre-rRNPs in the absence of the other was not simply a result of protein turnover when the Nip7/Nop2 subcomplex could not form. Each protein was present in whole cell extracts at wild-type levels when the other protein was depleted (Fig. 44B). We conclude that Nop2 and Nip7 form a subcomplex and that both are important for association of at least six other B-factors, as well as each other, with nascent ribosomes (Fig. 47D).

FIGURE 46

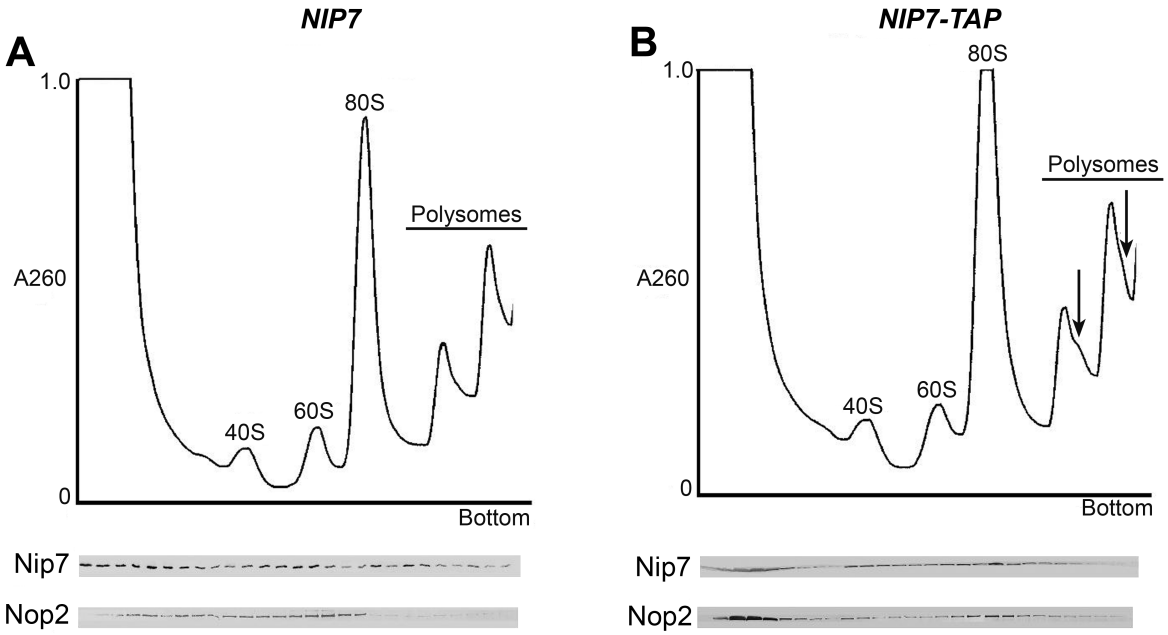

A
NIP7
1.0
A260
0
40S
60S
80S
Polysomes
Bottom
Nip7
Nop2
B
NIP7-TAP
1.0
A260
0
40S
60S
80S
Polysomes
Bottom
Nip7
Nop2

Figure 46: Nop2 and Nip7 co-sediment with preribosomes, but also with each other when the function of Nip7 is compromised by TAP-tagging.

(A) Nop2 and Nip7 co sediment with 66S preribosomes. Whole cell extracts were prepared from the wildtype *NIP7* strain grown in YEPD medium at 30 °C to mid-log phase, and were subjected to centrifugation on 7%-47% sucrose gradients. Fractions were collected and assayed by SDS-PAGE and western blotting for Nop2 and Nip7. A peak of Nop2 and Nip7 is evident in fractions 14-16 where 66S preribosomes sediment, and a second peak is seen near the top of the gradient in fractions 4-6. (B) Large amounts of Nop2 and Nip7 sediment in fractions near the top of a gradient using extracts from a *NIP7-TAP* strain than with wildtype *NIP7* extracts. Whole cell extracts from the *NIP7-TAP* yeast were subjected to centrifugation on 7%-47% sucrose gradients. Fractions were collected and assayed for Nop2 and Nip7 by western blotting. Significantly more Nop2 sediments in fractions 3-5, and less in fractions 14-16, in the *NIP7-TAP* extract compared to the wildtype *NIP7* extract. Additionally, the presence of the TAP-tag causes accumulation of halfmer polyribosomes indicated by arrows.

FIGURE 47

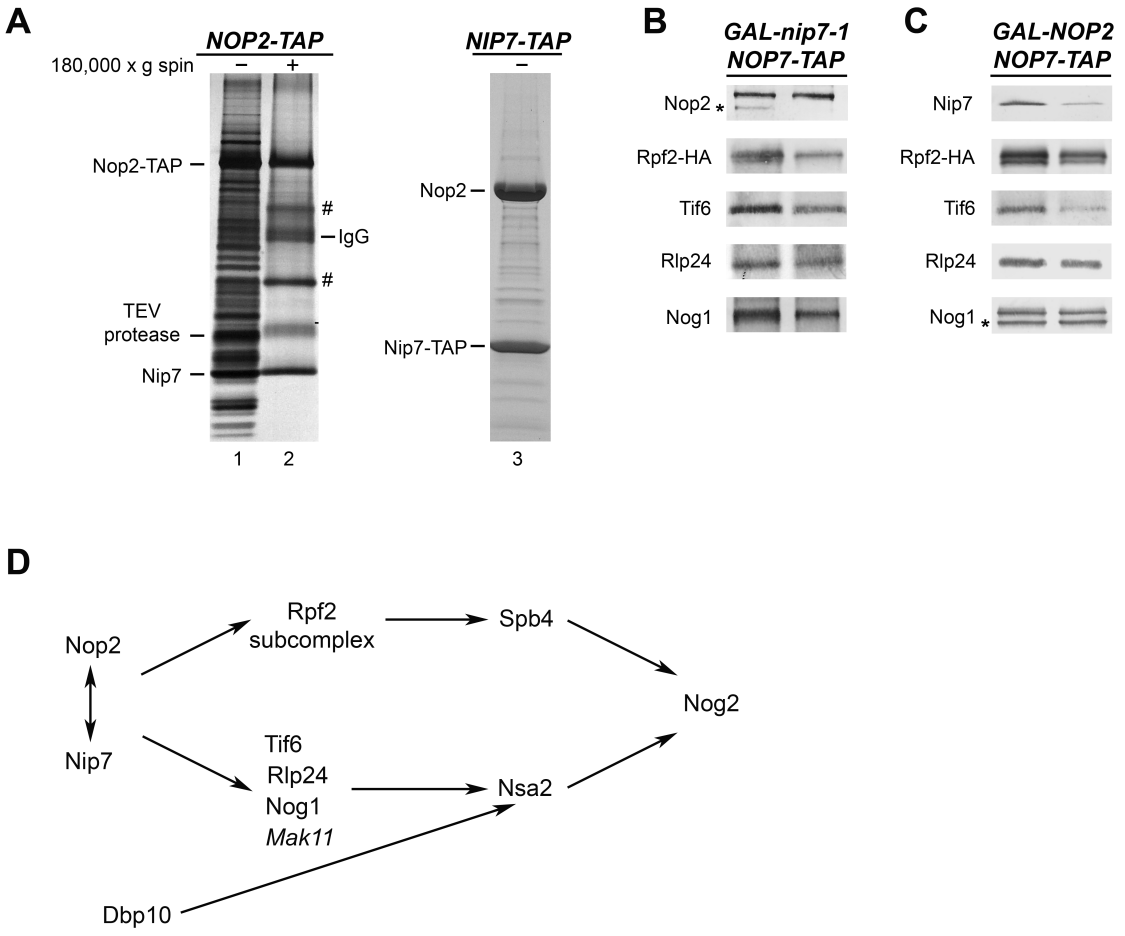

A
NOP2-TAP
NIP7-TAP
180,000 x g spin
–
+
–
Nop2-TAP
#
IgG
#
TEV
protease
Nip7
Nop2
Nip7-TAP
1
2
3
B
GAL-nip7-1
NOP7-TAP
Nop2 *
Rpf2-HA
Tif6
Rlp24
Nog1
C
GAL-NOP2
NOP7-TAP
Nip7
Rpf2-HA
Tif6
Rlp24
Nog1 *
D
Nop2
Nip7
Rpf2
subcomplex
Spb4
Nog2
Tif6
Rlp24
Nog1
Mak11
Nsa2
Dbp10

Figure 47: Nop2 and Nip7 form a subcomplex, are interdependent for assembly into pre-ribosomes, and function in recruiting of other B-factors.

(A) Nop2 and Nip7 form a heteromer *in vivo*. Yeast strains expressing TAP-tagged Nop2 or Nip7 were grown in YEPGlu medium to $3x10^7$ cells/ml. Whole cell extracts from the *NOP2-TAP* strain (lane 1) or the supernatants after high-speed centrifugation (lane 2) were subjected to affinity purification using Nop2-TAP, to purify Nop2-containing pre-ribosomes or subcomplexes, respectively. Purified proteins were identified by mass spectrometry. Proteins labeled with "#" are common contaminants in purified samples. Whole cell extract from the *NIP7-TAP* strain was subjected to affinity purification using Nip7-TAP (lane 3). Nop2 and Nip7 in these purified samples were identified by mass spectrometry. (B and C) Nop2 and Nip7 are interdependent for their assembly into pre-rRNPs, and important for incorporation of other B-factors into pre-ribosomes. *GAL-nip7-1* or *GAL-NOP2* yeast were grown in YEPGal or shifted to YEPGlu. Whole cell extracts were subjected to affinity purification, using Nop7-TAP to isolate pre-ribosomes. Amounts of B-factors present in the purified pre-ribosomes were analyzed by western blotting. Each pair of samples is shown as described in Figure 43A. Western blots showing the depletion of Nop2 or Nip7 from preribosomes, and the Nop7-TAP loading control are shown in Figure 43A. (D) Nop2 and Nip7 are important for the stable association of all of the B-factors.

Nog1, Rlp24, and Tif6 are interdependent for recruitment into pre-ribosomes.

Fromont-Racine and colleagues (Saveanu et al. 2001; Saveanu et al. 2003; Lebreton et al. 2006a; Saveanu et al. 2007; Lebreton et al. 2008) defined a hierarchy of recruitment among Mak11, Rlp24, Nog1, Nsa2, and Nog2 (boldface in Fig. 48C). To first investigate the relationship of Rlp24 and Nog1 with other B-factors for entry into nascent ribosomes, we surveyed the effects of depleting either of these two proteins on ribosome assembly. As previously observed by Saveanu *et al.* (2003), we found that amounts of Nsa2 and Nog2 in pre-ribosomes were diminished when expression of either *RLP24* or *NOG1* was turned off (Fig. 43A). Saveanu and colleagues had also found that Nog1 was absent from pre-rRNPs when Rlp24 was depleted, but that Rlp24 did not depend upon Nog1 for stable association with pre-ribosomes. However, when we depleted Nog1, we saw a decrease in levels of Rlp24 associated with purified pre-ribosomes (Fig. 48B). We also found that pre-ribosome-associated Tif6 decreased when either Nog1 or Rlp24 were depleted, but Rpf2, Nop2, and Nip7 were not affected (Fig. 48A and 48B). It is likely that the effect on Tif6 that we observe upon depleting Nog1 or Rlp24 is mediated through these two proteins rather than via downstream factors Nsa2 or Nog2, since we found that Nog2 is not necessary for docking of Tif6 with pre-rRNPs (Fig. 43B), and Lebreton and colleagues showed that Tif6 is not affected by depletion of Nsa2 (Lebreton et al. 2006a). This is also consistent with the observations that Nsa2 and Nog2 associate with pre-rRNPs several steps after Tif6 (Saveanu et al. 2001; Lebreton et al. 2006a). Together, our results and those of Fromont-Racine and colleagues demonstrate a network of physical and functional interactions among Tif6, Nog1 and Rlp24. These three proteins exhibit interdependence for association with pre-ribosomes and are required for later recruitment of Nsa2 and Nog2 (Fig. 48C).

FIGURE 48

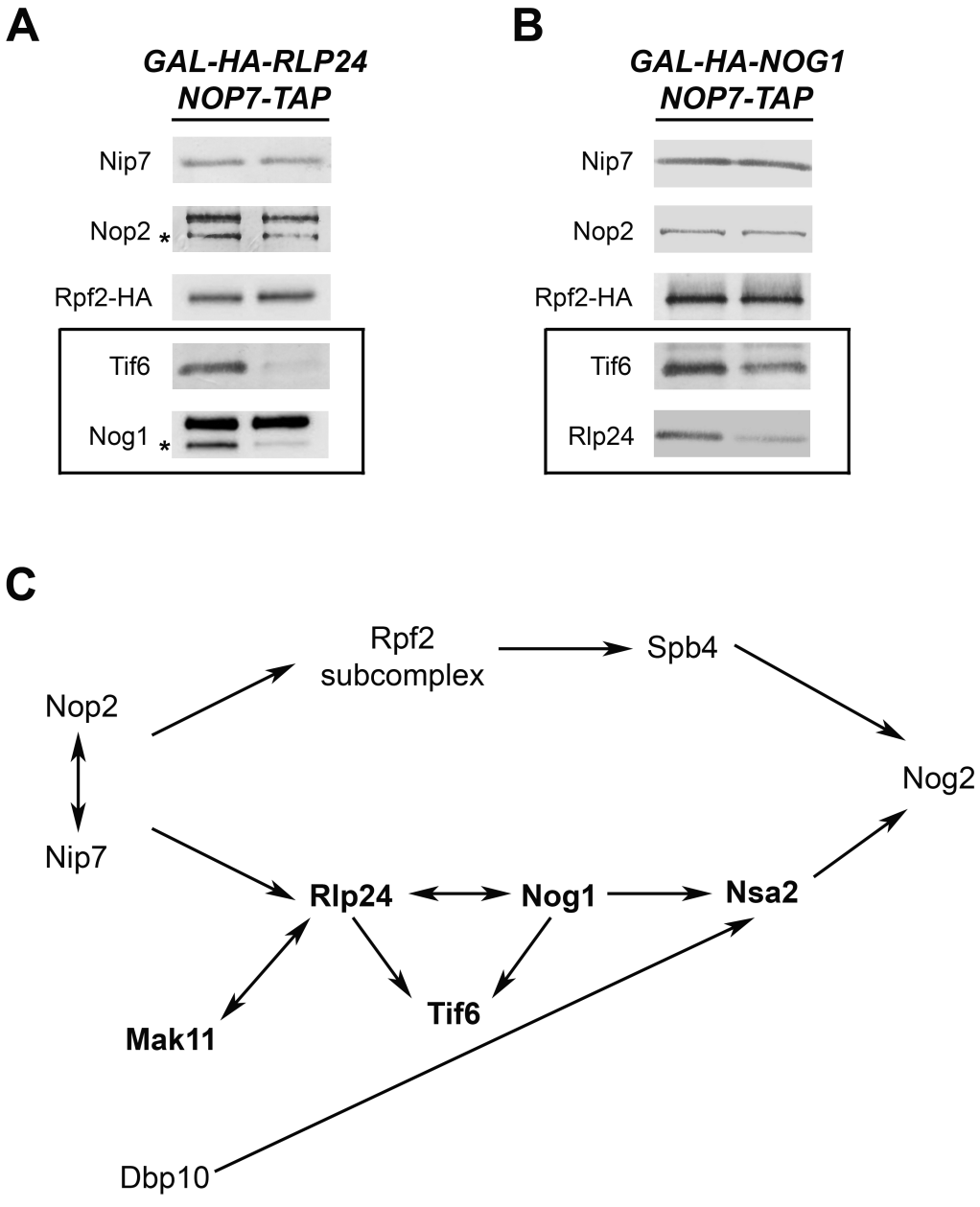

A
GAL-HA-RLP24
NOP7-TAP
Nip7
Nop2 *
Rpf2-HA
Tif6
Nog1 *
B
GAL-HA-NOG1
NOP7-TAP
Nip7
Nop2
Rpf2-HA
Tif6
Rlp24
C
Rpf2
subcomplex
Spb4
Nop2
Nog2
Nip7
Rlp24
Nog1
Nsa2
Tif6
Mak11
Dbp10

Figure 48: Nog1 and Rlp24 are important for association with pre-ribosomes of Tif6, as well as each other.

(A and B) Changes in amounts of pre-ribosomal proteins when either Rlp24 or Nog1 is depleted. *GAL-RLP24* or *GAL-NOG1* yeast were grown in YEPGal or shifted to YEPGlu for 16h to deplete either assembly factor. Pre-ribosomes were purified from whole cell lysates of undepleted and depleted cells using TAP-tagged Nop7. Western blotting was used to assay amounts of pre-ribosomal proteins. Each pair of samples is shown as described in Figure 3A. Western blots showing the depletion of Nog1 or Rlp24 from preribosomes, and the Nop7-TAP loading control are shown in Figure 43A. (C) Interdependence among Rlp24, Nog1, Tif6, Nsa2, and Nog2 for assembly into pre-ribosomes. Proteins in boldface were previously studied by Fromont-Racine and colleagues.

Tif6 and Dbp10 are important for association with pre-rRNPs of Rlp24, Nog1, Nsa2, and Nog2.

Tif6 is associated with pre-ribosomes containing $27SA_2$, 27SB, 25.5S and 7S pre-rRNAs and is found in both the nucleus and cytoplasm (Graindorge et al. 2005). Tif6 binds to r-protein L23 on the subunit interface of pre-ribosomes, and therefore prevents premature entry of nascent ribosomes into the translation pathway, by blocking association with 40S subunits (Gartmann et al. 2010). Assembly factors Sdo1 and Efl1 release Tif6 from pre-rRNPs, to enable recycling of Tif6 from the cytoplasm back to the nucleus (Senger et al. 2001; Menne et al. 2007). However, Tif6 also functions earlier in 60S subunit biogenesis. Depletion of Tif6 causes accumulation of 27SB pre-rRNA, by blocking pre-rRNA processing in the nucleolus (Basu et al. 2001). To investigate where Tif6 fits into the hierarchy of B-factor assembly into pre-ribosomes, we assayed the effects of depleting Tif6 on pre-ribosome constituents. We found that Rlp24, Nog1, Nsa2, and Nog2 were diminished, whereas Nop2, Nip7, and the Rpf2 subcomplex were not affected (Fig. 43A and Fig. 49A). Western blotting of whole cell extracts from the Tif6 and Rlp24 depleted strains also revealed that in the absence of Tif6, Rlp24 undergoes turnover, whereas Tif6 remains stable when Rlp24 is depleted (Fig. 44C). Therefore, our results (Fig. 48A, 48B and Fig 49A), together with those of Saveanu *et al.* (2003), show that association of Tif6, Rlp24 and Nog1 are mutually interdependent, but independent of assembly of Rpf2 and Spb4.

Dbp10 is a DEAD-box protein that routinely copurifies with 66S pre-ribosomes (Table 1). Depletion of Dbp10 or growing the cold-sensitive *dbp10-1* mutant at 18 ˚C leads to accumulation of 27SB pre-rRNA (Burger et al. 2000). We investigated the role of Dbp10 in recruiting proteins to nascent ribosomes, by purifying pre-ribosomes from a strain in

which Dbp10 was depleted. Western blotting revealed that levels of Rlp24, Nog1, Nsa2, and Nog2 were decreased, whereas Tif6, Nop2, Nip7, and r-protein L5 (representative of the Rpf2 subcomplex) were unaffected (Fig. 43A and Fig. 49B). The effects observed upon depletion of Dbp10 were relatively mild. This may reflect the transient nature of DBPs. While DBPs undoubtedly play a major role in ribosome assembly, they may not always be intimately associated with pre-ribosomes.

Taken together, our studies of the recruiting pathway of ten different assembly factors required for processing of 27SB pre-rRNA are summarized in the diagram in Figure 49C. Our data establish that many of the B-factors are recruited into early assembly intermediates in two independent pathways. These two pathways ultimately converge later in assembly to recruit the last factor, the GTPase Nog2.

FIGURE 49

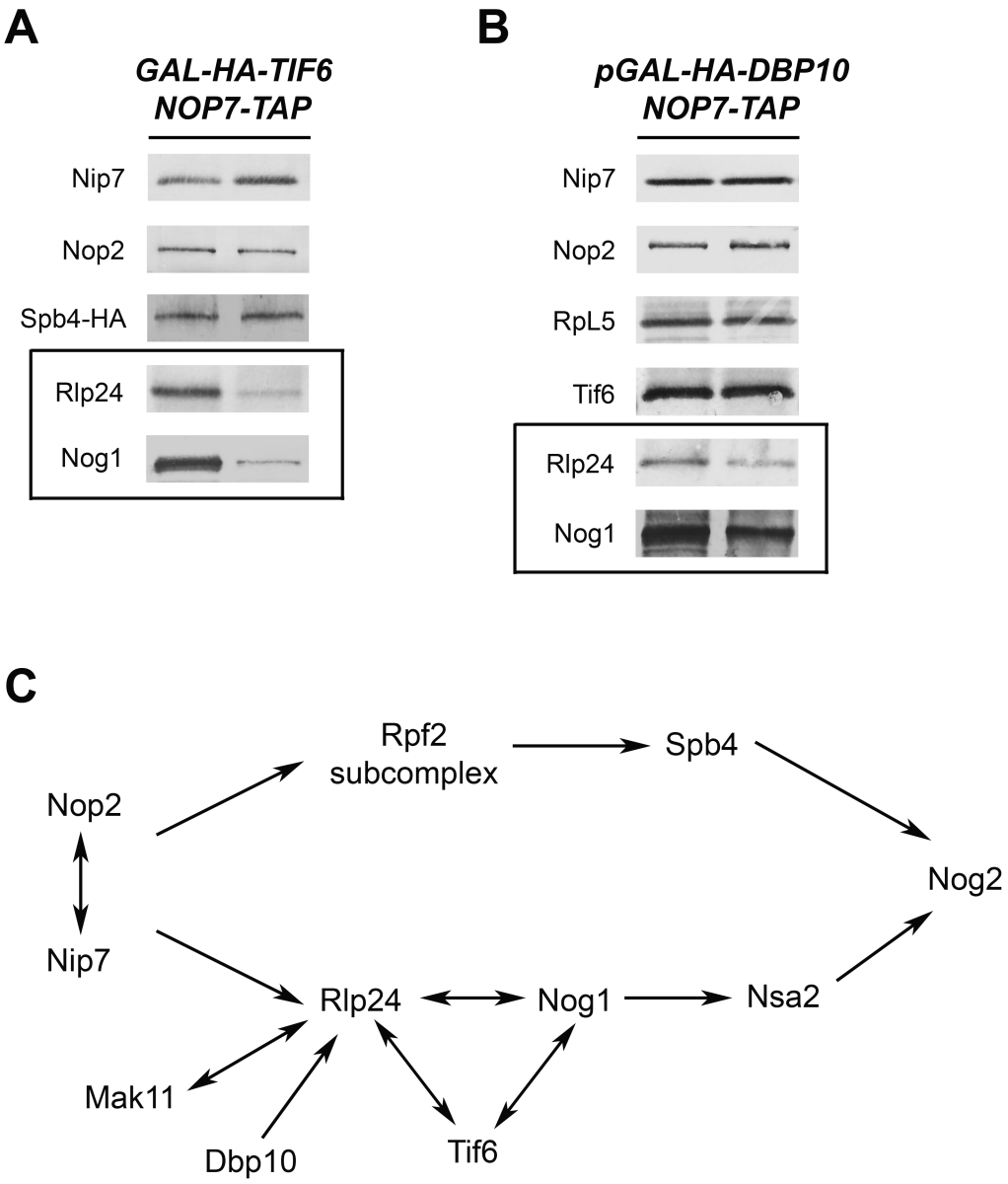

A
GAL-HA-TIF6
NOP7-TAP
Nip7
Nop2
Spb4-HA
Rlp24
Nog1
B
pGAL-HA-DBP10
NOP7-TAP
Nip7
Nop2
RpL5
Tif6
Rlp24
Nog1
C
Nop2
Nip7
Rpf2
subcomplex
Spb4
Nog2
Rlp24
Nog1
Nsa2
Mak11
Dbp10
Tif6

Figure 49: Both Tif6 and Dbp10 are required for assembly of Rlp24 and Nog1 into pre-ribosomes.

(A) Tif6 is required to recruit Rlp24 and Nog1 pre-rRNPs. Proteins present in pre-rRNPs purified from a *GAL-TIF6* strain grown in YEPGal or shifted to YEPGlu for 16h were resolved by SDS-PAGE and subjected to western blot analysis. Each pair of samples is shown as described in Figures 43A. Western blots showing the depletion of Tif6 from preribosomes, and the Nop7-TAP loading control are shown in Figure 43A. (B) Dbp10 is important for association of Rlp24 and Nog1 with pre-rRNPs. The *GAL-DBP10* strain was grown in YEPGal or shifted to YEPGlu for 16h to deplete Dbp10. Pre-ribosomes were purified from extracts prepared from each strain and proteins were resolved by SDS-PAGE. Pre-ribosomal proteins were assayed by western blotting. Each pair of samples is shown as described in Figure 43A. Western blots showing the depletion of Dbp10 from preribosomes, and the Nop7-TAP loading control are shown in Figure 43A. (C) Position in the association hierarchy for Tif6 and Dbp10.

The TOR protein kinase pathway regulates biogenesis of 60S ribosomal subunits via targeting the B-factors Rpf2, Spb4, Nog1, and Nog2.

The number of ribosomes in a cell, as well as their function, are adjusted in response to cellular growth rates, mediated in part by the protein kinase TOR (target of rapamycin) (Schmelzle and Hall 2000; Crespo and Hall 2002). TOR inactivation upon treatment of cells with rapamycin results in decreased transcription of rRNAs and nucleolar entrapment of pre-rRNPs, possibly via targeting Nog1, one of the B-factors (Honma et al. 2006; Vanrobays et al. 2008; Huber et al. 2009). To test whether other B-factors serve as targets of TOR kinase, we examined their levels in pre-ribosomes from cells treated with rapamycin. After treatment with rapamycin, pre-ribosomes remained largely intact, but levels of Rpf2, Spb4, Nog1, and Nog2 associated with pre-rRNPs decreased, while amounts of other B-factors remained the same (Fig. 50). As controls, we assayed levels of assembly factors and ribosomal proteins that do not function in 27SB pre-rRNA processing. These proteins remained stably associated with pre-ribosomal particles after treatment with rapamycin (Fig. 50). When amounts of B-factors in whole cell extracts were tested, we found that levels of Rpf2, Spb4, Nog2, and Nog1 decreased (Fig. 51). These data suggest that the TOR kinase pathway may regulate ribosome biogenesis in response to cellular growth rate via targeting a subset of B-factors. Failure to recruit or maintain Rpf2, Spb4, Nog2, and Nog1 in pre-rRNPs may block maturation of 60S ribosomal subunits, entrapping them within the nucleolus.

FIGURE 50

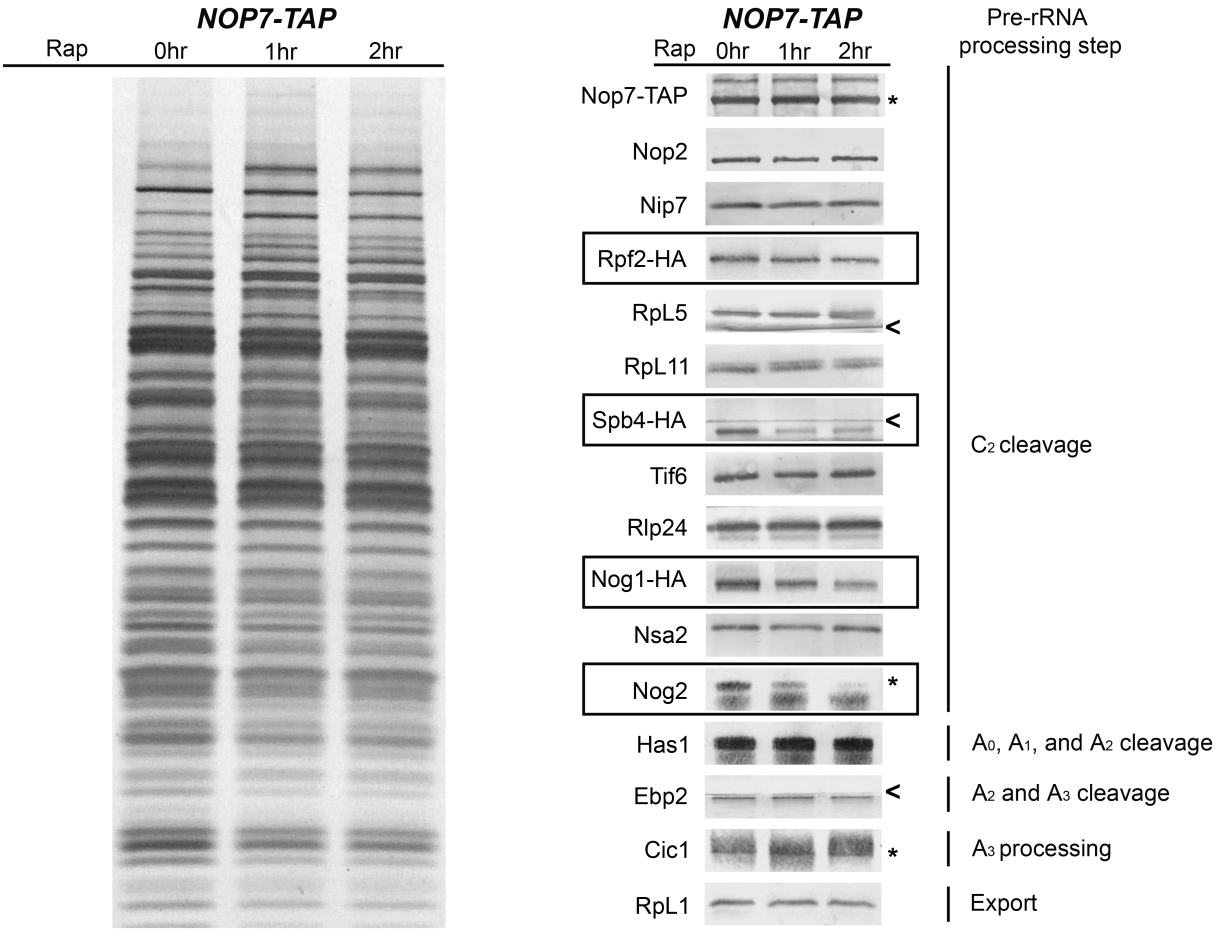

NOP7-TAP
Rap
0hr
1hr
2hr
NOP7-TAP
Rap
0hr
1hr
2hr
Pre-rRNA processing step
Nop7-TAP
Nop2
Nip7
Rpf2-HA
RpL5
RpL11
Spb4-HA
Tif6
Rlp24
Nog1-HA
Nsa2
Nog2
Has1
Ebp2
Cic1
RpL1
C2 cleavage
A0, A1, and A2 cleavage
A2 and A3 cleavage
A3 processing
Export

Figure 50: The TOR protein kinase pathway regulates assembly of 60S ribosomal subunits via targeting the B-factors Rpf2, Spb4, Nog1, and Nog2.

The Nop7-TAP strain was grown at 30°C in YEPGlu medium to $3x10^7$ cells/ml. Two more cultures were grown to $2x10^7$ cells/ml, and 200ng/ml rapamycin was added to each culture. These two cultures were then grown for another 1 or 2.5 hours to $3x10^7$ cells/ml. Whole cell extracts were subjected to single-step purification using TAP-tagged Nop7 to isolate 66S pre-ribosomes. Proteins present in the affinity-purified pre-ribosomes were resolved by SDS-PAGE and stained with silver (lanes 1-3), or subjected to western blot analysis (lanes 4-6). Proteins from untreated cells are in lanes 1 and 4, those from cells treated with rapamycin for 1 h are in lanes 2 and 5, and those from cells treated for 2.5 h are in lanes 3 and 6. Nop7-TAP serves as the loading control. Proteins with decreased association with pre-ribosomes upon treatment with rapamycin are boxed. The pre-rRNA processing step in which each protein tested functions is indicated.

FIGURE 51

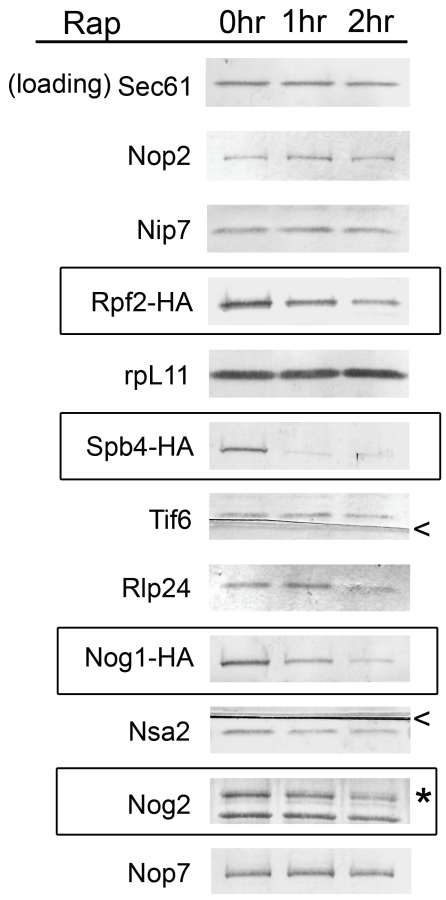

Rap
0hr 1hr 2hr
(loading) Sec61
Nop2
Nip7
Rpf2-HA
rpL11
Spb4-HA
Tif6
<
Rlp24
Nog1-HA
Nsa2
<
Nog2
*
Nop7

Figure 51: The amounts of B-factors Rpf2, Spb4, Nog1, and Nog2 are decreased in whole cell extract upon inactivation of TOR signaling.

The *NOP7-TAP* strain was grown as described in Figure 7. Whole cell extracts from rapamycin untreated or treated cells were assayed by SDS-PAGE and western blotting for amounts of B-factors upon inactivation of TOR signaling. Sec61 serves as a loading control. B-factors that change are boxed.

DISCUSSION

Our working hypothesis is that the numerous assembly factors associate with nascent ribosomes in a hierarchical and cooperative manner, through protein-protein or protein-RNA interactions, to drive forward the formation of consecutive assembly intermediates. Therefore, our approach to begin to uncover the precise roles of these factors is to systematically investigate physical or functional interactions among them.

Stable interactions among some assembly factors and r-proteins are evident by isolating assembly subcomplexes containing them. These subcomplexes might serve as smaller building blocks to minimize the complexity of assembly of these enormous ribonucleoprotein particles containing so many components. Importantly, identifying and characterizing these physical clusters of assembly factors will enable discovery of cofactors and substrates of these factors, thus unraveling their functions, and will also help define the local topology within pre-ribosomal particles.

Rearrangements of local structures within assembling ribosomes may be propagated by allosteric mechanisms to alter the global architecture of pre-rRNPs. Such reorganizations might affect recruitment or activity of assembly factors working in the same step of subunit biogenesis, even though these proteins may not physically interact. Thus, to obtain a comprehensive picture of ribosome assembly, it is necessary to "walk out" of neighborhoods defined by physical subcomplexes within pre-ribosomes, and to investigate interactions among all assembly factors that function together in one specific step of pre-rRNA processing and assembly. Studying molecules in one "functional cluster" will help to understand how these molecules coordinate their precise functions with each other in one assembly step.

We previously discovered that six assembly factors required for processing of $27SA_3$ pre-rRNA assemble early into pre-ribosomes, are mutually interdependent for association with pre-ribosomes, and are important for assembly of ribosomal proteins with domain I and II of 25S/5.8S rRNAs (Sahasranaman et al. 2011). Here we have studied recruitment of the factors required for the next step in pre-rRNA processing, removal of ITS2 from 27SB pre-rRNA. Previous experiments to map the relative timing of association of B-factors with pre-ribosomes demonstrated that seven of these proteins assembled rather early, with 90S pre-ribosomes or 66S particles containing $27SA_2$ pre-rRNA (Saveanu et al. 2003; Graindorge et al. 2005; Saveanu et al. 2007; Zhang et al. 2007; Garcia-Gomez et al. 2011). In contrast, Nsa2 and Nog2 assembled later, with 27SB pre-rRNA (Saveanu et al. 2001; Lebreton et al. 2006a). The entry points of Dbp10, Nip7, and Nop2 have not been studied. Experiments described in this paper are consistent with and extend previous results to generate a higher resolution picture of the assembly hierarchy.

Building on work from the Fromont-Racine group, we began by assaying the association of the late-entering B-factors, Nsa2 and Nog2, in the absence of the other B-factors. We show that all of the B-factors are required to recruit the GTPase Nog2, but only a subset (Nop2/Nip7, Dbp10, Tif6, Rlp24, and Nog1) are required to recruit Nsa2. Fromont-Racine and colleagues showed that Nsa2 is necessary to recruit Nog2. Here we show that in the absence of Rpf2 or Sbp4, Nsa2 is still recruited into pre-ribosomes, but Nog2 is not. Thus, Nsa2 alone is not sufficient to recruit the GTPase Nog2.

We then extended our model by systematically testing the interdependence of all the B-factors. We discovered that these B-factors are loaded into pre-ribosomes sequentially via two largely separate assembly routes that converge on Nog2 (Fig. 49C).

Association of Nop2 and Nip7 with each other and with pre-ribosomes is necessary for stable association of downstream B-factors, beginning with the Rpf2 subcomplex (Rpf2, Rrs1, r-proteins L5 and L11, and 5S rRNA), and Rlp24, Tif6, and Nog1. Members of each of these three sets of proteins are mutually interdependent for assembly and exhibit significant physical and genetic interactions with each other (Fig. 52). Furthermore, many contain RNA binding motifs and thus are likely to bind pre-rRNA. Taken together, these results suggest that processing of 27SB pre-rRNA requires formation of one or more assembly platforms of B-factor subcomplexes within pre-ribosomes, several steps before the processing event. In contrast, the last steps in recruiting of the B-factors occur later in assembly, after formation of 27SB pre-rRNA.

In the absence of each B-factor, other B-factors associate less well with pre-ribosomes, but to varying extents. Western blotting showed that the B-factors are usually not completely absent from pre-ribosomes, but rather diminished. The strongest effect that we observed in our mutants was the association of Nsa2 and Nog2. This probably reflects blocking assembly at a step before these proteins associate with pre-ribosomes. Conversely, effects on the association of other B-factors were often not as strong. One possibility is that we observe small changes in the levels of these proteins because we purify a different population of assembly intermediates in cells depleted of B-factors. We believe this is not the case since TAP-tagged Nop7 does not co-IP significantly different pre-rRNA intermediates in B-factor mutants (J. Talkish, data not shown). In fact, Nop7 co-IPs slightly greater amounts of 27SB pre-rRNA in the absence of the B-factors. Unlike Nsa2 and Nog2, the other B-factors associate with 35S or $27SA_2$ containing pre-ribosomes and remain associated through the lifetime of 27SB pre-rRNA. Since 27SB-containing pre-

ribosomes are the longest-lived intermediates and these intermediates accumulate in B-factor mutants, we predict that the small changes that we see might in fact be slightly underrepresented.

The experiments performed in this study fail to distinguish two possibilities that could occur in the absence of each B-factor: 1) The other B-factors fail to associate with pre-ribosomes. 2) The other B-factors associate with pre-ribosomes, but fail to be stably incorporated. We believe the former to be true regarding Nsa2 and Nog2, and the later regarding the other B-factors. Each B-factor in our model does not necessarily recruit the next through direct interaction, but rather may form a structure or niche in the pre-ribosome that allows stable incorporation of the next B-factor. Thus, each B-factor only stably associates with pre-ribosomes after stable incorporation of the preceding B-factors.

Our model shows that the B-factors associate with pre-ribosomes through two converging pathways that result in recruiting Nog2. Parallel assembly pathways that converge to a single intermediate have been observed in ribosome biogenesis, and are proposed to be quality control mechanisms (Perez-Fernandez et al. 2007; Lo et al. 2009; Mulder et al. 2010). Johnson and coworkers showed that cytoplasmic release of assembly factors occurs via parallel pathways that converge to trigger the release of Tif6 (Lo et al. 2010). This convergence of pathways may represent a quality control checkpoint to ensure Tif6 is not released before the assembling 60S subunit is competent for translation. Lamanna and Karbstein speculate that parallel assembly pathways may converge before irreversible steps in assembly (Lamanna and Karbstein 2010). They reason that irreversible steps should be tightly regulated and it is easier to survey a single intermediate rather than a number of different parallel intermediates before proceeding to the next step

of assembly. This may be reflected in the recruitment of Nog2 to pre-ribosomes. As the last known B-factor to associate with pre-ribosomes, Nog2 may be a key factor in triggering C_2 cleavage. Recruitment of Nog2 by two parallel pathways may ensure that it is not loaded onto pre-ribosomes prematurely, thus preventing premature cleavage at the C_2 site.

Of the twelve assembly factors required for processing of 27SB pre-rRNA, four are thought to exert their action by using the power of NTP hydrolysis. Involvement of this many NTPases during this step suggests substantial rearrangements may occur. Consistent with this, 27SB pre-rRNA is one of the most abundant pre-rRNA intermediates destined for 60S subunits, with a lifetime substantially longer than other pre-rRNAs (Kos and Tollervey 2010). The early assembling protein Spb4, a DBP and potential RNA dependent ATPase, and the late assembling factor Nsa2, are necessary to recruit the GTPase Nog2. Neither Spb4 nor Nsa2 alone is sufficient to recruit Nog2. Spb4 associates early with pre-ribosomes, whereas Nsa2 associates later. Temporal separation of the association of these two proteins may act as a proofreader of ribosome assembly, ensuring that Nog2 is recruited to the pre-ribosome only at the proper time. Because Sbp4 and Nog2 are at the end of the recruiting pathway (Fig. 49C), it is tempting to speculate that removal of ITS2 is triggered by the concerted action of these NTPases. Spb4 might be regulated by Nog2, analogous to regulation of the spliceosomal ATPase Brr2 by the GTPase Snu114 (Small et al. 2006). During spliceosome assembly, GTP-bound Snu114 activates Brr2, whereas GDP-bound Snu114 represses Brr2 function. Alternatively, Nog2 alone could harness the energy of GTP hydrolysis to cause a conformational switch within the pre-ribosome. In particular, the A_3 assembly factors Nop15 and Cic1 that bind to ITS2 may need to be removed or reorganized (Granneman et al. 2011). GTP hydrolysis may cause a structural change within

ITS2 that makes binding of Nop15 and Cic1 less favorable in the new conformation (Karbstein 2007). Consistent with Nog2 being a member of the myosin/kinesin superfamily of GTPases, Nog2 could also act in a mechanical fashion, using GTP hydrolysis to physically displace Cic1 or Nop15 (Leipe et al. 2002; Karbstein 2007).

Rearrangements before and during processing of 27SB pre-rRNA may also occur as a result of posttranslational modification of assembly factors. We show that the B-factors Rpf2, Spb4, Nog1 and Nog2 are specifically reduced in pre-ribosomes when the protein kinase TOR is inactivated. Based on our recruiting model, we would predict that if Nog1 were diminished in pre-ribosomes, Nsa2 would also be diminished. Contrary to this idea, we do not see a change in Nsa2 upon inactivation of TOR signaling. This may indicate that these proteins are not failing to be recruited to pre-ribosomes, but rather are recruited normally, but then prematurely dissociate from pre-ribosomes upon inactivation of TOR signaling. Interestingly, three of these B-factors are the putative NTPases Spb4, Nog1, and Nog2. These NTPases may fail to stably assemble into pre-ribosomes in the absence of posttranslational modifications. This could be analogous to r-protein S3, which must undergo a series of phosphorylation and dephosphorylation events in order to stably associate with pre-40S intermediates and promote formation of the 40S beak (Schafer et al. 2006).

Alternatively, inactivation of TOR signaling may repress expression of a subset of assembly factors. Nog1 was previously shown to be regulated by TOR kinase (Honma et al. 2006). Inactivation of TOR caused decreased transcription of *NOG1*. It was also shown that Nog1 is rapidly turned over, although independently of TOR signaling. We show that upon inactivation of TOR, levels of Rpf2, Spb4, Nog1, and Nog2 are diminished in whole cell

extracts. Expression of the genes encoding these proteins, as well as other assembly factors and r-proteins, is controlled and coordinated by a set of core promoter sequences termed the *Ribi* regulon (*Ri*bosome *bi*ogenesis) and RP regulon. Additionally, inactivation of TOR signaling represses expression of genes controlled by the *Ribi* and RP regulons (Cardenas et al. 1999; Powers and Walter 1999; Jorgensen et al. 2002; Miyoshi et al. 2003; Claypool et al. 2004; Jorgensen et al. 2004; Wade et al. 2006; Huber et al. 2009). Thus, Rpf2, Spb4, and Nog2 may be rapidly turned over, similarly to Nog1.

A current challenge in understanding ribosome biogenesis is determining where and how assembly factors contact the pre-ribosome. Recent studies that crosslink proteins to RNA with UV light have revealed the rRNA binding sites of some assembly factors (Bohnsack et al. 2009; Granneman et al. 2010; Granneman et al. 2011). Additionally, advances in cryo-EM have provided information about the locations of assembly factors in pre-ribosomes (Gartmann et al. 2010; Sengupta et al. 2010; Strunk et al. 2011), and higher resolution crystal structures of eukaryotic ribosomes are allowing better visualization of how r-proteins contact rRNA (Ben-Shem et al. 2011). While these techniques are powerful for determining how and where assembly factors contact the pre-ribosome, their application is limited in ribosome assembly. For example, not all assembly factors contact rRNA and thus cannot be cross-linked to determine their binding sites. Of those proteins that do bind RNA, crosslinking may not capture all RNA binding sites in these dynamic particles. Additionally, structural analyses often require a fairly homogenous purified sample. Because most assembly factors that function in 60S subunit biogenesis are present in more than one consecutive intermediate, obtaining homogenous samples for cryo-EM or

generating crystals is difficult. Therefore, other methods need to be employed to help predict and determine the binding sites of assembly factors.

We used known genetic and physical interactions among the B-factors to generate a model of the locations of some of these assembly factors (Fig. 52A). Nop2 and Nip7 form a subcomplex and are synthetically lethal with deletion of genes encoding r-proteins L26B or L17A respectively (Costanzo et al. 2010). These two r-proteins are adjacent to each other in domain I of 25S/5.8S rRNA, lying near the polypeptide exit tunnel. Consistent with the synthetic lethal interactions observed between these two r-proteins and the B-factors Nop2 and Nip7, L17 and L26 function in processing of 27SB pre-rRNA. This suggests that Nop2 and Nip7 might dock pre-ribosomes near these two r-proteins, close to the exit tunnel Fig. 52A).

Cryo-EM studies show that Tif6 binds L23 and L24 on the intersubunit side of assembling 60 subunits and functions to prevent premature association of the 60S and 40S subunits (Gartmann et al. 2010). Tif6 is one of the last assembly factors to be released from the assembling ribosome. Its removal is dependent on the Shwachman-Bodian-Diamond syndrome protein homologue Sdo1 and the GTPase Efl1 (Menne et al. 2007). Sdo1 was shown to interact with r-protein L3 in a two-hybrid screen, positioning Sdo1 near Tif6. Interestingly, Sdo1 was also shown to bind directly to Nip7 (Luz et al. 2009). Thus, there may be a physical connection between Nip7, Sdo1, and Tif6. This provides a testable model that Sdo1 may be involved in releasing not only Tif6, but other B-factors as well.

L5, L11, and 5S rRNA, which are members of the Rpf2 subcomplex, form the central protuberance (CP) near the top of 60S subunits (Ben-Shem et al. 2011). Thus it is likely that when Rpf2 and Rrs1 deliver L5, L11, and 5S rRNA to assembling ribosomes, they are

located in a comparable position. We speculate that Rpf2 and Rrs1 are located on the intersubunit side of the CP based on the following evidence: 1) Rrs1 was shown to interact with Ebp2 in both two-hybrid and PCA (protein complementation assay) screens (Tsujii et al. 2000; Tarassov et al. 2008). 2) Ebp2 exhibits two hybrid interactions with Brx1 (Shimoji et al. 2012). 3) Brx1 interacts with Tif6 by PCA (Tarassov et al. 2008). These three pieces of evidence suggest a chain of interactions beginning with Tif6, perpetuated through Brx1 and Ebp2, and ending with the Rpf2 subcomplex.

Nsa2 exhibits two-hybrid interactions with r-proteins L4, L15, and L18 (Lebreton et al. 2006a) (Fig. 52B), which are located adjacent to each other on the left edge of the 60S subunit when viewed from the intersubunit face. Nsa2 shares a number of both physical and genetic interactions with Rlp24, Nog1, and Mak11, suggesting that these proteins may associate with pre-ribosomes in close proximity to each other (Saveanu et al. 2003; Lebreton et al. 2006a). Consistent with this idea, our results, with those of Saveanu et al., show that Rlp24, Nog1, and Mak11 are interdependent for their assembly into pre-ribosomes and all three are required to recruit Nsa2. Interestingly, overexpression of the A_3-factor Nop7 suppresses mutations in *nog1* (Honma et al. 2006). Nop7 is a member of a group of mutually interdependent proteins required for processing $27SA_3$ pre-rRNA (Sahasranaman et al. 2011). UV crosslinking has shown most of the A_3-factors bind rRNA in domain I of 25S/5.8S rRNA or in ITS2, and in their absence these regions are not properly assembled (Granneman et al. 2011). Consistent with genetic interactions between Nog1 and Nop7, in the absence Nop7 and mutually interdependent A_3-factors, Nog1 and Rlp24 fail to associate with pre-ribosomes, suggesting they may also bind near the A_3-factors. Specifically, Nop7 was shown to bind rRNA near helix 54 in domain III (Fig. 52B). This

region of rRNA is in close proximity to the rRNA binding sites of L4, L15, and L18 further supporting the idea Rlp24, Nog1, Mak11, and Nsa2 bind the left edge of the 60S subunit. It is also interesting that inactivation of TOR signaling causes both Nog1 and Nop7 to associate less well with pre-ribosomes (Honma et al. 2006), suggesting this neighborhood could be a target of TOR regulation.

While we were unable to predict the binding sites of all B-factors, our model provides a number of important insights. First, we predict that a large majority of the B-factors are binding on the intersubunit face. Could some of these factors prevent premature subunit joining analogous to Tif6? Could Nog2 remove or reorganize these proteins analogous to other GTPases that function on the subunit interface (Lo et al. 2010)? Second, we predict that Rlp24, Nog1, and Nsa2 are binding near r-proteins L4, L15, and L18. These are in close proximity to the ITS2-proximal stem, where ITS2 would be predicted to be located in assembling 60S subunits. Our predictions for the location of these B-factors put them in prime position to facilitate the removal of ITS2.

FIGURE 52

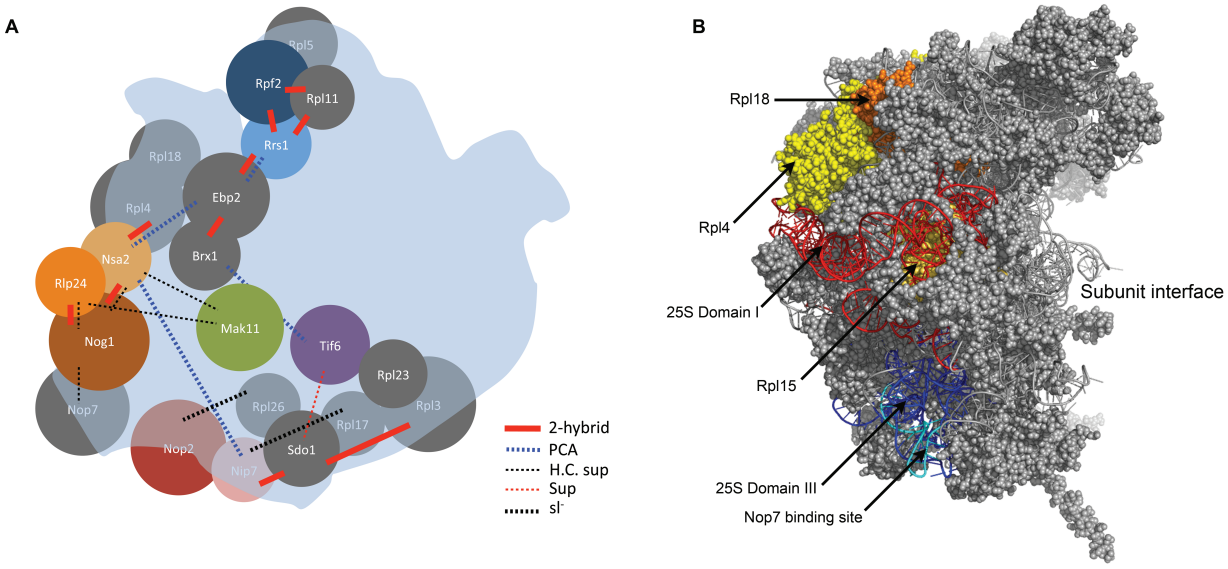

A
Rpl5
Rpf2
Rpl11
Rrs1
Rpl18
Ebp2
Rpl4
Nsa2
Brx1
Rlp24
Mak11
Nog1
Tif6
Rpl23
Rpl26
Rpl3
Rpl17
Nop7
Nop2
Sdo1
Nip7
2-hybrid
PCA
H.C. sup
Sup
sl-
B
Rpl18
Rpl4
25S Domain I
Subunit interface
Rpl15
25S Domain III
Nop7 binding site

Figure 52: Physical and genetic interactions provide clues about the location of the B-factors in pre-ribosomes.

(A) Predicted locations of B-factors in assembling 60S subunits. Binding sites of proteins were predicted using a combination of genetic and physical interactions and then superimposed on a schematic of the 60S subunit viewed form the intersubunit side. Grey circles indicate assembly factors and ribosomal proteins that were used as landmarks to help position the B-factors. PCA - protein complementation assay; H.C. sup – high-copy suppressor; Sup – extragenic suppressor; sl^- - synthetic lethal. (B) r-proteins L4, L15, and L18 are shown in the crystal structure of the 60S subunit as viewed from the crown view of the intersubunit face rotated right 90 °. Domain I and domain III of 25S rRNA are indicated in red and blue respectively. The Nop7 binding site determined by Granneman et al. (2011) is shown in cyan. Pymol images of the ribosome structure were generated using PDB files 3U5H and 3U5I.

MATERIALS AND METHODS

Construction of yeast strains

Yeast strains conditional for expression of *RPF2, RLP24, SPB4, NOG1, TIF6,* or *NOG2* were constructed as described by Longtine *et al.* (1998), as follows. Sequences containing a selectable marker, plus the *GAL1* promoter sequence followed by an ATG and codons encoding three copies of the hemaglutinin epitope (3HA), were amplified by PCR. The PCR products were transformed into yeast. Transformants were screened for correct integration of the *GAL1* promoter and the triple hemaglutinin (3HA) tag upstream and in-frame with the respective genes, by western blotting with anti-HA antisera. Strains conditional for expression of Nip7, Nop2, or Dbp10 were obtained from other laboratories (Hong et al. 1997; Zanchin et al. 1997; Burger et al. 2000), and contain a genomic knockout of the respective genes plus a plasmid bearing a *GAL* promoter fusion of each gene. For *NIP7*, we used the temperature-sensitive allele *nip7-1* fused to the *GAL* promoter. Because the Nip7-1 protein is functional at 30 °C but is less stable than wild-type Nip7 (Zanchin et al. 1997), Nip7-1 can be more rapidly depleted than with wild-type *NIP7* fused to the *GAL1* promoter.

Yeast strains expressing C-terminal TAP-tagged Nop7 or C-terminal 3HA-tagged proteins were created by PCR of the tag sequence and a selectable marker (*URA3* or *TRP1* for the TAP tag, and *HIS3* or *kanMX6* for the 3HA tag), transformation, and selection, as described in Rigaut *et al.* (1999) or Longtine *et al.* (1998), respectively. Transformants were screened by western blotting to identify those expressing the tagged proteins, and, in most cases, by polysome gradients for defects in ribosome assembly, which would indicate

effects of the tag on protein function. Sequences of oligonucleotides used as PCR primers are available upon request.

Growth of yeast strains and depletion of factors

Yeast strains used in this study are listed in Table 5. Unless otherwise noted, yeast were grown at 30 °C in YEPGlu medium (2% dextrose, 2% peptone, and 1% yeast extract), or YEPGal medium (2% galactose, 2% peptone, and 1% yeast extract). Cells were harvested during mid-logarithmic phase growth, at 3-5x10^7 cells/ml, except where otherwise indicated. The strains containing *GAL1* promoter fusions of B-factor genes were grown at 30 °C in YEPGal liquid medium to 3-5x10^7 cells/ml, or grown in YEPGal medium and shifted to YEPGlu for indicated times, to 3-5x10^7 cells/ml, to deplete the proteins *in vivo*. Depletion was assayed by western blotting of whole cell extracts with anti-HA antiserum, to measure amounts of the 3HA-tagged assembly factors (data not shown).

Sucrose gradient assays of ribosomes and polyribosomes

Pre-ribosomes, ribosomes, and polyribosomes were fractionated from 40 OD_{254} units of whole cell extracts on 7%-47%(w/v) sucrose gradients as described in Deshmukh *et al.* (1993), with the following modifications. Cycloheximide (5 mg) was added to cultures twenty minutes before harvesting cells. A Teledyne ISCO Foxy R1 density gradient fractionator was used to fractionate and analyze gradients.

Affinity purification of pre-ribosomes or pre-ribosome subcomplexes

Ribosome assembly intermediates were affinity-purified from whole cell extracts with magnetic Dynabeads (Invitrogen), using TAP-tagged assembly factor Nop7, as described in Sahasranaman *et al.* (2011). The Nop2/Nip7 subcomplex was purified as follows: extracts were prepared from a *NOP2-TAP* strain and pre-ribosomes and ribosomes were pelleted by centrifugation of whole cell extracts at 180,000xg for 2h at 4 °C, as described in Krogan *et al.* (2004). The supernatant was subjected to a second centrifugation at 180,000xg for 45 min at 4 °C. TAP-tagged Nop2 was used to affinity-purify the Nop2/Nip7 subcomplex from the supernatant as previously described (Rigaut et al. 1999).

Protein extractions, SDS-PAGE, and western blot analysis

Proteins in whole cell extracts were prepared for gel electrophoresis by dissolving the extract in SDS sample buffer. Proteins were recovered from sucrose gradient fractions or from eluates during affinity purification by precipitation with 10% TCA, and were subsequently suspended in SDS sample buffer. Proteins were resolved by SDS-PAGE on 4%-20% Novex precast gels (Invitrogen), and stained with silver by standard methods. To assay Nog2 protein by western blotting, NuPage 4%-12% Bis-Tris gels (Invitrogen) were used, since Nog2 comigrates with IgG on 4%-20% Novex gels. Proteins from whole-cell extracts, gradient fractions or purified pre-ribosomes were assayed by western blot analysis (Ausubel et al. 1994), with the following modification. To enable detection of multiple different proteins on one blot and to conserve antiserum, after electroblotting we cut nitrocellulose membranes into smaller sections based on the known mobility of the different proteins. Edges of cut membranes, when visible, are indicated by "<" in the Figures. TAP-tagged proteins were detected using alkaline phosphatase conjugated to IgG

(Pierce). 3HA-tagged proteins were identified with mouse monoclonal antibody 12CA5. Otherwise, antibodies specific for r-proteins or ribosomal assembly factors were used. AP-conjugated anti-mouse or anti-rabbit secondary antibodies (Promega) were used, and colorimetric detection was performed using NBT and BCIP (Promega). Often, two bands were seen for westerns with Nog2, Nop2, or Nog1. The band corresponding to the *bona fide* protein was confirmed by comigration on SDS-PAGE with silver-stained protein identified by mass spectrometry, or by decrease upon turning off expression of the corresponding gene, and is indicated with #.

ACKNOWLEDGEMENT

The authors thank the following people for generously providing strains: John Aris (*GAL-NOP2*), David Goldfarb and Nilson I. T. Zanchin (*GAL-nip7-1*), and Jesus de la Cruz (*GAL-DBP10*). We are grateful to the following people for generously providing antibodies: John Aris (Nop2), David Goldfarb (Nip7), Janine Maddock (Nog1), Cosmin Saveanu and Micheline Fromont-Racine (Rlp24, Nog2, Nsa2 and Tif6), and Jeff Brodsky (Sec61). We thank Susan Dowd for assistance with mass spectrometry.

5.2 Ebp2 and Brx1 function cooperatively in 60S ribosomal subunit assembly

This work was done in collaboration with Keiko Mizuta at the University of Hiroshima, Japan. Dr. Mizuta identified some very interesting synthetic lethal interactions between *ebp2* and *brx1* mutants and asked us if we could assist in pinpointing the molecular basis for this synthetic lethality. Together we found that the *ebp2 brx1* double mutants were defective in processing 27SA pre-rRNAs, whereas *brx1* mutants were not. Furthermore, we found that Ebp2 and Brx1 exhibited strong two-hybrid interactions, but that these interactions were abolished in *ebp2 brx1* double mutants. However, both proteins could still associate with 66S pre-ribosomes, but assembly was blocked. Last, we established a hierarchy of recruitment in which Ebp2 is necessary for Brx1 association, but not *vice versa*. Together our data suggest that Ebp2 and Brx1 do not necessarily need to interact to remain stably associated with pre-ribosomes, but do need to interact to properly function in 27SA pre-rRNA processing.

My contribution to this work included assaying pre-rRNA processing in Ebp2 and Brx1 depletion strains and *ebp2 brx1* single- and double mutants. Furthermore, I purified pre-ribosomes using Ebp2- and Brx1-TAP to determine their timing of association. This work was published in *Nucleic Acids Research* in May, 2012

5.2.1 Depletion of Ebp2 and Brx1 block processing of $27SA_2$ and $27SA_3$ pre-rRNAs.

To test the effect on pre-rRNA processing in the absence of Ebp2 or Brx1, strains were constructed in which the expression of each protein was placed under control of the *GAL* promoter. Cells were grown in galactose-containing medium to express each protein and then subsequently shifted to glucose-containing medium for 16 hours to deplete each

protein. Upon depletion of both proteins we observed an accumulation of $27SA_2$ and $27SA_3$ pre-rRNAs (Fig. 53). However, depletion of Ebp2 resulted in a slightly earlier pre-rRNA processing defect as evident by the greater accumulation of $27SA_2$ pre-rRNA, and a relatively small affect of 27SB pre-rRNA. On the other hand, depletion of Brx1 resulted in a "classic" A_3 phenotype; an accumulation of $27SA_3$ pre-rRNA and a subsequent decrease of $27SB_S$. These results are consistent with the established hierarchy in which Ebp2 assembles into pre-ribosomes prior to Brx1.

FIGURE 53

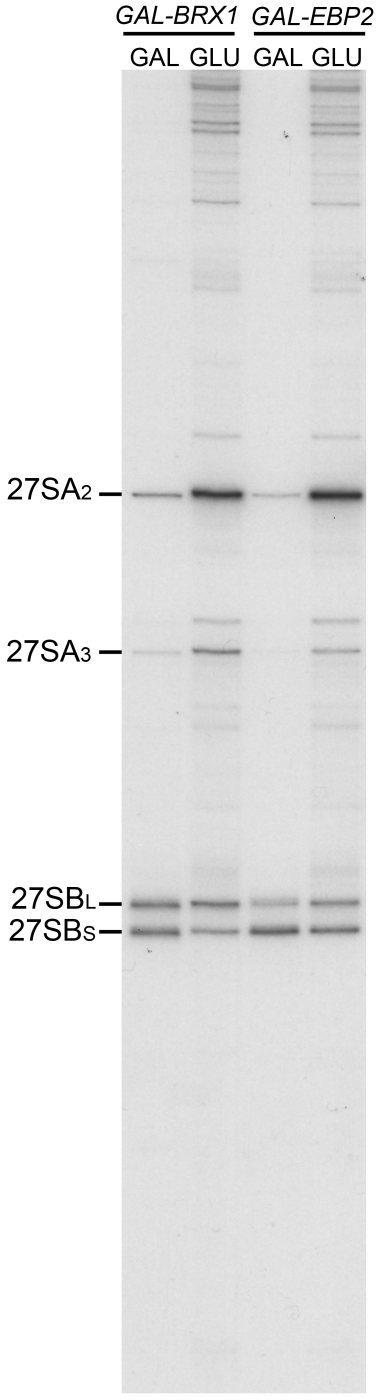


Figure 53: Ebp2 and Brx1 are required for processing 27SA2 and 27SA3 pre-rRNAs

The pre-rRNA processing defect in the absence of Ebp2 and Brx1. RNA was extracted from unshifted and shifted strains and assayed by primer extension with an oligonucleotide complementary to ITS2.

5.2.2 A combination of the *ebp2-14* and *brx1-102* or *brx1-172* mutations leads to synergistic defects in pre-rRNA processing.

Because *ebp2 brx1* double mutants are lethal at all temperatures, we constructed conditional lethal strains. To do so we built strains containing *ebp2-14 brx1-102* or *ebp2-14 brx1-172*, plus a plasmid containing wild-type HA-tagged *EBP2* under control of the *GAL* promoter. When these strains were shifted from galactose-containing medium to glucose-containing medium, the expression of *EBP2* was turned off and the phenotypes of the *ebp2 brx1* double mutant could be seen.

Because the *ebp2* single mutants are temperature sensitive, we examined pre-rRNA processing in the *brx1* and *ebp2* mutants grown at 25 °C and shifted to 37 °C, as well as the conditional double mutants grown at 25 °C, using primer extension. As shown in Figure 54, lanes 1-3, amounts of $27SA_2$, $27SA_3$, and 27SB in the *brx1-102* or *brx1-172* single mutants were similar to those in wild-type *BRX1* yeast. The *ebp2-14* mutant contained slightly higher levels of $27SA_2$ and $27SA_3$ pre-rRNAs compared to the wild-type strain (Fig. 54, lanes 4 and 5). Last, both double mutant strains shifted to glucose containing medium contained increased amounts of $27SA_2$ and $27SA_3$ pre-rRNAs compared to the unshifted strains expressing *EBP2* (Fig 54, lanes 6-9), or either single mutant alone. However, this affect was fairly minimal.

FIGURE 54

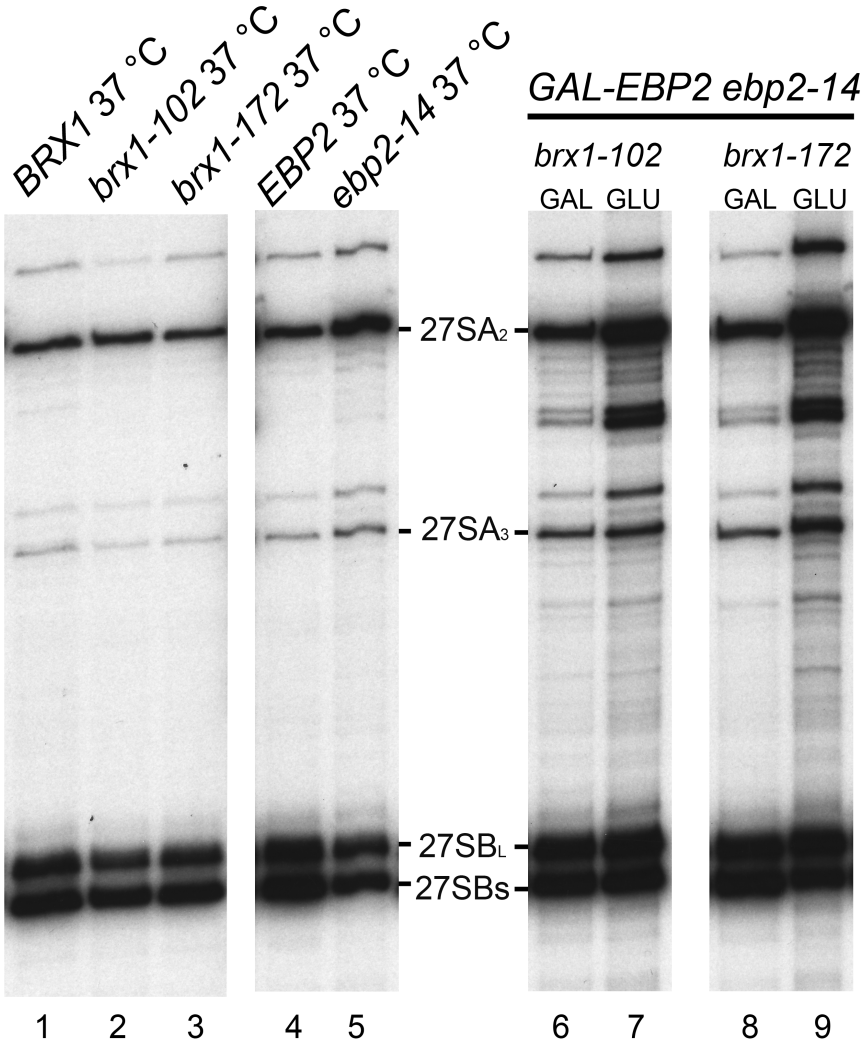

BRX1 37 °C
brx1-102 37 °C
brx1-172 37 °C
EBP2 37 °C
ebp2-14 37 °C
GAL-EBP2 ebp2-14
brx1-102
brx1-172
GAL GLU
GAL GLU
27SA2
27SA3
27SBL
27SBs
1 2 3 4 5 6 7 8 9

Figure 54: A combination of the *ebp2-14* and *brx1-102* or *brx1-172* mutations leads to synergeistic defects in pre-rRNA processing.

RNA was extracted from the indicated strains and assayed by primer extension using the ITS2-A oligonucleotide complementary to ITS2.

5.2.3 Ebp2 and Brx1 assemble into pre-ribosomes early, with pre-rRNPs containing 35S pre-rRNA.

We wanted to determine with which pre-ribosomal intermediates Ebp2 and Brx1 associate. Both proteins are routinely identified by mass spectrometry in pre-ribosomes affinity-purified using TAP-tagged early or middle assembly factors. To do so, we assayed with which of the consecutive pre-rRNA intermediates TAP-tagged Brx1 and Ebp2 co-purify. Nob1, a component of 43S pre-ribosomes, and an untagged strain were used as controls. Primer extension and northern blotting indicated that 35S, 27S, and 7S pre-rRNA co-purified with Brx1-TAP and Ebp2-TAP (Fig. 55). We also observed co-purification of 5.8S and 25S rRNAs with Brx1 and Ebp2, however these rRNAs were present in much lower quantities with Ebp2 suggesting that Ebp2 dissociates from pre-ribosomes prior to Brx1. Together these data suggest that Ebp2 and Brx1 associate with early pre-ribosomes containing 35S pre-rRNA and are present in each of the consecutive 66S pre-ribosomal intermediates.

FIGURE 55

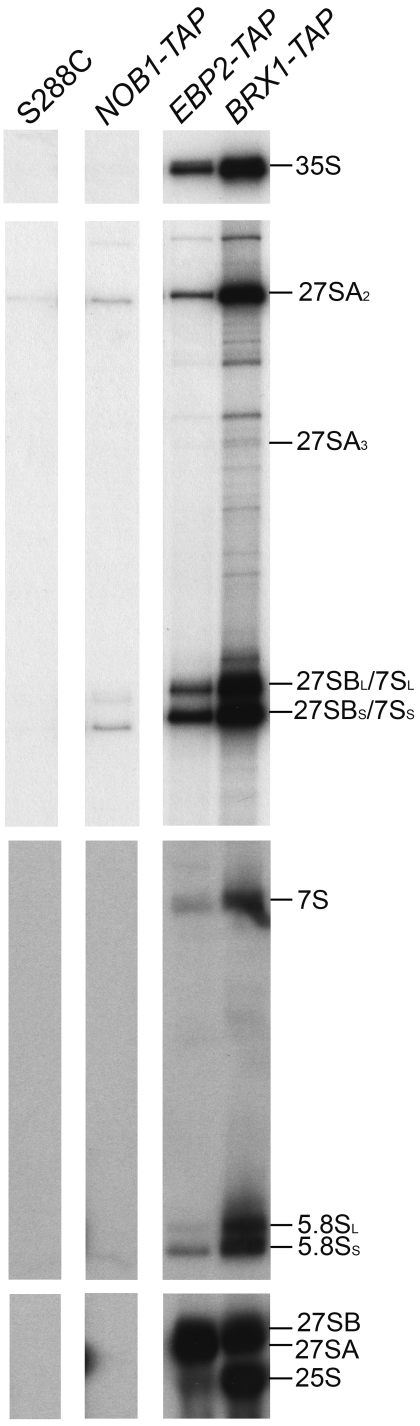

S288C
NOB1-TAP
EBP2-TAP
BRX1-TAP
35S
27SA2
27SA3
27SBL/7SL
27SBS/7SS
7S
5.8SL
5.8SS
27SB
27SA
25S

Figure 55: Ebp2 and Brx1 assemble into pre-ribosomes early, with pre-rRNPs containing 35S pre-rRNA.

TAP-tagged Ebp2 and Brx1 were used to affinity-purify pre-ribosomes. Pre-rRNAs contained in these particles were identified by primer extension and gel electrophoresis. The untagged parent strain S288C and Nob1-TAP were used as controls.

5.3 Timing of association of assembly factors

As discussed throughout this thesis, many assembly factors are present in different populations of pre-ribosomes, and thus their presence in discrete populations can be used as "landmarks" along the ribosome assembly pathway. To better understand the timing of association of assembly factors with pre-ribosomes, we obtained the Yeast TAP-Tagged ORF collection from Dr. Joseph Martens at the University of Pittsburgh. We affinity-purified particles using TAP-tagged assembly factors thought to be present in pre-ribosomes during early, middle, and late steps of assembly, and compared the pre-rRNAs they co-purify with those co-purified by Nop7, Brx1, and Nop4. These three assembly factors have previously been characterized and have been shown to be present in pre-ribosomes throughout assembly. Pre-rRNAs that co-purified with these factors were assayed by primer extension using an oligonucleotide complementary to ITS2, allowing simultaneous detection of $27SA_2$, $27SA_3$, and 27SB pre-rRNAs (Fig. 56). As controls, we used a Nob1-TAP strain (described in 5.2.3) and the untagged parent strain S288C. In general, we observed that Rrp5, Ssf1, Dbp7, Dbp6, Dbp2, Drs1, and Nsa1 associate with pre-ribosomes early in assembly (co-purified $27SA_2$ pre-rRNAs), Nog2, Nug1, Rix1, and Arx1 associate during middle steps (co-purified 27SB pre-rRNAs), and Lsg1 associates late in assembly (27S pre-rRNAs were undetectable). This work revealed that Rrp5 is associated only with early pre-ribosomes containing $27SA_2$ pre-rRNAs and has since been used routinely by the lab to assay changes in the composition of early pre-ribosomes.

FIGURE 56

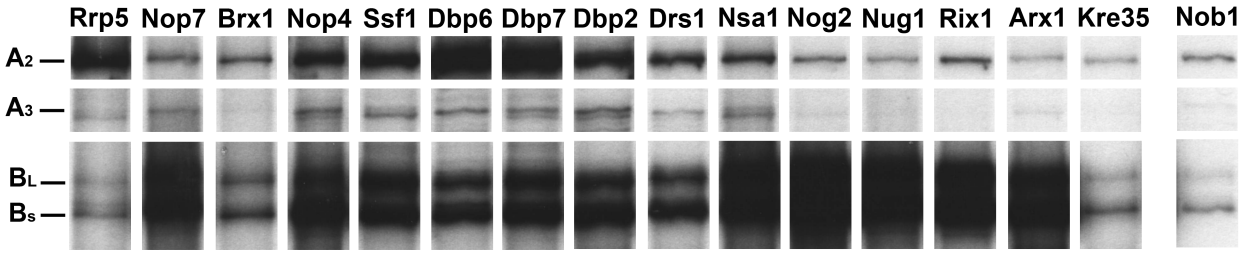

Rrp5
Nop7
Brx1
Nop4
Ssf1
Dbp6
Dbp7
Dbp2
Drs1
Nsa1
Nog2
Nug1
Rix1
Arx1
Kre35
Nob1
A2
A3
BL
Bs

Figure 56: Timing of association of 66S assembly factors

Pre-ribosomes were purified using each of the TAP-tagged proteins listed, and the pre-rRNAs contained within them were assayed by primer extension and PAGE using the ITS2-A oligonucleotide complementary to ITS2.

5.4 *In vivo* hydroxyl radical RNA structure probing in yeast

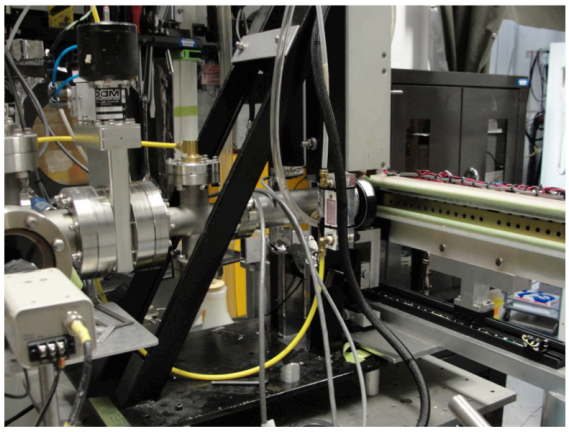
A current challenge to RNA structure probing is the relatively low number of reagents that can be used *in vivo.* Of the routinely used small molecules, DMS and recently developed SHAPE reagents are the only ones that can rapidly penetrate the cell wall. In an effort to develop new technologies for *in vivo* RNA structure probing in yeast, I performed *in vivo* hydroxyl radical footprinting at the National Synchrotron Light Source (beamline X28C) at Brookhaven National Laboratory. This technique was developed by Sarah Woodson's group to probe RNA structure in *E. coli*. Briefly, frozen cell pellets (5-10 μl) are placed in a cryo-cooled sample holder, and irradiated with synchrotron-generated x-rays to cause radiolysis of intracellular water and production of hydroxyl radicals (Fig. 57). The hydroxyl radicals produced are extremely short lived (10-20 μs) and cleave the RNA backbone in a solvent-accessible manner. These cleavages can then be detected by primer extension, providing tertiary information about RNA structure.

To develop this technique I first determined the optimal exposure time to achieve a good signal-to-noise ratio, while producing ~1 cleavage per RNA molecule. I exposed cells to the synchrotron-generated x-rays for 0-1000 ms, extracted RNA, and assayed the amount of cleavage by primer extension and PAGE, as well as agarose gel electrophoresis (Fig. 58A, 58B, and 58D). I determined that 100-200 ms was the optimal exposure time in yeast. Primer extension analysis of 5.8S rRNA revealed that it was cleaved in a solvent accessible manner. In general, 5.8S rRNA sequences that protrude from the surface of the ribosome were cleaved while those that were protected by r-proteins, or buried inside the ribosome were not (Fig. 58B and 59). I also performed hydroxyl radical footprinting in the *nop12Δ* strain but was surprised to find no differences in the cleavage pattern when

compared to wild-type (Fig. 58C.). It may be that Nop12 contacts the ITS2-proximal stem and helix 8 in such a way that it does not preclude the RNA backbone from being cleaved.

While the protocol I used was essentially the same as that described in Adilakshmi *et al*. 2006, there were a few differences. I found that including 5% glycerol in the TM buffer in which the cells are frozen significantly improved the quality of the RNA after phenol extraction. Glycerol is a scavenger of free radicals, however I found that addition of glycerol did not significantly change the exposure time needed to obtain cleavage of the RNA. Furthermore, I found that yeast required slightly longer exposure times than *E. coli* to achieve a good signal-to-noise ratio. The published protocol in Adilakshmi *et al*. (2006) reports an optimal exposure time for *E. coli* of ~200 ms, however more recently the Woodson lab has been using exposure times of ~75 ms (personal communication). Last, I can't stress enough how important it is to keep the cell pellets frozen at all times. I found that brief warming, even for a few seconds, is enough to significantly degrade the RNA.

FIGURE 57



• Irradiate frozen cells with x-rays generated by a synchrotron

↓

• This produces hydroxyl radical from water

↓

• Hydroxyl radicals cleave RNA in a solvent accessible manner

↓

• Detect cleavages by primer extension

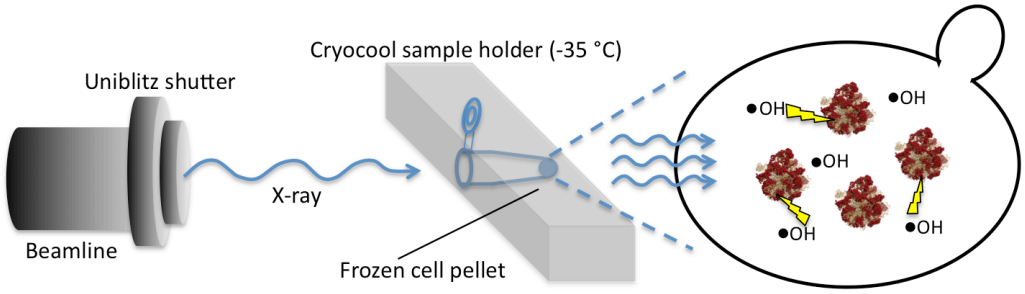


Figure 57: *In vivo* hydroxyl radical RNA structure probing in yeast

Shown is the experimental setup at the X28C beamline at the National Synchrotron Light Source. Tubes containing frozen cell pellets are placed in the cryocooled sample holder. Upon opening of the Uniblitz shutter, cells are irradiated with x-rays. This results in the radiolysis of water and production of hydroxyl radicals that cleave RNA in a solvent accessible manner.

FIGURE 58

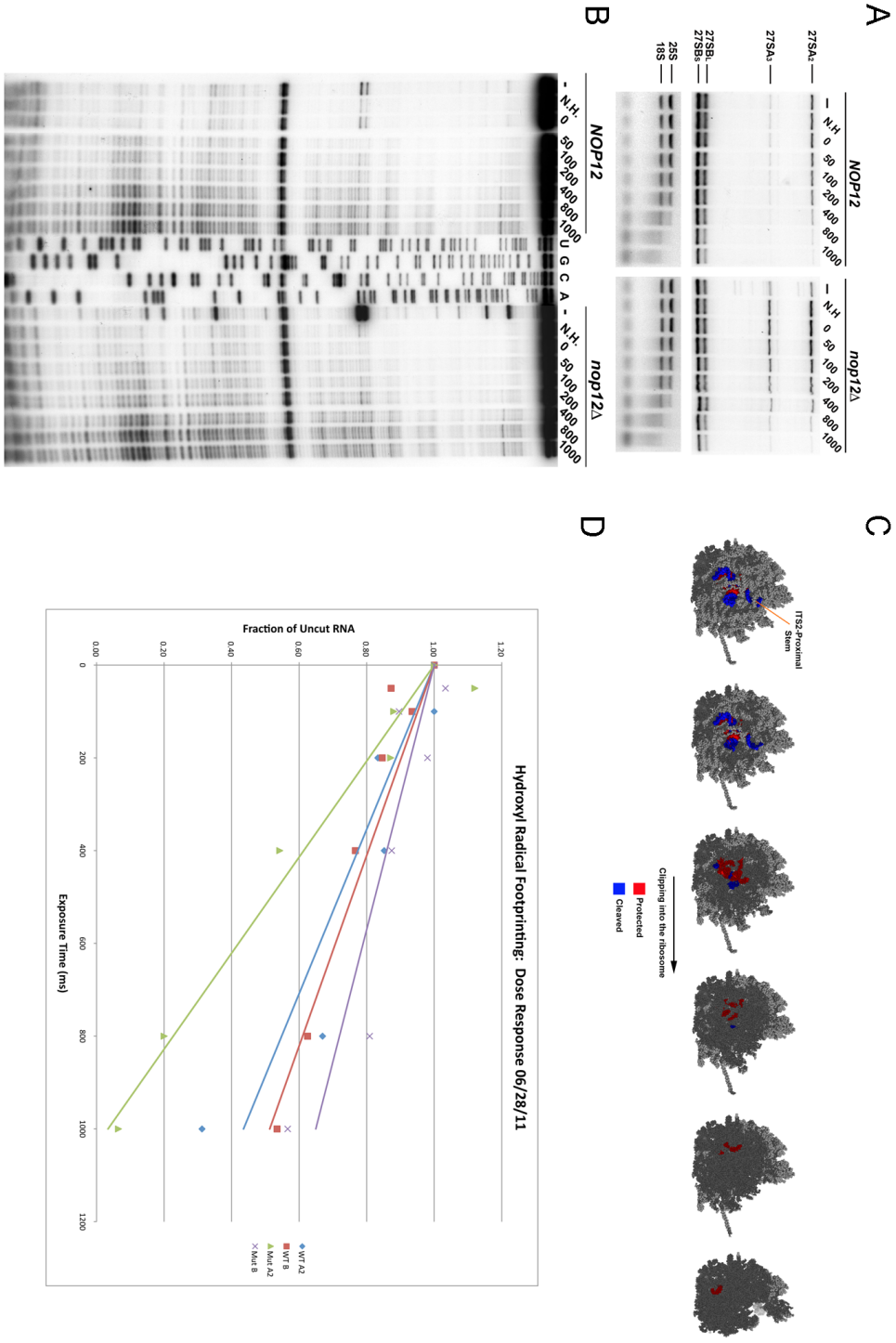

A
NOP12
nop12Δ
– NH4
0
50
100
200
400
800
1000
27SA2
27SA3
27SBL
27SBS
25S
18S
B
NOP12
nop12Δ
- NH4
0
50
100
200
400
800
1000
U
G
C
A
C
ITS1-Proximal Stem
Clipping into the ribosome
Protected
Cleaved
D
Hydroxyl Radical Footprinting: Dose Response 06/28/11
Fraction of Uncut RNA
Exposure Time (ms)
WT A2
WT B
Mut A2
Mut B

Figure 58: rRNA is cleaved in a dose-dependant manner by synchrotron-generated hydroxyl radicals.

(A) The optimal exposure time was determined by exposing cells to synchrotron-generated x-rays for 0-1000 ms and assaying the remaining amount of full-length 27S pre-rRNAs by primer extension. Ethidium bromide staining of agarose gels was used to assay the amount of 25S and 18S rRNAs remaining after exposure. (B) The cleavage pattern detected by primer extension and PAGE analysis of the ITS2-proximal stem and pre-5.8S rRNA in the presence and absence of Nop12. (C) Cleavage sites of 5.8S rRNA were plotted onto the crystal structure of yeast 60S ribosomes. Blue indicates cleavage, whereas red indicates protection. Shown are sequential slices into the core of the 60S subunit. (D) Quantification of the amount of full-length 27S pre-rRNAs assayed in (A).

FIGURE 59

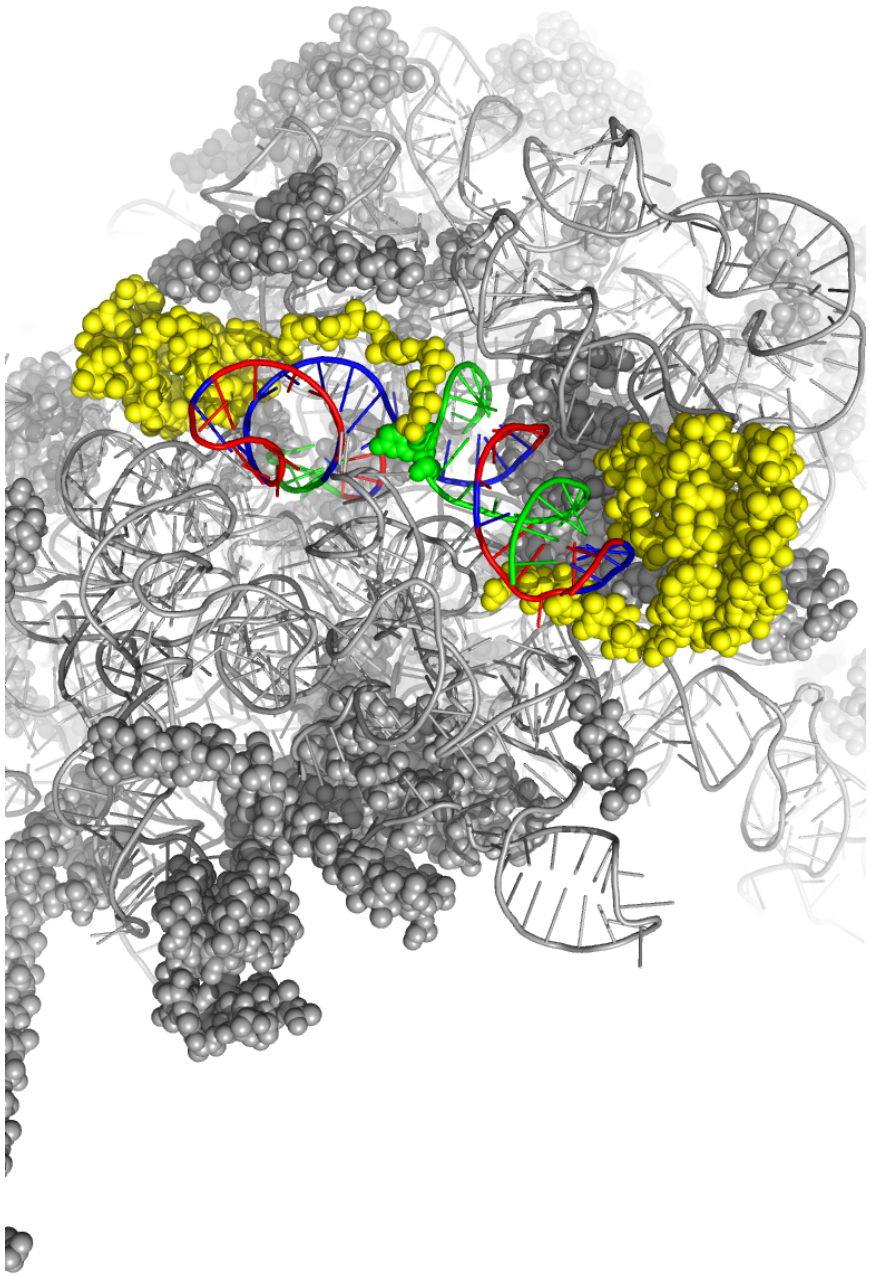


Figure 59: rRNA is cleaved in a solvent-accessible manner by syncrotron-generated hydroxyl radicals.

Shown is the crystal structure of the yeast 60S ribosomal subunit. The ITS2-proximal stem is shown in green and r-proteins L8 and L15 are shown in yellow. Red indicates areas of 5.8S rRNA that were cleaved by hydroxyl radicals, whereas blue represents areas that were protected.

5.5 Cic1 and Nop15 are required for proper folding of ITS2

Cic1 and Nop15 both have been shown to crosslink to sequences in ITS2. As discussed in Chapter 1 (1.6.6.3), ITS2 has been proposed to be dynamic, first folding into an open "ring" conformation (Fig. 60A) and then later refolding into a more compact "hairpin" conformation (Fig. 60B). To determine the role of these proteins in structuring this spacer I performed *in vivo* DMS probing of cells either expressing these proteins, or cells in which expression of Cic1 or Nop15 was shut off. Because these proteins are interdependent for their association with pre-ribosomes, changes in nucleotide reactivity in the absence of either were largely similar. I observed a number of nucleotides at or near the Cic1 and Nop15 binding sites with increased DMS reactivity (Fig. 60 and Fig. 61). A number of these nucleotides are predicted to be base-paired, suggesting helices near these proteins are not stably formed in their absence. Furthermore, I observed two nucleotides immediately 3' of the E site with decreased reactivity (C3021 and C3024). In the ring model, these two nucleotides do not participate in base pairs and thus should be reactive to DMS. However, in the hairpin model these two nucleotides are paired with G3044 and G3041, respectively. While doing these experiments, this work was published by Granneman *et al.* (2011) who observed the same changes. They proposed that Cic1 and Nop15 function to maintain ITS2 in the ring conformation, and in their absence ITS2 prematurely folds into the hairpin structure. I disagree with these results for two reasons. First, the DMS modification patter of ITS2 in wild-type cells does not provide enough information to distinguish between these two conformations. Second, if the model proposed by Granneman *et al*. were true, we should observe decreased modification of A3042 as well. However, this nucleotide becomes more reactive to DMS in the absence of Nop15 and Cic1. I believe the only

conclusion that can be drawn from these experiments is that ITS2 is not properly folded in the absence of these proteins.

FIGURE 60

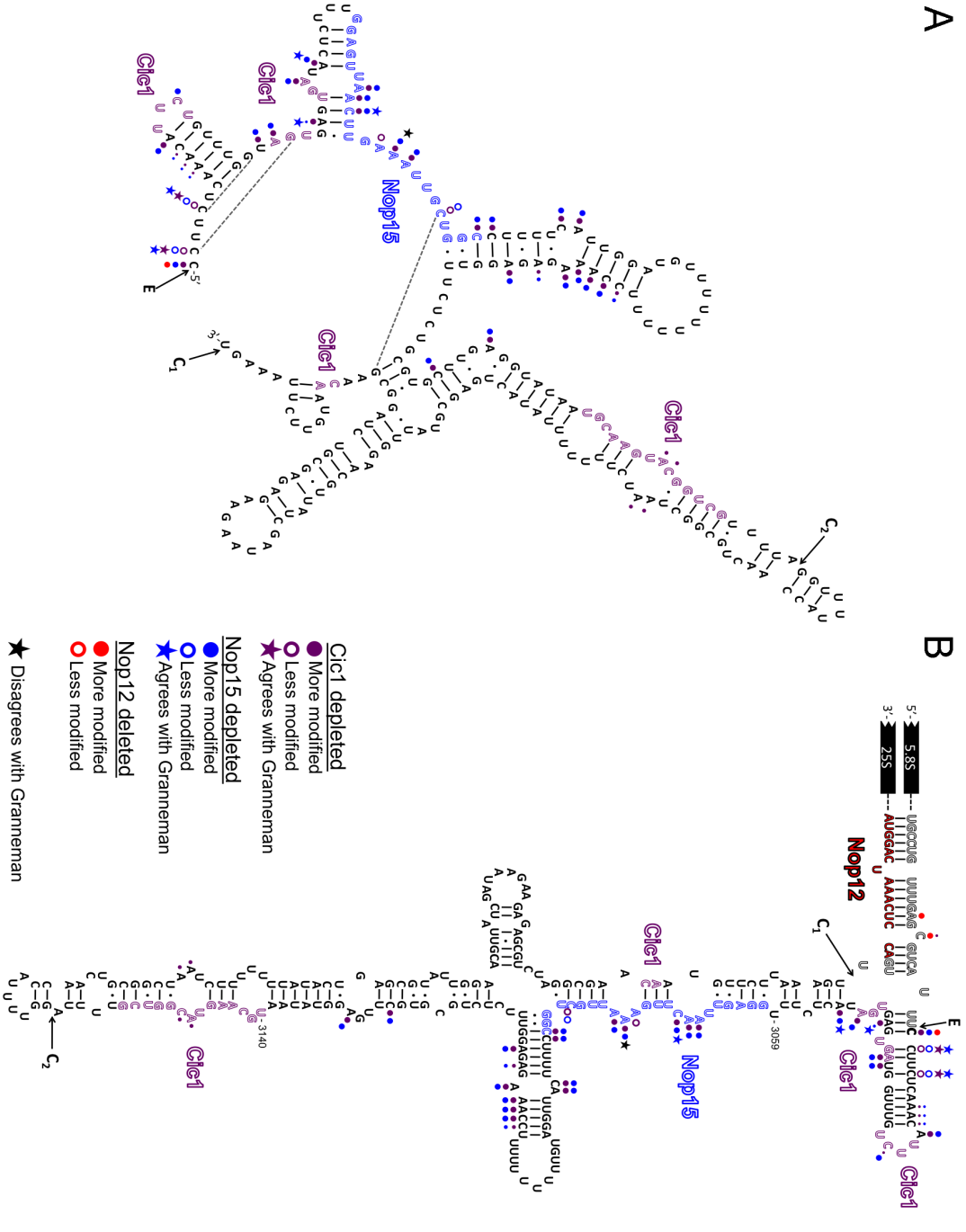

A
B
Nop15
Cic1
Nop12
Cic1 depleted
More modified
Less modified
Agrees with Granneman
Nop15 depleted
More modified
Less modified
Agrees with Granneman
Nop12 deleted
More modified
Less modified
Disagrees with Granneman

Figure 60: Cic1 and Nop15 are required for proper folding of ITS2

Shown are the secondary structures of ITS2 in the ring conformation (A) or the hairpin conformation (B). Differentially modified nucleotides in the absence of Cic1 and Nop15 are indicated with colored circles.

FIGURE 61

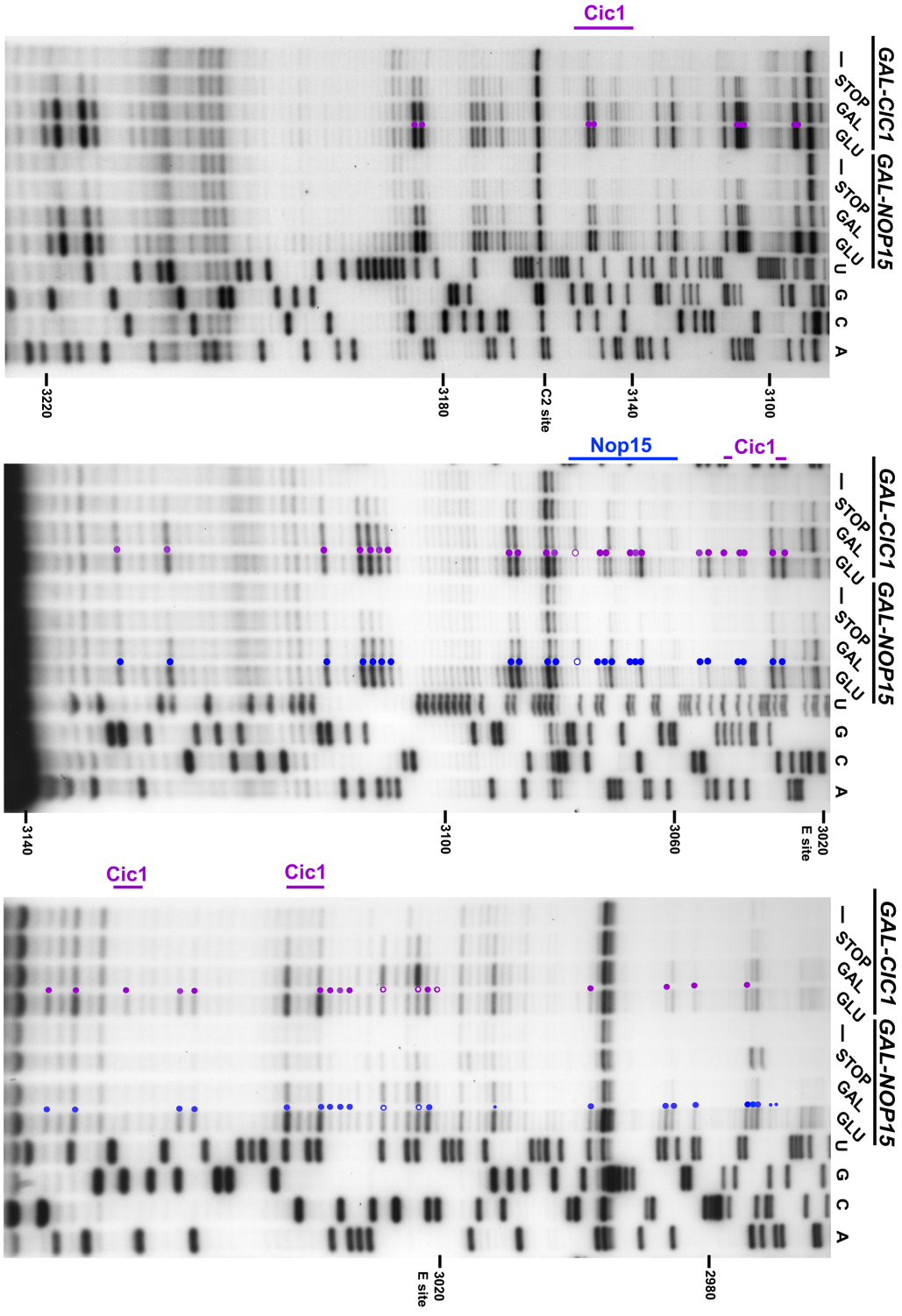

Cic1
GAL-CIC1
GAL-NOP15
— STOP
GAL
GLU
— STOP
GAL
GLU
U
G
C
A
3220
3180
C2 site
3140
3100
Nop15
Cic1
3140
3100
3060
3020
E site
Cic1
Cic1
3020
E site
2980

Figure 61: Cic1 and Nop15 are required for proper folding of ITS2

Shown are differentially modified nucleotides in the absence of Cic1 or Nop15 detected by primer extension and PAGE analysis. Differentially modified nucleotides are indicated as in Figure 60. Nucleotide positions corresponding to 35S pre-rRNA are indicated. Sites in ITS2 that have been previously shown to crosslink to Cic1 and Nop15 are shown.

5.6 Screening for mutations in genes synthetically lethal with *drs1* missense mutants

The assembly factor Nop7 was initially identified in a screen for genes synthetically lethal with *drs1-2* and *drs1-5* mutant alleles (Adams et al., 2002). Subsequently, Nop7 has been shown to interact with Drs1 both physically and functionally (Chapter 3, 3.2.2). These initial screens were not exhaustive and thus to search for other assembly factors that potentially function with, regulate, or are targets of Drs1, I and two undergraduates, Anna Park and Lynley Doonan, performed another screen with these *drs1* mutants. We used an *ade2 ade3 leu2 ura3 drs1*Δ haploid strain containing a *CEN URA3 ADE3 DRS1* plasmid and a *CEN LEU2* plasmid containing the *drs1* allele of interest (ether *drs1-2* or *drs1-5*). Colonies of this strain exhibit red/white sectoring due to partial loss of the *CEN URA3 ADE3 DRS1* plasmid at 30 °C. Cells were plated at a concentration of ~1000 cells/plate and then immediately subjected to a dose of UV irradiation that resulted in a ~15% survival rate. Cells were grown at 30 °C and colonies were screened for the nonsectoring red phenotype. Those colonies that displayed the nonsectoring red phenotype were plated on media containing 5-fluoroorotic acid (5-FOA) to determine if growth depends on the presence of the *CEN URA3 ADE3 DRS1* plasmid.

We screened ~115,000 mutagenized colonies and identified 16 that exhibited the nonsectoring phenotype and failed to grow on 5-FOA. However, upon loss of the *drs1 LEU2* plasmid from these candidates, and subsequent transformation of an unmutagenized *drs1 LYS2,* all of our candidates displayed the sectoring phenotype. This suggests that our initial phenotypes were due to additional mutations in the *drs1 LEU2* plasmid that resulted in nonfunctional Drs1.

5.7 Reducing the heterogeneity of pre-rRNAs for RNA structure probing

As discussed in Chapter 1 (1.6.5), a number of factors make probing the structure of pre-rRNAs *in vivo* a difficult task. This stems from the heterogeneous nature of pre-rRNAs. The first challenge is distinguishing the structure of pre-rRNAs from mature rRNAs. To solve this, we have designed oligonucleotide primers for primer extension that are complementary to the spacer sequences present only in pre-rRNAs. However, these spacers (ITS1 and ITS2) are present in more than one consecutive pre-rRNA intermediate, and thus our structure probing results represent the ensemble structures of all of these intermediates. One approach to purifying specific pre-rRNA intermediates is to use an assembly factor to purify a discrete interval of pre-ribosomal particles. However, due to the nature of the *in vivo* structure probing protocols, purification of assembly intermediates is not feasible after treatment of the cells with DMS and quenching with β-mercaptoethanol.

To address these issues, Jelena Jakovljevic and I have tried two different approaches to reduce the heterogeneity of pre-rRNAs after *in vivo* RNA structure probing and RNA extraction. The first approach we took was to simply run whole-cell RNA (10-100 ug) on agarose gels and cut out the band that represents 27S pre-rRNA (contains $27SA_2$, $27SA_3$, and 27SB pre-rRNAs). This approach is challenging for two reasons. First, because pre-rRNAs are present in much lower quantities than mature rRNAs, they are difficult to see by staining with ethidium bromide or GelStar nucleic acid stain (Lonza). Second, the resolution of our agarose gels only allows us to separate 27S pre-rRNA from 25S rRNA by a few millimeters. We were able to better visualize where 27S pre-rRNA ran on the gel by including on the same gel, pre-rRNAs that were affinity purified using Nop7-TAP. While we were able to enrich for 27S pre-rRNAs by excising the 27S pre-rRNA gel band, we found

that the integrity of our RNA was poor and our samples contained contaminating 25S rRNA. We also tried to "trough" 27S pre-rRNA by running our gels to separate 27S from 25S, cutting a trough in the gel above 27S, and then reversing the current and running 27S into the trough where it could subsequently be removed by pipetting. This greatly improved the integrity of our RNA and we were able to significantly enrich for 27S pre-rRNA, however our samples still contained amounts of 25S rRNA that would prevent further analysis of 27S pre-rRNA structure.

The second approach we tried was based off of protocols developed by the Nilsen laboratory, in which DNA oligonucleotides are splint-ligated onto the ends of RNAs of interest. The protocol relies on the ability of T4 DNA ligase to covalently join a DNA oligonucleotide to the 5' end of RNAs when the two ends are perfectly aligned. The ends are aligned by performing the ligation in the presence of a "bridge" oligonucleotide that hybridizes to both the oligonucleotide and the RNA of interest. Our experimental setup is as follows: 1) Biotin-conjugated DNA oligonucleotides are ligated to the 5' end of pre-rRNAs with the aid of bridge oligonucleotides complementary to the biotin-oligonucleotide and to the RNA of interest. 2) Following ligation, the RNA of interest is affinity-purified using streptavidin-coated beads. 3) The RNA of interest in eluted from the beads by briefly heating the sample to 95 °C to break the streptavidin-biotin interaction. 4) Eluted RNAs are assayed by primer extension, northern blotting, etc.

I designed DNA oligonucleotides of random sequence to be ligated to the 5' ends of $27SA_2$ and $27SA_3$ pre-rRNAs using bridge oligonucleotides complementary to these RNAs. I performed the splint ligations, affinity purifications, and assayed for purified RNAs by northern blotting. My first attempt did not result in obtaining any purified pre-rRNAs. I

think this approach still warrants consideration, but needs to be trouble-shooted more carefully. Before repeating any affinity purifications, I would first see if a ^{32}P-labled oligonucleotide can be splint ligated onto 27S pre-rRNA or 25S rRNA. This would at least allow me to determine if the splint ligation is working.

5.8 Mutational analysis of Drs1

To further characterize the role of Drs1 in ribosome biogenesis, Jelena Jakovljevic and I mutated key residues in the Walker A motif (K68A), Walker B motif (D385A), motif III (S416L), and the Q motif (Q258A), however we only assayed for defects in ribosome biogenesis in the D385A and S416L mutants. Previous studies on other RNA helicases predict that mutation of D385A in the Walker B motif should abolish ATP binding and hydrolysis, and mutation of S416L in motif III should uncouple ATP binding and hydrolysis from helicase activity. Furthermore, previous analysis of these mutations by the Baserga group showed they result in a dominant-negative growth defect when overexpressed in the presence of wild-type Drs1.

Amino acid changes were made by site-directed mutagenesis in a pRS315 plasmid containing *DRS1* (T. Ripmaster, JWB3013) (We used the company Retrogen, Inc). These plasmids were then transformed into the following strains: *GAL-HA-DRS1, GAL-HA-DRS1 NOP7*-TAP, *GAL-HA-DRS1 NOG2-TAP,*and *GAL-HA-DRS1 ARX1-TAP*. Upon depletion of endogenous wild-type Drs1, the effects of the D385A and S416L mutations on particle maturation and pre-rRNA processing were assayed by affinity purifications, northern blotting, and primer extension. In general, many of the defects we observed were largely similar to depletion of Drs1. Analysis of pre-rRNA processing by primer extension revealed a mild accumulation of $27SA_2$ and $27SA_3$ pre-rRNAs and a subsequent decrease in $27SB_S$ (Fig. 62A). SDS-PAGE analysis and silver staining of affinity-purified particles showed accumulation of high-molecular weight proteins similar to that observed upon depletion of Drs1 (Fig. 62B, compare to Fig. 26D). This was especially evident when mutant particles were purified using Nog2-TAP. All of the data and strains generated during this analysis

have been retained in Jelena's notebooks. Frozen stocks of these strains are retained in Jelena's strain box.

The fact that these mutant alleles confer a dominant-negative effect on growth when over expressed suggests these mutant proteins can assemble into particles, however all of our assays revealed phenotypes similar to the depletion of Drs1. One possibility is that these mutant proteins can associate with pre-ribosomes, but upon failure to bind or hydrolyze ATP they are not stably incorporated and fall out of particles. Another, more interesting possibility is that these mutations predicted to abolish ATP binding and hydrolysis block 27SA pre-rRNA processing. Our original analyses of *drs1* missense mutants suggest that the catalytic activity of Drs1 is required for 27SB pre-rRNA processing. These original mutants contained mutations near the conserved motifs for ATP binding and hydrolysis and thus might result in diminished catalytic activity, but not a complete loss of function. This would suggest that complete loss of ATP binding or hydrolysis by Drs1 blocks 27SA processing, whereas diminished activity blocks 27SB pre-rRNA processing. Similar results were seen by Dr. Jill Dembowski of our lab in her characterization of Has1. She found that mutations predicted to block Has1 activity block 27SB pre-rRNA processing, but complete loss of Has1 blocked 27SA pre-rRNA processing .

FIGURE 62

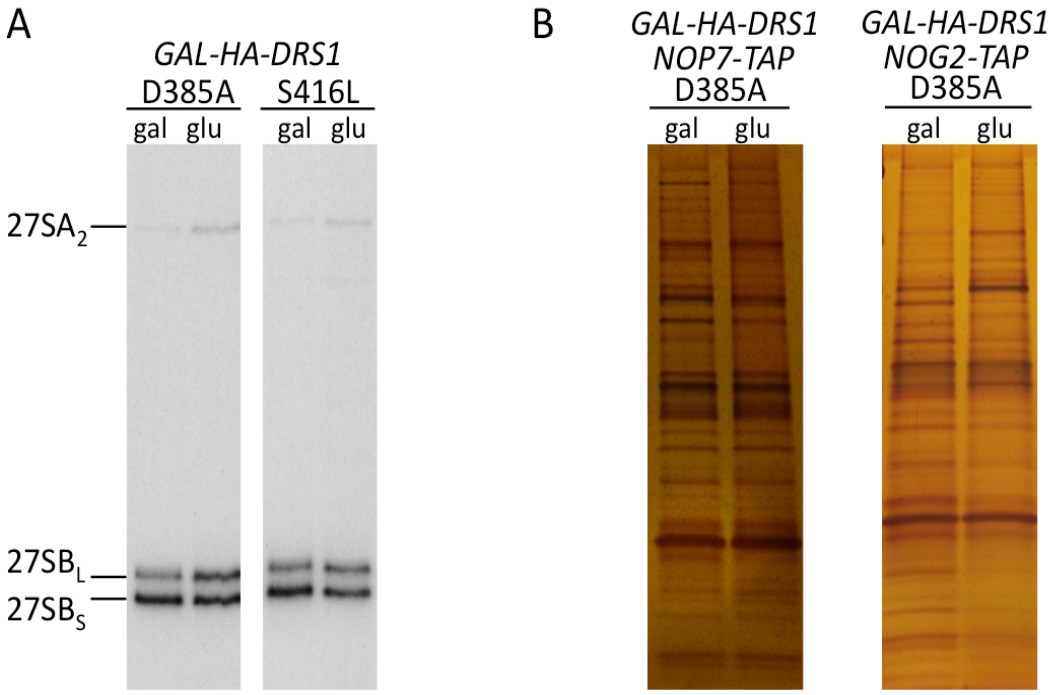
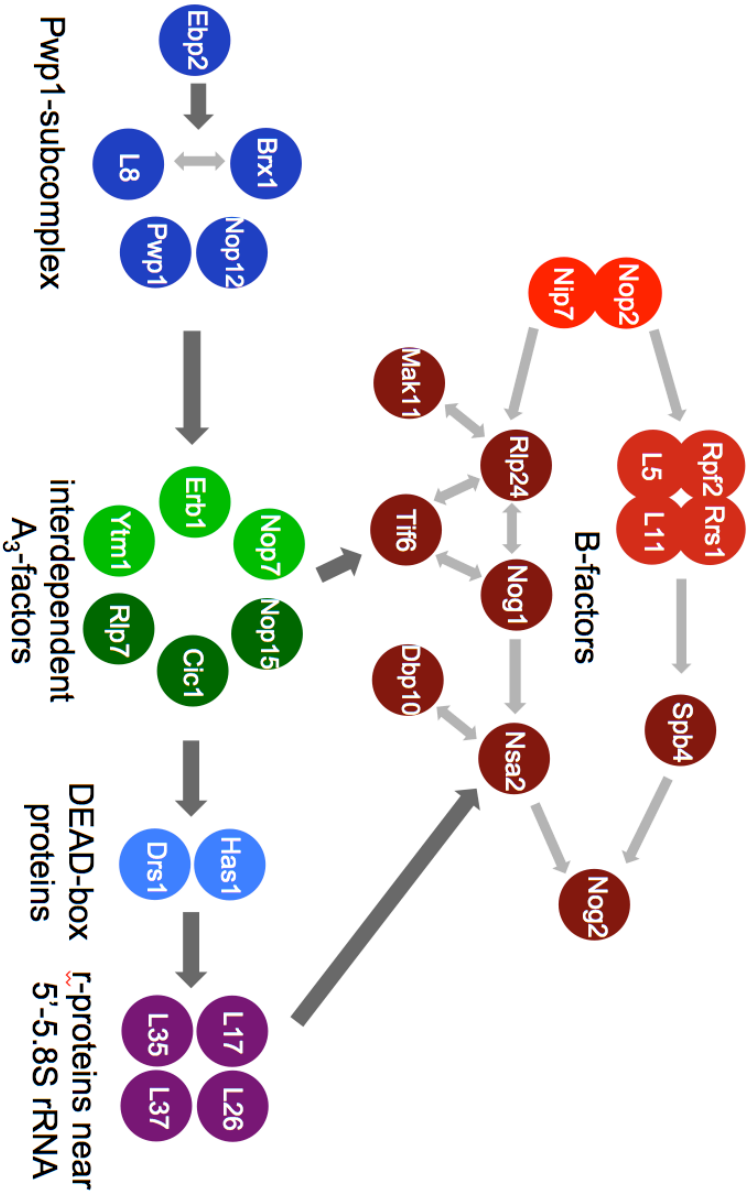

A
GAL-HA-DRS1
D385A
S416L
gal
glu
gal
glu
27SA2
27SBL
27SBS
B
GAL-HA-DRS1
NOP7-TAP
D385A
gal
glu
GAL-HA-DRS1
NOG2-TAP
D385A
gal
glu

Figure 62: Catalytically inactive *drs1* mutants block 27SA pre-rRNA processing

Representative data showing that the D385A and S416L *drs1* mutants block 27SA pre-rRNA processing (A) and cause the accumulation of high-molecular weight proteins in purified pre-ribosomes (B). The accumulation of high molecular weight proteins is most evident when pre-ribosomes are purified using Nog2-TAP.

5.9 Association hierarchy of proteins that function in 27S pre-rRNA processing

FIGURE 63



References

Adams, C.C., Jakovljevic, J., Roman, J., Harnpicharnchai, P., and Woolford, J.L., Jr. 2002. Saccharomyces cerevisiae nucleolar protein Nop7p is necessary for biogenesis of 60S ribosomal subunits. *RNA* **8**(2): 150-165.

Adams, P.L., Stahley, M.R., Gill, M.L., Kosek, A.B., Wang, J., and Strobel, S.A. 2004. Crystal structure of a group I intron splicing intermediate. *RNA* **10**(12): 1867-1887.

Adilakshmi, T., Bellur, D.L., and Woodson, S.A. 2008. Concurrent nucleation of 16S folding and induced fit in 30S ribosome assembly. *Nature* **455**(7217): 1268-1272.

Adilakshmi, T., Lease, R.A., and Woodson, S.A. 2006. Hydroxyl radical footprinting in vivo: mapping macromolecular structures with synchrotron radiation. *Nucleic Acids Res* **34**(8): e64.

Adilakshmi, T., Ramaswamy, P., and Woodson, S.A. 2005. Protein-independent folding pathway of the 16S rRNA 5' domain. *J Mol Biol* **351**(3): 508-519.

Agalarov, S.C., Selivanova, O.M., Zheleznyakova, E.N., Zheleznaya, L.A., Matvienko, N.I., and Spirin, A.S. 1999. Independent in vitro assembly of all three major morphological parts of the 30S ribosomal subunit of Thermus thermophilus. *Eur J Biochem* **266**(2): 533-537.

Anfinsen, C.B. 1973. Principles that govern the folding of protein chains. *Science* **181**(4096): 223-230.

Anfinsen, C.B., Haber, E., Sela, M., and White, F.H., Jr. 1961. The kinetics of formation of native ribonuclease during oxidation of the reduced polypeptide chain. *Proc Natl Acad Sci U S A* **47**: 1309-1314.

Anger, A.M., Armache, J.P., Berninghausen, O., Habeck, M., Subklewe, M., Wilson, D.N., and Beckmann, R. 2013. Structures of the human and Drosophila 80S ribosome. *Nature* **497**(7447): 80-85.

Armache, J.P., Jarasch, A., Anger, A.M., Villa, E., Becker, T., Bhushan, S., Jossinet, F., Habeck, M., Dindar, G., Franckenberg, S. et al. 2010a. Cryo-EM structure and rRNA model of a translating eukaryotic 80S ribosome at 5.5-A resolution. *Proc Natl Acad Sci U S A* **107**(46): 19748-19753.

-. 2010b. Localization of eukaryote-specific ribosomal proteins in a 5.5-A cryo-EM map of the 80S eukaryotic ribosome. *Proc Natl Acad Sci U S A* **107**(46): 19754-19759.

Ausubel, F.M., Brent, R., Kingston, R.E., Moore, D.D., Seidman, J.G., Smith, J.A., and Struhl, K. 1994. *Current protocols in molecular biology*. Wiley, New York.

Babiano, R., Badis, G., Saveanu, C., Namane, A., Doyen, A., Diaz-Quintana, A., Jacquier, A., Fromont-Racine, M., and de la Cruz, J. 2013. Yeast ribosomal protein L7 and its homologue Rlp7 are simultaneously present at distinct sites on pre-60S ribosomal particles. *Nucleic Acids Res*.

Babiano, R., Gamalinda, M., Woolford, J.L., Jr., and de la Cruz, J. 2012. Saccharomyces cerevisiae Ribosomal Protein L26 Is Not Essential for Ribosome Assembly and Function. *Mol Cell Biol* **32**(16): 3228-3241.

Ban, N., Nissen, P., Hansen, J., Moore, P.B., and Steitz, T.A. 2000. The complete atomic structure of the large ribosomal subunit at 2.4 A resolution. *Science* **289**(5481): 905-920.

Bassler, J., Grandi, P., Gadal, O., Lessmann, T., Petfalski, E., Tollervey, D., Lechner, J., and Hurt, E. 2001. Identification of a 60S preribosomal particle that is closely linked to nuclear export. *Mol Cell* **8**(3): 517-529.

Bassler, J., Kallas, M., Pertschy, B., Ulbrich, C., Thoms, M., and Hurt, E. 2010. The AAA-ATPase Rea1 drives removal of biogenesis factors during multiple stages of 60S ribosome assembly. *Mol Cell* **38**(5): 712-721.

Basu, U., Si, K., Warner, J.R., and Maitra, U. 2001. The Saccharomyces cerevisiae TIF6 gene encoding translation initiation factor 6 is required for 60S ribosomal subunit biogenesis. *Mol Cell Biol* **21**(5): 1453-1462.

Baudin, F., Ehresmann, C., Romby, P., Mougel, M., Colin, J., Lempereur, L., Bachellerie, J.P., Ebel, J.P., and Ehresmann, B. 1987. Higher-order structure of domain III in Escherichia coli 16S ribosomal RNA, 30S subunit and 70S ribosome. *Biochimie* **69**(10): 1081-1096.

Beltrame, M., Henry, Y., and Tollervey, D. 1994. Mutational analysis of an essential binding site for the U3 snoRNA in the 5' external transcribed spacer of yeast pre-rRNA. *Nucleic Acids Res* **22**(20): 4057-4065.

Ben-Shem, A., Garreau de Loubresse, N., Melnikov, S., Jenner, L., Yusupova, G., and Yusupov, M. 2011. The structure of the eukaryotic ribosome at 3.0 A resolution. *Science* **334**(6062): 1524-1529.

Benjamini, Y., Drai, D., Elmer, G., Kafkafi, N., and Golani, I. 2001. Controlling the false discovery rate in behavior genetics research. *Behav Brain Res* **125**(1-2): 279-284.

Berges, T., Petfalski, E., Tollervey, D., and Hurt, E.C. 1994. Synthetic lethality with fibrillarin identifies NOP77p, a nucleolar protein required for pre-rRNA processing and modification. *EMBO J* **13**(13): 3136-3148.

Berman, H.M., Westbrook, J., Feng, Z., Gilliland, G., Bhat, T.N., Weissig, H., Shindyalov, I.N., and Bourne, P.E. 2000. The Protein Data Bank. *Nucleic Acids Res* **28**(1): 235-242.

Bleichert, F. and Baserga, S.J. 2007. The long unwinding road of RNA helicases. *Mol Cell* **27**(3): 339-352.

Bohnsack, M.T., Kos, M., and Tollervey, D. 2008. Quantitative analysis of snoRNA association with pre-ribosomes and release of snR30 by Rok1 helicase. *EMBO Rep* **9**(12): 1230-1236.

Bohnsack, M.T., Martin, R., Granneman, S., Ruprecht, M., Schleiff, E., and Tollervey, D. 2009. Prp43 bound at different sites on the pre-rRNA performs distinct functions in ribosome synthesis. *Mol Cell* **36**(4): 583-592.

Brenowitz, M., Chance, M.R., Dhavan, G., and Takamoto, K. 2002. Probing the structural dynamics of nucleic acids by quantitative time-resolved and equilibrium hydroxyl radical "footprinting". *Curr Opin Struct Biol* **12**(5): 648-653.

Brink, M.F., Verbeet, M.P., and de Boer, H.A. 1993. Formation of the central pseudoknot in 16S rRNA is essential for initiation of translation. *EMBO J* **12**(10): 3987-3996.

Brion, P. and Westhof, E. 1997. Hierarchy and dynamics of RNA folding. *Annu Rev Biophys Biomol Struct* **26**: 113-137.

Brunel, C. and Romby, P. 2000. Probing RNA structure and RNA-ligand complexes with chemical probes. *Methods Enzymol* **318**: 3-21.

Buchmueller, K.L., Webb, A.E., Richardson, D.A., and Weeks, K.M. 2000. A collapsed non-native RNA folding state. *Nat Struct Biol* **7**(5): 362-366.

Buratti, E. and Baralle, F.E. 2004. Influence of RNA secondary structure on the pre-mRNA splicing process. *Mol Cell Biol* **24**(24): 10505-10514.

Burger, F., Daugeron, M.C., and Linder, P. 2000. Dbp10p, a putative RNA helicase from Saccharomyces cerevisiae, is required for ribosome biogenesis. *Nucleic Acids Res* **28**(12): 2315-2323.

Bussiere, C., Hashem, Y., Arora, S., Frank, J., and Johnson, A.W. 2012. Integrity of the P-site is probed during maturation of the 60S ribosomal subunit. *J Cell Biol* **197**(6): 747-759.

Butcher, S.E. and Pyle, A.M. 2011. The molecular interactions that stabilize RNA tertiary structure: RNA motifs, patterns, and networks. *Acc Chem Res* **44**(12): 1302-1311.

Cannone, J.J., Subramanian, S., Schnare, M.N., Collett, J.R., D'Souza, L.M., Du, Y., Feng, B., Lin, N., Madabusi, L.V., Muller, K.M. et al. 2002. The comparative RNA web (CRW) site: an online database of comparative sequence and structure information for ribosomal, intron, and other RNAs. *BMC Bioinformatics* **3**: 2.

Cardenas, M.E., Cutler, N.S., Lorenz, M.C., Di Como, C.J., and Heitman, J. 1999. The TOR signaling cascade regulates gene expression in response to nutrients. *Genes Dev* **13**(24): 3271-3279.

Cate, J.H., Gooding, A.R., Podell, E., Zhou, K., Golden, B.L., Kundrot, C.E., Cech, T.R., and Doudna, J.A. 1996. Crystal structure of a group I ribozyme domain: principles of RNA packing. *Science* **273**(5282): 1678-1685.

Chang, K.Y. and Tinoco, I., Jr. 1994. Characterization of a "kissing" hairpin complex derived from the human immunodeficiency virus genome. *Proc Natl Acad Sci U S A* **91**(18): 8705-8709.

Chauhan, S., Behrouzi, R., Rangan, P., and Woodson, S.A. 2009. Structural rearrangements linked to global folding pathways of the Azoarcus group I ribozyme. *J Mol Biol* **386**(4): 1167-1178.

Chauhan, S., Caliskan, G., Briber, R.M., Perez-Salas, U., Rangan, P., Thirumalai, D., and Woodson, S.A. 2005. RNA tertiary interactions mediate native collapse of a bacterial group I ribozyme. *J Mol Biol* **353**(5): 1199-1209.

Chauhan, S. and Woodson, S.A. 2008. Tertiary interactions determine the accuracy of RNA folding. *J Am Chem Soc* **130**(4): 1296-1303.

Chu, S., Archer, R.H., Zengel, J.M., and Lindahl, L. 1994. The RNA of RNase MRP is required for normal processing of ribosomal RNA. *Proc Natl Acad Sci U S A* **91**(2): 659-663.

Claypool, J.A., French, S.L., Johzuka, K., Eliason, K., Vu, L., Dodd, J.A., Beyer, A.L., and Nomura, M. 2004. Tor pathway regulates Rrn3p-dependent recruitment of yeast RNA polymerase I to the promoter but does not participate in alteration of the number of active genes. *Mol Biol Cell* **15**(2): 946-956.

Costa, M. and Michel, F. 1997. Rules for RNA recognition of GNRA tetraloops deduced by in vitro selection: comparison with in vivo evolution. *EMBO J* **16**(11): 3289-3302.

Costanzo, M., Baryshnikova, A., Bellay, J., Kim, Y., Spear, E.D., Sevier, C.S., Ding, H., Koh, J.L., Toufighi, K., Mostafavi, S. et al. 2010. The genetic landscape of a cell. *Science* **327**(5964): 425-431.

Cote, C.A., Greer, C.L., and Peculis, B.A. 2002. Dynamic conformational model for the role of ITS2 in pre-rRNA processing in yeast. *RNA* **8**(6): 786-797.

Craig, M.E., Crothers, D.M., and Doty, P. 1971. Relaxation kinetics of dimer formation by self complementary oligonucleotides. *J Mol Biol* **62**(2): 383-401.

Crespo, J.L. and Hall, M.N. 2002. Elucidating TOR signaling and rapamycin action: lessons from Saccharomyces cerevisiae. *Microbiol Mol Biol Rev* **66**(4): 579-591, table of contents.

Culver, G.M. 2003. Assembly of the 30S ribosomal subunit. *Biopolymers* **68**(2): 234-249.

Dammel, C.S. and Noller, H.F. 1993. A cold-sensitive mutation in 16S rRNA provides evidence for helical switching in ribosome assembly. *Genes Dev* **7**(4): 660-670.

Das, R., Kwok, L.W., Millett, I.S., Bai, Y., Mills, T.T., Jacob, J., Maskel, G.S., Seifert, S., Mochrie, S.G., Thiyagarajan, P. et al. 2003. The fastest global events in RNA folding: electrostatic relaxation and tertiary collapse of the Tetrahymena ribozyme. *J Mol Biol* **332**(2): 311-319.

Das, R., Laederach, A., Pearlman, S.M., Herschlag, D., and Altman, R.B. 2005. SAFA: semi-automated footprinting analysis software for high-throughput quantification of nucleic acid footprinting experiments. *RNA* **11**(3): 344-354.

de la Cruz, J., Kressler, D., Rojo, M., Tollervey, D., and Linder, P. 1998. Spb4p, an essential putative RNA helicase, is required for a late step in the assembly of 60S ribosomal subunits in Saccharomyces cerevisiae. *RNA* **4**(10): 1268-1281.

Deigan, K.E., Li, T.W., Mathews, D.H., and Weeks, K.M. 2009. Accurate SHAPE-directed RNA structure determination. *Proc Natl Acad Sci U S A* **106**(1): 97-102.

Dembowski, J.A., Kuo, B., and Woolford, J.L., Jr. 2013. Has1 regulates consecutive maturation and processing steps for assembly of 60S ribosomal subunits. *Nucleic Acids Res*.

Deshmukh, M., Tsay, Y.F., Paulovich, A.G., and Woolford, J.L., Jr. 1993. Yeast ribosomal protein L1 is required for the stability of newly synthesized 5S rRNA and the assembly of 60S ribosomal subunits. *Mol Cell Biol* **13**(5): 2835-2845.

Dez, C., Froment, C., Noaillac-Depeyre, J., Monsarrat, B., Caizergues-Ferrer, M., and Henry, Y. 2004. Npa1p, a component of very early pre-60S ribosomal particles, associates with a subset of small nucleolar RNPs required for peptidyl transferase center modification. *Mol Cell Biol* **24**(14): 6324-6337.

Dill, K.A. and Chan, H.S. 1997. From Levinthal to pathways to funnels. *Nat Struct Biol* **4**(1): 10-19.

Djebali, S., Davis, C.A., Merkel, A., Dobin, A., Lassmann, T., Mortazavi, A., Tanzer, A., Lagarde, J., Lin, W., Schlesinger, F. et al. 2012. Landscape of transcription in human cells. *Nature* **489**(7414): 101-108.

Dosil, M. and Bustelo, X.R. 2004. Functional characterization of Pwp2, a WD family protein essential for the assembly of the 90 S pre-ribosomal particle. *J Biol Chem* **279**(36): 37385-37397.

Dragon, F., Gallagher, J.E., Compagnone-Post, P.A., Mitchell, B.M., Porwancher, K.A., Wehner, K.A., Wormsley, S., Settlage, R.E., Shabanowitz, J., Osheim, Y. et al. 2002. A large nucleolar U3 ribonucleoprotein required for 18S ribosomal RNA biogenesis. *Nature* **417**(6892): 967-970.

Draper, D.E., Grilley, D., and Soto, A.M. 2005. Ions and RNA folding. *Annu Rev Biophys Biomol Struct* **34**: 221-243.

Dunbar, D.A., Dragon, F., Lee, S.J., and Baserga, S.J. 2000. A nucleolar protein related to ribosomal protein L7 is required for an early step in large ribosomal subunit biogenesis. *Proc Natl Acad Sci U S A* **97**(24): 13027-13032.

Duronio, R.J., Gordon, J.I., and Boguski, M.S. 1992. Comparative analysis of the beta transducin family with identification of several new members including PWP1, a nonessential gene of Saccharomyces cerevisiae that is divergently transcribed from NMT1. *Proteins* **13**(1): 41-56.

Dutca, L.M., Gallagher, J.E., and Baserga, S.J. 2011. The initial U3 snoRNA:pre-rRNA base pairing interaction required for pre-18S rRNA folding revealed by in vivo chemical probing. *Nucleic Acids Res* **39**(12): 5164-5180.

Ehresmann, C., Baudin, F., Mougel, M., Romby, P., Ebel, J.P., and Ehresmann, B. 1987. Probing the structure of RNAs in solution. *Nucleic Acids Res* **15**(22): 9109-9128.

El Hage, A., French, S.L., Beyer, A.L., and Tollervey, D. 2010. Loss of Topoisomerase I leads to R-loop-mediated transcriptional blocks during ribosomal RNA synthesis. *Genes Dev* **24**(14): 1546-1558.

Emery, B., de la Cruz, J., Rocak, S., Deloche, O., and Linder, P. 2004. Has1p, a member of the DEAD-box family, is required for 40S ribosomal subunit biogenesis in Saccharomyces cerevisiae. *Mol Microbiol* **52**(1): 141-158.

Fabian, G.R. and Hopper, A.K. 1987. RRP1, a Saccharomyces cerevisiae gene affecting rRNA processing and production of mature ribosomal subunits. *J Bacteriol* **169**(4): 1571-1578.

Fatica, A., Cronshaw, A.D., Dlakic, M., and Tollervey, D. 2002. Ssf1p prevents premature processing of an early pre-60S ribosomal particle. *Mol Cell* **9**(2): 341-351.

Fatica, A., Oeffinger, M., Dlakic, M., and Tollervey, D. 2003a. Nob1p is required for cleavage of the 3' end of 18S rRNA. *Mol Cell Biol* **23**(5): 1798-1807.

Fatica, A., Oeffinger, M., Tollervey, D., and Bozzoni, I. 2003b. Cic1p/Nsa3p is required for synthesis and nuclear export of 60S ribosomal subunits. *RNA* **9**(12): 1431-1436.

Ferre-D'Amare, A.R., Zhou, K., and Doudna, J.A. 1998. Crystal structure of a hepatitis delta virus ribozyme. *Nature* **395**(6702): 567-574.

Ferreira-Cerca, S., Poll, G., Gleizes, P.E., Tschochner, H., and Milkereit, P. 2005. Roles of eukaryotic ribosomal proteins in maturation and transport of pre-18S rRNA and ribosome function. *Mol Cell* **20**(2): 263-275.

Ferreira-Cerca, S., Poll, G., Kuhn, H., Neueder, A., Jakob, S., Tschochner, H., and Milkereit, P. 2007. Analysis of the in vivo assembly pathway of eukaryotic 40S ribosomal proteins. *Mol Cell* **28**(3): 446-457.

Freed, E.F., Bleichert, F., Dutca, L.M., and Baserga, S.J. 2010. When ribosomes go bad: diseases of ribosome biogenesis. *Mol Biosyst* **6**(3): 481-493.

Freier, S.M., Kierzek, R., Jaeger, J.A., Sugimoto, N., Caruthers, M.H., Neilson, T., and Turner, D.H. 1986. Improved free-energy parameters for predictions of RNA duplex stability. *Proc Natl Acad Sci U S A* **83**(24): 9373-9377.

Gadal, O., Strauss, D., Petfalski, E., Gleizes, P.E., Gas, N., Tollervey, D., and Hurt, E. 2002. Rlp7p is associated with 60S preribosomes, restricted to the granular component of the nucleolus, and required for pre-rRNA processing. *J Cell Biol* **157**(6): 941-951.

Gallagher, J.E., Dunbar, D.A., Granneman, S., Mitchell, B.M., Osheim, Y., Beyer, A.L., and Baserga, S.J. 2004. RNA polymerase I transcription and pre-rRNA processing are linked by specific SSU processome components. *Genes Dev* **18**(20): 2506-2517.

Gamalinda, M., Jakovljevic, J., Babiano, R., Talkish, J., de la Cruz, J., and Woolford, J.L., Jr. 2013. Yeast polypeptide exit tunnel ribosomal proteins L17, L35 and L37 are necessary to recruit late-assembling factors required for 27SB pre-rRNA processing. *Nucleic Acids Res*.

Garcia-Gomez, J.J., Lebaron, S., Froment, C., Monsarrat, B., Henry, Y., and de la Cruz, J. 2011. Dynamics of the putative RNA helicase Spb4 during ribosome assembly in Saccharomyces cerevisiae. *Mol Cell Biol* **31**(20): 4156-4164.

Gartmann, M., Blau, M., Armache, J.P., Mielke, T., Topf, M., and Beckmann, R. 2010. Mechanism of eIF6-mediated inhibition of ribosomal subunit joining. *J Biol Chem* **285**(20): 14848-14851.

Geerlings, T.H., Vos, J.C., and Raue, H.A. 2000. The final step in the formation of 25S rRNA in Saccharomyces cerevisiae is performed by 5'-->3' exonucleases. *RNA* **6**(12): 1698-1703.

Giaever, G., Chu, A.M., Ni, L., Connelly, C., Riles, L., Veronneau, S., Dow, S., Lucau-Danila, A., Anderson, K., Andre, B. et al. 2002. Functional profiling of the Saccharomyces cerevisiae genome. *Nature* **418**(6896): 387-391.

Graindorge, J.S., Rousselle, J.C., Senger, B., Lenormand, P., Namane, A., Lacroute, F., and Fasiolo, F. 2005. Deletion of EFL1 results in heterogeneity of the 60 S GTPase-associated rRNA conformation. *J Mol Biol* **352**(2): 355-369.

Granato, D.C., Machado-Santelli, G.M., and Oliveira, C.C. 2008. Nop53p interacts with 5.8S rRNA co-transcriptionally, and regulates processing of pre-rRNA by the exosome. *FEBS J* **275**(16): 4164-4178.

Granneman, S., Gallagher, J.E., Vogelzangs, J., Horstman, W., van Venrooij, W.J., Baserga, S.J., and Pruijn, G.J. 2003. The human Imp3 and Imp4 proteins form a ternary complex with hMpp10, which only interacts with the U3 snoRNA in 60-80S ribonucleoprotein complexes. *Nucleic Acids Res* **31**(7): 1877-1887.

Granneman, S., Petfalski, E., Swiatkowska, A., and Tollervey, D. 2010. Cracking pre-40S ribosomal subunit structure by systematic analyses of RNA-protein cross-linking. *EMBO J* **29**(12): 2026-2036.

Granneman, S., Petfalski, E., and Tollervey, D. 2011. A cluster of ribosome synthesis factors regulate pre-rRNA folding and 5.8S rRNA maturation by the Rat1 exonuclease. *EMBO J* **30**(19): 4006-4019.

Groeneveld, H., Thimon, K., and van Duin, J. 1995. Translational control of maturation-protein synthesis in phage MS2: a role for the kinetics of RNA folding? *RNA* **1**(1): 79-88.

Guthrie, C., Nashimoto, H., and Nomura, M. 1969. Structure and function of E. coli ribosomes. 8. Cold-sensitive mutants defective in ribosome assembly. *Proc Natl Acad Sci U S A* **63**(2): 384-391.

Halic, M., Becker, T., Pool, M.R., Spahn, C.M., Grassucci, R.A., Frank, J., and Beckmann, R. 2004. Structure of the signal recognition particle interacting with the elongation-arrested ribosome. *Nature* **427**(6977): 808-814.

Harnpicharnchai, P., Jakovljevic, J., Horsey, E., Miles, T., Roman, J., Rout, M., Meagher, D., Imai, B., Guo, Y., Brame, C.J. et al. 2001. Composition and functional characterization of yeast 66S ribosome assembly intermediates. *Mol Cell* **8**(3): 505-515.

Held, W.A., Mizushima, S., and Nomura, M. 1973. Reconstitution of Escherichia coli 30 S ribosomal subunits from purified molecular components. *J Biol Chem* **248**(16): 5720-5730.

Helser, T.L., Baan, R.A., and Dahlberg, A.E. 1981. Characterization of a 40S ribosomal subunit complex in polyribosomes of Saccharomyces cerevisiae treated with cycloheximide. *Mol Cell Biol* **1**(1): 51-57.

Henras, A.K., Soudet, J., Gerus, M., Lebaron, S., Caizergues-Ferrer, M., Mougin, A., and Henry, Y. 2008. The post-transcriptional steps of eukaryotic ribosome biogenesis. *Cell Mol Life Sci* **65**(15): 2334-2359.

Henry, Y., Wood, H., Morrissey, J.P., Petfalski, E., Kearsey, S., and Tollervey, D. 1994. The 5' end of yeast 5.8S rRNA is generated by exonucleases from an upstream cleavage site. *EMBO J* **13**(10): 2452-2463.

Hierlmeier, T., Merl, J., Sauert, M., Perez-Fernandez, J., Schultz, P., Bruckmann, A., Hamperl, S., Ohmayer, U., Rachel, R., Jacob, A. et al. 2012. Rrp5p, Noc1p and Noc2p form a protein module which is part of early large ribosomal subunit precursors in S. cerevisiae. *Nucleic Acids Res*.

Holbrook, S.R. 2008. Structural principles from large RNAs. *Annu Rev Biophys* **37**: 445-464.

Holmes, K.L. and Culver, G.M. 2005. Analysis of conformational changes in 16 S rRNA during the course of 30 S subunit assembly. *J Mol Biol* **354**(2): 340-357.

Holzel, M., Rohrmoser, M., Schlee, M., Grimm, T., Harasim, T., Malamoussi, A., Gruber-Eber, A., Kremmer, E., Hiddemann, W., Bornkamm, G.W. et al. 2005. Mammalian WDR12 is a novel member of the Pes1-Bop1 complex and is required for ribosome biogenesis and cell proliferation. *J Cell Biol* **170**(3): 367-378.

Hong, B., Brockenbrough, J.S., Wu, P., and Aris, J.P. 1997. Nop2p is required for pre-rRNA processing and 60S ribosome subunit synthesis in yeast. *Mol Cell Biol* **17**(1): 378-388.

Honma, Y., Kitamura, A., Shioda, R., Maruyama, H., Ozaki, K., Oda, Y., Mini, T., Jeno, P., Maki, Y., Yonezawa, K. et al. 2006. TOR regulates late steps of ribosome maturation in the nucleoplasm via Nog1 in response to nutrients. *EMBO J* **25**(16): 3832-3842.

Horsey, E.W., Jakovljevic, J., Miles, T.D., Harnpicharnchai, P., and Woolford, J.L., Jr. 2004. Role of the yeast Rrp1 protein in the dynamics of pre-ribosome maturation. *RNA* **10**(5): 813-827.

Huber,A., Bodenmiller, B., Uotila, A., Stahl, M., Wanka, S., Gerrits, B., Aebersold, R., and Loewith, R. 2009. Characterization of the rapamycin-sensitive phosphoproteome reveals that Sch9 is a central coordinator of protein synthesis. *Genes Dev* **23**(16): 1929-1943.

Hughes, J.M. 1996. Functional base-pairing interaction between highly conserved elements of U3 small nucleolar RNA and the small ribosomal subunit RNA. *J Mol Biol* **259**(4): 645-654.

Hughes, J.M. and Ares, M., Jr. 1991. Depletion of U3 small nucleolar RNA inhibits cleavage in the 5' external transcribed spacer of yeast pre-ribosomal RNA and impairs formation of 18S ribosomal RNA. *EMBO J* **10**(13): 4231-4239.

Ingolia, N.T., Brar, G.A., Rouskin, S., McGeachy, A.M., and Weissman, J.S. 2012. The ribosome profiling strategy for monitoring translation in vivo by deep sequencing of ribosome-protected mRNA fragments. *Nat Protoc* **7**(8): 1534-1550.

Jakovljevic, J., Gamalinda, M., Talkish, J., Alexander, L., Linneman, J., Milkereit, P., and Woolford, J.L., Jr. 2012. Ribosomal proteins L7 and L8 function in concert with six A3 assembly factors to propagate assembly of domain I of 25S rRNA in yeast 60S ribosomal subunits. *RNA* **18**: 1805-1822.

Jiang, M., Sullivan, S.M., Walker, A.K., Strahler, J.R., Andrews, P.C., and Maddock, J.R. 2007. Identification of novel Escherichia coli ribosome-associated proteins using isobaric tags and multidimensional protein identification techniques. *J Bacteriol* **189**(9): 3434-3444.

Jorgensen, P., Nishikawa, J.L., Breitkreutz, B.J., and Tyers, M. 2002. Systematic identification of pathways that couple cell growth and division in yeast. *Science* **297**(5580): 395-400.

Jorgensen, P., Rupes, I., Sharom, J.R., Schneper, L., Broach, J.R., and Tyers, M. 2004. A dynamic transcriptional network communicates growth potential to ribosome synthesis and critical cell size. *Genes Dev* **18**(20): 2491-2505.

Joseph, N., Krauskopf, E., Vera, M.I., and Michot, B. 1999. Ribosomal internal transcribed spacer 2 (ITS2) exhibits a common core of secondary structure in vertebrates and yeast. *Nucleic Acids Res* **27**(23): 4533-4540.

Ju, Q. and Warner, J.R. 1994. Ribosome synthesis during the growth cycle of Saccharomyces cerevisiae. *Yeast* **10**(2): 151-157.

Kallstrom, G., Hedges, J., and Johnson, A. 2003. The putative GTPases Nog1p and Lsg1p are required for 60S ribosomal subunit biogenesis and are localized to the nucleus and cytoplasm, respectively. *Mol Cell Biol* **23**(12): 4344-4355.

Karbstein, K. 2007. Role of GTPases in ribosome assembly. *Biopolymers* **87**(1): 1-11.

-. 2011. Inside the 40S ribosome assembly machinery. *Curr Opin Chem Biol* **15**(5): 657-663.

Karbstein, K. and Doudna, J.A. 2006. GTP-dependent formation of a ribonucleoprotein subcomplex required for ribosome biogenesis. *J Mol Biol* **356**(2): 432-443.

Kean, J.M. and Draper, D.E. 1985. Secondary structure of a 345-base RNA fragment covering the S8/S15 protein binding domain of Escherichia coli 16S ribosomal RNA. *Biochemistry* **24**(19): 5052-5061.

Kertesz, M., Wan, Y., Mazor, E., Rinn, J.L., Nutter, R.C., Chang, H.Y., and Segal, E. 2010. Genome-wide measurement of RNA secondary structure in yeast. *Nature* **467**(7311): 103-107.

Kim, S.H., Suddath, F.L., Quigley, G.J., McPherson, A., Sussman, J.L., Wang, A.H., Seeman, N.C., and Rich, A. 1974. Three-dimensional tertiary structure of yeast phenylalanine transfer RNA. *Science* **185**(4149): 435-440.

Klein, D.J., Schmeing, T.M., Moore, P.B., and Steitz, T.A. 2001. The kink-turn: a new RNA secondary structure motif. *EMBO J* **20**(15): 4214-4221.

Kos, M. and Tollervey, D. 2005. The Putative RNA Helicase Dbp4p Is Required for Release of the U14 snoRNA from Preribosomes in Saccharomyces cerevisiae. *Mol Cell* **20**(1): 53-64.

-. 2010. Yeast pre-rRNA processing and modification occur cotranscriptionally. *Mol Cell* **37**(6): 809-820.

Kressler, D., Hurt, E., and Bassler, J. 2010. Driving ribosome assembly. *Biochim Biophys Acta* **1803**(6): 673-683.

Kressler, D., Hurt, E., Bergler, H., and Bassler, J. 2011. The power of AAA-ATPases on the road of pre-60S ribosome maturation--molecular machines that strip pre-ribosomal particles. *Biochim Biophys Acta* **1823**(1): 92-100.

Kressler, D., Linder, P., and de La Cruz, J. 1999. Protein trans-acting factors involved in ribosome biogenesis in Saccharomyces cerevisiae. *Mol Cell Biol* **19**(12): 7897-7912.

Kressler, D., Roser, D., Pertschy, B., and Hurt, E. 2008. The AAA ATPase Rix7 powers progression of ribosome biogenesis by stripping Nsa1 from pre-60S particles. *J Cell Biol* **181**(6): 935-944.

Krogan, N.J., Peng, W.T., Cagney, G., Robinson, M.D., Haw, R., Zhong, G., Guo, X., Zhang, X., Canadien, V., Richards, D.P. et al. 2004. High-definition macromolecular composition of yeast RNA-processing complexes. *Mol Cell* **13**(2): 225-239.

Kufel, J., Dichtl, B., and Tollervey, D. 1999. Yeast Rnt1p is required for cleavage of the pre-ribosomal RNA in the 3' ETS but not the 5' ETS. *RNA* **5**(7): 909-917.

Kumar, A. and Warner, J.R. 1972. Characterization of ribosomal precursor particles from HeLa cell nucleoli. *J Mol Biol* **63**(2): 233-246.

Lafontaine, D. and Tollervey, D. 1995. Trans-acting factors in yeast pre-rRNA and pre-snoRNA processing. *Biochem Cell Biol* **73**(11-12): 803-812.

Lamanna, A.C. and Karbstein, K. 2009. Nob1 binds the single-stranded cleavage site D at the 3'-end of 18S rRNA with its PIN domain. *Proc Natl Acad Sci U S A* **106**(34): 14259-14264.

-. 2010. An RNA conformational switch regulates pre-18S rRNA cleavage. *J Mol Biol* **405**(1): 3-17.

Lapik, Y.R., Fernandes, C.J., Lau, L.F., and Pestov, D.G. 2004. Physical and functional interaction between Pes1 and Bop1 in mammalian ribosome biogenesis. *Mol Cell* **15**(1): 17-29.

Lau, C.K., Bachorik, J.L., and Dreyfuss, G. 2009. Gemin5-snRNA interaction reveals an RNA binding function for WD repeat domains. *Nat Struct Mol Biol* **16**(5): 486-491.

Lau, N.C., Lim, L.P., Weinstein, E.G., and Bartel, D.P. 2001. An abundant class of tiny RNAs with probable regulatory roles in Caenorhabditis elegans. *Science* **294**(5543): 858-862.

Lawley, P.D. and Brookes, P. 1963. Further Studies on the Alkylation of Nucleic Acids and Their Constituent Nucleotides. *Biochem J* **89**: 127-138.

Lebaron, S., Schneider, C., van Nues, R.W., Swiatkowska, A., Walsh, D., Bottcher, B., Granneman, S., Watkins, N.J., and Tollervey, D. 2012. Proofreading of pre-40S ribosome maturation by a translation initiation factor and 60S subunits. *Nat Struct Mol Biol* **19**(8): 744-753.

Lebreton, A., Rousselle, J.C., Lenormand, P., Namane, A., Jacquier, A., Fromont-Racine, M., and Saveanu, C. 2008. 60S ribosomal subunit assembly dynamics defined by semi-quantitative mass spectrometry of purified complexes. *Nucleic Acids Res* **36**(15): 4988-4999.

Lebreton, A., Saveanu, C., Decourty, L., Jacquier, A., and Fromont-Racine, M. 2006a. Nsa2 is an unstable, conserved factor required for the maturation of 27 SB pre-rRNAs. *J Biol Chem* **281**(37): 27099-27108.

Lebreton, A., Saveanu, C., Decourty, L., Rain, J.C., Jacquier, A., and Fromont-Racine, M. 2006b. A functional network involved in the recycling of nucleocytoplasmic pre-60S factors. *J Cell Biol* **173**(3): 349-360.

Leipe, D.D., Wolf, Y.I., Koonin, E.V., and Aravind, L. 2002. Classification and evolution of P-loop GTPases and related ATPases. *J Mol Biol* **317**(1): 41-72.

Lescoute, A. and Westhof, E. 2006. The interaction networks of structured RNAs. *Nucleic Acids Res* **34**(22): 6587-6604.

Leshin, J.A., Heselpoth, R., Belew, A.T., and Dinman, J. 2011. High throughput structural analysis of yeast ribosomes using hSHAPE. *RNA Biol* **8**(3): 478-487.

Liang, X.H. and Fournier, M.J. 2006. The helicase Has1p is required for snoRNA release from pre-rRNA. *Mol Cell Biol* **26**(20): 7437-7450.

Liebeg, A. and Waldsich, C. 2009. Probing RNA structure within living cells. *Methods Enzymol* **468**: 219-238.

Lilley, D.M. 1998. Folding of branched RNA species. *Biopolymers* **48**(2-3): 101-112.

Lindahl, L., Archer, R.H., and Zengel, J.M. 1992. A new rRNA processing mutant of Saccharomyces cerevisiae. *Nucleic Acids Res* **20**(2): 295-301.

Lo, K.Y., Li, Z., Bussiere, C., Bresson, S., Marcotte, E.M., and Johnson, A.W. 2010. Defining the pathway of cytoplasmic maturation of the 60S ribosomal subunit. *Mol Cell* **39**(2): 196-208.

Lo, K.Y., Li, Z., Wang, F., Marcotte, E.M., and Johnson, A.W. 2009. Ribosome stalk assembly requires the dual-specificity phosphatase Yvh1 for the exchange of Mrt4 with P0. *J Cell Biol* **186**(6): 849-862.

Longtine, M.S., McKenzie, A., 3rd, Demarini, D.J., Shah, N.G., Wach, A., Brachat, A., Philippsen, P., and Pringle, J.R. 1998. Additional modules for versatile and economical PCR-based gene deletion and modification in Saccharomyces cerevisiae. *Yeast* **14**(10): 953-961.

Lucks, J.B., Mortimer, S.A., Trapnell, C., Luo, S., Aviran, S., Schroth, G.P., Pachter, L., Doudna, J.A., and Arkin, A.P. 2011. Multiplexed RNA structure characterization with selective 2'-hydroxyl acylation analyzed by primer extension sequencing (SHAPE-Seq). *Proc Natl Acad Sci U S A* **108**(27): 11063-11068.

Luz, J.S., Georg, R.C., Gomes, C.H., Machado-Santelli, G.M., and Oliveira, C.C. 2009. Sdo1p, the yeast orthologue of Shwachman-Bodian-Diamond syndrome protein, binds RNA and interacts with nuclear rRNA-processing factors. *Yeast* **26**(5): 287-298.

Lygerou, Z., Allmang, C., Tollervey, D., and Seraphin, B. 1996. Accurate processing of a eukaryotic precursor ribosomal RNA by ribonuclease MRP in vitro. *Science* **272**(5259): 268-270.

Mangiarotti, G., Turco, E., Perlo, C., and Altruda, F. 1975. Role of precursor 16S RNA in assembly of E. coli 30S ribosomes. *Nature* **253**(5492): 569-571.

McManus, C.J. and Graveley, B.R. 2011. RNA structure and the mechanisms of alternative splicing. *Curr Opin Genet Dev* **21**(4): 373-379.

Menne, T.F., Goyenechea, B., Sanchez-Puig, N., Wong, C.C., Tonkin, L.M., Ancliff, P.J., Brost, R.L., Costanzo, M., Boone, C., and Warren, A.J. 2007. The Shwachman-Bodian-Diamond syndrome protein mediates translational activation of ribosomes in yeast. *Nat Genet* **39**(4): 486-495.

Merino, E.J., Wilkinson, K.A., Coughlan, J.L., and Weeks, K.M. 2005. RNA structure analysis at single nucleotide resolution by selective 2'-hydroxyl acylation and primer extension (SHAPE). *J Am Chem Soc* **127**(12): 4223-4231.

Merl, J., Jakob, S., Ridinger, K., Hierlmeier, T., Deutzmann, R., Milkereit, P., and Tschochner, H. 2010. Analysis of ribosome biogenesis factor-modules in yeast cells depleted from pre-ribosomes. *Nucleic Acids Res* **38**(9): 3068-3080.

Miles, T.D., Jakovljevic, J., Horsey, E.W., Harnpicharnchai, P., Tang, L., and Woolford, J.L., Jr. 2005. Ytm1, Nop7, and Erb1 form a complex necessary for maturation of yeast 66S preribosomes. *Mol Cell Biol* **25**(23): 10419-10432.

Milkereit, P., Gadal, O., Podtelejnikov, A., Trumtel, S., Gas, N., Petfalski, E., Tollervey, D., Mann, M., Hurt, E., and Tschochner, H. 2001. Maturation and intranuclear transport of pre-ribosomes requires Noc proteins. *Cell* **105**(4): 499-509.

Milkereit, P., Strauss, D., Bassler, J., Gadal, O., Kuhn, H., Schutz, S., Gas, N., Lechner, J., Hurt, E., and Tschochner, H. 2003. A Noc complex specifically involved in the formation and nuclear export of ribosomal 40 S subunits. *J Biol Chem* **278**(6): 4072-4081.

Miller, O.L., Jr. and Beatty, B.R. 1969. Visualization of nucleolar genes. *Science* **164**(3882): 955-957.

Mitchell, P., Petfalski, E., and Tollervey, D. 1996. The 3' end of yeast 5.8S rRNA is generated by an exonuclease processing mechanism. *Genes Dev* **10**(4): 502-513.

Miyoshi, K., Shirai, C., and Mizuta, K. 2003. Transcription of genes encoding trans-acting factors required for rRNA maturation/ribosomal subunit assembly is coordinately regulated with ribosomal protein genes and involves Rap1 in Saccharomyces cerevisiae. *Nucleic Acids Res* **31**(7): 1969-1973.

Mizushima, S. and Nomura, M. 1970. Assembly mapping of 30S ribosomal proteins from E. coli. *Nature* **226**(5252): 1214.

Moazed, D. and Noller, H.F. 1986. Transfer RNA shields specific nucleotides in 16S ribosomal RNA from attack by chemical probes. *Cell* **47**(6): 985-994.

Moazed, D., Stern, S., and Noller, H.F. 1986. Rapid chemical probing of conformation in 16 S ribosomal RNA and 30 S ribosomal subunits using primer extension. *J Mol Biol* **187**(3): 399-416.

Morita, D., Miyoshi, K., Matsui, Y., Toh, E.A., Shinkawa, H., Miyakawa, T., and Mizuta, K. 2002. Rpf2p, an evolutionarily conserved protein, interacts with ribosomal protein L11 and is essential for the processing of 27 SB Pre-rRNA to 25 S rRNA and the 60 S ribosomal subunit assembly in Saccharomyces cerevisiae. *J Biol Chem* **277**(32): 28780-28786.

Mougel, M., Eyermann, F., Westhof, E., Romby, P., Expert-Bezancon, A., Ebel, J.P., Ehresmann, B., and Ehresmann, C. 1987. Binding of Escherichia coli ribosomal protein S8 to 16 S rRNA. A model for the interaction and the tertiary structure of the RNA binding site. *J Mol Biol* **198**(1): 91-107.

Mulder, A.M., Yoshioka, C., Beck, A.H., Bunner, A.E., Milligan, R.A., Potter, C.S., Carragher, B., and Williamson, J.R. 2010. Visualizing ribosome biogenesis: parallel assembly pathways for the 30S subunit. *Science* **330**(6004): 673-677.

Narla, A. and Ebert, B.L. 2010. Ribosomopathies: human disorders of ribosome dysfunction. *Blood* **115**(16): 3196-3205.

Nierhaus, K.H. 1991. The assembly of prokaryotic ribosomes. *Biochimie* **73**(6): 739-755.

Nierhaus, K.H. and Dohme, F. 1974. Total reconstitution of functionally active 50S ribosomal subunits from Escherichia coli. *Proc Natl Acad Sci U S A* **71**(12): 4713-4717.

Nissan, T.A., Bassler, J., Petfalski, E., Tollervey, D., and Hurt, E. 2002. 60S pre-ribosome formation viewed from assembly in the nucleolus until export to the cytoplasm. *EMBO J* **21**(20): 5539-5547.

Nissan, T.A., Galani, K., Maco, B., Tollervey, D., Aebi, U., and Hurt, E. 2004. A pre-ribosome with a tadpole-like structure functions in ATP-dependent maturation of 60S subunits. *Mol Cell* **15**(2): 295-301.

Nissen, P., Ippolito, J.A., Ban, N., Moore, P.B., and Steitz, T.A. 2001. RNA tertiary interactions in the large ribosomal subunit: the A-minor motif. *Proc Natl Acad Sci U S A* **98**(9): 4899-4903.

Novikova, I.V., Hennelly, S.P., and Sanbonmatsu, K.Y. 2012. Structural architecture of the human long non-coding RNA, steroid receptor RNA activator. *Nucleic Acids Res* **40**(11): 5034-5051.

O'Donohue, M.F., Choesmel, V., Faubladier, M., Fichant, G., and Gleizes, P.E. 2010. Functional dichotomy of ribosomal proteins during the synthesis of mammalian 40S ribosomal subunits. *J Cell Biol* **190**(5): 853-866.

Oeffinger, M., Leung, A., Lamond, A., and Tollervey, D. 2002. Yeast Pescadillo is required for multiple activities during 60S ribosomal subunit synthesis. *RNA* **8**(5): 626-636.

Oeffinger, M. and Tollervey, D. 2003. Yeast Nop15p is an RNA-binding protein required for pre-rRNA processing and cytokinesis. *EMBO J* **22**(24): 6573-6583.

Oeffinger, M., Zenklusen, D., Ferguson, A., Wei, K.E., El Hage, A., Tollervey, D., Chait, B.T., Singer, R.H., and Rout, M.P. 2009. Rrp17p is a eukaryotic exonuclease required for 5' end processing of Pre-60S ribosomal RNA. *Mol Cell* **36**(5): 768-781.

Ohtake, Y. and Wickner, R.B. 1995. Yeast virus propagation depends critically on free 60S ribosomal subunit concentration. *Mol Cell Biol* **15**(5): 2772-2781.

Osheim, Y.N., French, S.L., Keck, K.M., Champion, E.A., Spasov, K., Dragon, F., Baserga, S.J., and Beyer, A.L. 2004. Pre-18S ribosomal RNA is structurally compacted into the SSU processome prior to being cleaved from nascent transcripts in Saccharomyces cerevisiae. *Mol Cell* **16**(6): 943-954.

Pan, J., Thirumalai, D., and Woodson, S.A. 1997. Folding of RNA involves parallel pathways. *J Mol Biol* **273**(1): 7-13.

Pan, T. and Sosnick, T.R. 1997. Intermediates and kinetic traps in the folding of a large ribozyme revealed by circular dichroism and UV absorbance spectroscopies and catalytic activity. *Nat Struct Biol* **4**(11): 931-938.

Panse, V.G. and Johnson, A.W. 2010. Maturation of eukaryotic ribosomes: acquisition of functionality. *Trends Biochem Sci* **35**(5): 260-266.

Peattie, D.A. and Gilbert, W. 1980. Chemical probes for higher-order structure in RNA. *Proc Natl Acad Sci U S A* **77**(8): 4679-4682.

Pendrak, M.L. and Roberts, D.D. 2011. Ribosomal RNA processing in Candida albicans. *RNA* **17**(12): 2235-2248.

Perez-Fernandez, J., Roman, A., De Las Rivas, J., Bustelo, X.R., and Dosil, M. 2007. The 90S preribosome is a multimodular structure that is assembled through a hierarchical mechanism. *Mol Cell Biol* **27**(15): 5414-5429.

Pertschy, B., Saveanu, C., Zisser, G., Lebreton, A., Tengg, M., Jacquier, A., Liebminger, E., Nobis, B., Kappel, L., van der Klei, I. et al. 2007. Cytoplasmic recycling of 60S preribosomal factors depends on the AAA protein Drg1. *Mol Cell Biol* **27**(19): 6581-6592.

Pertschy, B., Schneider, C., Gnadig, M., Schafer, T., Tollervey, D., and Hurt, E. 2009. RNA helicase Prp43 and its co-factor Pfa1 promote 20 to 18 S rRNA processing catalyzed by the endonuclease Nob1. *J Biol Chem* **284**(50): 35079-35091.

Pestov, D.G., Stockelman, M.G., Strezoska, Z., and Lau, L.F. 2001. ERB1, the yeast homolog of mammalian Bop1, is an essential gene required for maturation of the 25S and 5.8S ribosomal RNAs. *Nucleic Acids Res* **29**(17): 3621-3630.

Pley, H.W., Flaherty, K.M., and McKay, D.B. 1994. Model for an RNA tertiary interaction from the structure of an intermolecular complex between a GAAA tetraloop and an RNA helix. *Nature* **372**(6501): 111-113.

Poll, G., Braun, T., Jakovljevic, J., Neueder, A., Jakob, S., Woolford, J.L., Jr., Tschochner, H., and Milkereit, P. 2009. rRNA maturation in yeast cells depleted of large ribosomal subunit proteins. *PLoS One* **4**(12): e8249.

Poot, R.A., Pleij, C.W., and van Duin, J. 1996. The central pseudoknot in 16S ribosomal RNA is needed for ribosome stability but is not essential for 30S initiation complex formation. *Nucleic Acids Res* **24**(19): 3670-3676.

Poot, R.A., Tsareva, N.V., Boni, I.V., and van Duin, J. 1997. RNA folding kinetics regulates translation of phage MS2 maturation gene. *Proc Natl Acad Sci U S A* **94**(19): 10110-10115.

Porschke, D. and Eigen, M. 1971. Co-operative non-enzymic base recognition. 3. Kinetics of the helix-coil transition of the oligoribouridylic--oligoriboadenylic acid system and of oligoriboadenylic acid alone at acidic pH. *J Mol Biol* **62**(2): 361-381.

Powers, T., Daubresse, G., and Noller, H.F. 1993. Dynamics of in vitro assembly of 16 S rRNA into 30 S ribosomal subunits. *J Mol Biol* **232**(2): 362-374.

Powers, T. and Noller, H.F. 1995. Hydroxyl radical footprinting of ribosomal proteins on 16S rRNA. *RNA* **1**(2): 194-209.

Powers, T. and Walter, P. 1999. Regulation of ribosome biogenesis by the rapamycin-sensitive TOR-signaling pathway in Saccharomyces cerevisiae. *Mol Biol Cell* **10**(4): 987-1000.

Rashid, R., Liang, B., Baker, D.L., Youssef, O.A., He, Y., Phipps, K., Terns, R.M., Terns, M.P., and Li, H. 2006. Crystal structure of a Cbf5-Nop10-Gar1 complex and implications in RNA-guided pseudouridylation and dyskeratosis congenita. *Mol Cell* **21**(2): 249-260.

Rietveld, K., Van Poelgeest, R., Pleij, C.W., Van Boom, J.H., and Bosch, L. 1982. The tRNA-like structure at the 3' terminus of turnip yellow mosaic virus RNA. Differences and similarities with canonical tRNA. *Nucleic Acids Res* **10**(6): 1929-1946.

Rigaut, G., Shevchenko, A., Rutz, B., Wilm, M., Mann, M., and Seraphin, B. 1999. A generic protein purification method for protein complex characterization and proteome exploration. *Nat Biotechnol* **17**(10): 1030-1032.

Rinn, J.L. and Chang, H.Y. 2012. Genome regulation by long noncoding RNAs. *Annu Rev Biochem* **81**: 145-166.

Ripmaster, T.L., Vaughn, G.P., and Woolford, J.L., Jr. 1992. A putative ATP-dependent RNA helicase involved in Saccharomyces cerevisiae ribosome assembly. *Proc Natl Acad Sci U S A* **89**(23): 11131-11135.

Rodriguez-Galan, O., Garcia-Gomez, J.J., and de la Cruz, J. 2013. Yeast and human RNA helicases involved in ribosome biogenesis: current status and perspectives. *Biochim Biophys Acta* **1829**(8): 775-790.

Rohl, R. and Nierhaus, K.H. 1982. Assembly map of the large subunit (50S) of Escherichia coli ribosomes. *Proc Natl Acad Sci U S A* **79**(3): 729-733.

Rosado, I.V., Dez, C., Lebaron, S., Caizergues-Ferrer, M., Henry, Y., and de la Cruz, J. 2007. Characterization of Saccharomyces cerevisiae Npa2p (Urb2p) reveals a low-molecular-mass complex containing Dbp6p, Npa1p (Urb1p), Nop8p, and Rsa3p involved in early steps of 60S ribosomal subunit biogenesis. *Mol Cell Biol* **27**(4): 1207-1221.

Rotenberg, M.O., Moritz, M., and Woolford, J.L., Jr. 1988. Depletion of Saccharomyces cerevisiae ribosomal protein L16 causes a decrease in 60S ribosomal subunits and formation of half-mer polyribosomes. *Genes Dev* **2**(2): 160-172.

Russell, R., Millett, I.S., Doniach, S., and Herschlag, D. 2000. Small angle X-ray scattering reveals a compact intermediate in RNA folding. *Nat Struct Biol* **7**(5): 367-370.

Russell, R., Millett, I.S., Tate, M.W., Kwok, L.W., Nakatani, B., Gruner, S.M., Mochrie, S.G., Pande, V., Doniach, S., Herschlag, D. et al. 2002a. Rapid compaction during RNA folding. *Proc Natl Acad Sci U S A* **99**(7): 4266-4271.

Russell, R., Zhuang, X., Babcock, H.P., Millett, I.S., Doniach, S., Chu, S., and Herschlag, D. 2002b. Exploring the folding landscape of a structured RNA. *Proc Natl Acad Sci U S A* **99**(1): 155-160.

Sachs, A.B. and Davis, R.W. 1990. Translation initiation and ribosomal biogenesis: involvement of a putative rRNA helicase and RPL46. *Science* **247**(4946): 1077-1079.

Sahasranaman, A., Dembowski, J., Strahler, J., Andrews, P., Maddock, J., and Woolford, J.L., Jr. 2011. Assembly of Saccharomyces cerevisiae 60S ribosomal subunits: role of factors required for 27S pre-rRNA processing. *EMBO J* **30**(19): 4020-4032.

Samaha, R.R., O'Brien, B., O'Brien, T.W., and Noller, H.F. 1994. Independent in vitro assembly of a ribonucleoprotein particle containing the 3' domain of 16S rRNA. *Proc Natl Acad Sci U S A* **91**(17): 7884-7888.

Saveanu, C., Bienvenu, D., Namane, A., Gleizes, P.E., Gas, N., Jacquier, A., and Fromont-Racine, M. 2001. Nog2p, a putative GTPase associated with pre-60S subunits and required for late 60S maturation steps. *EMBO J* **20**(22): 6475-6484.

Saveanu, C., Namane, A., Gleizes, P.E., Lebreton, A., Rousselle, J.C., Noaillac-Depeyre, J., Gas, N., Jacquier, A., and Fromont-Racine, M. 2003. Sequential protein association with nascent 60S ribosomal particles. *Mol Cell Biol* **23**(13): 4449-4460.

Saveanu, C., Rousselle, J.C., Lenormand, P., Namane, A., Jacquier, A., and Fromont-Racine, M. 2007. The p21-activated protein kinase inhibitor Skb15 and its budding yeast homologue are 60S ribosome assembly factors. *Mol Cell Biol* **27**(8): 2897-2909.

Schafer, T., Maco, B., Petfalski, E., Tollervey, D., Bottcher, B., Aebi, U., and Hurt, E. 2006. Hrr25-dependent phosphorylation state regulates organization of the pre-40S subunit. *Nature* **441**(7093): 651-655.

Schmelzle, T. and Hall, M.N. 2000. TOR, a central controller of cell growth. *Cell* **103**(2): 253-262.

Schmitt, M.E. and Clayton, D.A. 1993. Nuclear RNase MRP is required for correct processing of pre-5.8S rRNA in Saccharomyces cerevisiae. *Mol Cell Biol* **13**(12): 7935-7941.

Schneider, C.A., Rasband, W.S., and Eliceiri, K.W. 2012. NIH Image to ImageJ: 25 years of image analysis. *Nat Methods* **9**(7): 671-675.

Senger, B., Lafontaine, D.L., Graindorge, J.S., Gadal, O., Camasses, A., Sanni, A., Garnier, J.M., Breitenbach, M., Hurt, E., and Fasiolo, F. 2001. The nucle(ol)ar Tif6p and Efl1p are required for a late cytoplasmic step of ribosome synthesis. *Mol Cell* **8**(6): 1363-1373.

Sengupta, J., Bussiere, C., Pallesen, J., West, M., Johnson, A.W., and Frank, J. 2010. Characterization of the nuclear export adaptor protein Nmd3 in association with the 60S ribosomal subunit. *J Cell Biol* **189**(7): 1079-1086.

Shajani, Z., Sykes, M.T., and Williamson, J.R. 2011. Assembly of bacterial ribosomes. *Annu Rev Biochem* **80**: 501-526.

Shepard, P.J. and Hertel, K.J. 2008. Conserved RNA secondary structures promote alternative splicing. *RNA* **14**(8): 1463-1469.

Shimoji, K., Jakovljevic, J., Tsuchihashi, K., Umeki, Y., Wan, K., Kawasaki, S., Talkish, J., Woolford, J.L., Jr., and Mizuta, K. 2012. Ebp2 and Brx1 function cooperatively in 60S ribosomal subunit assembly in Saccharomyces cerevisiae. *Nucleic Acids Res*.

Shuai, K. and Warner, J.R. 1991. A temperature sensitive mutant of Saccharomyces cerevisiae defective in pre-rRNA processing. *Nucleic Acids Res* **19**(18): 5059-5064.

Sigurdsson, S., Dirac-Svejstrup, A.B., and Svejstrup, J.Q. 2010. Evidence that transcript cleavage is essential for RNA polymerase II transcription and cell viability. *Mol Cell* **38**(2): 202-210.

Silverman, S.K., Zheng, M., Wu, M., Tinoco, I., Jr., and Cech, T.R. 1999. Quantifying the energetic interplay of RNA tertiary and secondary structure interactions. *RNA* **5**(12): 1665-1674.

Small, E.C., Leggett, S.R., Winans, A.A., and Staley, J.P. 2006. The EF-G-like GTPase Snu114p regulates spliceosome dynamics mediated by Brr2p, a DExD/H box ATPase. *Mol Cell* **23**(3): 389-399.

Spitale, R.C., Crisalli, P., Flynn, R.A., Torre, E.A., Kool, E.T., and Chang, H.Y. 2012. RNA SHAPE analysis in living cells. *Nat Chem Biol* **9**(1): 18-20.

Staley, J.P. and Woolford, J.L., Jr. 2009. Assembly of ribosomes and spliceosomes: complex ribonucleoprotein machines. *Curr Opin Cell Biol* **21**(1): 109-118.

Staple, D.W. and Butcher, S.E. 2005. Pseudoknots: RNA structures with diverse functions. *PLoS Biol* **3**(6): e213.

Stern, S., Moazed, D., and Noller, H.F. 1988. Structural analysis of RNA using chemical and enzymatic probing monitored by primer extension. *Methods Enzymol* **164**: 481-489.

Stern, S., Powers, T., Changchien, L.M., and Noller, H.F. 1989. RNA-protein interactions in 30S ribosomal subunits: folding and function of 16S rRNA. *Science* **244**(4906): 783-790.

Stout, C.D., Mizuno, H., Rubin, J., Brennan, T., Rao, S.T., and Sundaralingam, M. 1976. Atomic coordinates and molecular conformation of yeast phenylalanyl tRNA. An independent investigation. *Nucleic Acids Res* **3**(4): 1111-1123.

Strezoska, Z., Pestov, D.G., and Lau, L.F. 2002. Functional inactivation of the mouse nucleolar protein Bop1 inhibits multiple steps in pre-rRNA processing and blocks cell cycle progression. *J Biol Chem* **277**(33): 29617-29625.

Strunk, B.S. and Karbstein, K. 2009. Powering through ribosome assembly. *RNA* **15**(12): 2083-2104.

Strunk, B.S., Loucks, C.R., Su, M., Vashisth, H., Cheng, S., Schilling, J., Brooks, C.L., 3rd, Karbstein, K., and Skiniotis, G. 2011. Ribosome assembly factors prevent premature translation initiation by 40S assembly intermediates. *Science* **333**(6048): 1449-1453.

Strunk, B.S., Novak, M.N., Young, C.L., and Karbstein, K. 2012. A translation-like cycle is a quality control checkpoint for maturing 40S ribosome subunits. *Cell* **150**(1): 111-121.

Suddath, F.L., Quigley, G.J., McPherson, A., Sneden, D., Kim, J.J., Kim, S.H., and Rich, A. 1974. Three-dimensional structure of yeast phenylalanine transfer RNA at 3.0angstroms resolution. *Nature* **248**(443): 20-24.

Sun, C. and Woolford, J.L., Jr. 1994. The yeast NOP4 gene product is an essential nucleolar protein required for pre-rRNA processing and accumulation of 60S ribosomal subunits. *EMBO J* **13**(13): 3127-3135.

Sykes, M.T. and Williamson, J.R. 2009. A complex assembly landscape for the 30S ribosomal subunit. *Annu Rev Biophys* **38**: 197-215.

Szep, S., Wang, J., and Moore, P.B. 2003. The crystal structure of a 26-nucleotide RNA containing a hook-turn. *RNA* **9**(1): 44-51.

Talkington, M.W., Siuzdak, G., and Williamson, J.R. 2005. An assembly landscape for the 30S ribosomal subunit. *Nature* **438**(7068): 628-632.

Talkish, J., Zhang, J., Jakovljevic, J., Horsey, E.W., and Woolford, J.L., Jr. 2012. Hierarchical recruitment into nascent ribosomes of assembly factors required for 27SB pre-rRNA processing in Saccharomyces cerevisiae. *Nucleic Acids Res* **40**(17): 8646-8661.

Tamura, M. and Holbrook, S.R. 2002. Sequence and structural conservation in RNA ribose zippers. *J Mol Biol* **320**(3): 455-474.

Tarassov, K., Messier, V., Landry, C.R., Radinovic, S., Serna Molina, M.M., Shames, I., Malitskaya, Y., Vogel, J., Bussey, H., and Michnick, S.W. 2008. An in vivo map of the yeast protein interactome. *Science* **320**(5882): 1465-1470.

Thirumalai, D., Lee, N., Woodson, S.A., and Klimov, D. 2001. Early events in RNA folding. *Annu Rev Phys Chem* **52**: 751-762.

Tollervey, D. 1996. Trans-acting factors in ribosome synthesis. *Exp Cell Res* **229**(2): 226-232.

Tollervey, D., Lehtonen, H., Carmo-Fonseca, M., and Hurt, E.C. 1991. The small nucleolar RNP protein NOP1 (fibrillarin) is required for pre-rRNA processing in yeast. *EMBO J* **10**(3): 573-583.

Trapman, J., Retel, J., and Planta, R.J. 1975. Ribosomal precursor particles from yeast. *Exp Cell Res* **90**(1): 95-104.

Traub, P. and Nomura, M. 1968. Structure and function of E. coli ribosomes. V. Reconstitution of functionally active 30S ribosomal particles from RNA and proteins. *Proc Natl Acad Sci U S A* **59**(3): 777-784.

Tsujii, R., Miyoshi, K., Tsuno, A., Matsui, Y., Toh-e, A., Miyakawa, T., and Mizuta, K. 2000. Ebp2p, yeast homologue of a human protein that interacts with Epstein-Barr virus nuclear antigen 1, is required for pre-rRNA processing and ribosomal subunit assembly. *Genes Cells* **5**(7): 543-553.

Tsuno, A., Miyoshi, K., Tsujii, R., Miyakawa, T., and Mizuta, K. 2000. RRS1, a conserved essential gene, encodes a novel regulatory protein required for ribosome biogenesis in Saccharomyces cerevisiae. *Mol Cell Biol* **20**(6): 2066-2074.

Tullius, T.D. and Greenbaum, J.A. 2005. Mapping nucleic acid structure by hydroxyl radical cleavage. *Curr Opin Chem Biol* **9**(2): 127-134.

Udem, S.A. and Warner, J.R. 1972. Ribosomal RNA synthesis in Saccharomyces cerevisiae. *J Mol Biol* **65**(2): 227-242.

Ulbrich, C., Diepholz, M., Bassler, J., Kressler, D., Pertschy, B., Galani, K., Bottcher, B., and Hurt, E. 2009. Mechanochemical removal of ribosome biogenesis factors from nascent 60S ribosomal subunits. *Cell* **138**(5): 911-922.

Underwood, J.G., Uzilov, A.V., Katzman, S., Onodera, C.S., Mainzer, J.E., Mathews, D.H., Lowe, T.M., Salama, S.R., and Haussler, D. 2010. FragSeq: transcriptome-wide RNA structure probing using high-throughput sequencing. *Nat Methods* **7**(12): 995-1001.

van der Sande, C.A., Kwa, M., van Nues, R.W., van Heerikhuizen, H., Raue, H.A., and Planta, R.J. 1992. Functional analysis of internal transcribed spacer 2 of Saccharomyces cerevisiae ribosomal DNA. *J Mol Biol* **223**(4): 899-910.

van Meerten, D., Girard, G., and van Duin, J. 2001. Translational control by delayed RNA folding: identification of the kinetic trap. *RNA* **7**(3): 483-494.

Vanrobays, E., Leplus, A., Osheim, Y.N., Beyer, A.L., Wacheul, L., and Lafontaine, D.L. 2008. TOR regulates the subcellular distribution of DIM2, a KH domain protein required for cotranscriptional ribosome assembly and pre-40S ribosome export. *RNA* **14**(10): 2061-2073.

Venema, J. and Tollervey, D. 1999. Ribosome synthesis in Saccharomyces cerevisiae. *Annu Rev Genet* **33**: 261-311.

Wade, C.H., Umbarger, M.A., and McAlear, M.A. 2006. The budding yeast rRNA and ribosome biosynthesis (RRB) regulon contains over 200 genes. *Yeast* **23**(4): 293-306.

Walter, A.E., Turner, D.H., Kim, J., Lyttle, M.H., Muller, P., Mathews, D.H., and Zuker, M. 1994. Coaxial stacking of helixes enhances binding of oligoribonucleotides and improves predictions of RNA folding. *Proc Natl Acad Sci U S A* **91**(20): 9218-9222.

Warf, M.B. and Berglund, J.A. 2010. Role of RNA structure in regulating pre-mRNA splicing. *Trends Biochem Sci* **35**(3): 169-178.

Warner, J.R. 1999. The economics of ribosome biosynthesis in yeast. *Trends Biochem Sci* **24**(11): 437-440.

Watts, J.M., Dang, K.K., Gorelick, R.J., Leonard, C.W., Bess, J.W., Jr., Swanstrom, R., Burch, C.L., and Weeks, K.M. 2009. Architecture and secondary structure of an entire HIV-1 RNA genome. *Nature* **460**(7256): 711-716.

Weeks, K.M. 2010. Advances in RNA structure analysis by chemical probing. *Curr Opin Struct Biol* **20**(3): 295-304.

Wehner, K.A. and Baserga, S.J. 2002. The sigma(70)-like motif: a eukaryotic RNA binding domain unique to a superfamily of proteins required for ribosome biogenesis. *Mol Cell* **9**(2): 329-339.

Weitzmann, C.J., Cunningham, P.R., Nurse, K., and Ofengand, J. 1993. Chemical evidence for domain assembly of the Escherichia coli 30S ribosome. *FASEB J* **7**(1): 177-180.

Wells, S.E., Hughes, J.M.X., Igel, A.H., and Ares, M. 2000. Use of dimethysulfate to probe RNA structure in vivo. *Methods in Enzymology* **318**: 479-493.

Wery, M., Ruidant, S., Schillewaert, S., Lepore, N., and Lafontaine, D.L. 2009. The nuclear poly(A) polymerase and Exosome cofactor Trf5 is recruited cotranscriptionally to nucleolar surveillance. *RNA* **15**(3): 406-419.

Wilkinson, K.A., Gorelick, R.J., Vasa, S.M., Guex, N., Rein, A., Mathews, D.H., Giddings, M.C., and Weeks, K.M. 2008. High-throughput SHAPE analysis reveals structures in HIV-1 genomic RNA strongly conserved across distinct biological states. *PLoS Biol* **6**(4): e96.

Wimberly, B.T., Brodersen, D.E., Clemons, W.M., Jr., Morgan-Warren, R.J., Carter, A.P., Vonrhein, C., Hartsch, T., and Ramakrishnan, V. 2000. Structure of the 30S ribosomal subunit. *Nature* **407**(6802): 327-339.

Woodson, S.A. 2000. Compact but disordered states of RNA. *Nat Struct Biol* **7**(5): 349-352.

-. 2008. RNA folding and ribosome assembly. *Curr Opin Chem Biol* **12**(6): 667-673.

-. 2010. Compact intermediates in RNA folding. *Annu Rev Biophys* **39**: 61-77.

-. 2012. RNA folding pathways and the self-assembly of ribosomes. *Acc Chem Res* **44**(12): 1312-1319.

Woolford, J.L., Jr. 1991. The structure and biogenesis of yeast ribosomes. *Adv Genet* **29**: 63-118.

Woolford, J.L., Jr. and Warner, J.R. 1991. In *The Molecular and Cellular Biology of the Yeast Saccharomyces: Genome Dynamics, Protein Synthesis, and Energetics*, (ed. J.R. Broach, J.R. Pringle, and E.W. Jones), pp. 587-626. Cold Spring Harbor Laboratory Press.

Wu, K., Wu, P., and Aris, J.P. 2001. Nucleolar protein Nop12p participates in synthesis of 25S rRNA in Saccharomyces cerevisiae. *Nucleic Acids Res* **29**(14): 2938-2949.

Xue, Y., Bai, X., Lee, I., Kallstrom, G., Ho, J., Brown, J., Stevens, A., and Johnson, A.W. 2000. Saccharomyces cerevisiae RAI1 (YGL246c) is homologous to human DOM3Z and encodes a protein that binds the nuclear exoribonuclease Rat1p. *Mol Cell Biol* **20**(11): 4006-4015.

Yeh, L.C. and Lee, J.C. 1990. Structural analysis of the internal transcribed spacer 2 of the precursor ribosomal RNA from Saccharomyces cerevisiae. *J Mol Biol* **211**(4): 699-712.

Yeh, L.C., Thweatt, R., and Lee, J.C. 1990. Internal transcribed spacer 1 of the yeast precursor ribosomal RNA. Higher order structure and common structural motifs. *Biochemistry* **29**(25): 5911-5918.

Yoon, J.H., Abdelmohsen, K., and Gorospe, M. 2012. Posttranscriptional Gene Regulation by Long Noncoding RNA. *J Mol Biol*.

Zanchin, N.I., Roberts, P., DeSilva, A., Sherman, F., and Goldfarb, D.S. 1997. Saccharomyces cerevisiae Nip7p is required for efficient 60S ribosome subunit biogenesis. *Mol Cell Biol* **17**(9): 5001-5015.

Zarrinkar, P.P. and Williamson, J.R. 1994. Kinetic intermediates in RNA folding. *Science* **265**(5174): 918-924.

Zhang, J., Harnpicharnchai, P., Jakovljevic, J., Tang, L., Guo, Y., Oeffinger, M., Rout, M.P., Hiley, S.L., Hughes, T., and Woolford, J.L., Jr. 2007. Assembly factors Rpf2 and Rrs1 recruit 5S rRNA and ribosomal proteins rpL5 and rpL11 into nascent ribosomes. *Genes Dev* **21**(20): 2580-2592.

Zhang, W., Morris, Q.D., Chang, R., Shai, O., Bakowski, M.A., Mitsakakis, N., Mohammad, N., Robinson, M.D., Zirngibl, R., Somogyi, E. et al. 2004. The functional landscape of mouse gene expression. *J Biol* **3**(5): 21.

Zhuang, X., Bartley, L.E., Babcock, H.P., Russell, R., Ha, T., Herschlag, D., and Chu, S. 2000. A single-molecule study of RNA catalysis and folding. *Science* **288**(5473): 2048-2051.

Zhuang, X., Kim, H., Pereira, M.J., Babcock, H.P., Walter, N.G., and Chu, S. 2002. Correlating structural dynamics and function in single ribozyme molecules. *Science* **296**(5572): 1473-1476.